Drying of water based foundry coatings: Innovative test, process design and optimization methods

di Muoio, Giovanni Luca; Tiedje, Niels Skat; Johansen, Bjørn Budolph

Publication date:
2015

Document Version
Publisher's PDF, also known as Version of record

Drying of water based foundry coatings: Innovative test, process design and optimization methods

PhD Thesis

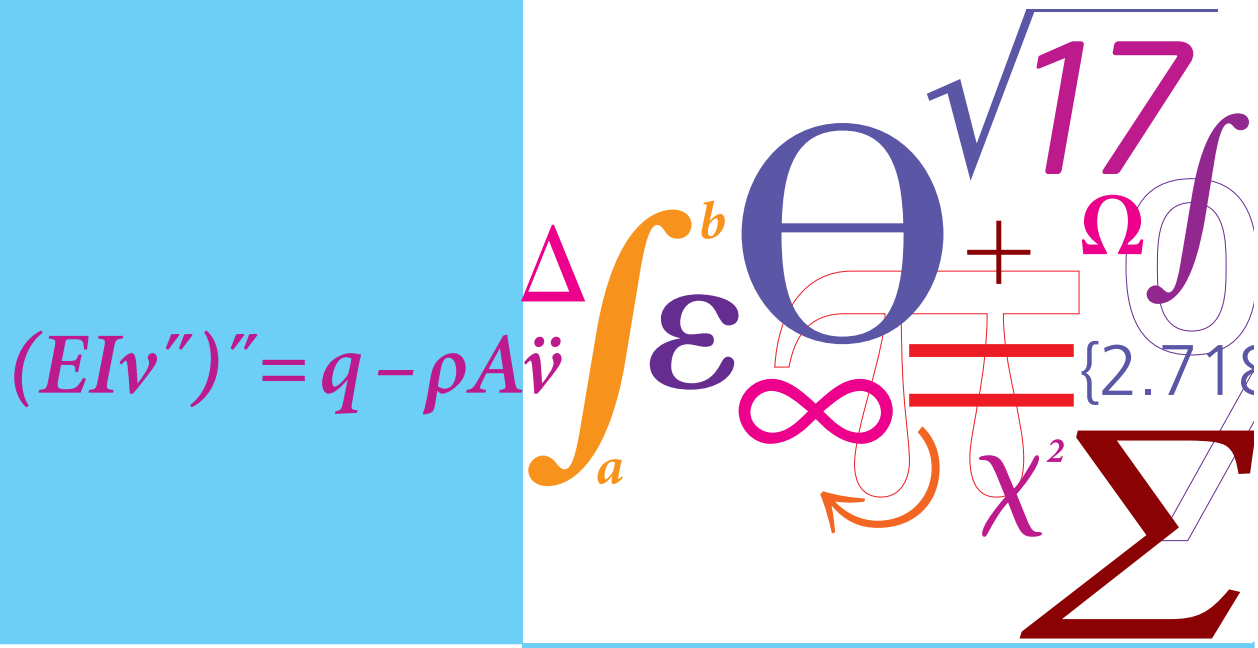

Giovanni Luca Di Muoio
February 2015

DTU Mechanical Engineering
Department of Mechanical Engineering

Drying of water based foundry coatings: Innovative test, process design and optimization methods

Industrial PhD Thesis

Giovanni Luca Di Muoio

University Supervisor: Niels Skat Tiedje, PhD. (Associate Professor)

Department of Mechanical Engineering, Technical University of Denmark

Company Supervisor: Bjørn Budolph Johansen (Technology Director)

Casting Technology Department, Global Castings A/S

March 2012 – February 2015

Drying of water based foundry coatings: Innovative test, process design and optimization methods

To my family and friends

"*It always seems impossible until it is done.*"
Nelson Mandela

"*Well, I suggest you gentlemen invent a way to put a square peg in a round hole. Rapidly*."
Gene Kranz, Flight Director, Apollo 13 Mission

"...perfection is finally attained not when there is no longer anything to add, but when there is no longer anything to take away..."
Antoine de Saint-Exupery

Synopsis

This work has been carried out in in partial fulfilment of the requirements for the award of the degree of Doctor of Philosophy (PhD) at the Technical University of Denmark. Associate Professor Niels Skat Tiedje has been the university supervisor from March 2012 to February 2015. Casting Technology Director Bjørn Budolph Johansen has been the company supervisor from March 2012 to June 2014.

In this Industrial PhD Thesis we present the main results of several tests and simulations carried out from 2011 to 2014 at Global Castings A/S (former Vestas Wind Systems A/S) and at the Technical University of Denmark with the overall aim to optimize the drying process of water based foundry coatings.

Drying of foundry coatings is a relatively new process in the foundry industry that followed the introduction of water as a solvent. In order to avoid moisture related quality problems and reach production capacity goals there is a need to understand how to design, control and optimize drying processes. The main focus of this project was on the critical parameters and properties to be controlled in production in order to achieve a stable and predictable drying process. We propose for each of these parameters simple methods for testing both at laboratory and production scale so that material characterization and model validation can be carried out also for materials different from the ones considered in this study. Additionally, we present the application of calculation methods and advanced simulation tools on real industrial cases. These tools have been developed in order to simulate and optimize the drying process and reduce drying time and power consumption as well as production process design time and cost of expensive drying equipment.

Results show that test methods from other industries can be used or adapted to better control drying processes of water based foundry coatings. Critical drying process related properties were obtained in the several laboratory tests performed and calculation and simulation methods were developed. Additionally, examples of improvement on full scale industrial production line are shown.

Keywords: Drying Process Design, Water Based Coating, Furan Sand, Test Methodologies, Simulation, Process Control

Synopsis (Danish)

Denne afhandling er udført som en del af kravet til at opnå ph.d.-graden på DTU. Lektor Niels Skat Tiedje har været vejleder på Universitetet fra marts 2012 til februar 2015. Støberidirektør Bjørn Budolph Johansen har været firmavejleder fra marts 2012 til juni 2014.I denne erhvervs-ph.d. afhandling præsenteres hovedresultaterne af adskillige forsøg og simuleringer udført fra 2011 til 2014 på Global Castings A/S (tidligere Vestas Wind Systems A/S) og DTU med hovedformålet at optimere tørring af støbeforme coatede med vandbaserede støberisværter.

Tørring af støberisværter er en forholdsvis ny proces indenfor støberibranchen, der er kommet med indførelse af vand som opløsningsmiddel til sværter. For at undgå problemer med kvaliteten pga. fugtighed og for at imødekomme behovet for at holde produktionstiden lavest muligt, er det nødvendigt at forstå hvordan man konstruerer, kontrollerer og optimerer tørringsprocessen. Hovedtemaet i dette projekt er at analysere og beskrive de kritiske procesparametre og fysiske egenskaber hos sværten som skal kontrolleres i produktionen for at opnå en stabil og forudsigelig tørreproces.

I en serie indledende forsøg undersøges hvilke procesparametre, der er væsentlige for tørringsprocessen. Baseret på de indledende forsøg er der udført en række studier af specifikke parametres indflydelse på procesbetingelserne og hvordan materialeegenskaber påvirker tørreprocessen.

I projektet udvikles enkle metoder til kvalitetskontrol af materialer og produktionsprocesser der kan anvendes i en produktion og/eller i laboratoriet. Analysemetoderne anvendes både til materialekarakterisering og til at validere de modeller for tørring, der udvikles i projektet.
Til slut demonstreres, ved hjælp at eksempler fra et produktionsmiljø, hvordan projektets resultater kan anvendes i praksis herunder vises hvordan både en enkel model og også mere avancerede simuleringsværktøjer kan anvendes i industrien. Disse værktøjer er blevet udviklet for at kunne simulere og optimere tørringsprocessen samt reducere tørretiden og energiforbruget i produktion smat for at reducere tiden til udvikling og konstruktion af tørreanlæg.

Resultaterne viser at forsøgsmetoder fra andre industrier kan anvendes eller tilpasses til bedre at kontrollere tørringsprocesser af vandbaserede støberibelægninger. Kritiske tørreprocessers egenskaber blev analyseret i de omfattende laboratorieforsøg og beregningsmodeller til brug i produktion er udviklet. Endvidere demonstreres det hvordan metoderne kan bruges til at forbedre produktionsprocesserne i praksis i en industriel produktionsline.

Nøgleord:
Konstruktion af tørringsproces, vandbaseret belægning, furan sand, forsøgsmetodik, simulering, proces kontrol.

Supplements

This thesis is composed of a main body where the background, objective, methods and results are presented as well as two appendices. One appendix where the published papers (supplements) originated form the different work packages are documented and a second appendix where experimental equipment main specifications are described.

A list of the papers at the basis of this thesis is provided below:

Supplement I

G. L. Di Muoio, N. S. Tiedje, B. B. Johansen, Critical Control Variables For The Coating Process Of Furan Bonded Sand With Water Based Foundry Coatings, Word Foundry Congress, 14-21 May 2014, Bilbao, Spain

Supplement II

G. L. Di Muoio, N. S. Tiedje, Achieving Control of Coating Process in your Foundry, Archives of Foundry Engineering, Issue 3, 2015

Supplement III

G. L. Di Muoio, N. S. Tiedje, Evaporation Rates of Water Based Foundry Coatings on Furan Bonded Sands, International Foundry Research

Supplement IV

G. L. Di Muoio, N. S. Tiedje, B. B. Johansen, Investigation of Moisture Levels in Water Based Foundry Coating and Furan Sands Using and Automatic Vapor Sorption Analyzer, 19th International Drying Symposium (IDS 2014), Lyon, France, August 24-27, 2014

Supplement V

G. L. Di Muoio, N. S. Tiedje, B. B. Johansen, Automatic Vapour Sorption Analysis as New Methodology for Assessing Moisture Content of Water Based Foundry Coating and Furan Sands, 10th International Symposium on the Science and Processing of Cast Iron – SPCI10, 9-13 Nov, Mar Del Plata, Argentina

Supplement VI

G. L. Di Muoio, N. S. Tiedje, Moisture Diffusion Coefficients Determination of Furan Bonded Sands and Water Based Foundry Coatings, International Journal of Cast Metal Research, 2/2015 (June 2015)

Supplement VII

G. L. Di Muoio, N. S. Tiedje, B. B. Johansen, Measurement of Moisture in Foundry Coating Using Resistance Based Measuring Devices, 19th International Drying Symposium (IDS 2014), Lyon, France, August 24-27, 2014

Supplement VIII

Giovanni Luca Di Muoio, A. Della Rocca, N. S. Tiedje, CFD Study for the Optimization of the Drying Process of Foundry Moulds used in the Production of Wind Turbine Components, Int. Journal of Engineering Research and Application

Supplement IX

G. L. Di Muoio, N. S. Tiedje, When dry is dry? Process design rules, simulations and industrial cases on the drying of water based foundry coatings, International Foundry Research, 3/2015 (September)

Supplement X

G.L. Di Muoio, G. Bertuzzi, J. O. Frandsen, An Innovative Integrated CAE Approach for The Design and Optimization of Foundry Moulding Boxes, CastTech 2nd International Conference, 20-21 Nov 2014, Bielefeld , Germany

Acknowledgments

I want to thank my supervisors for Niels Skat Tiedje and Bjørn Budolph Johansen for the support and the hard work to make this project successful, from the initial application for funding to the daily problems.

The management team at Global Castings provided me with ongoing support and allowed me to carry out this project even through difficult transition times for the company.

Torben Hansen, Niels Ole Jeppesen and Torbjørn Skaland for the support in the very early stages of this project in Vestas Castings Xuzhou. Jens Karsten Siersbæk and Claus Rasmussen who gave me the opportunity to work for the first time on drying process optimization at VCX and gave me very useful on the job training in project management.

My many (some former) colleagues at Global Castings helped in many aspects of the project (and not only) in different factories across the world. In particular Xu Yunlong, Yang Yanchu, Shi Feng, Chen Peng, Wang Ruirong, Zhao Peigen, Tommy Karlsson, Kjetil Odinsen, Kalojan Simeonov.

My colleagues Jens Ole Frandsen, Giacomo Bertuzzi and Emanuele Spessot for helping me in many other projects allowing me to focus on my Phd.

The professors at DTU in particular Dr. Jesper Hattel, Dr. Jepser Thorborg and Dr. Cem Tutum for the good lectures and discussions and colleagues at DTU that provided me help along the project.

The many PhD students and in particular Alessandro Della Rocca and Pietro Albicocco for their help at different stages in the project.

Danilo Tomaselli for making me discover my passion for swimming and allowing me to achieve and maintain an optimal psychophysical balance during my PhD studies.

Andrea Mazzucco for the critical support on the heat exchange coefficient determination.

I am indebted to Denmark and The Danish Institute for Science, Technology and Innovation for the framework and the funding needed in order to carry out such a successful industrial PhD programme.

My family, friends and Rebecca for the always present support and capacity to bear with me.

Table of Contents

List of Figures

List of Tables

List of Symbols

A_{sample} coated area of sample [m^2]

CF evaporation rate correction factor [ ]

$CT_{dry,\ coat}$ or DCT thickness of dry coating [kg/m^2]

CT_{water} or WT or CT_{H2O} thickness of water [kg/m^2]

$CT_{H2O,\ init}$ initial thickness of water [kg/m^2]

$CT_{wet,coat}$ or WCT thickness of wet coating [kg/m^2]

CWF Coating Water Fraction (CWF) [%]

D diffusion coefficient [$m^2\ s^{-1}$]

Δt time step used in numerical solution [s]

Δ_{H20} mass of evaporated water in time Δt [kg]

ER_{avg} average water evaporation rate [$kg/m^2/h$]

ER water evaporation rate [$kg/m^2/h$]

h or HTC heat exchange coefficient [$W/(m^2K)$]

L thickness of the sample [m]

M_e adsorbed mass of water at equilibrium [kg]

M_t adsorbed mass of water at time t [kg]

$MC_{W.B.}$ or $U_{\%}$ moisture of coating layer on wet basis [%]

R electrical resistance [Ohm]

RH ai relative humidity [%]

ρ density [kg/m^3]

t time [s]

t_{dry} drying time [hours]

W_{dry} weight of coated sample after drying [g]

W_{water} weight of water in the coating layer [g]

W_{wet} weight of coated sample after coating [g]

$W_{dry,\ coat}$ weight of dry coating [g]

$W_{wet,coat}$ weight of wet coating [g]

W_{sand} weight of sample before coating [g]

x space [m]

X moisture [ ]

X_i initial moisture content [%]

X_e moisture content at equilibrium [ ]

X_t moisture content at time t [ ]

X* nondimensional moisture [ ]

1. Introduction

1.1 - Background & Motivation

Global Castings foundries produce cast iron component that constitute the most critical load bearing structure of the nacelle and of the hub and are vital to the construction and performance of the wind turbine. As turbines with higher power rating are designed every year, the need for increased size and better quality castings is set and, as a consequence, more stringent demands are posed on the production processes in terms of capacity, quality and process control.

The production of castings starts with the preparation of a mould, made of chemically bonded sand, which will give the shape to the final casting. This sand mould is then coated with a refractory coating to prevent the sand from melting and sticking onto the casting (creating surface defects and a surface difficult to machine). Finally the molten iron is poured into the mould and after cooling down the part is extracted, cleaned, machined and sent to the final assembly factory (Figure 1.1).

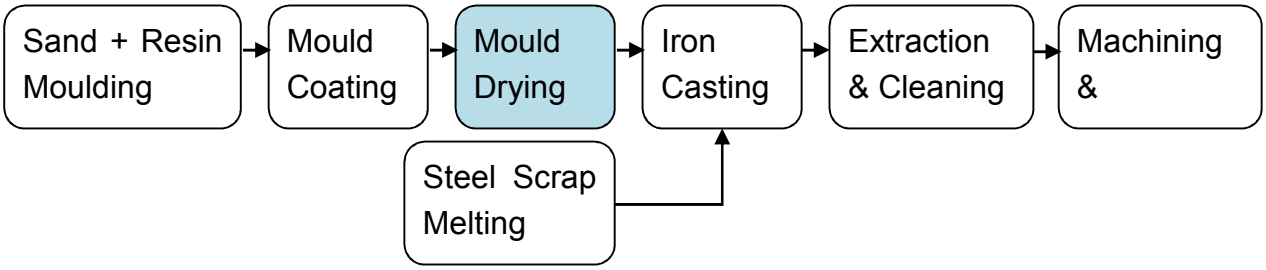

Figure 1.1 Summary of production flow in Global Castings foundries.

Drying of foundry coatings is a relatively new process in the foundry industry that followed the introduction of water as a solvent. Previously used alcohol based coatings were dried by burning, a fast but unsafe process due to the high flames generated (Figure 1.2). Additionally alcohol fumes and combustion gases are released in production environment posing health and safety risks for the operators.

Figure 1.2 Drying of alcohol based coated mould generating 6 m high flames (on the right), and operator standing nearby (on the left).

Water was introduced as a solvent to eliminate such risks, but in order to avoid moisture related defects in the castings ([1-3]) a drying step for the coated moulds is needed (Figure 1.3). The duration of the drying process (drying time) and the final amount of residual moisture needs to be predicted and controlled so that process capacity and quality can be maintained.

In this work, we focus on the critical process parameters and properties to be controlled in order to achieve a stable drying process (Figure 1.4). The term stability means that we are able to predict the final moisture level and the drying time (the time needed to reach the specified moisture level) of a mould and keep these within a narrow range.

In particular, we need identify, for each of these parameters, simple methods for testing and measuring so that material characterization and model validation can be carried out easily also for materials different from the ones considered in this study. Simple calculation methods and more advanced simulation tools are needed in order to simulate the drying process and reduce design time and cost of expensive drying equipment.

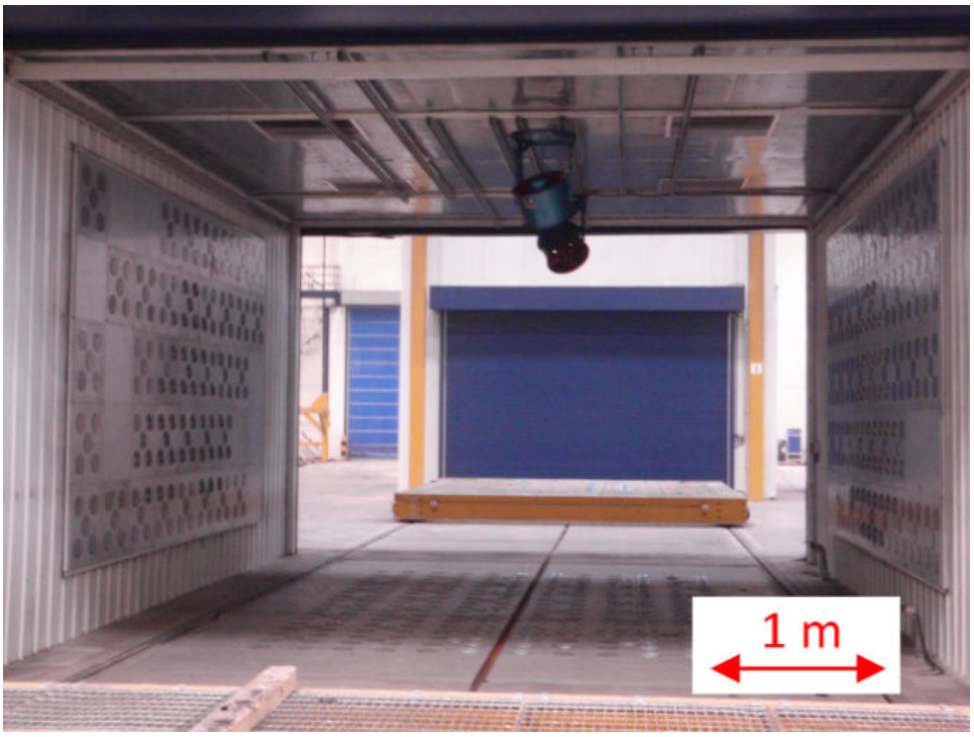

Figure 1.3 Example of a drying cabinet used for the drying of water based coatings applied on sand moulds in the production of large size wind turbine components.

Production Step	Moulding	Coating	Drying	Assembly
Critical Parameter	Mould Properties	Coating Layer Properties	- Drying Time - Residual Moiture	- Moisture Pick Up - Storage Time

Figure 1.4 Critical parameters influencing the drying process at each production step.

1.2 - Literature Review

In the following sections we provide a quick review to clarify the state of the art in the different areas covered in this project.

1.2.1 - Foundry Coating

The use of coating is critical is the production of good quality castings as it is the only means of separation between the sand and the molten metal [4] and properties of the coating can significantly affect the quality of the final parts [5].

The coatings are suspensions composed mainly by refractory filler (typically zircon, graphite or olivine) and a liquid carrier (alcohol or water) [6]. Water based coatings have been recently introduced in the market and adopted in Global Casting foundries, these coatings are non-flammable, nontoxic and cheaper compared to alcohol based coatings. On the other hand, the drying process is usually slower or more expensive, since the water must be removed by evaporation either in ambient conditions or in a drying oven [6,7].

General coating properties are described in [8] and a review of possible methods for assessing foundry coating properties is presented by Nwaogu [4]. However there are thousands of different formulations for foundry coating available from suppliers and there is therefore a need to create simple test and evaluation methodologies to be used at factories as well as identifying relevant properties of the foundry coatings that today are not being measured.

Once test methodologies and critical parameters are identified it will then be possible to implement these controls in production to guarantee stable properties of the coating layer and therefore of the casting surface quality [9].

1.2.2 - Coating Layer Properties

The energy used in the drying process and therefore the cost are are heavily dependent on coating layer properties (such as water content and coating penetration) [9,10]. Coating layer properties can influence surface quality and veining defects in a casting [7,11-13].

For production of large castings (5-30 tons) flow coating, brush coating and spray coating can be used (dipping would be very unpractical). Flow coating (**Figure** 1.5) is the most commonly used method as it leads to better and more uniform coating layer properties [5,9], as compared to spray and brush coating. It is therefore the focus of this study.

Figure 1.5 Flow coating of large size mould for wind turbine parts production.

Even though flow coating is known to be a more stable process compared to spraying, there are still several variables that can affect the coating layer properties [13-15]. Additionally these properties can depend on particular setup of specific factories.

Another fundamental aspect in controlling the coating process is the ability to measure and monitor the variables affecting the process (i.e. coating density, coating viscosity, mould properties, etc…) and to measure the properties of the resulting coating layer. This is something that today can only be done partially by the available methods such as wheel or comb [9] (**Figure** 1.6).

There is therefore needed to investigate the possible variables that can influence the coating layer properties for the specific coating and mould properties typical of Global Casting factories and possible simple methods to measure coating layer properties in production.

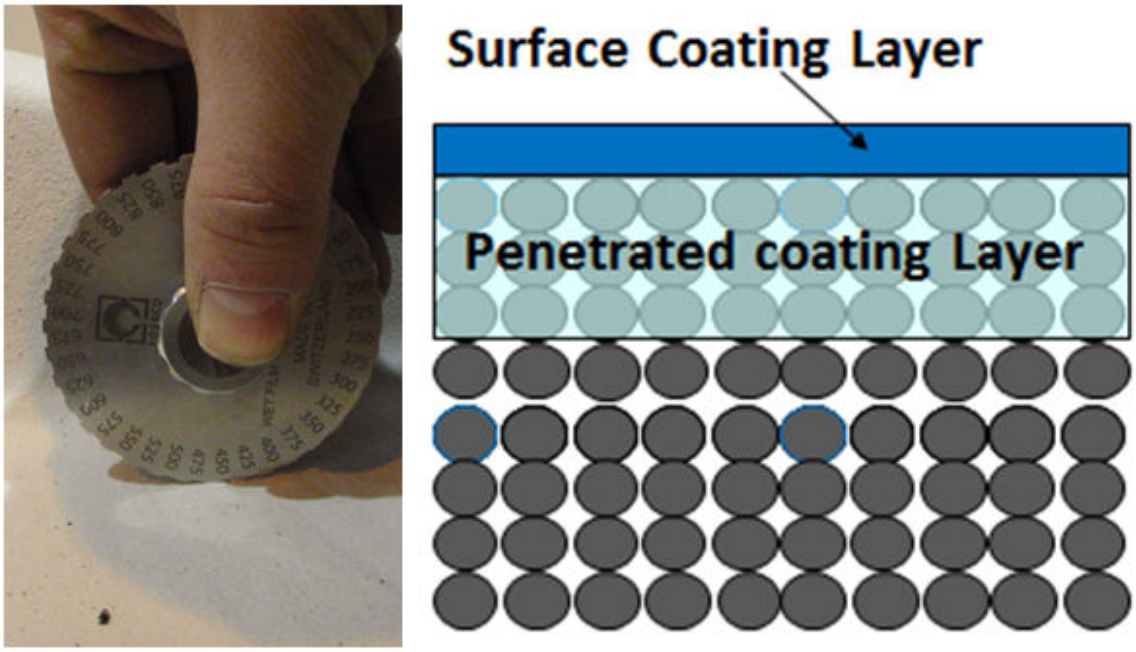

Figure 1.6 Standard coating thickness measuring wheel (right), actual measured thickness is only the surface layer (left).

1.2.3 - Evaporation Rates and Drying Time

In the foundry industry, moulds are normally dried in forced air convection ovens (Figure 1.3) or in ambient conditions depending on the needed drying time. Drying times, however, are heavily influenced by the type of coating used, the initial amount of water in the coating layer and the conditions of the drying air [9,10,17].

Typically water based coatings contain more than 30% of water [Supplement I] at the time of application. Drying of moulds is needed in order to reduce the moisture of the coating to a minimum and to lower the risk of vapour and gas defects [1,2,18-20].

A proper understanding of the drying behaviour of water based coatings can help to correctly dimension drying equipment, therefore helping to reduce investment cost, power usage and risk of vapour defects which finally lowers the cost of the produced castings.

In the drying industry it is common practice to characterize materials drying behaviour with laboratory tests where the sample is dried while the water loss is monitored by measuring the weight variation of the sample [21]. From the weight measurement is then possible to obtain important drying properties such as evaporation rates and characteristic drying curves [22,23]

(**Figure** 1.7). These properties are normally not available in literature for foundry coatings and bonded sands. Testing is therefore required in order to determine such properties.

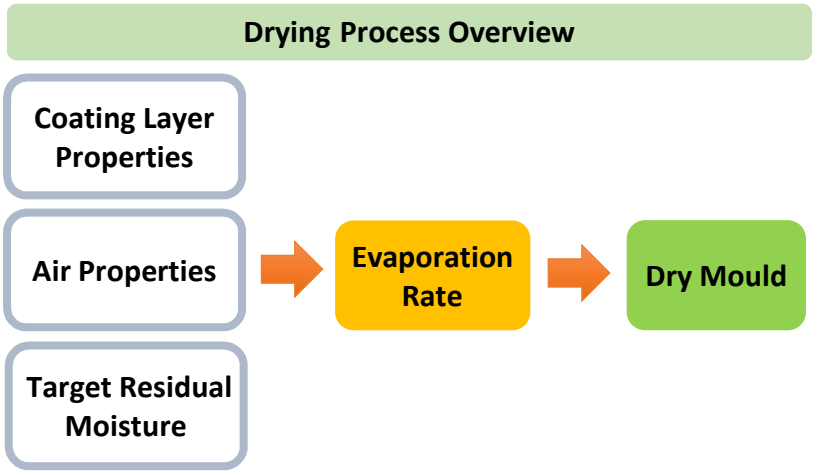

Figure 1.7 Drying process parameters overview.

1.2.4 - Residual Moisture Levels

When cast parts are produced, the molten metal in contact with the mould causes the production of gases that can lead to defects and scrapped items (Figure 1.8). These gases are composed by a mixture of water vapour, decomposition products of the coating and moulding materials and from gases dissolved in the molten iron [1,2]. Gas defects can be correlated directly to vapour generated in the mould and coating material due to high level of residual moisture after the drying process [18-20]. In particular for furan sands, water vapour is a significant component of the gases generated during the decomposition [24]. Moisture is present in furan sand as product of the binder and catalyst reaction but its amount can change over time [20]. Literature shows that gas defects probability can be predicted by simulation if models are calibrated with experimental data for the specific binding system used [25-27]. Other studies shows that gas evolution rates can vary for different materials [28-31].

All the current studies however focus on different classes of binding system and foundry material but do not provide information about the influence of parameters such as temperature, air humidity and dust levels and about different brands of furan binders used in Global Castings production facilities (Figure 1.9).

Sorption/desorption curves are typically used in other industries (such as food, wood, paper) to design and optimise drying processes (by knowing the initial moisture and final moisture achievable at the drier's air humidity and temperature levels) [21,22], to provide limits for production processes control and monitoring, to predict shelf life by knowing what moisture level a material will reach in an environment at a given air humidity (i.e. shelf life prediction in food packaging depends on moisture content) [32] or to predict possible moisture migration between different materials [22,32]. These curves are a property of the material and show how its moisture levels vary as a function of relative humidity at a given temperature. In particular they will show the minimum possible level of moisture achievable in given environmental conditions for a given material.

These test are normally not used in the foundry industry but are thought to be relevant by the authors to improve the understanding of the foundry material behaviour with respect to moisture.

Figure 1.8 Example of moisture related casting defect,

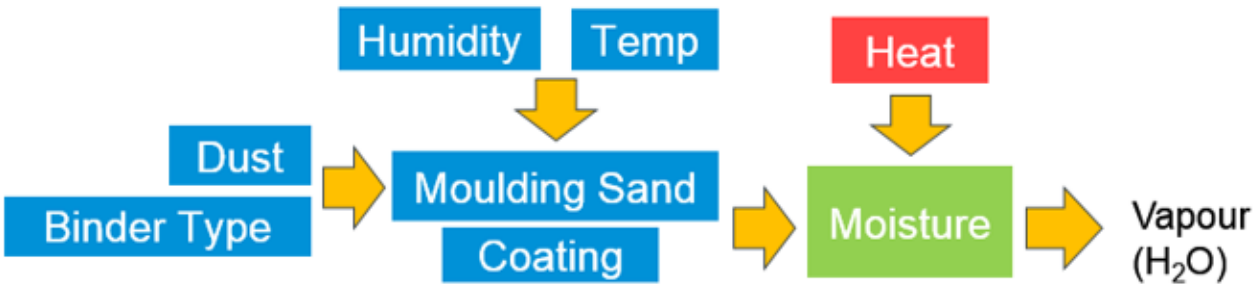

Figure 1.9 Parameters affecting vapour generation in a castings process.

1.2.5 - Moisture Diffusion

The critical parameter needed to model moisture adsorption behaviour of foundry moulds and cores is the moisture diffusion coefficient [33]. Such coefficient, typically obtained from laboratory tests, is needed in order to predict more precisely how the moisture distribution in a mould changes when conditions in the surrounding environment are varying. For example, foundry cores and moulds are exposed to a varying environment for different time after drying in a drying cabinet at low relative humidity and high temperature (Figure 1.10).

In the drying industry moisture diffusion coefficients are used to design driers used mainly in food and wood industry [33]. Coefficients are determined with different methods in different industries [33-39]. Literature shows that the moisture diffusion coefficients can be affected by many factors (like temperature and moisture) [33] and also by methods used to obtain and analyse the data [34]. Data for moisture diffusivity coefficients is available for general classes of materials (like wood, milk, paper, sand, etc…) [33] but not for materials used in the foundry industry like furan sands and water based coatings. There is therefore no standard foundry methodology to predict moisture diffusion coefficients in foundry materials.

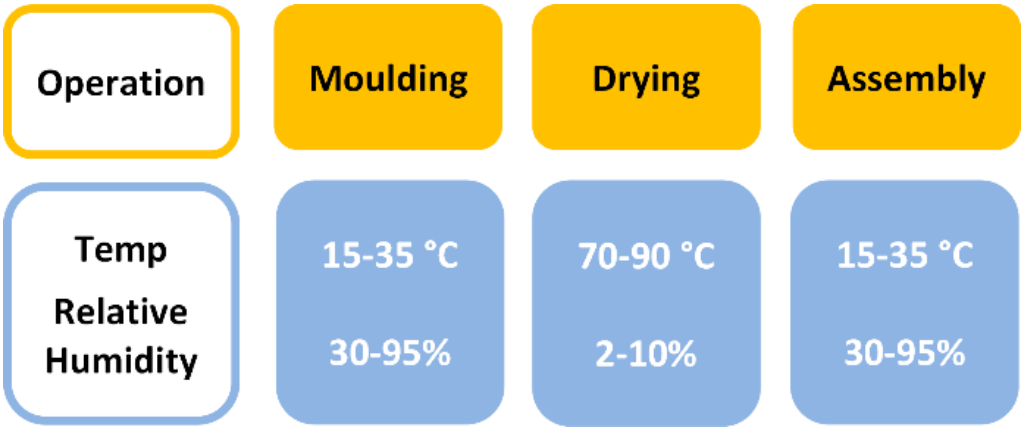

Figure 1.10 Production process steps for a furan sand mould coated with water based coating and correspondent ranges of environment conditions.

1.2.6 - Moisture Measurement Methods

For large foundry moulds there is a need to find a suitable, easy to use indirect measuring methods for assessing the residual moisture content since direct gravimetric methods would be unpractical and non-capable of detecting the small weight variations caused by moisture.

In the drying industry, moisture in material can be measured indirectly by measuring changes in electrical properties [33-35]. There are several factors that can affect the measurement accuracy (such as transducer design, leakage currents, electrode shape, material moisture uniformity, etc. [36]) and the correlation between the considered electrical property of the material and moisture is different from one material to another.

A tool providing a measure of coating moisture on a relative scale is used by Schultze [9]. But there are no commercial moisture measuring tools that are specifically calibrated for foundry coatings.

1.2.7 - Process Design and Simulation

Continuous pressure on the foundries for costs reduction makes necessary a special approach to the process design where tools are optimized and costs are minimized maintaining or improving the degree of quality of the casted items.

For the drying process there is a need to establish simple rules for hand calculations and preliminary dimensioning of the process, as well as more complex models that can be used for optimization of the processes.

CAE tools are needed in order to shorten the design time and lower final cost of the products therefore maximizing the revenues (Figure 1.11) [40,41] but are not always used to their full extent in foundry industry. In a similar way CFD simulations can be used as a tool to decrease the design time and lower the possible risk and costs related to the start- up of drying operations [41,42] but practical application in the foundry literature a lacking.

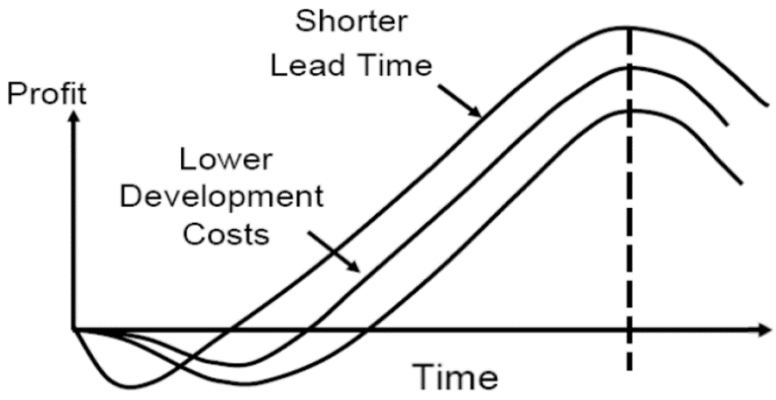

Figure 1.11 Effects of CAE tools on product lifecycle.

1.2.8 - Management of the Design Process

The way a design process and relative risks are managed heavily influences the outcome of the final products [43,44]. Possible problems generated in a design project are shown in Figure 1.12. Problems in first part of the list are typically cause by issues with the management process, while problems in the latter part of the list are more closely related with technology.

There is a needed to define design procedures and rules in order to be able to optimize design processes and therefore cost minimize risk and costs of final products.

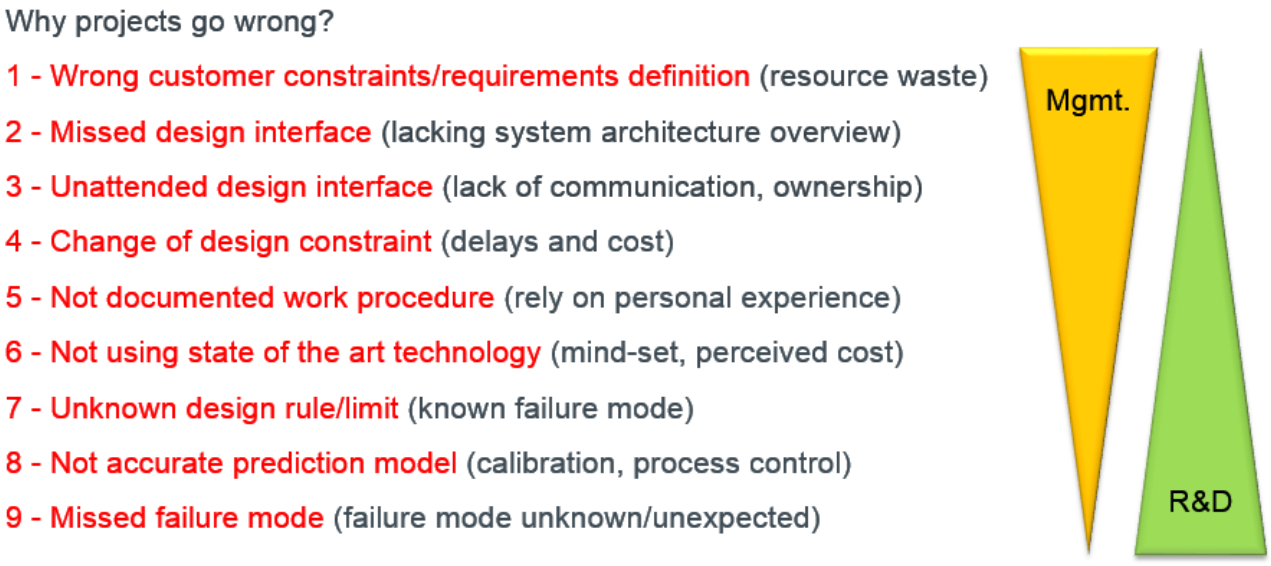

Figure 1.12 Possible problems generated in a design project. The first part of the list are typically caused by issues with the management process, while problems in the latter part of the list are closely related with technology.

1.3 - Main Objectives

In this section we summarize the main objective for the different areas investigated.

1.3.1 - Coating Properties

The first series of experiments focuses on determining how coating properties, such as viscosity and density, are affected by temperature and water content, as well as to compare different methods for assessing such properties.

Therefore the main objectives of this first test campaign are:

- To determine in which measure different variables affect coating properties like viscosity and density
- Check the sensibility and accuracy of different measuring methods for assessing coating properties
- Quantify how water content in the coating is affected by coating density
- Suggest which variables should be controlled in production
- Eliminate non influent variables from next experimental campaign in order to reduce experimental effort

1.3.2 - Coating Layer Properties

The second series of experiments has the objective to determine how coating layer thickness properties are affected by variable that can be varied in Global Castings factories.

As a consequence the main objectives of this second set of experiments are:

- To determine if and how different parameters known from literature and industry are affecting coating layer properties
- To suggest control strategies for the influent parameters in order to achieve repeatable coating and drying processes
- Identify possible non-linear effects and variations in process stability
- Investigate the relation between variables easily measured in production and coating layer properties.

1.3.3 - Evaporation Rates and Drying Time

Once coating layer properties are known evaporation rates are needed in order to be able to compute drying time.

The objective of this section is to test and model the evaporation rates for water based foundry coating used at Global Castings. In particular we aim at:

- Building an experimental setup to be able accurately control drying conditions and measure evaporation rates for furan bonded sand samples coated with water based foundry coating
- Run experiments to identify the effect of different factors such as coating layer properties and air conditions
- Obtain equations and design map for evaporation rates and characteristic curves to be used in process design
- Suggest possible variables that should be monitored and controlled in production

1.3.4 - Residual Moisture Levels

In this section there are mainly two objectives: fist to identify the effects of different variables on residual moisture levels of furan sand moulds and water based foundry coatings, the next is to test the capabilities a new test methodology (vapour sorption analysis) that is normally not used in foundry business. In particular we want to:

- identify how the moisture content in foundry coating and in sands bonded with different brands of furan binders are affected by relative humidity, temperature and dust levels
- to understand which parameters have the highest effect on moisture levels in the considered material and therefore on the generation of water vapour and the risk of gas defects
- to create a set of data that can be used for the design and control of driers of furan moulds and foundry coatings
- to support foundry engineers making the right choices when optimizing the production and drying process of coated furan sand moulds.
- to provide a new methodology for testing foundry coatings and binding systems based on technology already used in other industries

1.3.5 - Moisture Diffusion

Tests in this section are aimed at determining moisture diffusion coefficients in furan sands and water based foundry coatings. The main objectives are to:

- Obtain moisture diffusion coefficients and determine the effect of different factors on the moisture diffusion of furan bonded sands and of water based coatings.
- Compare two possible test methods and verify repeatability of results and identify advantages and disadvantage of the two methods
- Show how it is possible to use these coefficients for the estimation of moisture in a foundry mould

1.3.6 - Moisture Measurement Methods

The test campaigns in this section are aimed at the comparison of different moisture tools and the calibration of the tools for specific water based foundry coating used at Global Castings. In particular we want to:

- Compare the performance of a self-developed resistance based moisture measuring device versus two commercial tools calibrated for concrete and wood.
- Compare the stability of the output for different wire types and cable length needed for use in large foundry moulds
- Ultimately determine how the setup can provide the most accurate results in a factory installation
- Calibrate of the self-developed tool by comparing gravimetric moisture measurements with resistance measurements

1.3.7 - Process Design and Simulation

With regard to process design and simulation we want to provide an overview of tools for the preliminary dimensioning of drying processes as well as for the optimization. In particular we want to:

- Provide simple hand calculation procedures for preliminary estimations
- Provide more accurate equations to be used in numerical solvers for the optimization of drying processes
- Use CFD simulations to reduce the risk and costs involved in the drying of large foundry moulds for wind turbines applications

1.3.8 - Management of the Design Process

In this section we present a case where a novel approach to the design of foundry tools is presented with the objective to simplify the workflow of the design and the optimization process of a foundry mould with the aid of CAE (Computer Aided Engineering) tools. In particular we want to:

- Show that the tooling process of a foundry can be optimized with tools coming from product development methodology
- These of state of the art CAE tools can help to reduce design time, increase the level of optimization of the tools and ultimately lower costs and increase revenues

1.3.9 - Thesis Outline

In Chapter 1 an introduction of the back ground and motivations as well as the state of the art summary are provided for the different research areas.

In Chapter 2 an overview of the methods used for the different experimental campaigns is presented as well as calculation and simulation methods for process simulation.

Chapter 3 presents the main results achieve for each area.

In Chapter 4 a discussion of the results with respect to original objectives of the project and practical implications is presented

Chapter 5 summarizes the main conclusions and future work.

References are provided in Chapter 6.

In Appendix A the published papers (supplements) originated form the different work packages are documented.

In Appendix B experimental equipment main specifications are described.

In this thesis we provide an overview and only the most relevant information for each areas and chapter. Full detail, in particular about methods and results, for each area investigated can be found in the different supplements as described in Table 1.1

Table 1.1 Overview of the areas investigated and supplements where full detailed can be found.

Investigation phase	Investigated Area	Related Supplement
1	Coating Properties	I
2	Coating Layer Properties	I,II
3	Evaporation Rates and Drying time	III
4	Residual Moisture Levels	IV,V
5	Moisture Diffusion	VI
6	Moisture Measurement	VII
7	Drying Process Design and Simulation	VIII,IX
8	Management of the Design Process	X

2. Methods

2.1 - Background and Overview

In order to characterize and optimize the drying process our approach (Figure **2.**1) is to start with experiments at laboratory scale with the aim to test different properties and provide preliminary tools of assessment with low cost and risk. Hand calculations are then performed to support the initial choice of process parameters levels, for example in order to estimate the drying time. Advanced CFD simulations are used when there is a need to optimize the process for a given geometry or when direct solution of equations is not possible in a simple way. Finally, full scale tests are used for final verification and adjustments.

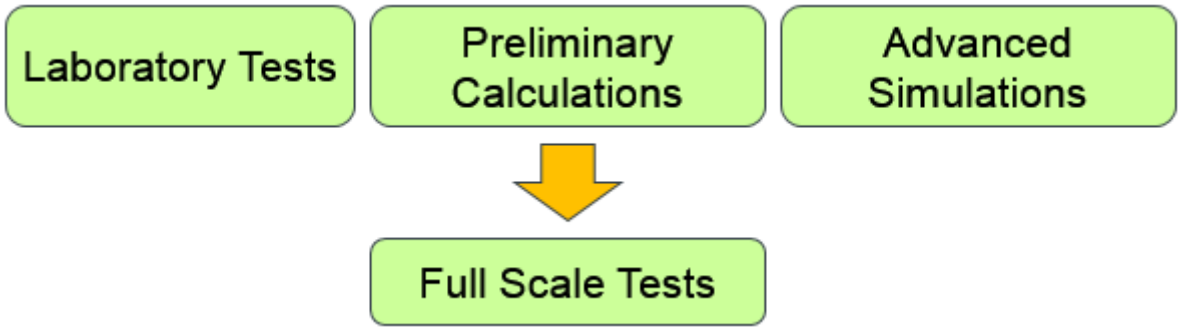

Figure 2.1 Approach to the characterization and optimization of drying process used in this work.

Figure **2.**2 provides an overview of the test and modelling phases that constitute main part of this work. In each phase the main variables investigated are also shown.

In the next sections we describe the most important features and aspects of different methods used in the difference phases. Detailed description of the methods and design of experiments can be found in the different supplements according to Table 1.1 and in Appendix B.

What is important to point out is that the levels used for the test variables are the typical high and low values allowed in production. Full and fractional factorial planes are used and addition of center points was done to investigate nonlinear behavior.

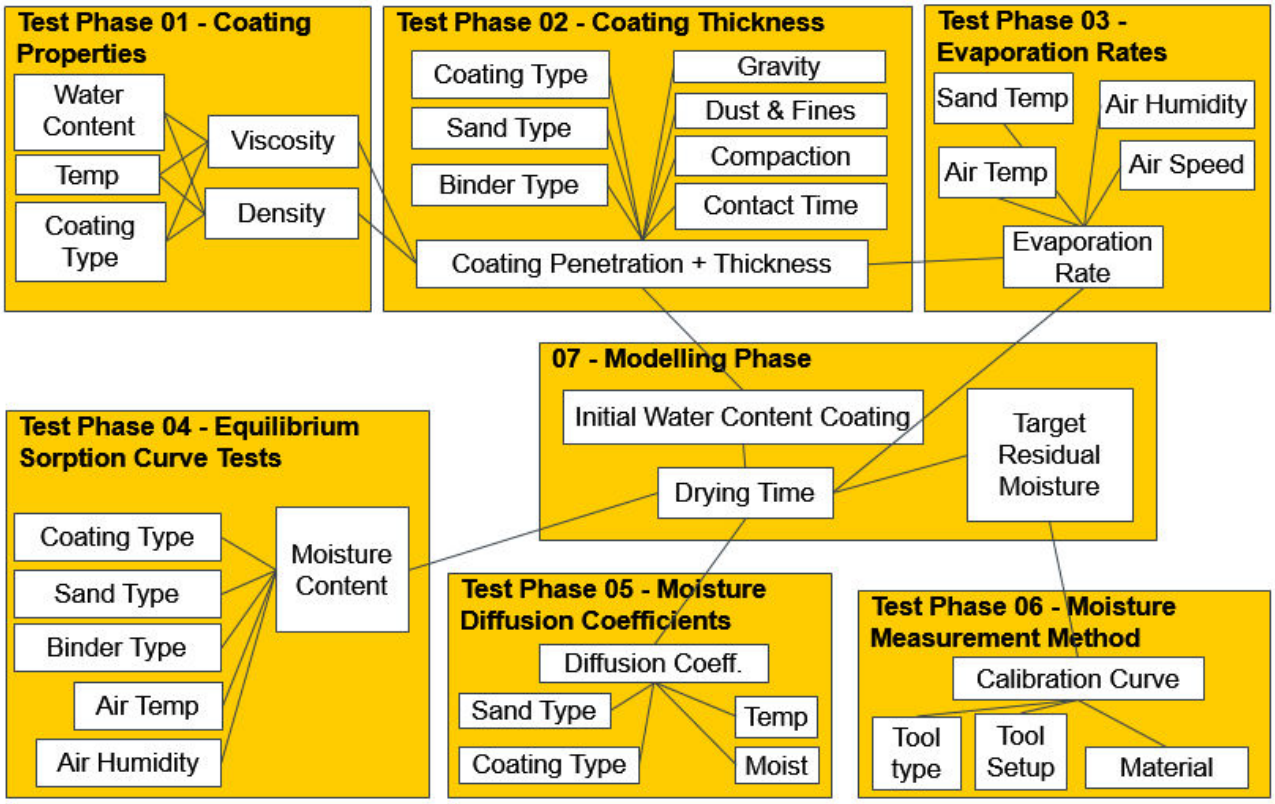

Figure 2.2 Overview of properties affecting coating penetration and thickness.

2.2 - Coating Properties Tests

The first series of experiments has the objective to determine how coating properties such as viscosity and density are affected by temperature and water content as well as to compare different methods for assessing such properties. A review of the possible methods for assessing coating properties is presented by Nwaogu [4] and Tracton[8]. Additionally, we chose to compare standard methods used in production, such as flow cup (equipped with a self-developed time measurement system) and Baume stick, against a laboratory rotational viscometer.

2.2.1 - Cup Time Measurement

In this study, in an attempt to improve the accuracy of this measurement, an experimental setup has been designed to reduce the time measurement error (Figure **2.**3). A sliding pin labelled “B” in figure C has been inserted in the flow cup “A” with an extension wire for its extraction. The weight of the cup is recorded via a load cell connected to a PC where the data is stored for subsequent processing.

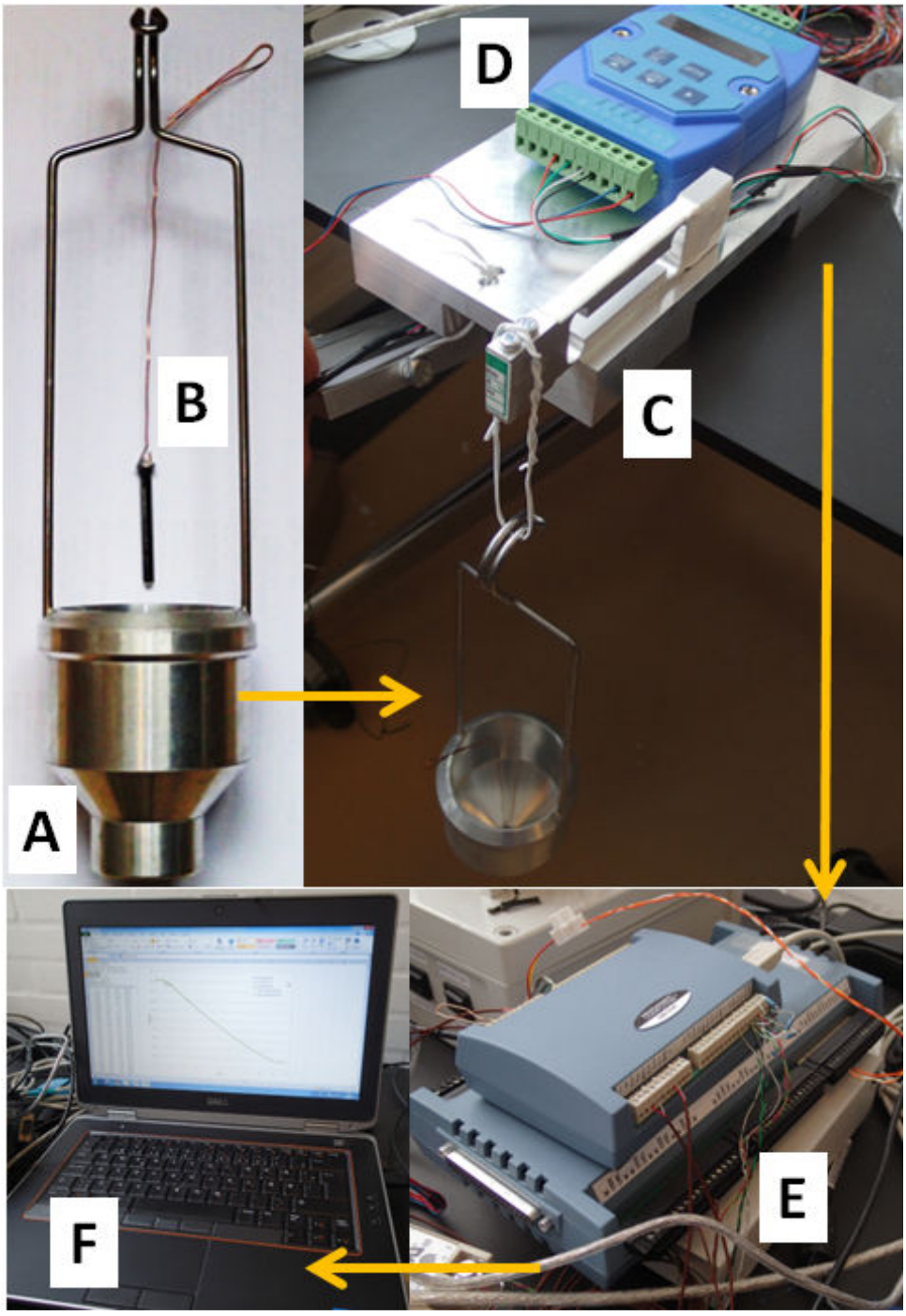

Figure 2.3 Experimental setup for cup time measurement: a) 4mm flow cup, b) sliding pin, c) load cell, d) signal conditioner, e) acquisition card, f) computer.

In order to minimize measurement system errors, the load cell has an accuracy of +/- 0.12 grams and a full scale of 600 grams (while total weight of the cup and coating are below 500 g), and the data acquisition systems uses a sampling frequency of 100 Hz (cup times measured should be between 10 and 20 seconds).

After the acquisition, we plot the weight of the cup versus time and extract the cup time measurement from the curve (Figure **2.**4).

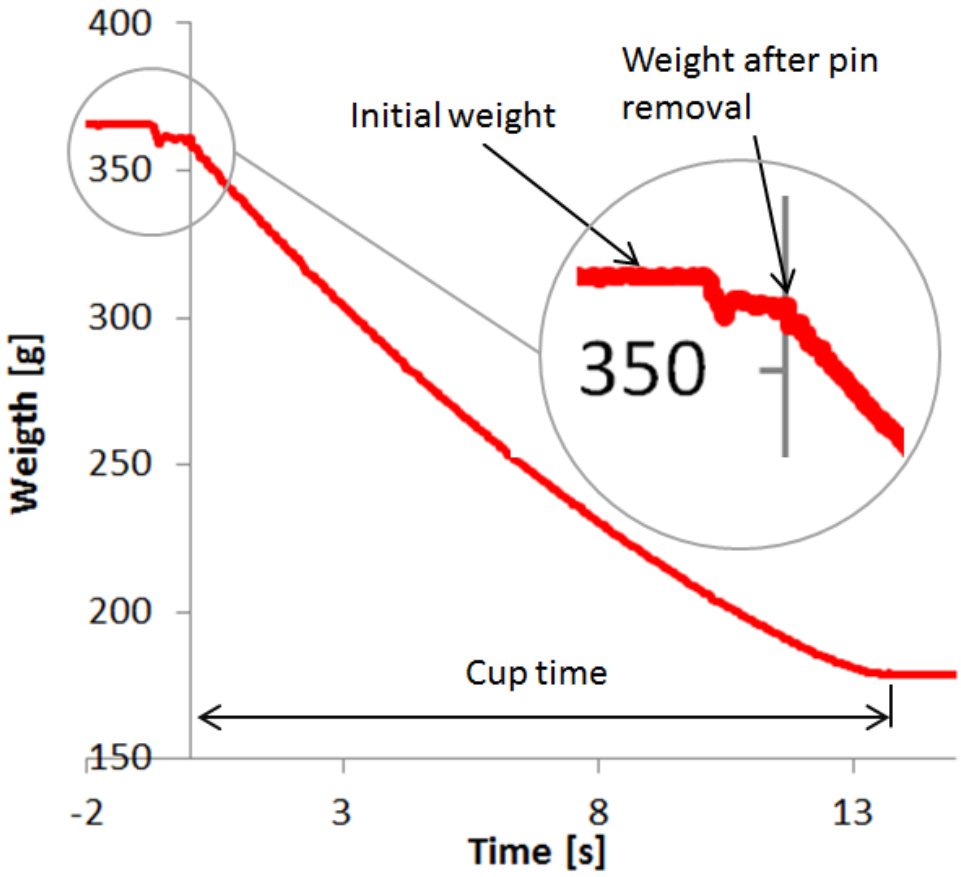

Figure 2.4 Cup time measurement from acquired data.

2.2.2 - Baumé Measurement

The Baumé measurements are taken as typically done in the industry. The coating is mixed thoroughly and allowed to settle for one minute. Then the Baumé stick is immersed in the coating, when there is no more movement, the reading is taken (Figure **2.**5). The resolution of the Baumé stick used is 2°Bé, so it is not expected that this method will reveal small variations in density of the coating.

Figure 2.5 Baume measurement setup.

2.2.3 - Viscosity Measurement

Viscosity is typically not measured directly in production, but it is known to be a critical parameter in coating performance [4,8]. Typically for paints the viscosity should increase when shear rate decreases. In this way dripping of coating can be reduced after application.

In this study, we use an Elcometer 2300 RV rotational viscometer with a L3 spindle type (Figure **2.**6). With this setup it is possible to measure viscosity with a resolution of 10mPas at any given rpm (rotation per minute). The maximum viscosity measurable is 400.000mPas at 0.3 RPM and 600mPas at 200 RPM. The accuracy of the measurement is +/-1% of the maximum viscosity measurable at a

given RPM, in particular the accuracy is 6 mPas at 30 RMP and 40 mPas 200 RMP (see plots in the results section).

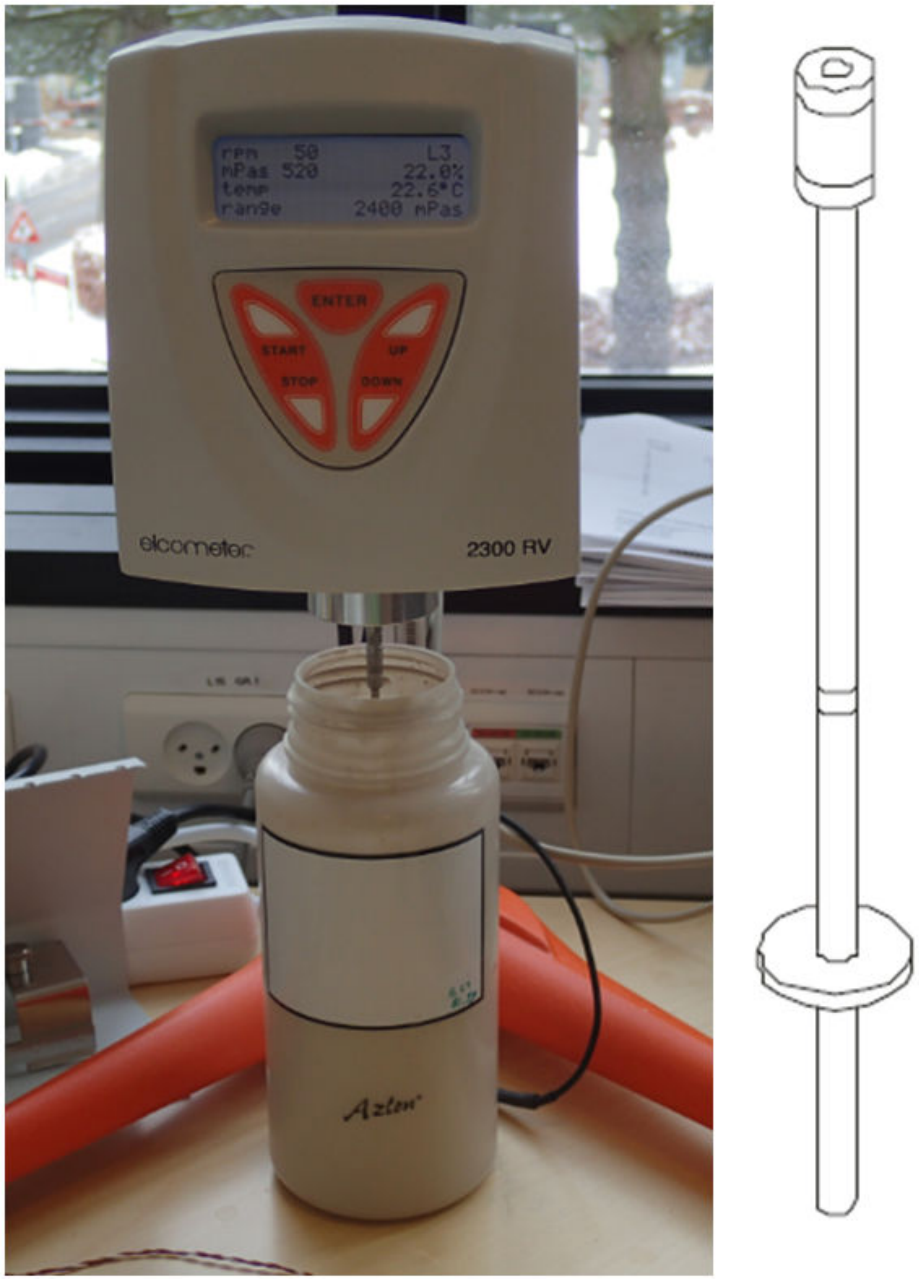

Figure 2.6 Experimental setup for viscosity measurement.

2.2.4 - Water Content Measurement

Coating water content is normally not measured in production. This property directly affects drying time, so it is important to understand how it varies with coating density.

For these tests, a MJ33 moisture analyser from Mettler Toledo is used (Figure **2.**7). The measurement technique allows to reach accuracies of 0.05 %.

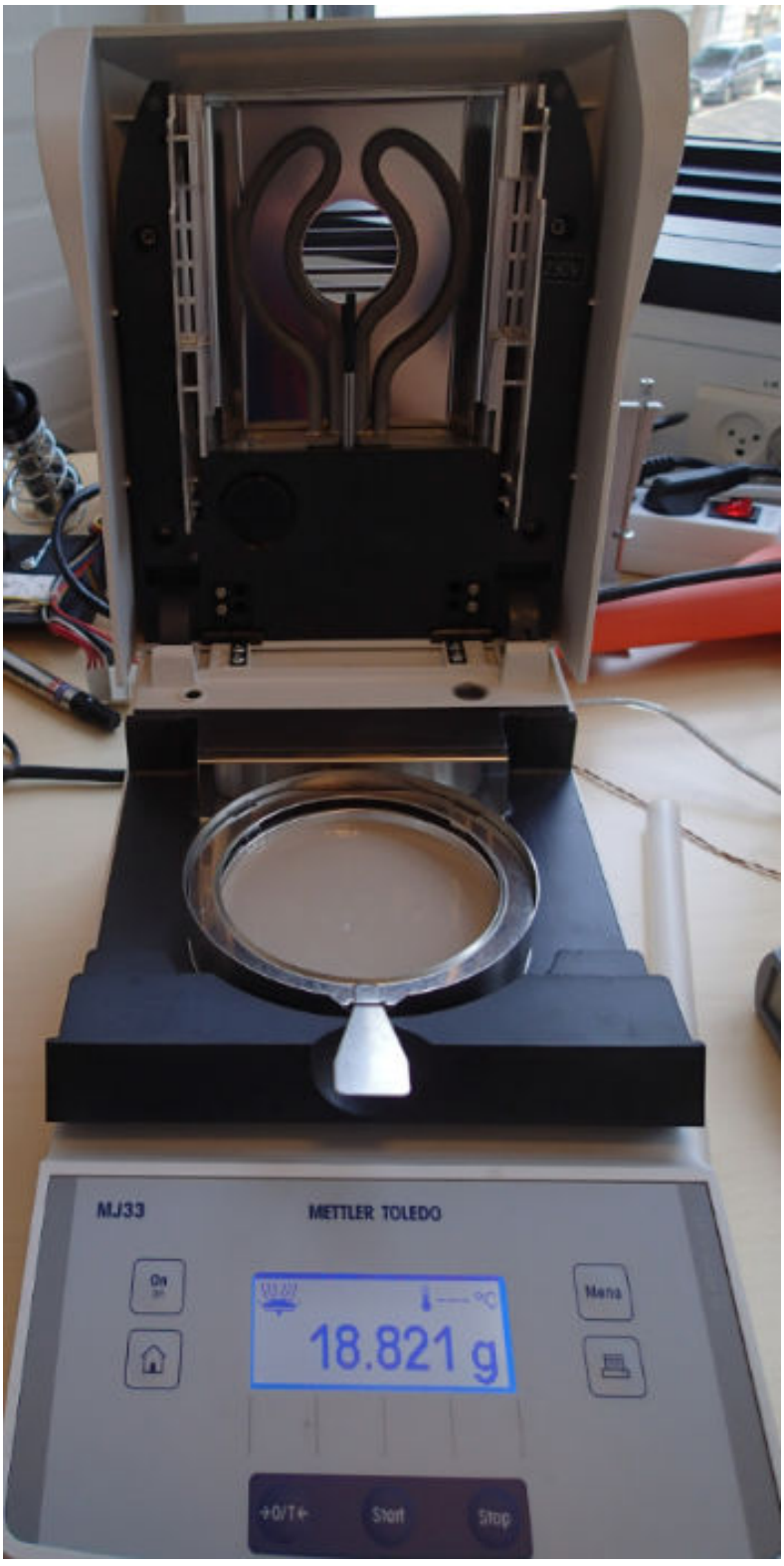

Figure 2.7 Experimental setup for coating water content measurement.

2.3 - Coating Layer Properties Tests

2.3.1 - Design of Experiments

The second series of experiments has the objective to determine how coating layer properties are affected by process variables. In particular process variables considered are: coating density, binder system type, gravity, dust levels, compaction and dipping time.

Specific coating layer properties are defined for this study and calculated from weight variations of the test samples or also measured from pictures taken with a stereomicroscope. The response variables considered for this study are:

- **Wet Coating Thickness (WCT)** [kg/m^2] represents the quantity of material (solids + water) added to the coated surface
- **Dry Coating Thickness (DCT)** [kg/m^2] shows how much solid material has been added to the surface and it is therefore a better indication of the final dry coating layer properties. Also cost of coating consumption is dependent on this quantity.
- **Wet Coating Water Content/Thickness (WT)** [kg/m^2] is quantity of water per square meter of coated area. Heavily influences drying time and the energy required for the drying process.
- **Coating Water Fraction** (**CWF**) [%] represents the fraction of water in the coating absorbed by the sample. This property is useful to understand, by comparison with the original water content of the coating, if there is any adsorption of water from the coating to the sand sample.
- **Penetration depth** [mm] is a measure of how deep the coating will penetrate into the coated surface and is measured from pictures taken with a stereo microscope. This property can affect drying time since the drying front requires more time to reach deeper into the mould.
- **Sand Density** [kg/m^3] is calculated from the measured volume and weight of the tested specimens to verify if compaction has an effect on this parameter and therefore if it is possible to use density measurements to assess compaction of sand moulds.

Calculation details for each property can be found in Supplement I.

Commercially available tools for measurement of coating thickness (like wheel and comb) have not been used for mainly two reasons: firstly because these tools cannot measure the coating

penetration into the sand, secondly because the samples would be damaged by removal of the coating and it would have not been possible to carry out more accurate gravimetric analyses.

High and low levels used for the variables in coating layer properties tests are shows in Table 2.1. Sand type and binder type are combined to reflect the two furan based recipes used in the factories.

Dust and fines levels are chosen to be the minimum possible level (0.00 % dust and 0.10% fines) and the maximum allowed level in the factories (0.2 % dust and 2 % fines).

Low compaction is achieved by filling the test specimens without vibration and no compaction load applied while it cures. High compaction is achieved by applying a weight of 1 kg on a sample of 18 mm diameter. This will generate, in the compacted specimen, a pressure of 38 kPa, representative of the pressure present at the bottom of a mould with a height of about 2.5-3 m (assuming hydrostatic pressure distribution and a sand density of about 1450 kg/m^3).

Coating density levels are chosen to be the upper and lower boundaries of the current specification (1790 kg/m^3 and 2042 kg/m^3).

The variable “Coating type” indicates two different batches of the same commercial coating supplied to two different factories (VCM and VCK).

Dipping times are chosen as 2 seconds (to represent a single quick pass during flow coating process) and 2 minutes (to represent the area where the coating is gathered, that are inevitably formed during the coating of a large mould).

Gravity effect represents the fact the coated surface might be facing upwards or downwards and gravity might speed up or slow down the penetration on the coating in the sand surface of the mould.

To estimate the non-linear effects and repeatability in the experiments centre points experiments were added out with the following conditions: medium compaction, coating density of 1908 kg/m3, dipping time of 5 seconds and sample facing down.

All tests are carried out at temperature between 22 and 25 C.

Table 2.1 High and low levels used for the varibales in coating layer properties tests.

Variable	Number of Levels	Level 1	Level 2
Sand Recipe	2	VCM HA 1%	VCK Dyn 1%
Dust & Fines	2	0.00%/0.10% Dust/Fines	0.20%/2.00% Dust/Fines
Compaction	2	High (1 kg weight)	Low (no weight)
Coating Density	2	1790	2042
Coating Type	2	VCM	VCK
Dipping Time	2	2	120
Gravity Effect	2	Sample facing up	Sample facing down

2.3.2 - Test Procedure

The first step in the sample preparation procedure is to sieve sand to remove the dust and to sieve filter dust to remove larger particles. Dust and fines are the added to the sieved sand as well as binder and catalyst to achieve the desired levels.

Cylindrical moulds of 18mm diam and 50mm depth are then filled with the sand batches and weights are applied to the mould where high level of compation is needed (Figure **2.**8).

Sand mould dimensions, used to calculate the volume, and weight are taken and recorded for each mould. Weight measurements for calculation of coating layer properties are carried out for the empty moulds, cured mould, freshly coated mould and the dry mould.

The coating of the mould is carried out either by immersion of the sample facing down in the coating or by placing on top of the sample a container that fits the moulds facing up and then pouring the coating in the container (Figure **2.**9).

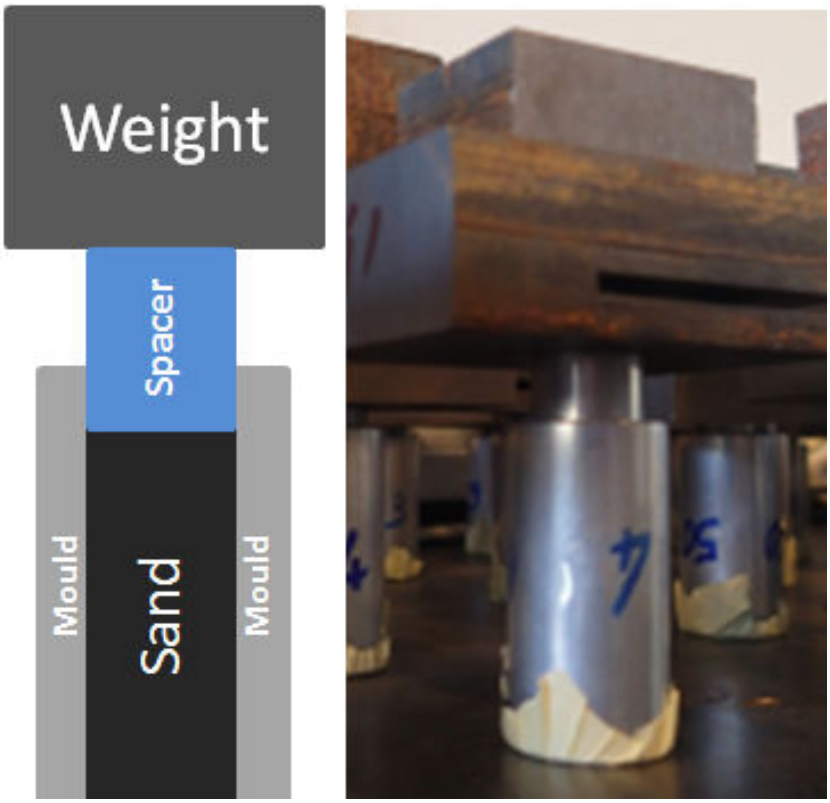

Figure 2.8 Moulding of high compaction sample with 1kg weight.

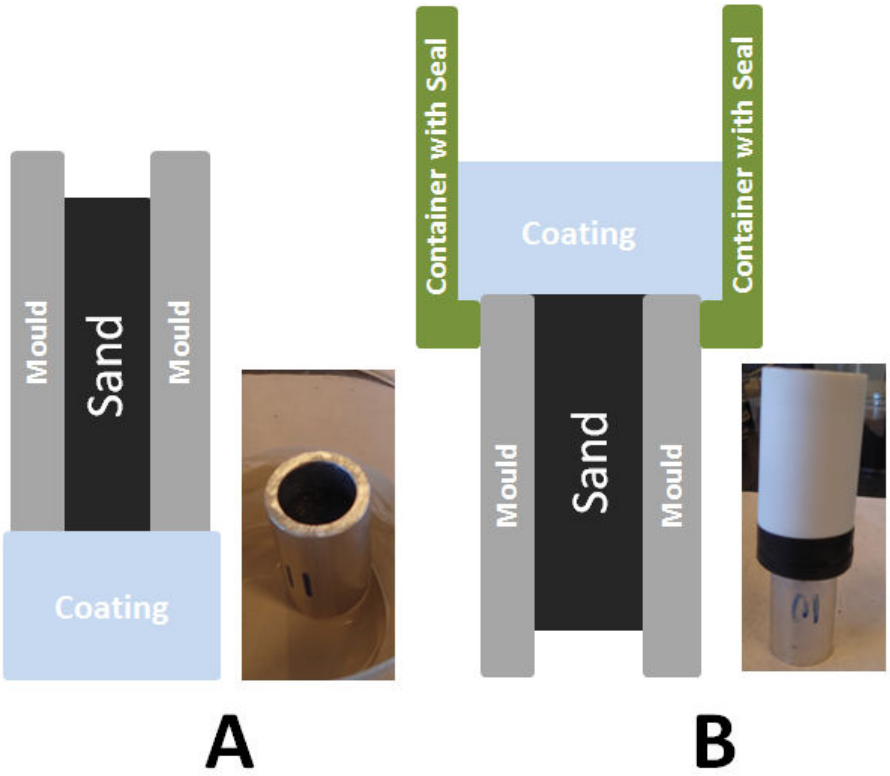

Figure 2.9 Coating with: a) coated face down and b) coated face upwards

After the final weight measurement, the samples are extracted from the mould and ground along the length to obtain a flat surface. Images of the sample section are then taken with a stereomicroscope with an 8X magnification factor and saved. Coating penetration depth measurements are then taken by analyzing each image in a photo editing software (Figure **2.**10Fig. 19).

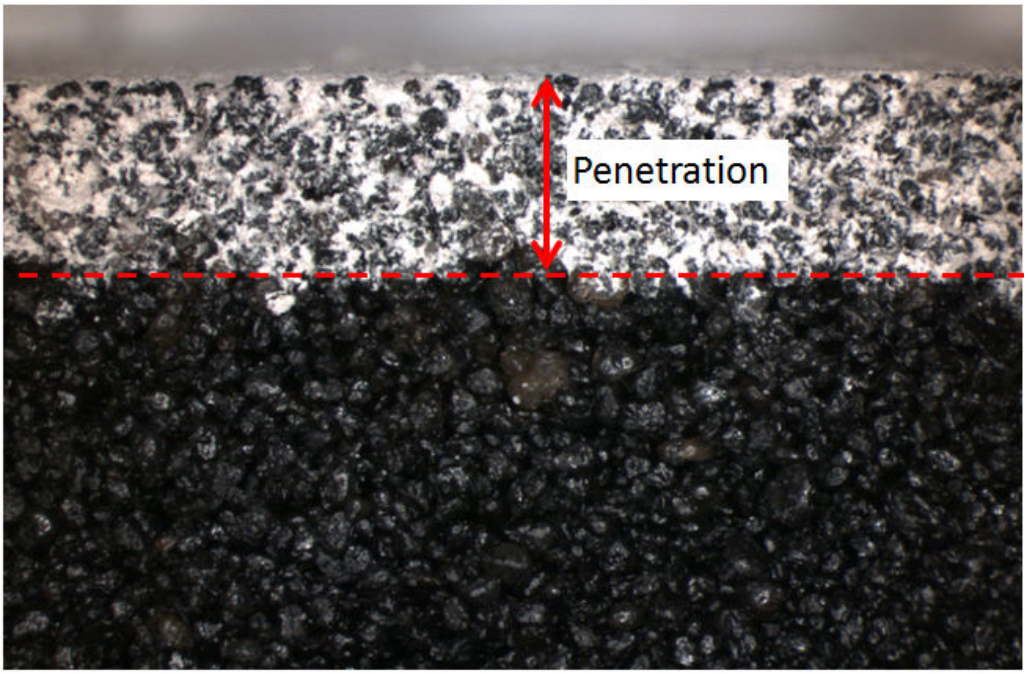

Figure 2.10 Coating penetration measurement.

2.4 - Evaporation Rates Tests

2.4.1 - Sample Preparation

Sand samples (Figure **2.**11) are prepared in a similar way as described in section 2.3.2. The main difference is that cylindrical moulds are now of 25 mm diameter (instead of 18) and that a special mould material (PVC-U) is chosen for its good resistance to acids and solvents, to minimize moisture adsorption and maximize thermal insulation on the sides of the specimen. This is done to minimize possible errors coming from weight variations of the mould.

After curing, each sample is coated right before the drying process is started. During drying the weight of the sample is recorded (drying setup described in section 2.4.2) and additionally the

weight of the sample is measured before coating, after coating and after drying on a precision laboratory scale with +/- 0.1 mg accuracy.

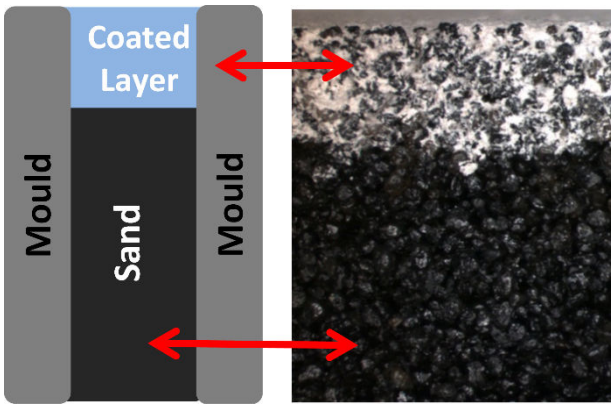

Figure 2.11 Coated furan sand mould used in the drying tests.

2.4.2 - Drying Setup

The drying operation is performed in a specially designed experimental setup (Figure **2.**12, Figure **2.**13 and Figure **2.**14). Air speed, humidity and temperature are measured as well as sample weight and surface temperature. All the data from the sensors are transferred from the acquisitions card to a computer. Then, a program developed in the data acquisition software DasyLab stores the data for subsequent analysis and provides real time feedback to control to the heaters, the humid air supply and dry air supply. In this way is possible to maintain the desired drying conditions within an accuracy of +/- 0.1 m/s for the air speed, +/- 2 °C for the temperature and +/- 3 % for the relative humidity (see appendix B for details on equipment accuracy). With regard to the measurement of surface temperature of the sample, a non-contact infrared sensor is used in order to avoid possible effects of contact on the weight measurement (see appendix B for details).

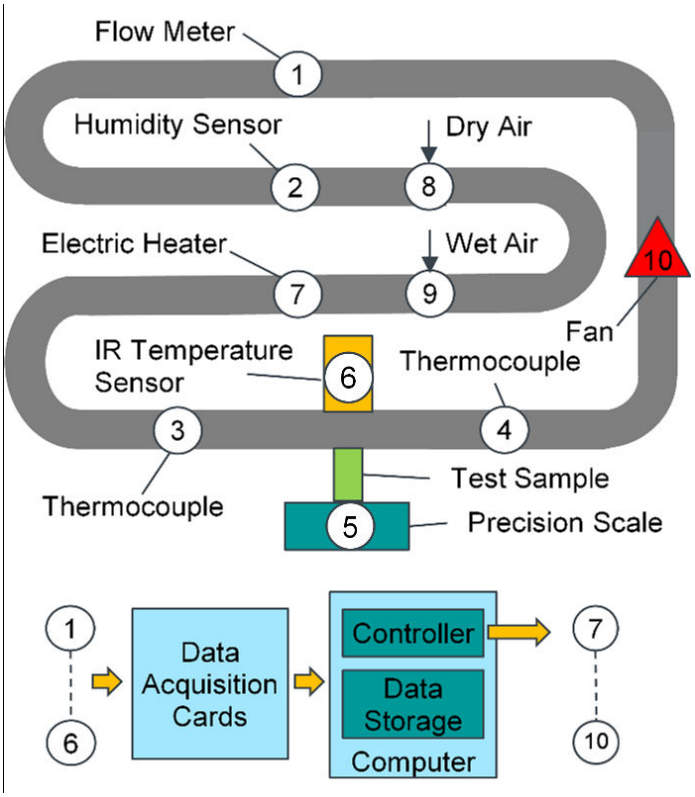

Figure 2.12 Experimental setup used for the drying tests.

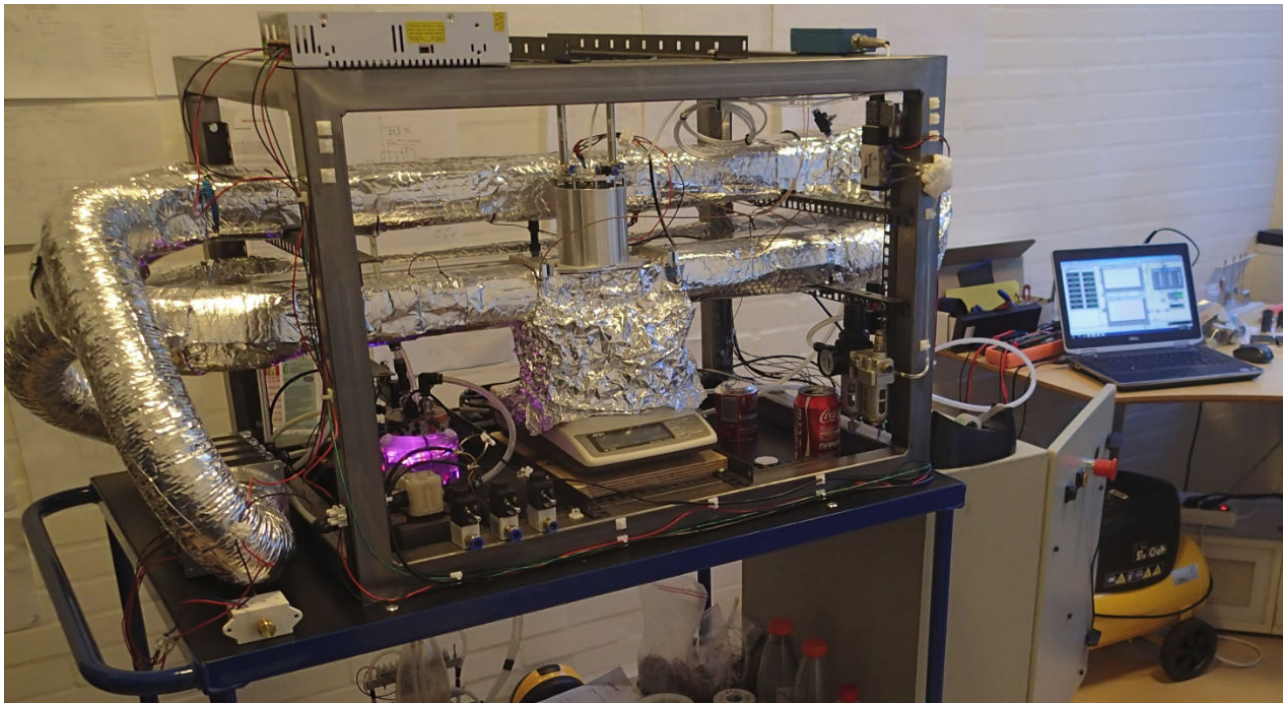

Figure 2.13 Picture of experimental setup for drying tests.

Figure 2.14 Picture of acquisition cards and power supplies for the experimental drying setup.

2.4.3 - Design of Experiments

Experiments are carried out to understand the effect of thickness, air speed and air properties on the drying behaviour.

2.4.3.1 - Experimental Plan - Thickness Effect

In order to determine the effect of the coating layer thickness on the drying behaviour, the coating parameters levels are chosen according to Table 2.2 in other to obtain coating layer thicknesses representative of the ones used in real production. The ranges (maximum and minimum levels) of the each parameter is chosen to be representative of the highest and lowest limits allowed by the factory specifications. More details about the levels used and sample preparation can be found in Supplement I and II. For each coating conditions 6 samples are produced for a total of 36 sample.

Air speed levels are chosen as 0.8 m/s, 1.5 m/s and 2.5 m/s (AS1, AS2 and AS3 Table 2.3). These values will provide, in the test duct used for the tests, similar values of heat transfer coefficients to

the ones achieved in the factory. In particular AS1 replicates the values normally achieved by natural convection, AS3 represents values obtained with forced convection and AS2 provides a centre point for the experimental plan.

With regard to drying air conditions, we choose the values of low relative humidity at 30 °C, 50 °C and 70 °C (levels AC1, AC4, AC7 in Table 2.4) normally achievable in production. The temperatures are chosen to represent drying conditions typically used in the factories considered. Low relative humidities are chosen for these tests to limit the drying time (especially for samples with high coating thickness) and to isolate the effect of thickness.

For each set of drying conditions (AC1-AS1, AC4-AS2 and AC7-AS3) two samples coated with the same coating conditions are dried. In this way an experimental plan of 3 (air conditions) x 6 (coating conditions) is replicated two times and provides a total of 36 runs.

Table 2.2 High and coating parameters levels used to achieve different coating layer thicknesses.

Coating Thickness Level	Sand Comp.	Coating Density [kg/m^3]	Gravity Effect	Dipping Time [s]
CT1	High	2042	Down	2
CT2	Med	1908	Down	5
CT3	Low	1790	Up	120
CT4	Low	1908	Up	120
CT5	Low	1908	Up	15
CT6	High	1790	Down	2

Table 2.3 High and air speed levels used in the drying tests.

Air Speed Levels	Air Speed [m/s]	Heat Exchange Coeff. [W/m^{2}K]
AS1	0,8	3,5-4
AS2	1,5	7,5-8
AS3	2,5	13-15

2.4.3.2 - Experimental Plan - Air Properties Effect

To determine the effects of different air conditions we now choose only one coating level (CT2 in Table 1) that is the centre point of the specification values used in the factory and therefore represent what the target coating thickness should be.

A total of 9 air conditions levels are used (Table 2.4) that are representative of drying conditions normally achievable in foundry environment and drying cabinets. As shown in Figure **2.**15 we can see that relative humidity conditions are normally limited by low limits that are determined by the typical minimum air humidity present in the ambient air (assuming 100% of fresh air is supplied to the drying cabinet) and by the maximum limit where the risk of condensation during drying becomes high due to the increased dew point (this can happen especially when air is recirculated in the drying cabinet to reduce energy losses).
Each of the air drying conditions is tested at the three air speed levels described in Table 2 for a total of 27 runs.

Table 2.4 Air temperature and humidity levels used in the drying tests.

Air Conditions Levels	Temperature [C]	Dew Point [C]	Relative Humidity [%]
AC1	30	4	20
AC2	30	18	50
AC3	30	26	80
AC4	50	10	10
AC5	50	25	25
AC6	50	32	40
AC7	70	10	5
AC8	70	25	10
AC9	70	40	23

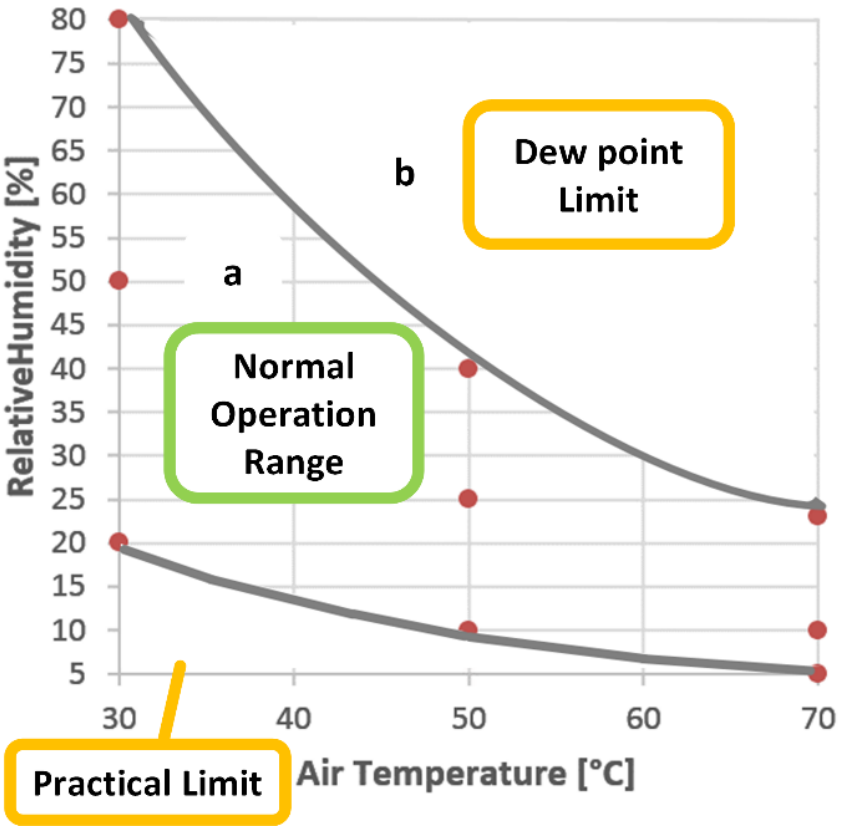

Figure 2.15 Design space limits for air temperature and humidity.

2.4.3.3 - Drying Properties Definitions

In order to understand how water is removed from the sample coating thickness properties such as water thickness and moisture described in Section 2.3.1 are calculated from the logged weight curve (Figure **2.**16).

Drying relevant properties are then calculated (detailed calculation method is shown in Supplement III) such as:

- **Drying time t_{dry} [hours]** that is the time at which the samples reaches a moisture of 1% time (Figure 2.17a)
- **Average evaporation rate ER_{avg} [kg/m²/h]** representing the average amount water evaporated from the sample in the drying period and therefore useful to estimate drying time and evaporation energy required for drying
- I**nstant evaporation rate ER [kg/m²/h]** representing the amount of water evaporating from the sample at each instant during the drying and obtained by deriving the weight with

respect to time. This parameter is useful to calculate instant amount of power required for the evaporation time (Figure 2.17b)

- The **maximum evaporation rate ER_{max} [kg/m²/h]** useful to calculate the maximum amount of power required for evaporation time (Figure 2.17c)

From the sample surface temperature plot as a function of time (Figure 2.17c), we can define:

- **t_1** as the time at which the surface water of the sample evaporates at a constant temperature (initial plateau of the curve)
- **t_2** the time at which the surface temperature of the sample reached the second higher plateau but more moisture can be present in lower layers.
- **(t_1/t_{dry})** fraction of drying time where water evaporated is coming from the surface
- **$((t_{dry}-t_2)/t_{dry})$** fraction of drying time where water evaporated is coming from the layers below the surface

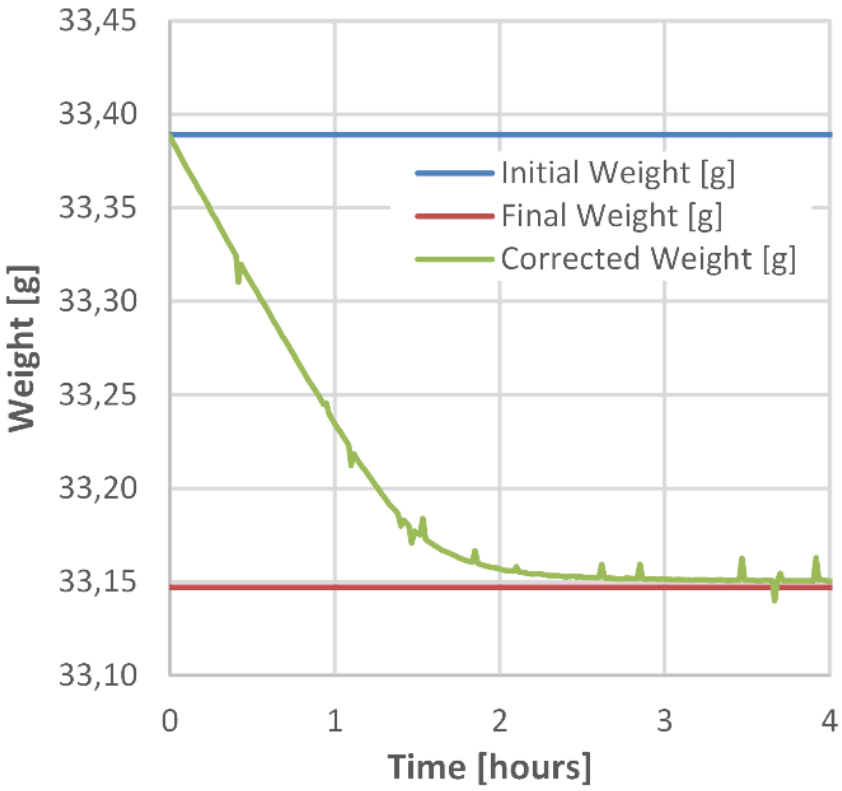

Figure 2.16 Coated sample weight variation during drying.

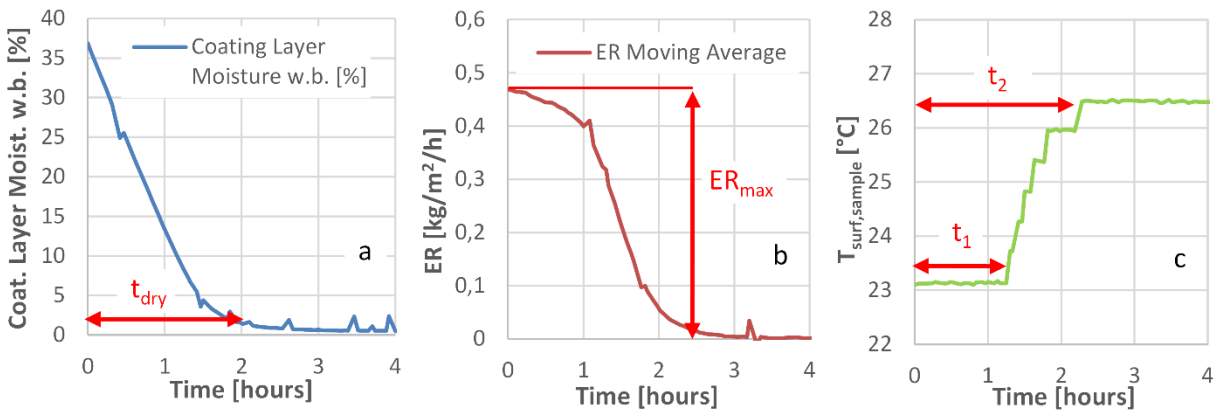

Figure 2.17 Drying parameters used in this study: a) drying time, b) maximum evaporation rate and c) surface temperature transition times.

Characteristic curves are used to describe the evaporation rate as a function of the coating moisture. These curve can help to understand changes in material behaviour that are needed when designing a dryer. In order to obtain these curves, we plot the ratio between the evaporation rate and the maximum evaporation rate (ER/ER_{max}) versus the coating layer moisture divided by the initial moisture (Figure 2.18).

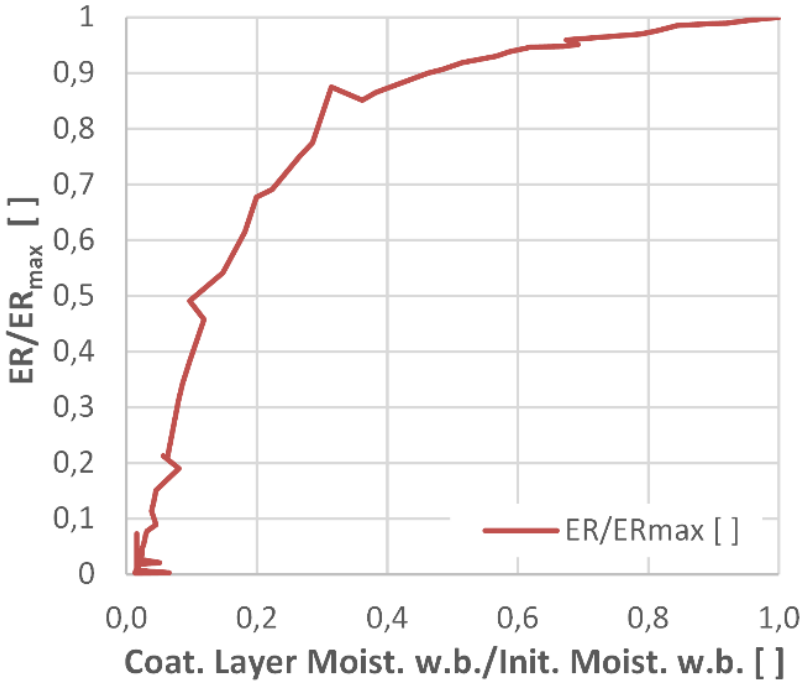

Figure 2.18 Example of characteristic drying curve of furan sand sample coated with water based foundry coating.

2.5 Residual Moisture Tests

2.5.1 - Automatic Vapour Sorption Analysis

In order to obtain the equlibrium moisture values for furan sands and coating Atomatic Vapour Sorption Analysis tecnique sample granular samples must be prepared.

For the bonded sand, the sample preparation starts by mixing sand, binder and catalyst, followed by curing for one week at 23-25 °C and 45-50% RH and finally manual crushing (Figure 2.19a) (for easier handling during tests). Binder addition was 1% of sand weight and catalyst addition was 40% of binder weight as per factory specification.

The coating samples were obtained by drying the liquid coating (typically containing an initial moisture of 30-40% on wet basis) at same conditions and time used for the sand samples and then manually crushing the dry coating into powder (Figure 2.19b). Pure dust and un-bonded sand were taken directly from filter bags and silos in the factory and then let equilibrate at the same temperature and humidity conditions as described for the other samples.

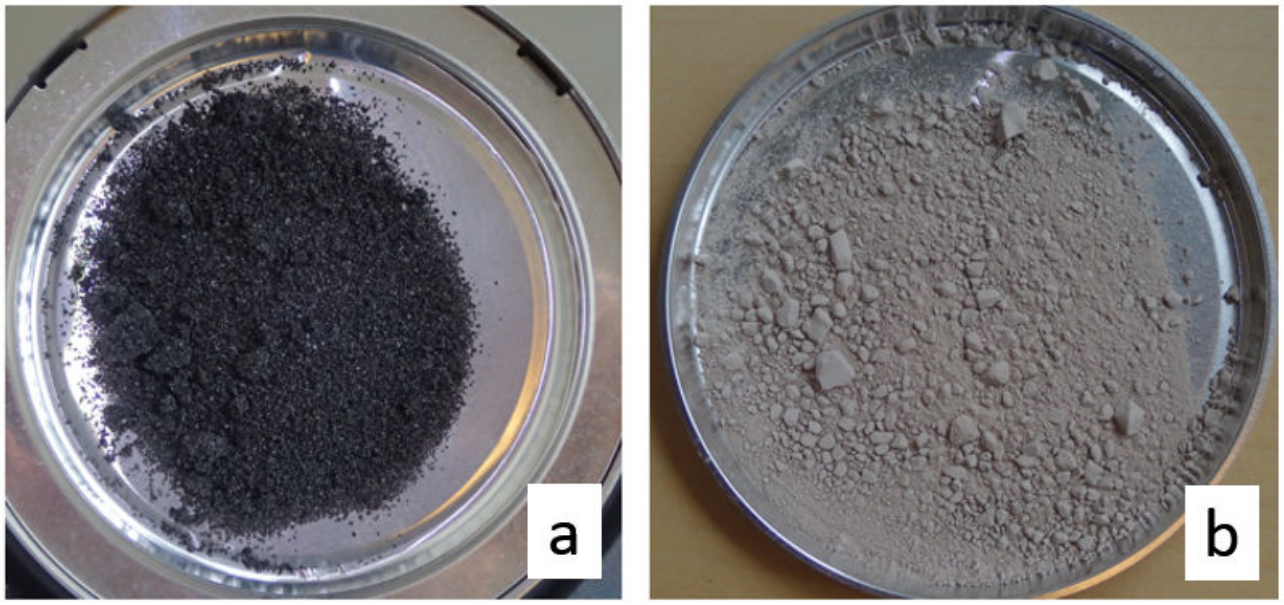

Figure 2.19 Materials preparation: a) crushed sand and b) crushed coating.

After sample preparation and equlibration at 23-25 °C and 45-50% RH for a week, a sample of each type was tested in an automatic moisture analyzer with an accuracy of 0.05% on measured moisture value. The automatic moisture analyzer was set to dry the sample at a temperature of 105 °C. The

wet basis moisture values are used as input in the automatic vapor sorption analyser to compute the sample moisture values during the sorption tests since it is not possible for the automatic moisture analyzer to dry the samples at 105 °C (see Supplement IV and V for detailed procedure and and equaitons).

The automatic vapor sorption analyser used for this study (Figure 2.20) is equipped with a precision scale with +/- 0.1 mg accuracy, a dew point sensor with 0.5 % RH accuracy and infrared sensor for temperature control. The moisture level can be controlled by supplying either wet air or dry air.

The sorption/desorption tests were carried out by loading a sample of about 10-12g in the automatic sorption analyzer and inputting the initial moisture of the sample at 23-25 °C and 45-50% RH (Fig.3.b) from the previous tests. After sealing the cover, the machine starts recording weight variation and changing temperature and relative humidity according to the test plan.

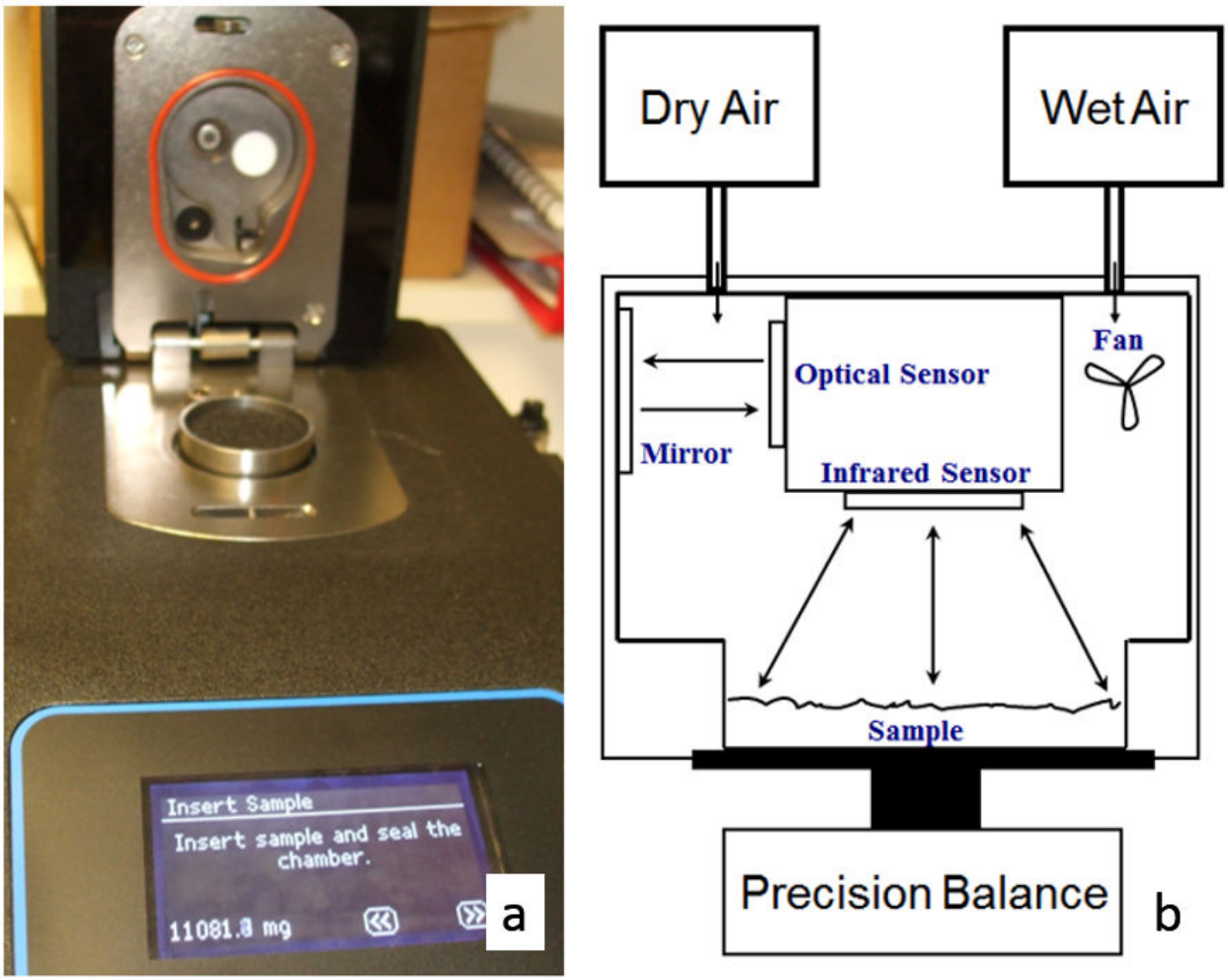

Figure 2.20 Test Setup: a) initial moisture level measurement, b) automatic vapour sorption analyser and c) schematic.

In order to obtain the sorption/desorption curves, the temperature is held constant at the selected test temperature while the air humidity is changed stepwise in 5% increments. The current moisture content of the sample is calculated based on the weight variation and recorded (see Supplement IV and V for equations). If the variation in moisture is less then 0.02% in one hour, the sample is considered equilibrated and the air humidity can be changed to the value required by the next step (Figure 2.21).

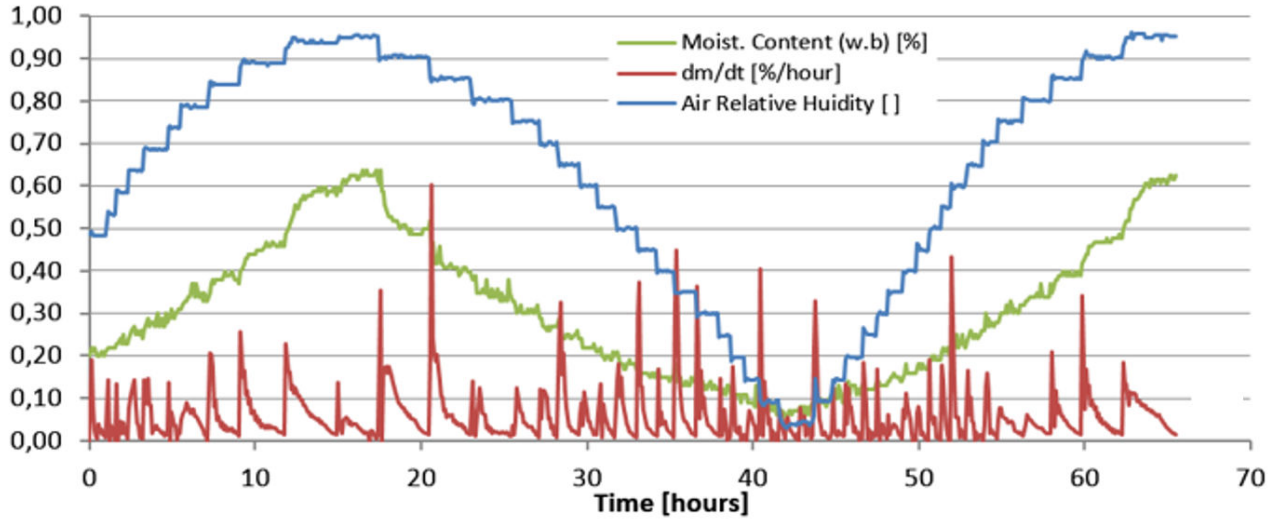

Figure 2.21 Example of sorption tests data.

Each test begins at 50% RH and the air humidity is incresed stepwise up to 95% to initialise the sample (Fig.4b), then the desorption phase starts (humidity is decresed step-wise to 5% RH) and finally the adsorption phase is carried out (humidity is increased stepwise to 95% RH). In order to obtain the final sorption curve, the moisture level of each equilibrium point is plotted versus the air humidity as in **Figure 2.**22. Sorption curves are plotted in the results section without the initialization steps.

Finally, 3rd degree polynomial equations are fitted to the experimentally obtained sorption and desorption curves, the curves coefficients are reported in Supplement V.

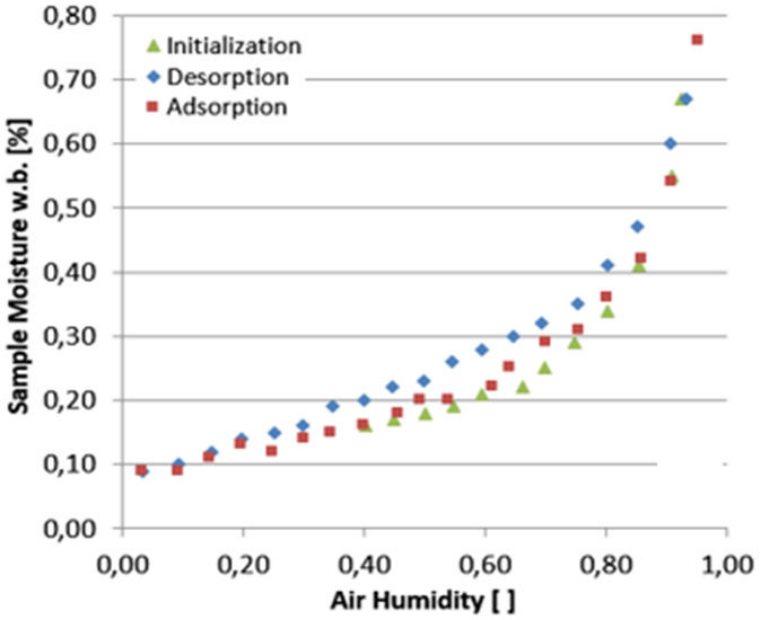

Figure 2.22 Example of equilibrated points (initialization, desorption and sorption curve).

2.5.2 - Experimental Plan

To investigate the effect of different variables, the experimental plan described in Table 2.5 was designed. First, the effect of temperature on the two main classes of material is studied (coating and GCX F sand). Then the effect of dust levels are investigated (no dust and 2% dust) and different binder system brands (GCX S, GCM and GCGG). Finally pure dust and un-bonded sand were tested to provide baselines for comparison.

Table 2.5 Overview of experimental for residual moisture tests.

Material	Temperature [°C]		
	15	25	35
Coating	X	X	X
GCX F	X	X	X
GCK No Dust		X	
GCK 2% Dust		X	
GCX S		X	
GCM		X	
GCGG		X	
Pure Dust		X	
Un-bonded Sand		X	

The temperature levels were chosen as the minimum (15°C), typical (25°C) and maximum (35°C) temperature allowed in the produciton facilities. Similarly, dust levels representing the maximum allowed (2%) and the minimum possibly achievable levels. The binder brands are the same as used in the considered production facilities.

2.6 - Moisture Diffusion Tests

Two different methods were used to run moisture adsorption tests. A manual method, in which a simple (but slow), low cost equipment is used and an automatic test methodology (Automatic Vapour Sorption Analysis described in section 2.5.1) where more costly (but faster) equipment is used. In this way, it is possible not only to determine the diffusion coefficient, but also to compare the results from the two methods and give recommendations to the foundry industry on which test methods to use to estimate moisture diffusion coefficients.

2.6.1 - Manual Test Method

In the manual tests method furan sand samples are moulded in a cylindrical mould of 18 mm diameter and 50 mm depth in the same way described in Section 2.3.2. In order to represent the possible ranges of density of a real production mould, some moulds are left un-compacted, while on the others a 1 kg weight (equivalent to the pressure of sand for a 2.5 m high mould) is added right after filling. In this way, it will be possible to achieve different sand density of the samples and to determine the possible effect on the moisture diffusion coefficients.

Samples are cured for 48 hours at room conditions (23-25 °C and 35-45% RH), followed by a period of equilibration of 48 hours where samples are placed in a sealed container where silica gel is used to keep air relative humidity at 5-7% (Figure 2.23). In this way, we equilibrate the moisture of the sample to replicate the situation of a mould which has been through a drying step.

Figure 2.23 Equilibration of sand sample at 5-7% RH before moisture adsorption diffusion tests.

After equilibration at 5 % RH, the sample is placed on a precision scale connected to a computer that records weight changes. The air around the sample will be either at laboratory conditions (23-25 °C and 35-45% RH) or near saturation (23-25 °C and 95% RH). In order to achieve the 95% RH test condition, a water soaked cloth is added on the wall of the sample chamber (Figure 2.24).

This procedure is aiming at reproducing the process of a mould taken out from a drying step and placed in environment where the humidity can vary from 30 to 95% RH (as shown in figure 2). However due to limitations of the manual method, only the two above described values of relative humidity are used in these experiments.

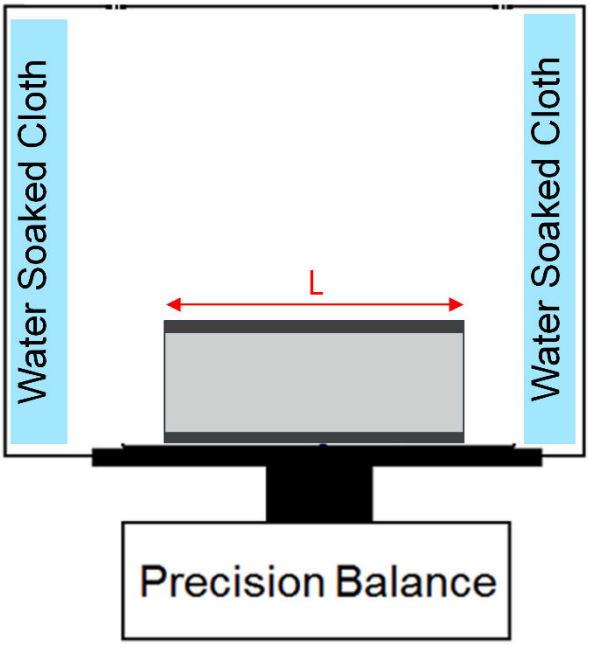

Figure 2.24 Schematic test setup for manual sorption tests.

The experimental plan for manual tests can be summarised as in Table 2.6where two possible sand binder recipes (GCK and GCM) were tested at two humidity levels.
The plan is repeated for low and high compaction sample and replicated two times, for a total of 16 runs.

Table 2.6 Overview of experimental plan for manual sorption tests.

Material	**Temperature [°C]**	
	25	
	Relative Humidity [%]	
	40	95
GCK	X	X
GCM	X	X

The sample moisture can be calculated from the weight variation (Supplement VI) and is defined on wet basis as it is common practice in foundry industry.

The dry weight is obtained by drying the sample at 105 °C for 30 minutes.

2.6.2 - Automatic Tests Method

For the automatic tests method, an automatic vapour sorption analyser is used with the same test methodology described in section 2.5.1.
The same test data used to obtain the sorption curve and equilibrium moisture levels can be used to determine the moisture diffusion coefficients.
The same experimental plan described in Table 2.5 Overview of experimental for residual moisture tests.is used.

2.6.3 - Diffusion Coefficients Determination

In order to obtain diffusion coefficients from the test data, approximated solutions of the diffusion equation are fitted to the measured weight curves. The solution is expressed in a ratio between the adsorbed mass of water by the sample at the time t (M_t) and the equilibrated mass of the sample M_e and approximated as below [45,46,Supplement VI]:

$$\frac{M_t}{M_e} = \frac{4}{L}\sqrt{\frac{Dt}{\pi}} \qquad \text{for } \frac{M_t}{M_e} < 0.5$$

Eq.2.1a

$$\frac{M_t}{M_e} = 1 - \frac{8}{\pi^2}\exp\left(-\frac{\pi^2 D}{L^2}t\right) \qquad \text{for } \frac{M_t}{M_e} > 0.5 \qquad \text{Eq.2.1b}$$

Where D is the diffusion coefficient and L the thickness of the sample as shown in figures 4 and 6.
Both approximations of the solution must fit experimental data in the correspondent range of M_t/M_e using the same diffusion coefficient (Figure 2.25 Example of experimental data fitted with the two approximated solutions Eq.2.1a and Eq.2.1.b.).

For the manual sorption tests, the fitting is performed using the final equilibrated mass value reached at the specific test relative humidity (40% or 95% RH).

For the automatic sorption test, the fitting is carried out for each test step (time for which the relative humidity is kept constant). In this way it is possible to obtain a diffusion coefficient for each value of relative humidity used in test steps (full details in Supplement VI).

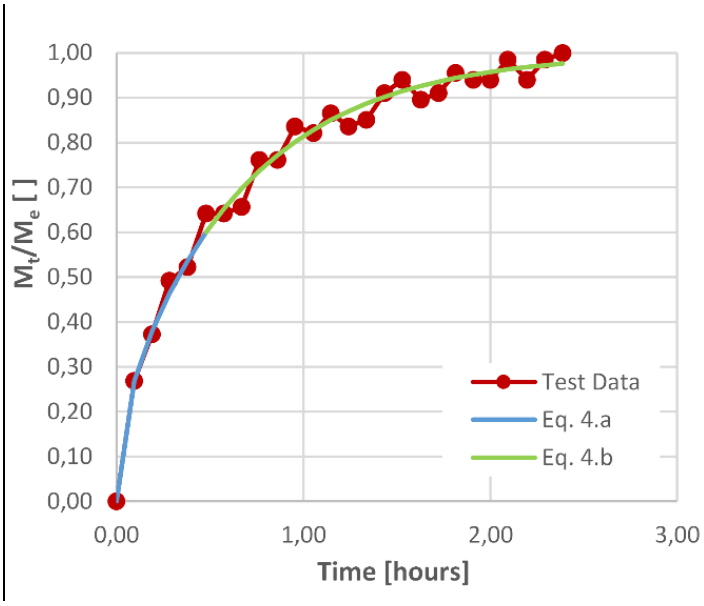

Figure 2.25 Example of experimental data fitted with the two approximated solutions Eq.2.1a and Eq.2.1.b.

2.7 - Moisture Measurement Tests

In this section we present two sets of tests: in the first set we compare the performance of commercial tools with a self-developed and built device (Figure 2.26). In the second set of tests we want to obtain a correlation between the moisture in the considered foundry coating and the measured resistance.

2.7.1 - Moisture Tools Comparison Tests

The tool choice is based on different capabilities of the tools. Tool A (Figure 2.26.a) can provide moisture readings for concrete and has been used in some of Global Castings production facilities to give indications on the moisture level of the considered coating. However, it was found to significantly loose accuracy when extension wires were used to reach into hard to measure locations in the mould, and it seemed to have a significant error for readings above 1% due to different properties of concrete and the considered coating. Additionally, Tool A can only provide visual

output so that no automatic logging is possible by connecting to a data acquisition system. The only advantages of Tool A is that it is battery powered and it is rugged for industrial use.

Tool B (Figure 2.26b) provides an analogue voltage signal from 0 to 10 V, is calibrated for wood and it requires an external power supply. The hope is that it could be used also for foundry coatings if its performance is good in the relevant range.

Tool C (Figure 2.26c) is a prototype transducer designed to have a nominal voltage response V_{out} that can be converted to a resistance R_{meas} using a known relationship (Supplement VII). It is powered by an external power supply.

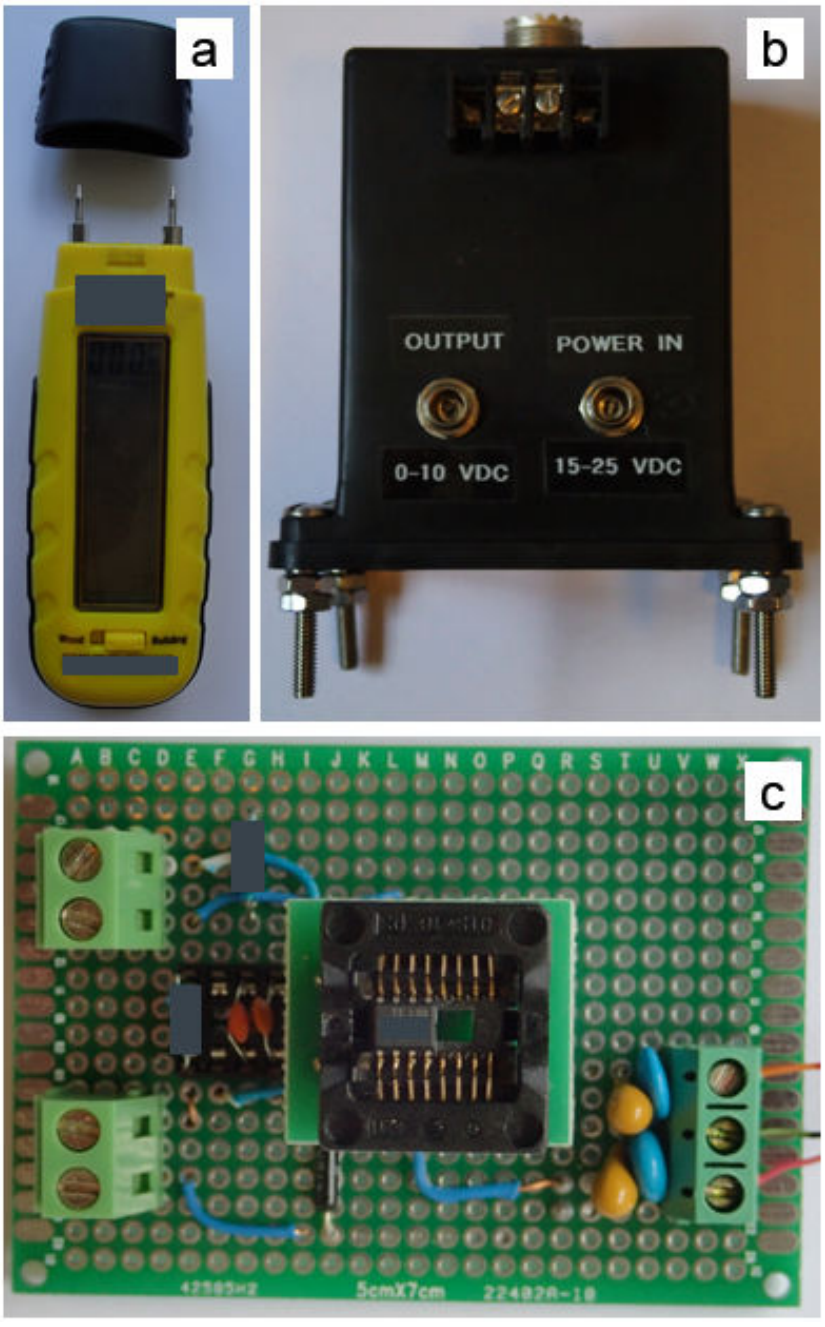

Figure 2.26 Transducers used in the performance comparison a) Tool A, b) Tool B and c) Tool C.

The transducers are tested using a bank of resistors ranging from 10 kOhm to 200 GOhm (Supplement VII).

The objectives of the tests are to determine if the tools can provide stable and meaningful reading across the considered resistance range (Figure 2.27). Three test configuration were used: 30 cm wire (to minimize leakage currents) to be used as a reference or best case, 15 m standard wires (used in production environment to do measurements in hard to reach areas) and 15 m Teflon coated wires (expected to reduce the effect of leakage currents).

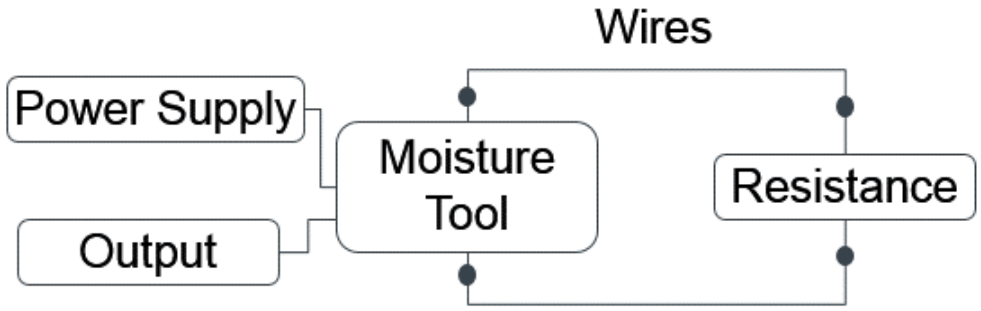

Figure 2.27 Schematic of experimental setup for moisture tool comparison tests.

2.7.2 - Moisture-Resistance Correlation Tests

In order to obtain a correlation between moisture in the coating and resistance we have designed a Teflon sample holder (

Figure **2.28**) that can accommodate two electrodes and provide support for a layer of coating of 1 mm thickness. The electrodes are spaced 15 mm from each other and Teflon was chosen for its high resistivity and its low sensitivity to moisture in order to minimize leakage currents.

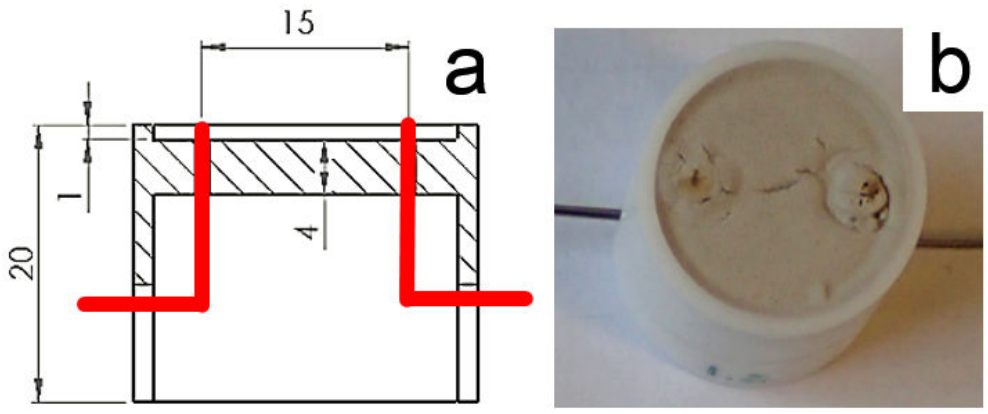

Figure 2.28 a) Schematic of coating sample holder with electrodes and b) picture with coating.

The coated sample holder is placed on a scale with +/-0.1 mg accuracy and connected to a computer and a data logging software. The coated surface of the sample is facing upwards and inserted by few millimeters in an air duct where air at 45-55% RH and 24-26 C is supplied at a speed of 1 m/s. This provides similar drying conditions for all the tests. The electrodes are connected to the moisture tool C by flexible copper wires, as shown in Figure 2.29, to minimize any weight measurement errors.

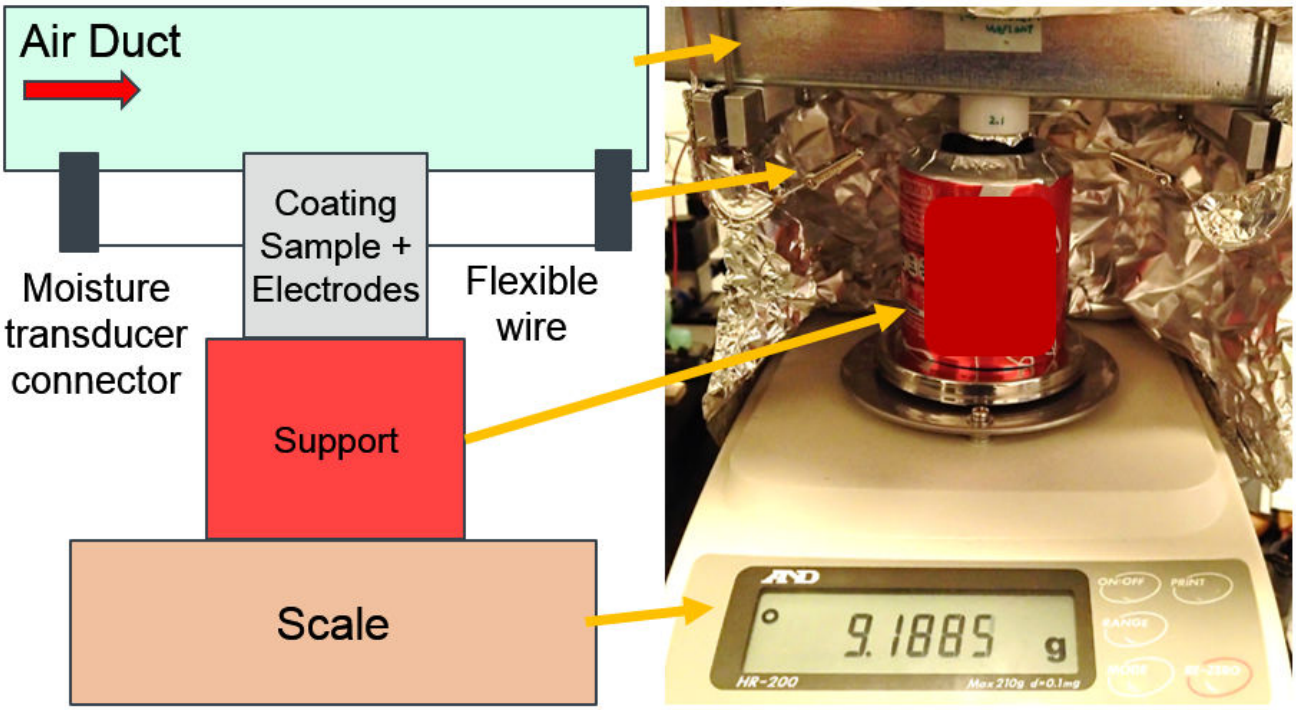

Figure 2.29 Experimental apparatus for logging of weight and resistance during drying.

The moisture in the coating layer is calculated from the logged weigth on a wet basis (Supplement VI) and then it is plotted versus the resistance R calculated from the logged voltage (Supplement VII).

The above described method is used to simplify the measurement of a non-equilibrium moisture condition of the coating being dried. The advantages of such a setup is shorter test time and increased accuracy due to minimal handling of the coating sample.

2.7.3 - Moisture Measurements Method for Large Moulds

In order to be able to measure moisture in large size moulds production electrodes can be installed as shown in Figure 2.30. Moisture can then be monitored by one of the moisture tools described in section 2.7.1.

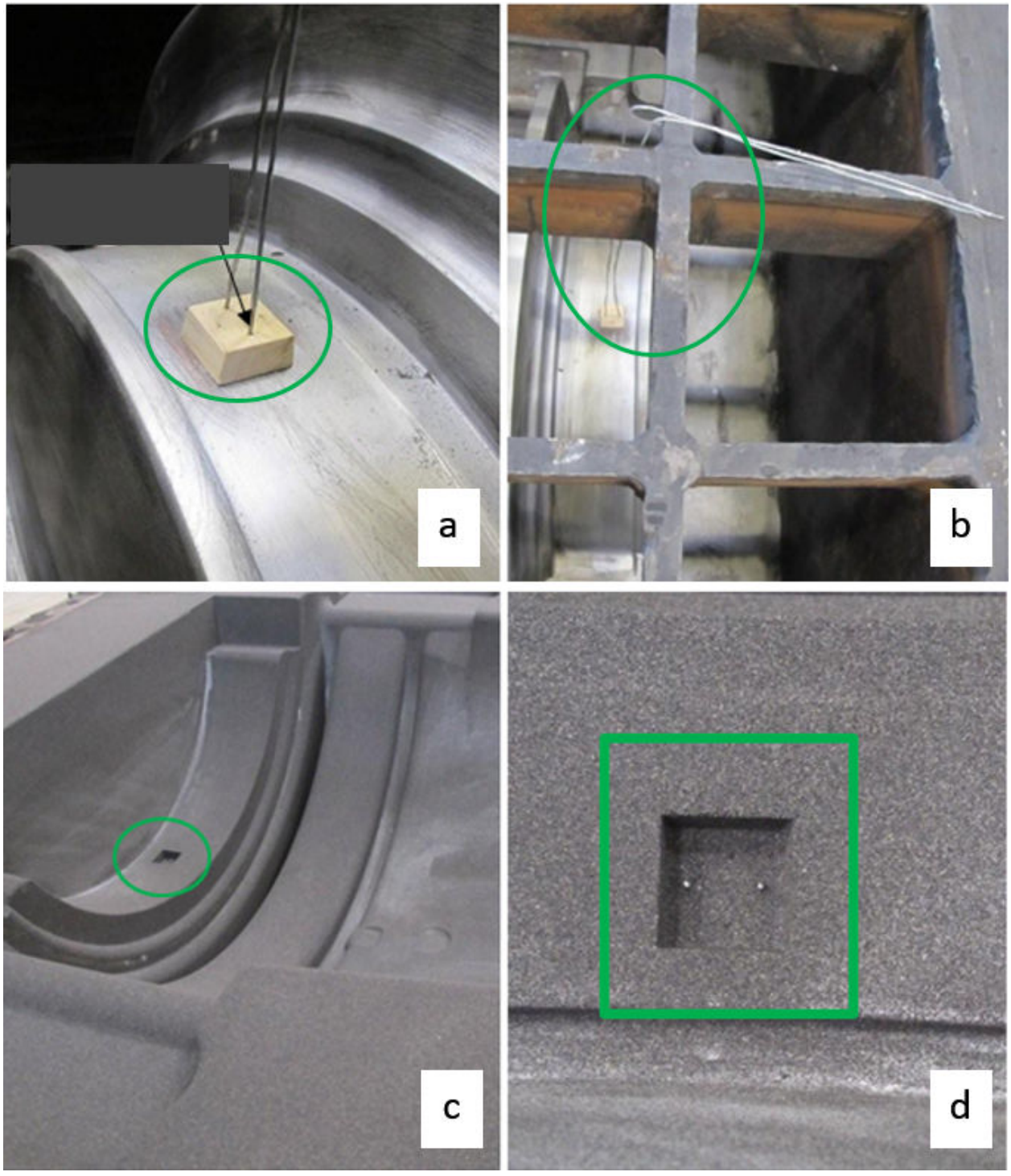

Figure 2.30 Moisture measurements setup for large sized sand moulds. a) Electrode support on pattern, b) wires installation, c) measuring point overview,) measuring point close up.

2.7.4 - Infra Red Thermography

Temperature measurements can be used for identifying areas with higher moisture content. This is because water will tend to evaporate and subtract heat from the mould surface. This is a qualitative measurement technique but allows for a quick check of large areas and identification of cold spots. This is needed in the production of large size castings like the ones produced at Global Castings. For our work we choose a Trotec LV InfraRed thermal camera with an accuracy of+/- 2 degree Celsius (Figure 2.31).

Figure 2.31 Infrared camera for temperature surface measurement in large moulds.

2.8 - Process Design and Simulations

2.8.1 - Drying Time Hand Calculation Methods

The typical goal in production is to avoid bottlenecks. The objective is therefore to make sure that the drying time of the moulds is equal or shorter than the needed production time.

For constant drying air conditions the estimation of drying time can be carried out with the following manual calculation procedure (Supplement VIII):

1) Determine average evaporation rate from a design map (Figure 2.32). Design maps are functions of air properties, coating thickness and type (Eq.2.2) and can be determined with drying experiments as describe in secion 2.4.3 and Supplment III:

$$ER_{avg} = ER_{avg}(T_{air}, RH_{air}, V_{air}, CT_{H2O,init}, X_{final}) \quad \text{Eq.2.2}$$

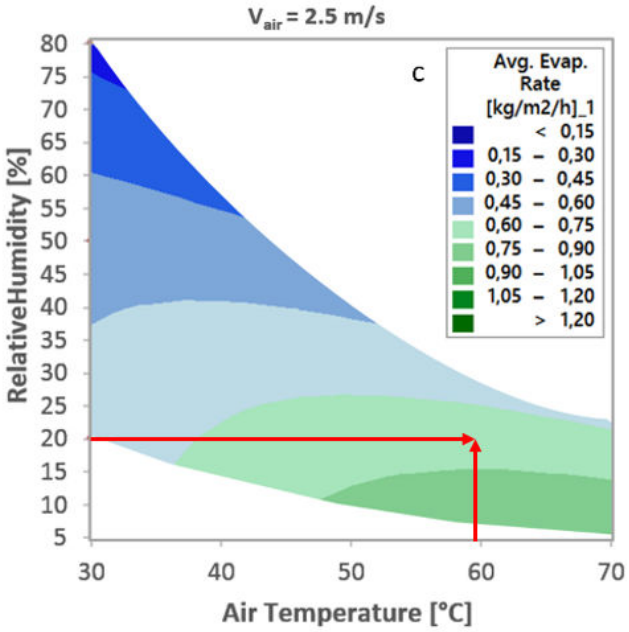

Figure 2.32 Average evaporation rates design maps for air speeds of 2.5 m/s, initial water thickness of < 1 kg/m2 and final moisture of < 1 %.

2) Calculate estimated drying time by dividing the initial amount of water in the coating layer by the evaporation rate, as show in Eq.2.3:

$$t_{dry} = \frac{CT_{H2O,init}}{ER_{avg}}$$ Eq.2.3

The estimated drying time can then be compared with the production requirements and changes to the drying air condition or coating process can be made if needed.

2.8.2 - Drying Time Numerical Calculation Methods

If there is a need to simulate varying conditions of drying air like changes in temperature, relative humidity or air speed it is possible to follow a numerical approach. In the numerical approach the properties are assumed constant only for a small amount of time Δt compared to total the length of the drying process. In this case the solution is carried out as follows:

1) Determine maximum evaporation rate from experimental equations in the form of Eq.2.4. Maximum evaporation rates are only functions of air properties and can be determined experimentally as shown in [Supplement III]:

$$ER_{max} = ER_{max}(T_{air}, RH_{air}, V_{air})$$ Eq. 2.4

2) Use the ratio between current coating moisture level and initial moisture (for the first time step the ratio is 1) and the initial water thickness to obtain the correction factor from Eq.2.5 or Figure 2.33:

$$CF \quad = CF \quad (CT_{H2O,init}, X_{current})$$ Eq. 2.5

3) Calculate current evaporation rate as:

$$ER_{current} = ER_{max}\, CF$$ Eq. 2.6

4) Calculate water evaporated (Eq.2.7) and new moisture level at the next time step:

$$\Delta_{H2O} = \; ER_{current} \Delta t$$ Eq.2.7

5) Update drying air properties and start a new iteration from step 1.

The calculation is stopped when the calculated residual moisture is less than 1%.

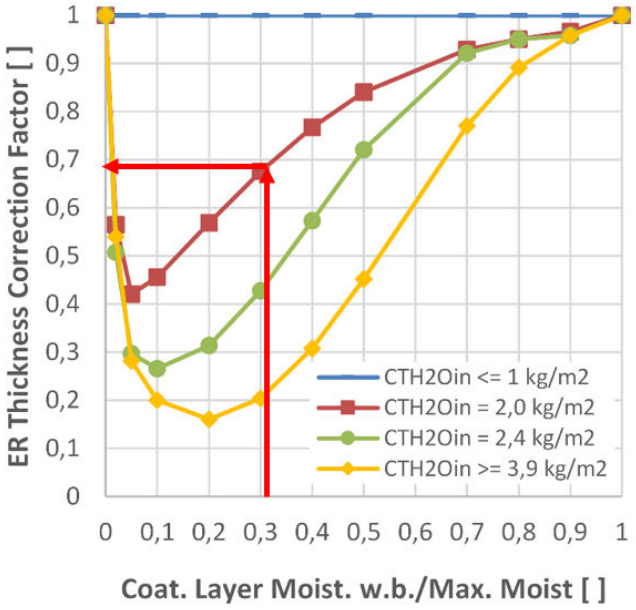

Figure 2.33 Experimental Correction factor for evaporation rate calculation based on initial coating water thickness and current moisture in the coating layer.

2.8.3 - Adsorbed Moisture After Drying

The adsorbed mass of water Mt at the time t, for a core of flat shape and thickness L, can be calculated with equation 2.8 where M_i is the initial mass of the core and X_e is the equilibrium moisture from the sorption curve (Figure 2.22). The ratio between M_t/M_e is calculated from equations 2.1a and 2.1b obtained from approximate solutions of the diffusion equation (Supplement 6). The diffusion coefficient D can be determined by laboratory tests as described in section 2.6.

$$M_t = M_e \frac{M_t}{M_e} = M_i X_e \frac{M_t}{M_e} \qquad \text{Eq.2.8}$$

For complex geometries or for calculating the actual moisture distribution in a core or mould 3D solvers can be used where diffusion coefficients obtained in Supplement VI can be used.

2.8.4 - CFD Simulations Method

In order to efficiently dry large coated moulds it is important to avoid areas with low air recirculation. Computational fluid dynamic (CFD) simulation methodology can be used to simulate forced air convection around foundry moulds and optimize the air flow around the moulds to shorten the drying time.

In our study first we compare the performance of different fans with the objective to choose a fan model to be used in the subsequent mould drying simulations. Then, mould drying simulations are carried out by modelling three representative geometries typical of wind turbine parts produced at Global Castings such as a hub, main foundation and a main bearing house in a 3D software. These geometries are then imported in a fluid flow solver where complete Navier-Stokes equations coupled with energy transport equations are solved. Moisture transfer and evaporation are not modelled in order to reduce the modelling effort and reduce the overall computational time, while the velocity field and heat transfer coefficient are used to evaluate the effectiveness of different fan layouts.

Detailed description of simulation methodology can be found in Supplement IX.

2.9 - Management of the Design Process

Based on methodology typically used for development of new products [42] a new desing process is introduced at Global Castings for the desing of foundry moulds. Supplement X shows the applicaiton of such a methodology to the optimization of foundry mouldbox

The newly introduced desing process (Figure 2.34) starts by defining a clear set of requirements coming from the customer. Then, two main iterative desing loops are used to initially define the design concept and then to finalize the detailed design.

The first loop is iterated until all the stakeholders approve the desing concept and no more changes are needed to the the concept. The second loop is iterated until test and 0 series are completed succesfully.

Whitin the detailed design phase one more iteration loop are present (Figure 2.35). In these loops, the necessary calculations and simulations are performed and the design is optimized until all the constraints coming from the customer requirements are satisfied.

Tools such as value stream mapping, interface diagram and gant charts are used to support this process and their detailed application is shown in Supplement X.

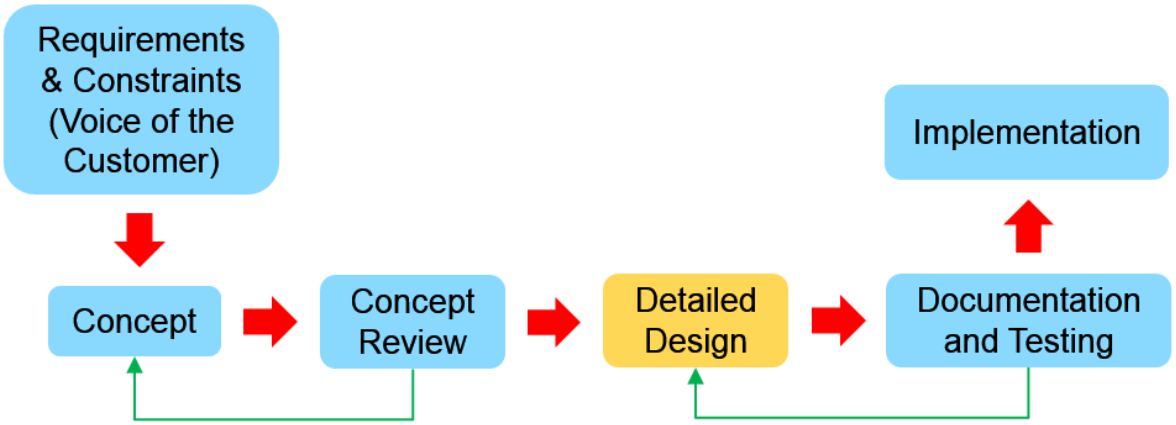

Figure 2.34 Overall view of new design process.

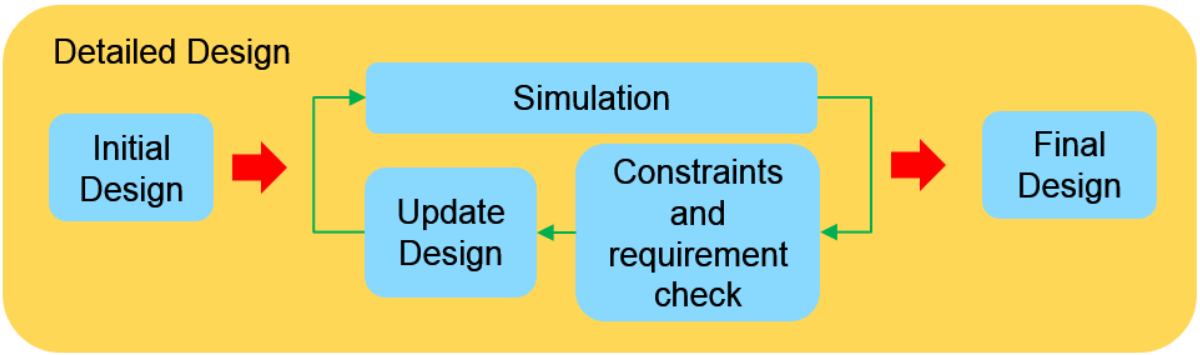

Figure 2.35 Schematics of detailed design phase of the new design process.

3. Main Results

In this chapter we present the main results from the investigations in the different area. Full details can be found in the different supplements according to Table 1.1 and in Appendix B.

3.1 - Coating Properties Tests Results

3.1.1 - Cup Time Tests Results

Main effects plot (Figure 3.1) graphically shows how cup time are increasing significantly with density but only have small fluctuation with respect of other variables.

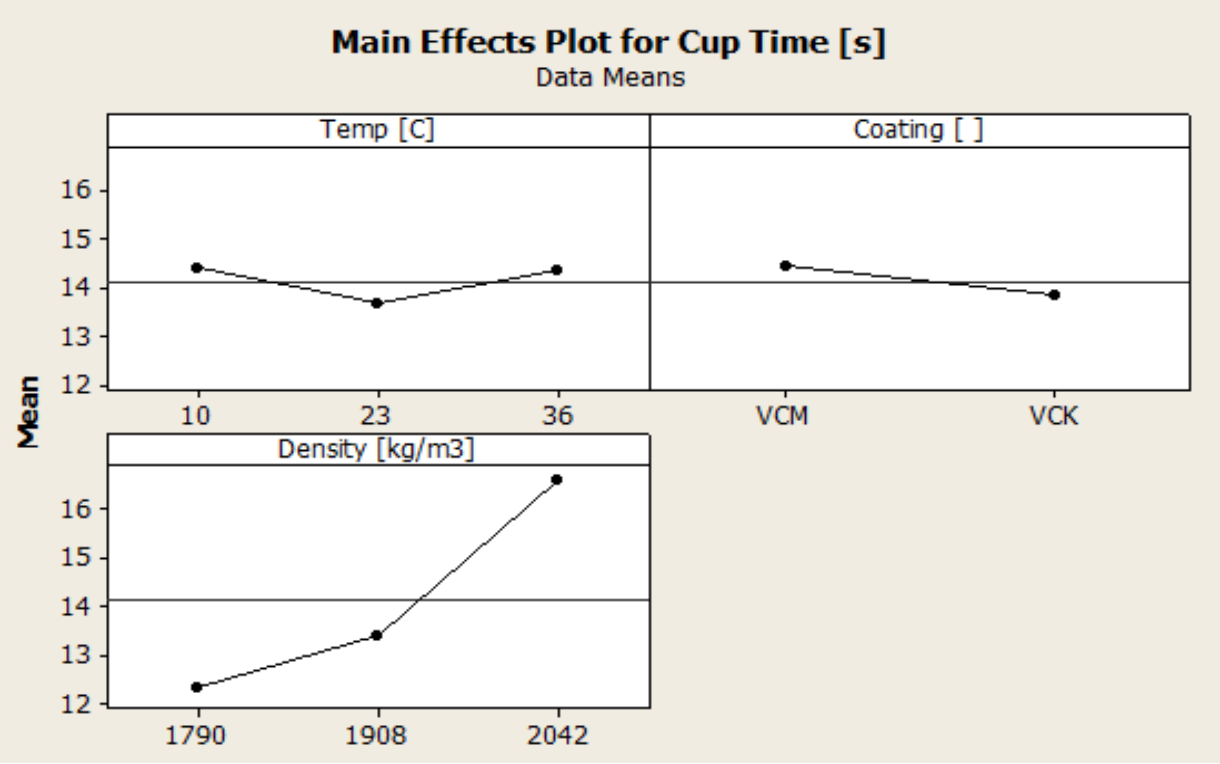

Figure 3.1 Main effect plots for cuptime.

It can also be noticed that when density decreases from 1908 kg/m^3 to 1790 kg/m^3, cup time decreases from about 13,5s to 12,5s. This difference might be difficult to measure with a manual cup time measurement.

Finally, in the main effect plot of density on cup time, we can see that the relation between cup time and density is nonlinear.

3.1.2 - Baume Tests Results

The main effect plot (Figure 3.2) shows how the baume reading increses when measuring at 36°C. Both temperature and density have an effect on Baume measurements.

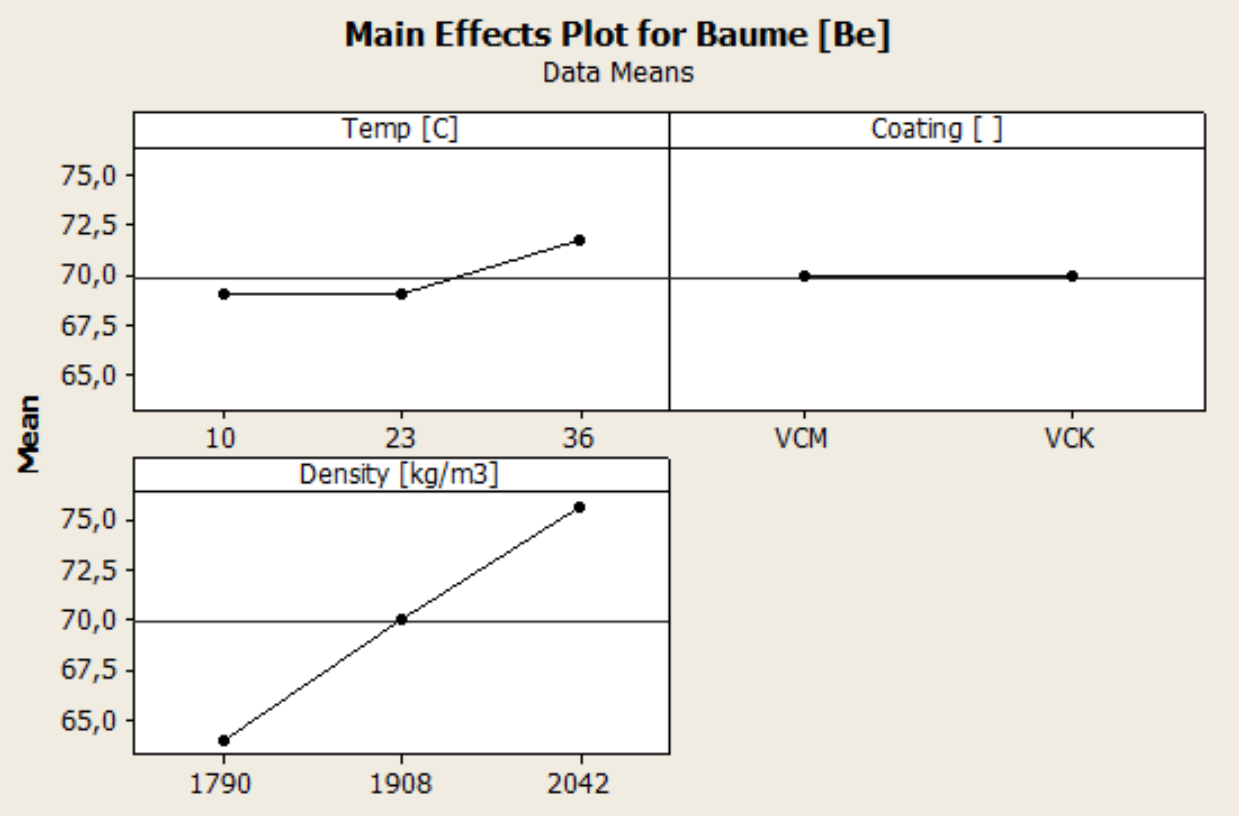

Figure 3.2 Main effect plots for Baume.

3.1.3 - Rotational Viscosity Tests Results

Figure 3.3 reports the results from the rotational viscosity tests for all the considered coating samples at 23 °C. It can be seen that test speed does have an effect on absolute value (the higher the speed the lower the viscosity) but it does not change the shape of the curves compared to each other.

It also can be noticed that the higher the density of the coating the higher the viscosity.

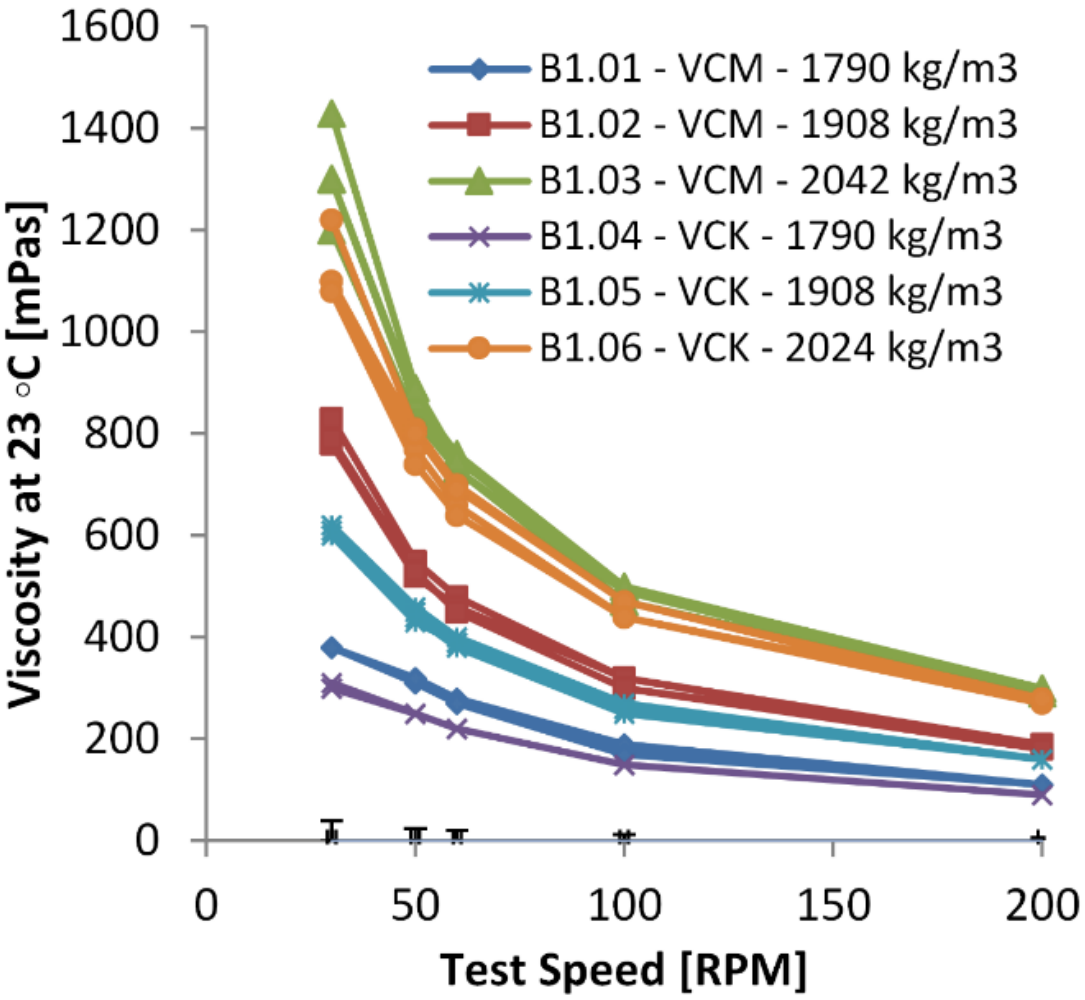

Figure 3.3 Viscosity measurements carried on two different batches of coating with three different densities at 23 °C. Two full sweeps performed for the different test speeds resulting in four measurements for the middle test levels values and two measurements for maximum and minimum test speed levels. Viscosity can be directly correlated with density however results can be compared only if the test speed is the same [Supplement I].

Figure 3.4 shows the viscosity test resutls for VCM coating with a density of 1908 kg/m^3 at the three different test temperatues. It can bee seen that temperature has a minor effect at low test speeds that can only by detected by the rotational viscometer.

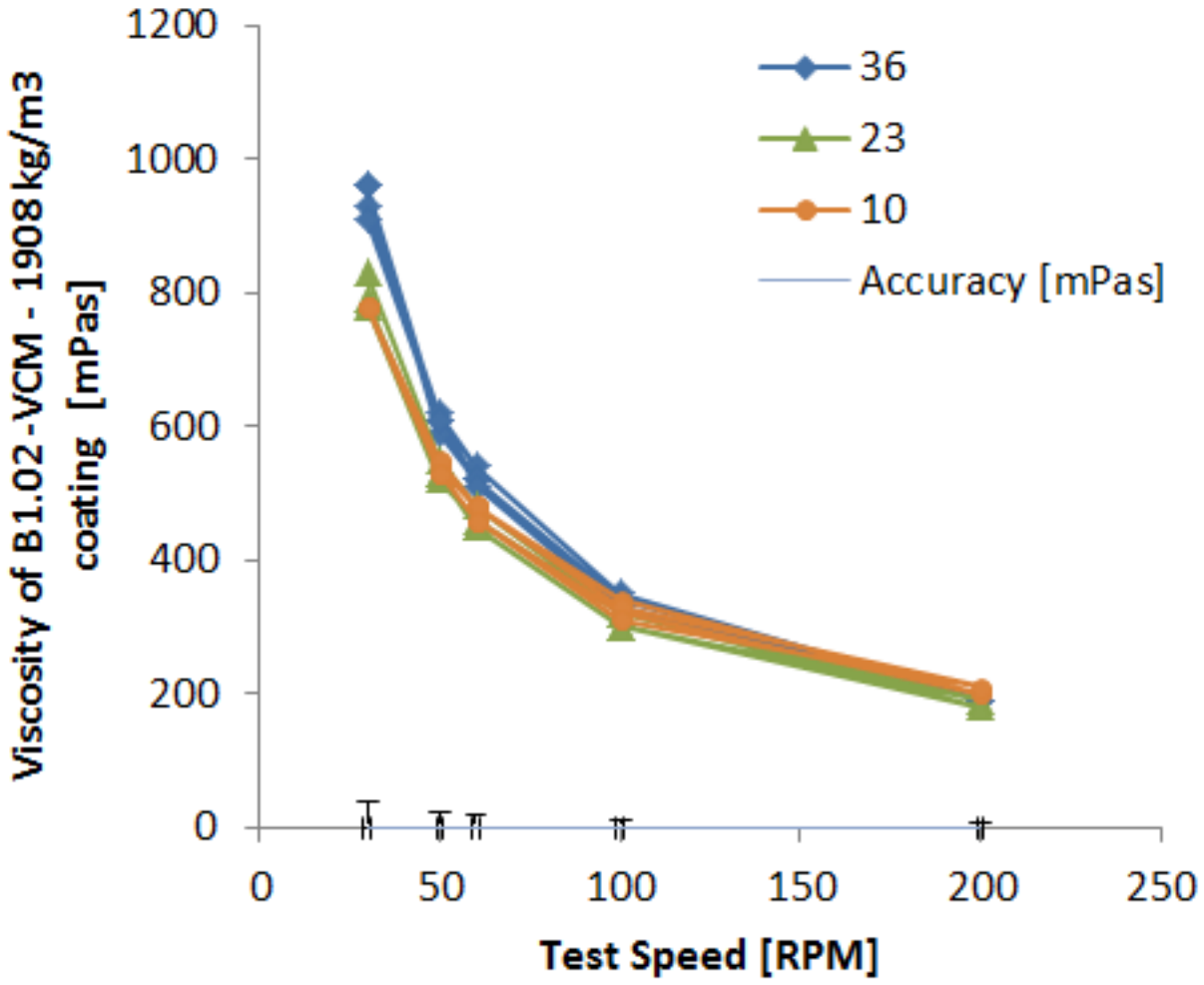

Figure 3.4 Viscosity tests results for VCM coating with a density of 1908 kg/m3.

3.1.4 - Water Content Tests Results

Water content result are reported in Figure 3.5. We can see that for both coating batches we have a water content of about 43% for a density of 1790 kg/m^3, 38% for a density of 1908 kg/m^3 and 34 % for a density of 2042 kg/m^3. This is a significant difference considering all these value of densities are allowed by the current specificaiton. This means that, if control limits are not tightened, a significant variation of the initial moisture level in the mould coating is possible with consequent variation in drying time and coating layer properties.

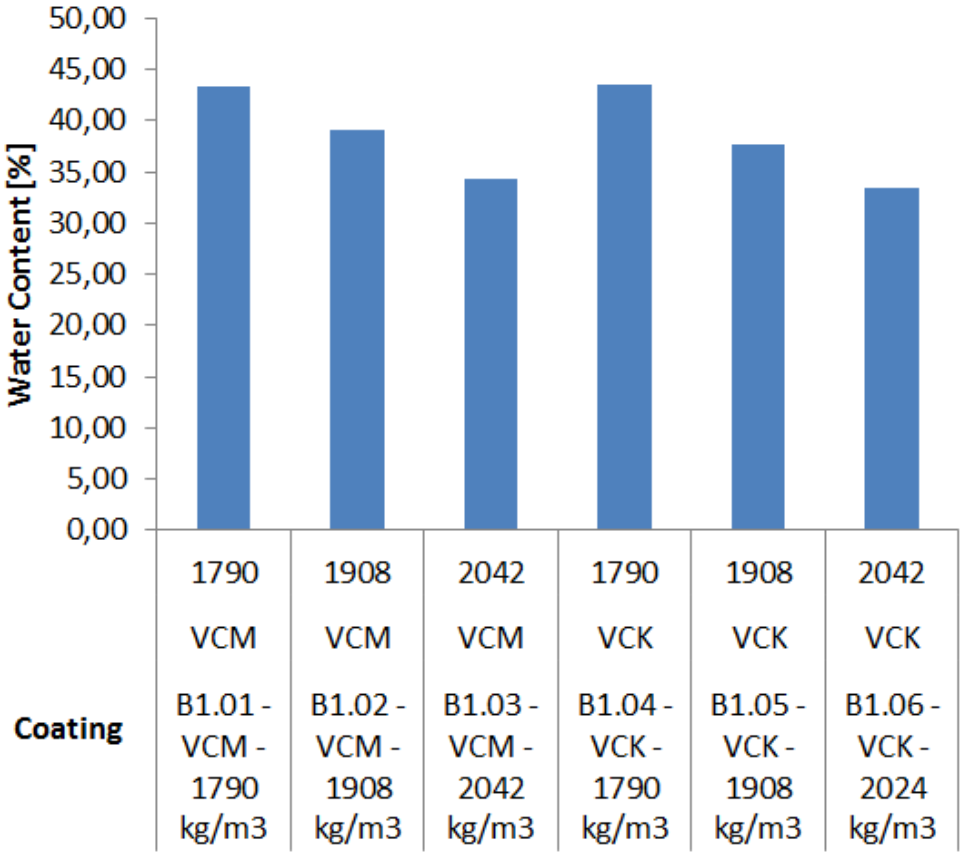

Figure 3.5 Moisture content results for different coatings.

3.2 - Coating Layer Properties Tests Results

3.2.1 - Fractional Factorial Designs Results (main effects)

From Figure 3.6 we can notice that for wet coating thickness the most relevant effect is sand compaction followed by dipping time and gravity effect. Second order interactions have smaller effects.

Similar analysis are carried out for the other coating thickness properties and summarized in Table 3.1. We can see that the most important factors are compaction, coating density, dipping time and gravity.

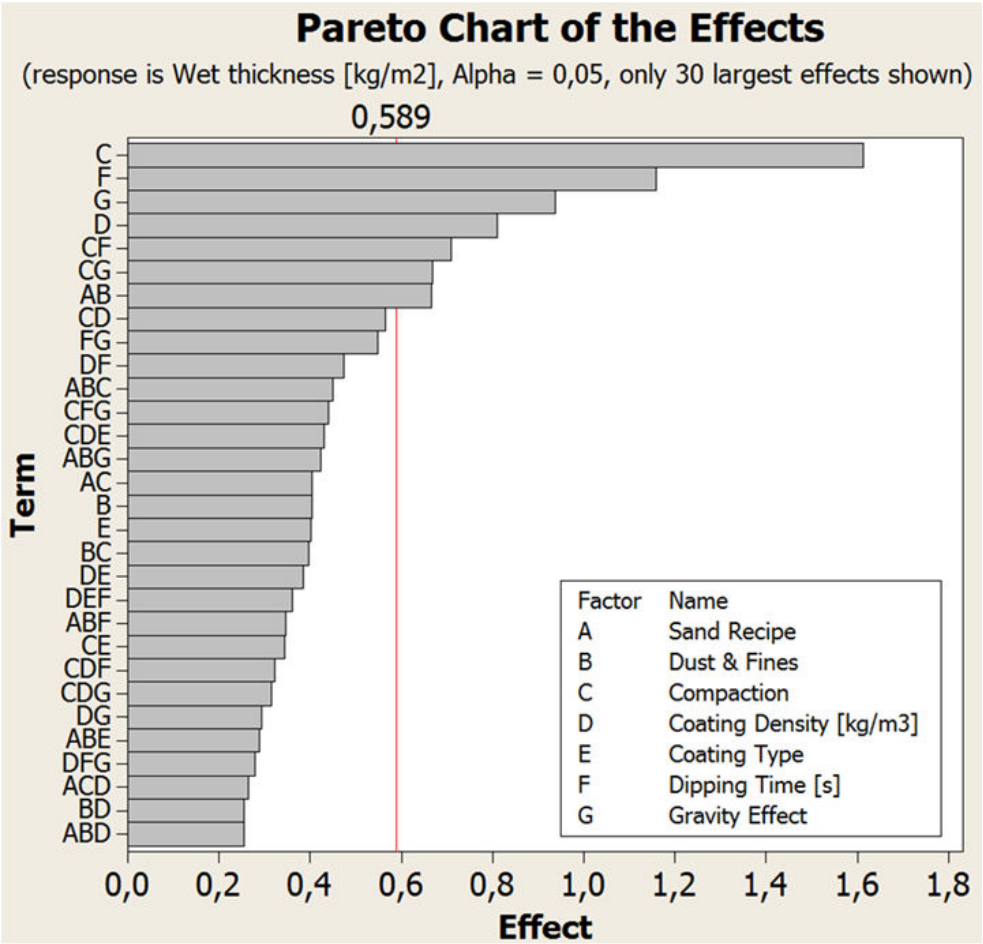

Figure 3.6 Pareto chart of effects for wet coating thickness (up to 3rd order interection inlcuded).

Table 3.1 Summary of main effects that are relevant for each coating layer property. Lowest numbers used to indicate the largest effects.

	Wet Coat. Thick. [kg/m^2]	Dry Coat. Thick. [kg/m^2]	Water Thick. [kg/m^2]	Coat. Water Fract. [%]	Penetration [mm]	Sand Den. [kg/m^3]
Sand Recipe						2
Dust & Fines			(5)			
Comp.	1	1	1	(2)	2	1
Coating Density	4		2	1	1	
Coating Type						
Dipping Time	2	2	3		3	
Gravity	3	3	4		(4)	

The effets of varying these most important factors are illustrated in Figure 3.7 for the dry coating thickness. We can see that low compaction generates a larger variation compared to high compaction. For high compaction dry thickness is typically between 0.8 kg/m^2 and 1.5 kg/m^2, while for low compaction is above 1.2 kg/m^2. The worst combination is for low compaction, 120s dipping time and with the sample facing up, in this case dry coating thickness varies from about 1.5 kg/m^2 to more than 6 kg/m^2.

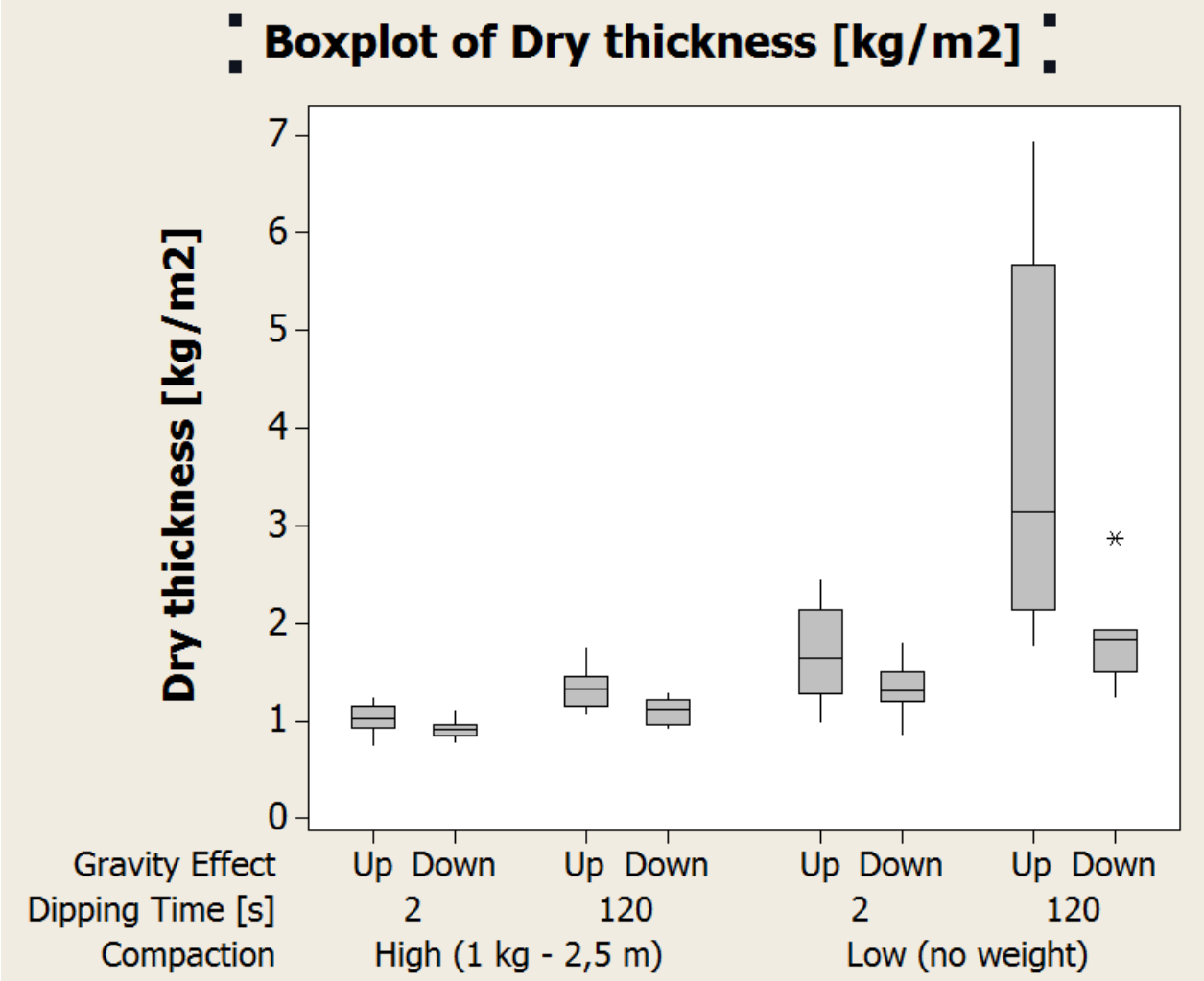

Figure 3.7 Box plots of dry coating thickness as a function of most relevant effects.

In **Figure 3.**8 we see that, when other levels are kept constant, samples facing up always have a higher water thickness. We can also see that water thickness can vary from less than 0.5 kg/m^3 to more than 3 kg/m^2 depending on the levels chosen.

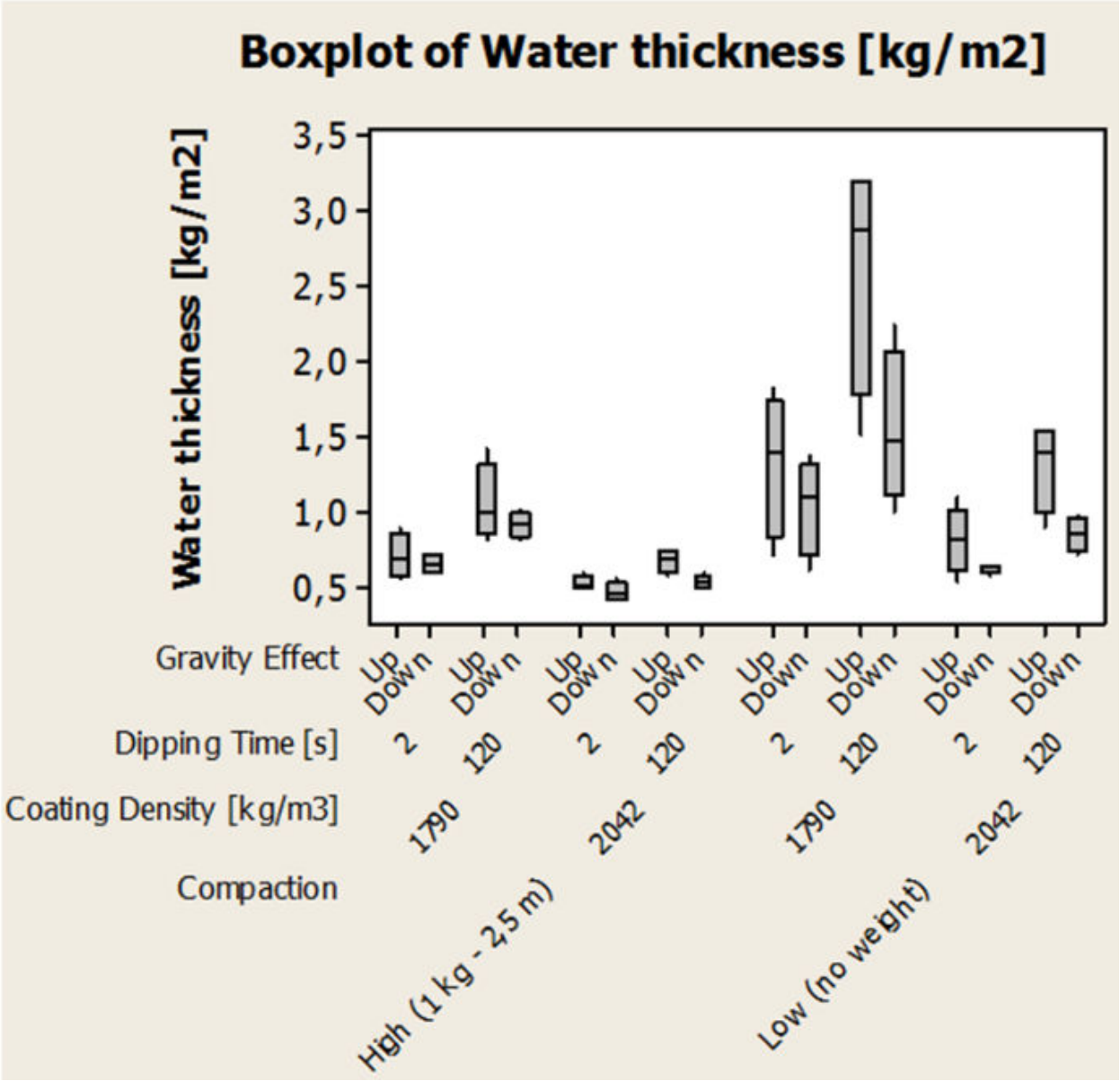

Figure 3.8 Water thickness deposited on furan sand samples using different levels of sand compaction, coating density, dipping time and gravity. The amount of water can vary from 0.5 kg/m^2 to more than 3.0 kg/m^2.

3.2.2 - Centre Points Addition Results (non-linearity)

The first results for the addition of centre points (Figure 3.9) show the effect of sand depth (and relative compaction pressure) on the achieved sand density. In the figure we can see that the function is non-linear. In particular sand density decreases significantly for low sand depths and the

scatter increases substantially. It is therefore important for small moulds (depth lower than 1 m) to make sure that manual compaction methods and vibration are used.

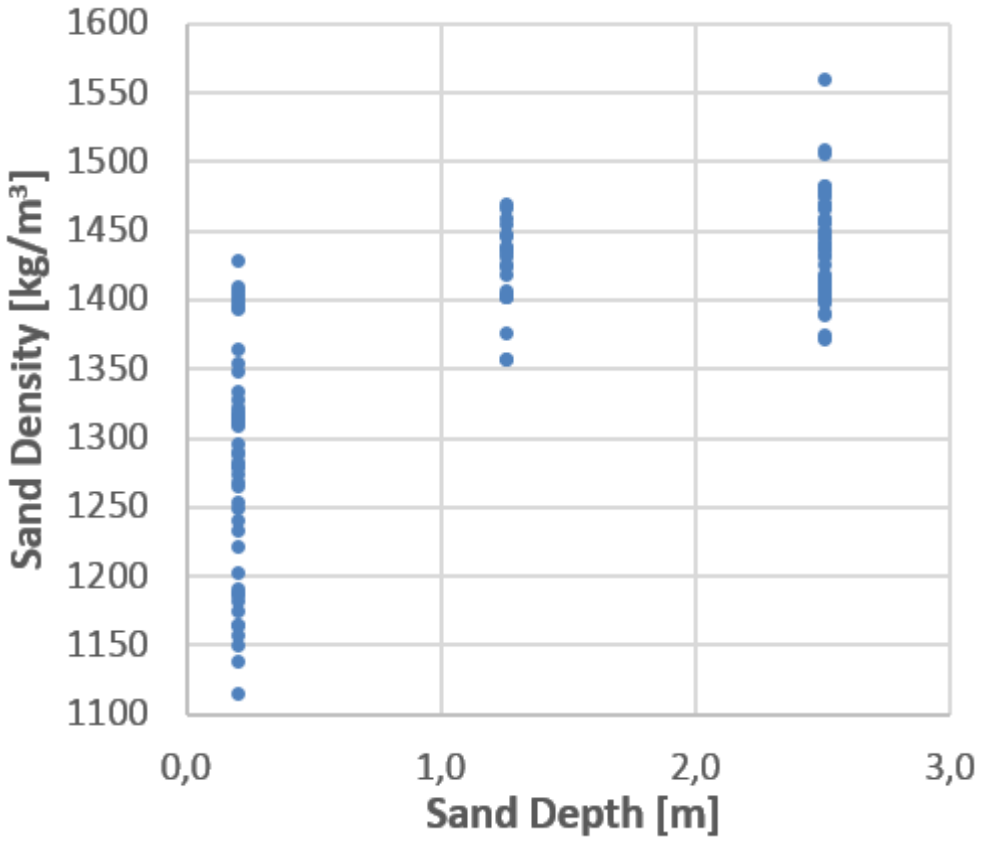

Figure 3.9 Sand density of samples as a function of mould depth.

Figure 3.10 shows how water thickness depends heavily on the sand density and scatter increases substantially for sand densities below 1350 kg/m^3.

The effect of coating density is shown in Figure 3.11. In this case we see that the scatter in water thickness decreases as the coating density increases. It appears that there is a threshold density above which the scatter is reduced by a factor of 3. The threshold is near a coating density of 2042 kg/m^3.

The effect of time is represented in **Figure 3.**12. Again we see a strong non-linear correlation where water thickness increases substantially with dipping time as well as scatter does. It is therefore important to coat samples with fast passes and avoid pools of coating that will increase substantially the water thickness layer.

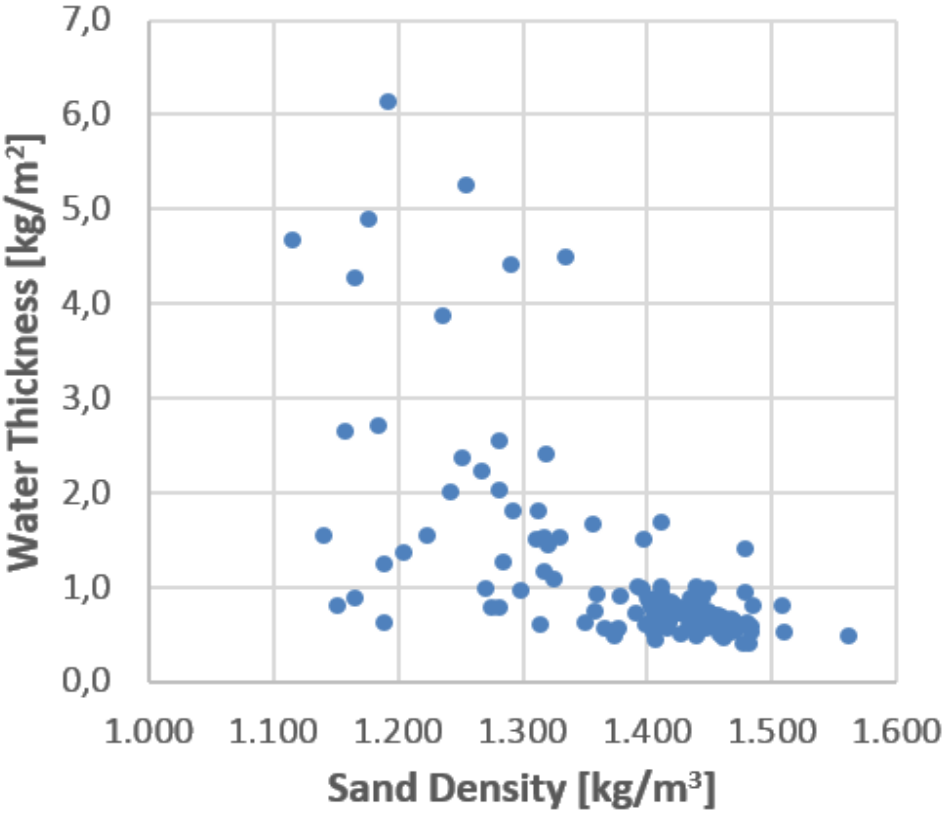

Figure 3.10 Water thickness as a function of sand density.

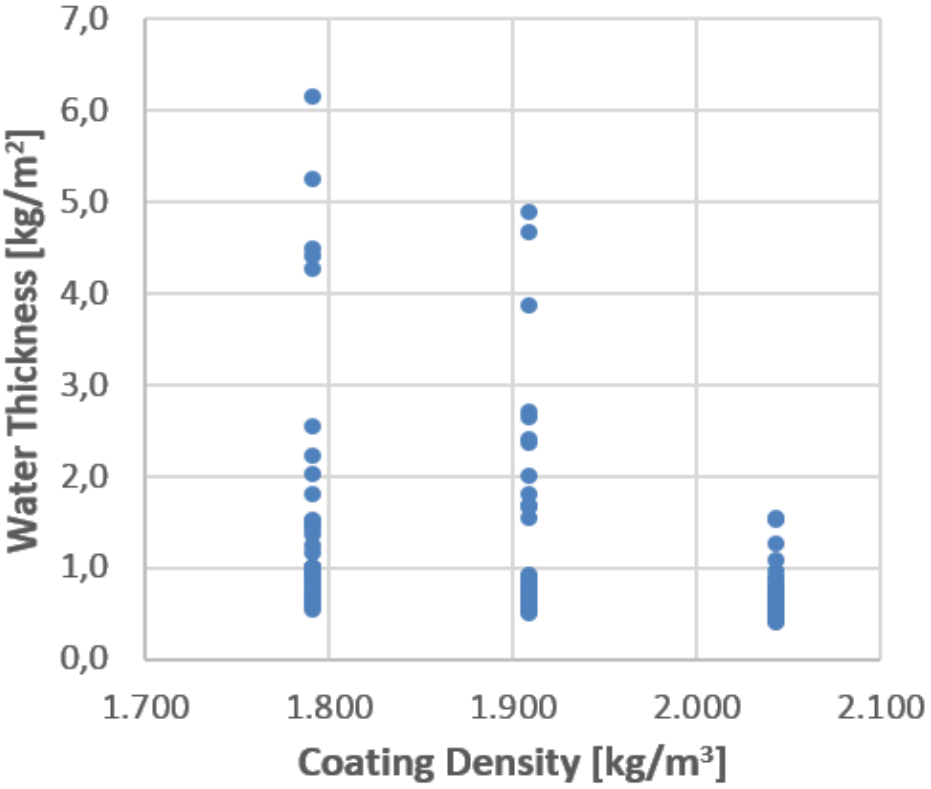

Figure 3.11 Water thickness as a function of coating density.

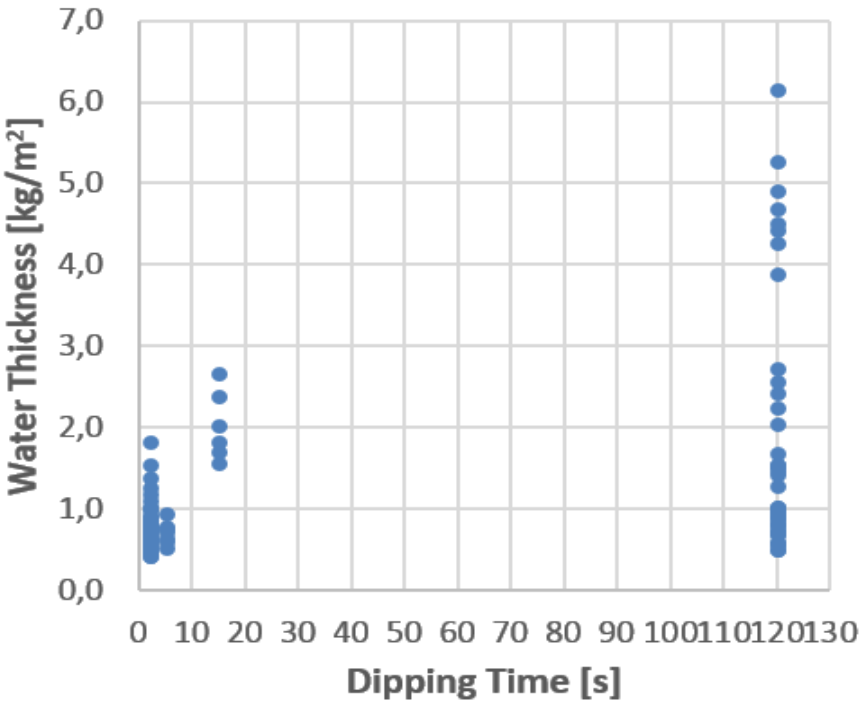

Figure 3.12 Water thickness as a function of dipping time.

Figure 3.13 shows measurements of coating penetration that can be carried out on production moulds. This measurements can be directly correlated to the amount of water in the coating layer (Figure 3.14).

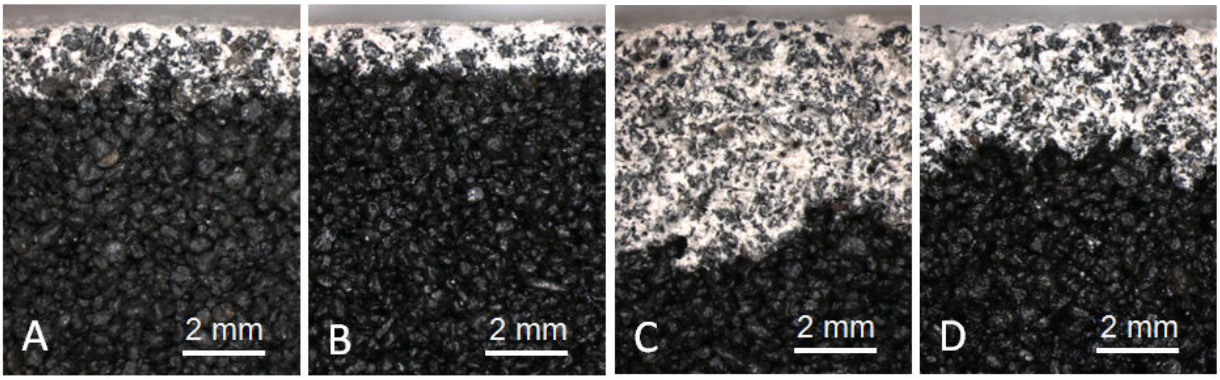

Figure 3.13 Coating penetration achieved with different levels of sand compaction, coating density, dipping time and gravity effect [Supplement I].

Figure 3.15 shows the water thickness on samples coated with tightly controlled coating conditions, in particular we used good sand compaction, 1908 kg/m^2 coating density, 5 seconds dipping time and sample facing down while being coated to reduce the gravity effect. We can see that it is possible to achieve control of the coating layer within a tight range by controlling relevant process variables.

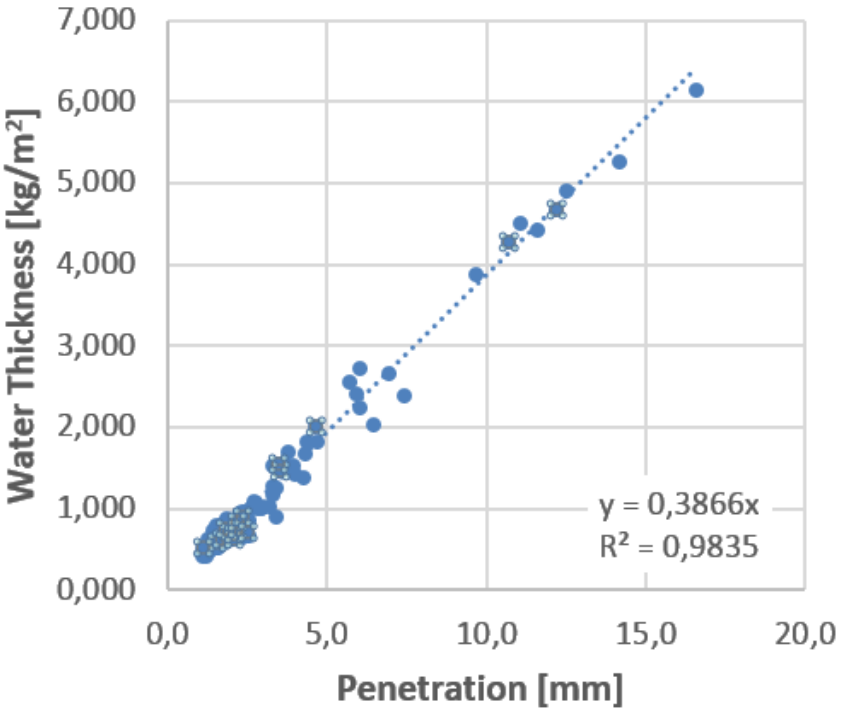

Figure 3.14 Coating penetration can be directly correlated to water thickness. This allows to predict of coating layer water amount in large moulds.

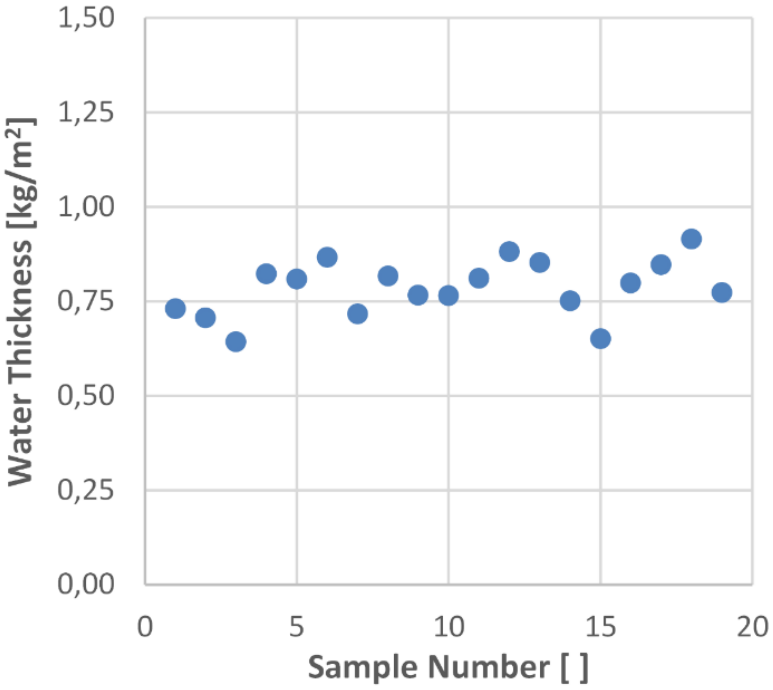

Figure 3.15 Water thickness on samples coated with tightly controlled coating conditions. It is possible to achieve control of coating layer by controlling relevant process variables.

3.3 - Evaporation Rates Tests Results

3.3.1 - Thickness Effect

In order to understand the effect of coating layer thickness, we plot the average evaporation rates as a function the initial coating layer water thickness. If we look at the results for drying conditions AC1 and AS1 (Figure 3.16), we can see that the average evaporations rate is clearly a function of the initial water thickness. In particular ER_{avg} seems to be constant for initial water thicknesses below 1 kg/m^2 and it drops significantly (almost to 35% of the original value) for water thicknesses above 4 kg/m^2.

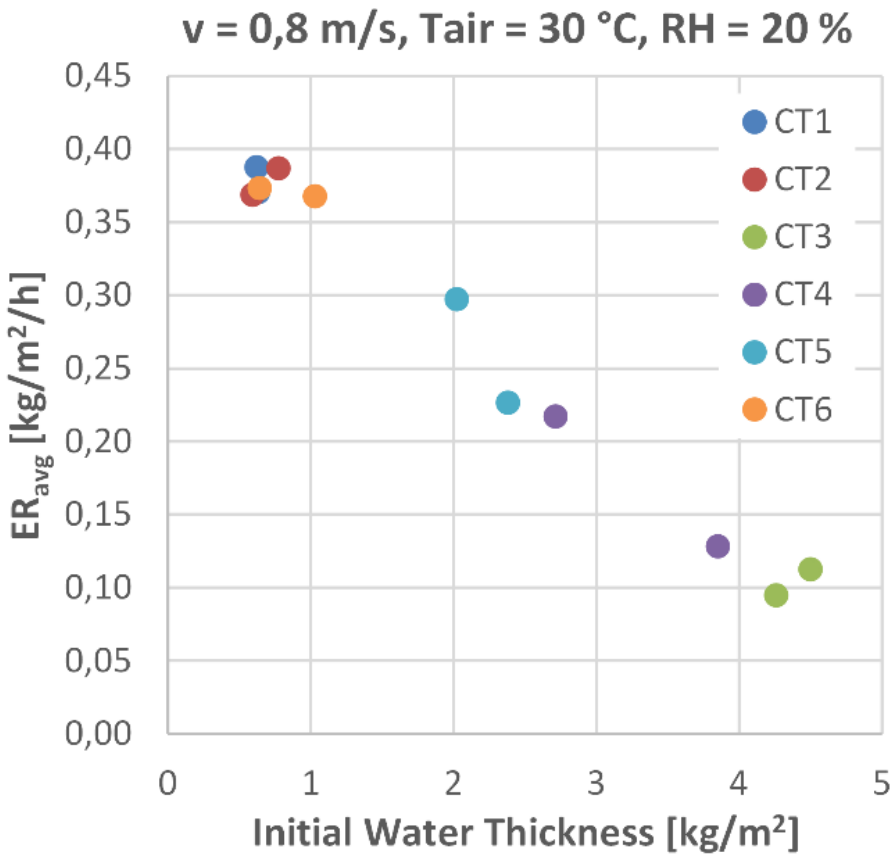

Figure 3.16 Average evaporation rates as a function of initial water thickness for air condition AC1.

Figure 3.17a shows the effect of drying conditions and water thickness on the average evaporation rate. We can see that for all the drying conditions ER_{avg} is constant for initial water thicknesses below 1 kg/m^2. If we look at the evaporation rate values, we see that the thickness effect varies for the different air conditions. In particular, from the AC7 to AC1 the evaporation rate increases from 0.38

kg/m²/h to 1.2 kg/m²/h (about 300% increase) for initial thicknesses below 1 kg/m², while for thicknesses above 4 kg/m² the increase is only from 0.10 kg/m²/h to 0.2 kg/m²/h (about 200% increase). These results confirm that it is extremely important to control the coating layer thickness in order to achieve control of the drying time.

The effect of the evaporation rate variation on the drying time can be seen in **Figure 3.**17b. We can see that the drying time increases linearly with the initial water thicknesses for values below 1 kg/m², this reflects the fact that a linear increase initial water to be evaporated and a constant drying rate will provide a linear increase in drying time. On the other hand, for thicknesses above 1 kg/m² the drying time increases more than linearly with increases of initial water thickness. This is because not only there is more water to be evaporated but also because the evaporation rate is decreasing. We can therefore conclude that to minimize drying time a water coating thickness below 1 kg/m² should be used.

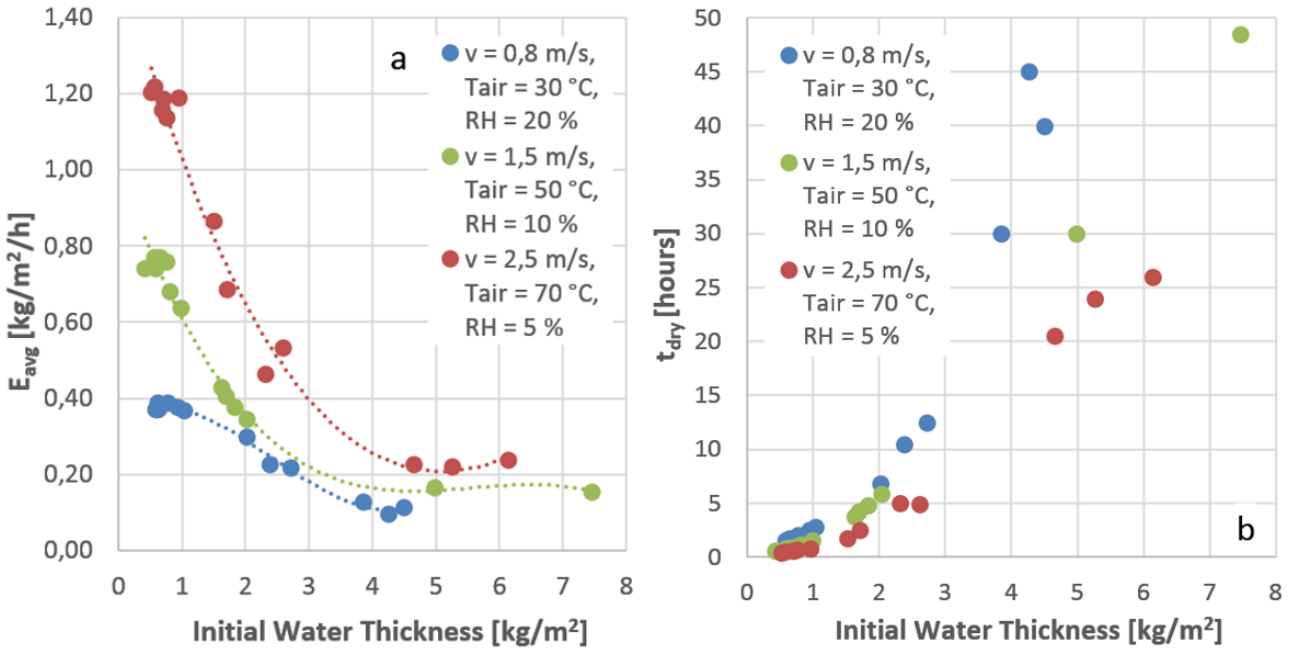

Figure 3.17 Effect of air conditions and initial water thickness on a) average evaporation rate and b) drying time.

In Figure 3.18a we can see that the ER_{max}/ER_{avg} ratio is typically between 2 and 3 for initial water thicknesses below 1 kg/m² while it increases up to 14 for initial water thicknesses of 6 kg/m². This means that driers dimensioned on ER_{max} in order to avoid problems with condensation will have to be significantly over dimensioned if coating thicknesses exceeding 1 kg/m² are to be dried.
Figure 3.18b we see that for samples with less than 1 kg/m² of initial water thickness the ratio t_1/t_{dry} is comprised between 0.20 (for AC7) and 0.40 (for AC1), therefore for at least 20% of drying time

evaporation from the surface to the air is the driving phenomena. For higher water thicknesses the t_1/t_{dry} ratio drops to less than 0.05 therefore, in this case, for most of the drying time diffusion from the inner layers is the driving phenomena.

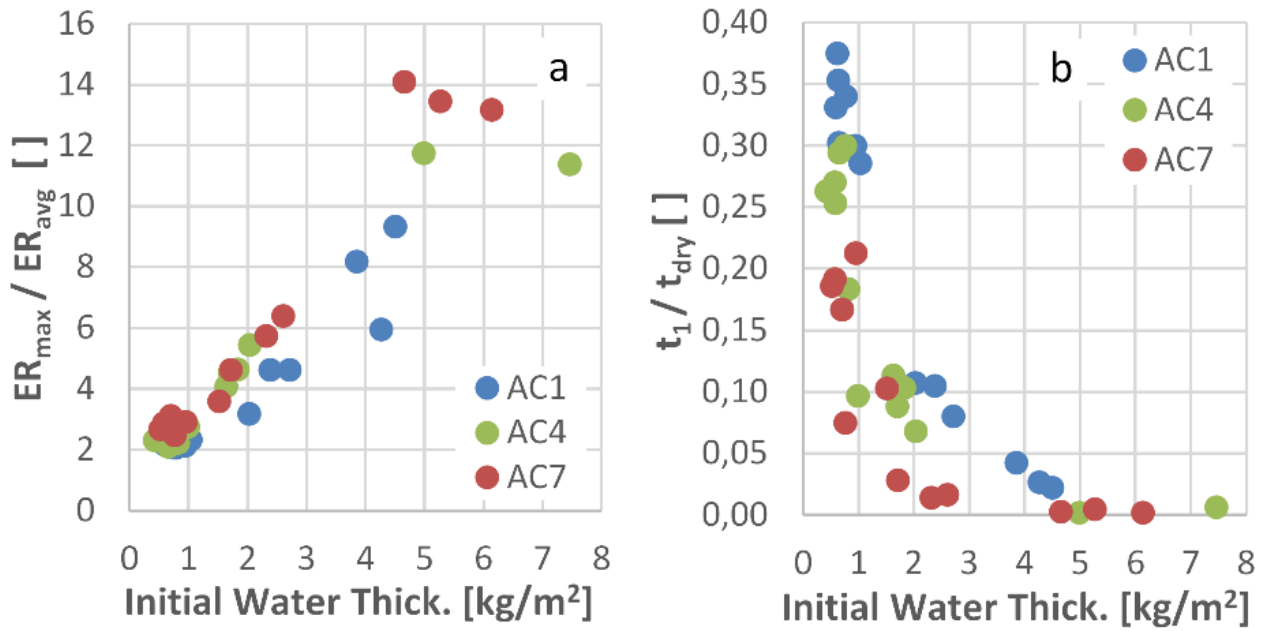

Figure 3.18 Effect of air conditions and initial water thickness on a) ER_{max}/ER_{avg} ratio and b) surface temperature transition times t_1.

The above results can be summarised by stating that the initial coating thickness is the main factor determining the evaporation rate, and therefore drying time, of water based coated furan sand moulds. In particular, for low initial water thicknesses, evaporation from the surface to the air is determining the evaporation rate. In this case, it is mainly the combination of temperature, humidity and velocity that controls the drying time. While for samples with higher thicknesses, diffusion of water from the inner layers of the samples to the surface is the determining phenomena. For high initial water thicknesses, evaporation is slower and air conditions effect is less relevant than for low initial water thicknesses.

3.3.2 - Effect of Air Properties

Figure 3.19 shows the average evaporation rates for the tests where air properties are varied. We can clearly see that increasing air speed and temperature will increase evaporation rate, while increasing relative humidity decreases the evaporation rate. In particular, we can see that there is a non-linear the relation between relative humidity and evaporation rate, especially for the higher

values. Additionally we note that, by varying air drying conditions in the considered range it is possible to achieve variations of average evaporation rates from 0.1 to 1.2 kg/m^2/h (1200 % increase), this confirms that good control of air drying conditions is critical to controlling evaporation rates and therefore the drying time.

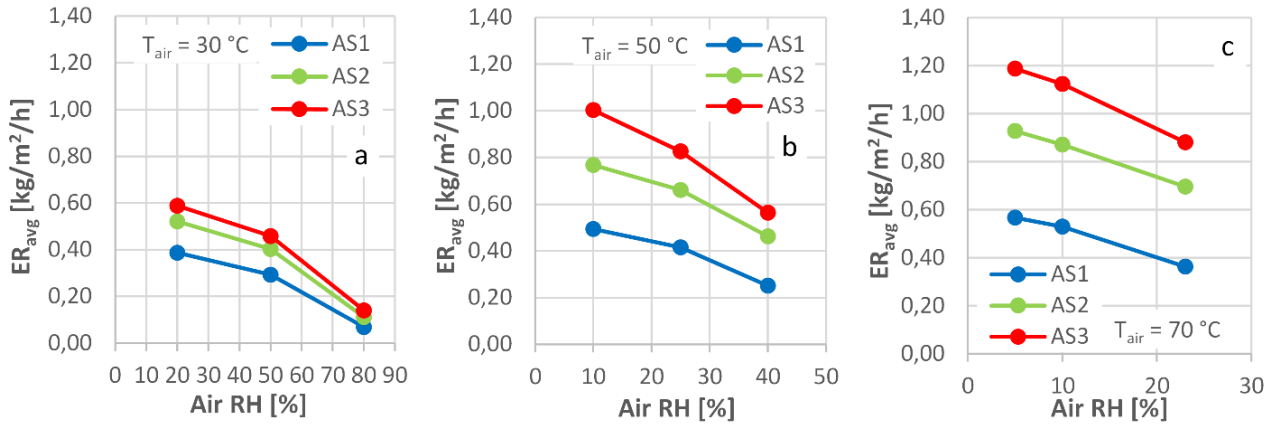

Figure 3.19. Average evaporation rates results a) at 30 °C, b) 50 °C and c) 70 °C.

Figure 3.20 shows that the ER_{max}/ER_{avg} ratio varies between 1.4 and 3.0. It is therefore necessary to over dimension the drier power from 40% to 300% compared to the average power needed depending on the drying conditions used. In particular low relative humidity gives higher ER_{max}/ER_{avg} ratios.

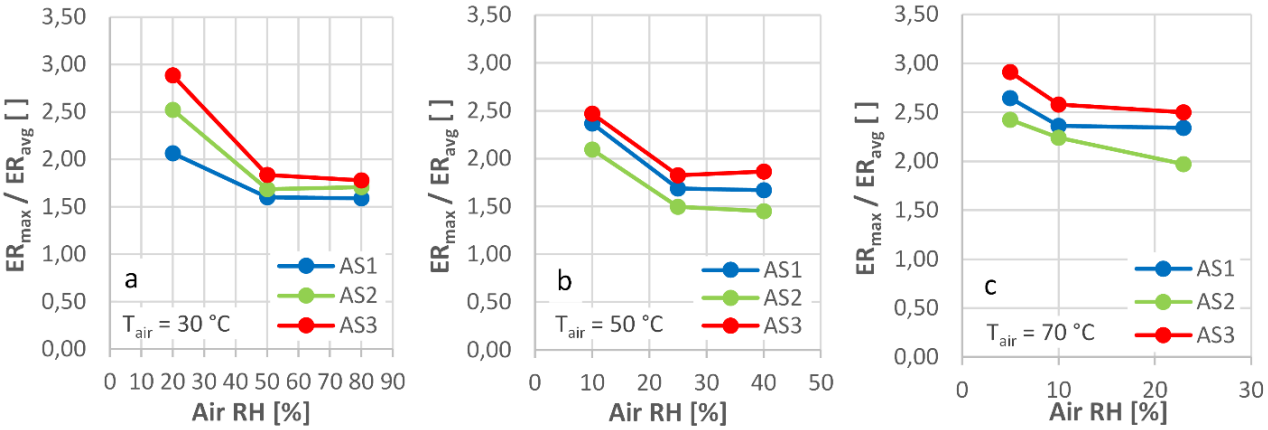

Figure 3.20 ER_{max}/ER_{max} ratio results at 30 °C (a), 50 °C (b) and 70 °C (c).

In order to provide a useful tool for the drying process and equipment design the experimental data has been fitted with a second order polynomial (Eq.3.1) where V_{air} is expressed in m/s, T_{air} in °C and RH in %. The coefficient of determination obtained is 99.31 %.

The polynomial is then used to build design maps that drying process designers can use a simple tool (Figure 3.21 and Supplement III).

$$ER_{avg} = -0.556 + 0{,}4022\,V_{air} + 0{,}02264\,T_{air} + 0{,}01611\,RH - 0{,}1031\,V_{air}^2 - 0{,}000178\,T_{air}^2 - 0{,}000085\,RH^2 + 0{,}004368\,V_{air}T_{air} - 0{,}001980\,V_{air}\,RH \quad - 0{,}000371 T_{air}\,RH \qquad \text{Eq.3.1}$$

$$R^2 = 99.31\%$$

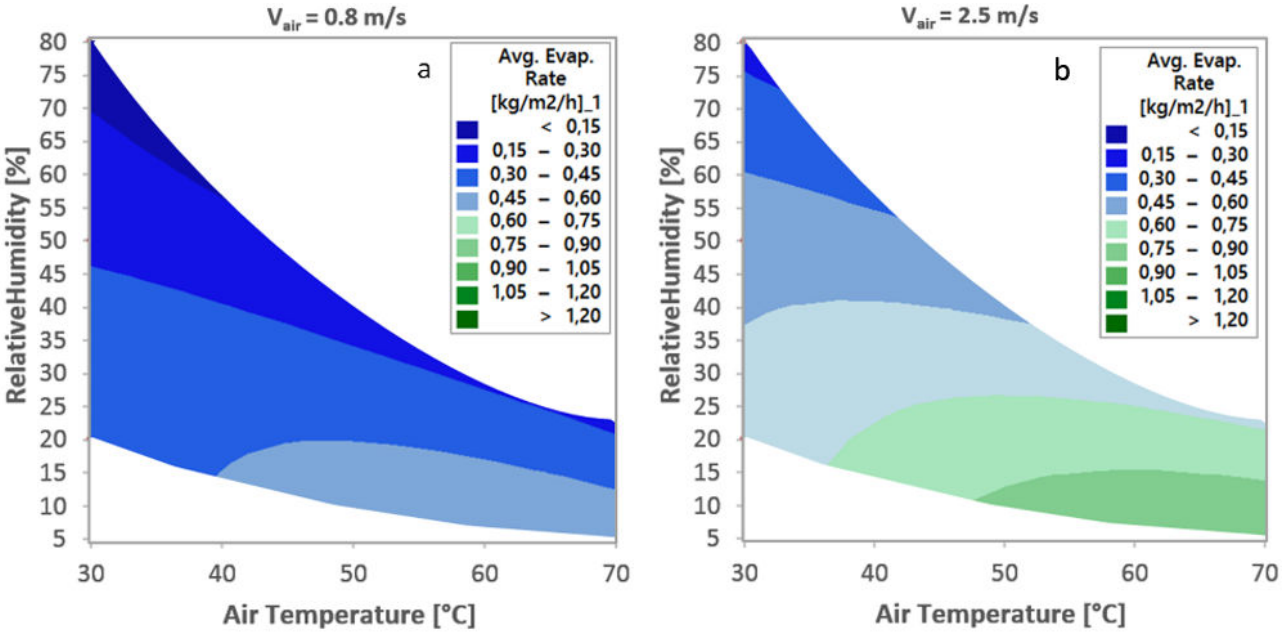

Figure 3.21 Average evaporation rates design maps for air speeds of a) 0.8 m/s and b) 2.5 m/s.

As a final check, we plot surface temperature of the samples during the initial drying stage ($T_{surf,min}$) versus the wet bulb temperature of the air used for the drying. As we can see (Figure 3.22) there is good overall agreement except for low and high wet bulb temperature situations. For low wet bulb temperatures (Figure 3.22a) the sample is drying at higher temperature, this is because initial temperature of the sample (25 °C) is above the wet bulb temperature (16 °C). For high wet bulb temperature (Figure 3.22b) the sample is drying at lower temperature, this is because initial temperature of the sample (25 °C) is significantly below the wet bulb temperature (45 °C).

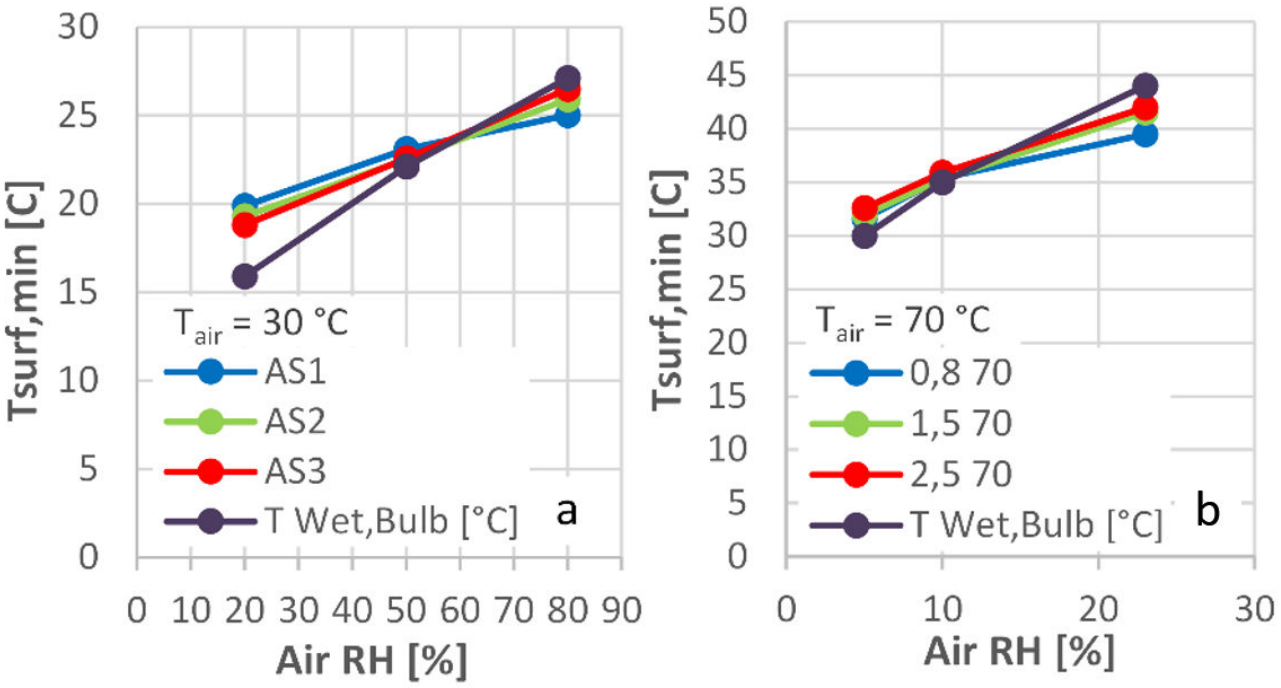

Figure 3.22 Initial surface temperature results for drying a) at 30 °C and b) at 70 °C versus air wet bulb temperature.

3.3.3 - Characteristic Curves

Drying curves are used to understand how the water is released from the material as a function of moisture. Thanks to these curves it is possible to calculate evaporation rates based on the residual moisture in the sample and therefore improve the accuracy of drying simulations. As described in [22] these curves are function of material type and should be independent of drying condition.

In this last result section we analyse the effect of initial water thickness and drying conditions on the characteristic drying curves.

In Figure 3.23a we can see how for increasing initial water thicknesses the shape of the curve is heavily affected. Coating density does not have significant effect on the curves shape (Figure 3.23b) Air conditions seem to have minor effects (Figure 3.23c), especially in the initial stages of drying (moisture ratio above 0.9) when the evaporation rate has its maximum. Also, in air conditions effect curves the noise is more visible since supply of dry and wet are was used more frequently and the high levels of air speed were used.

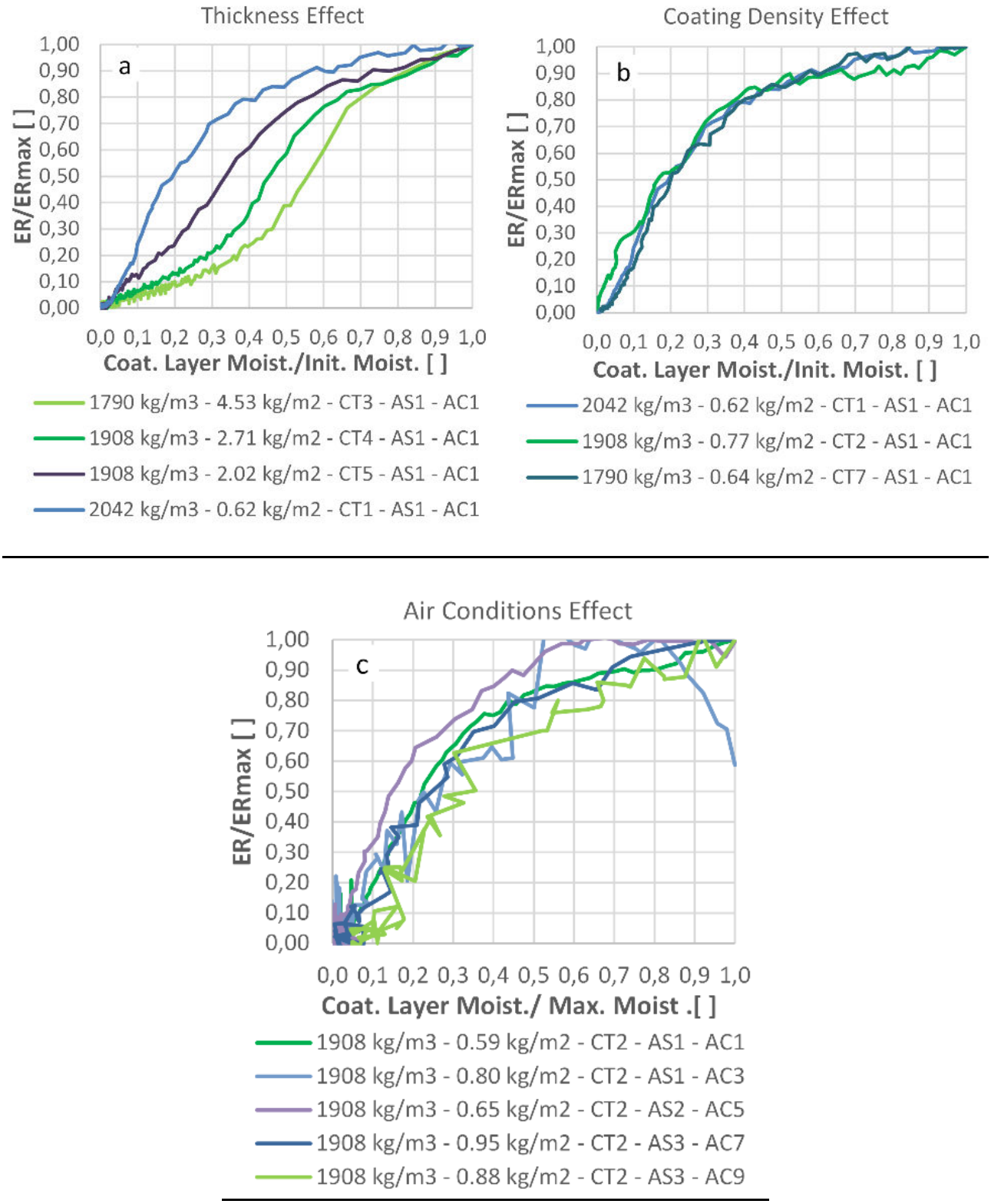

Figure 3.23 Effect of coating thickness (a), density (b) and drying condition (c) on the characteristic drying curves.

3.4 - Residual Moisture Tests Results

At the end of the drying process the coating and mould materials will, over time, tend to reach a residual moisture level in equilibrium with the surrounding air conditions. In order to quantify the residual moisture and to help define the moisture level at which the mould and coating under production conditions should be considered dry, this section presents the results of the residual moisture tests carried out in this study.

Figure 3.24 a and 5 show the sorption curves respectively for GCX F furan bonded sand and for foundry coating at 15 °C, 25 °C and 35 °C. It can be seen that, for both materials, temperature does not have a significant effect. On the other hand, air humidity has a major effect. For both materials, moisture can be as low as 0.1% at 5% RH and become as high as 0.6% at 95% RH. Even though the absolute values seem small, we need to notice that from 0.10 % to 0.60% there is a variation of 600%. Additionally, large amounts of moulding sands are used in each mould. For example a 40 tons mould might contain as low as 40 kg of water at 0.1% moisture (if dried at 5% RH for enough time) or as much 240 kg of water at 0.6 % moisture (if stored for enough time at 95% RH). It is therefore important to be aware of this variation when designing the drying process. In a similar way factory environment conditions and venting channels routings in the moulds should be chosen based the required values of residual moisture allowed in the mould.

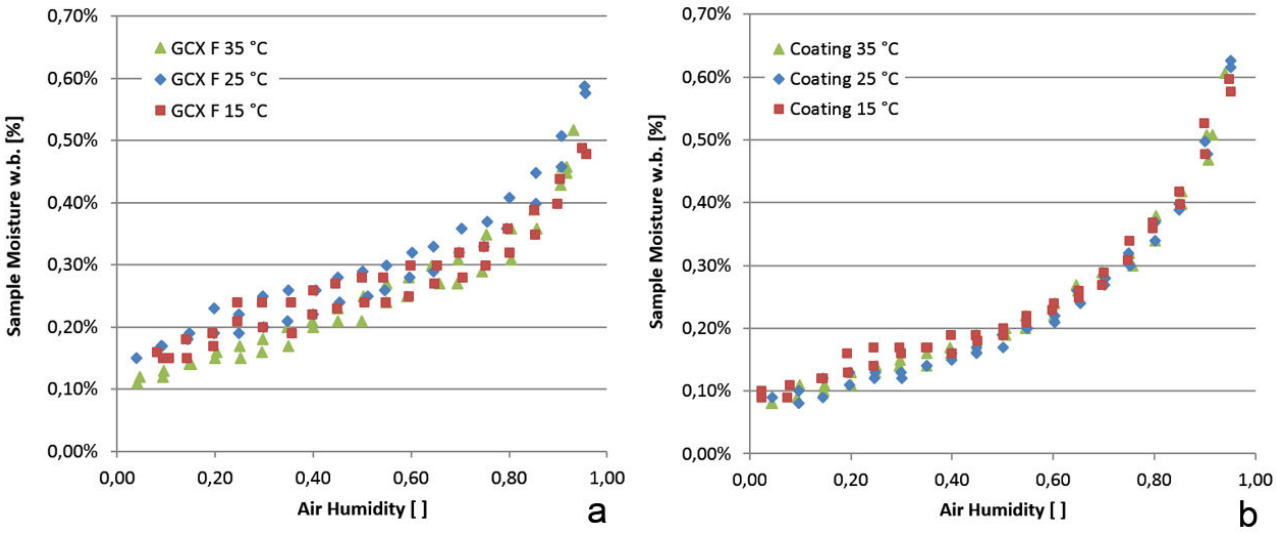

Figure 3.24 Sorption curves at 15 °C, 25 °C and 35 °C for a) sand and b) coating.

Another important conclusion is that the hysteretic behaviour between adsorption and desorption is fairly limited especially for the coating. For the moulding sand, where there is slightly more

hysteresis, the difference between sorption and desorption curve is typically less than 0.05% in moisture.

Figure 3.25a shows that the effect of a 2% dust addition causes a small increase in moisture levels, for example from 0.20% to 0.24% at 50% relative humidity. However, pure dust can contain from 0.30% to 1.70% moisture, it is therefore important to reduce dust segregation in silos to avoid lumps of dust in the moulds.

Figure 3.25b shows a comparison between moulding sands bonded with different binder types and un-bonded sand. It can be seen that un-bonded sand has the smallest moisture content (between 0.04% and 0.20%), it has no hysteresis between adsorption and desorption and moisture value is a linear function of air humidity. When adding binder the behaviour becomes nonlinear and the moisture level increases up to 4 times that of the un-bonded sand. This is a confirmation of the hydrophilic nature of furan binding systems.

Also we can see that a binder like GCM has significantly lower moisture level compared to the other binders, and it could therefore be used in moulds that are more prone to gas defects. For example, considering a 40 ton mould at 90 % RH where GCM binder is used, it will have a moisture of 0.30 % and therefore a water content of 120 kg. On the other hand if GCK or GCGG binders are used, the same mould will have a moisture content of about 0.55 % at 90% RH, which translates to a water content of 220 kg (almost double the one of VCM binder). Finally, the highest moisture content is 0.75%, given by GCGG binder at 95% RH, this translates in a quantity of 300 kg of water for a 40 tons mould.

These results show that different amounts and brands of furan binders can have different performance with respect to moisture content. Sorption tests can help to quantify these performances and to choose the right material recipe.

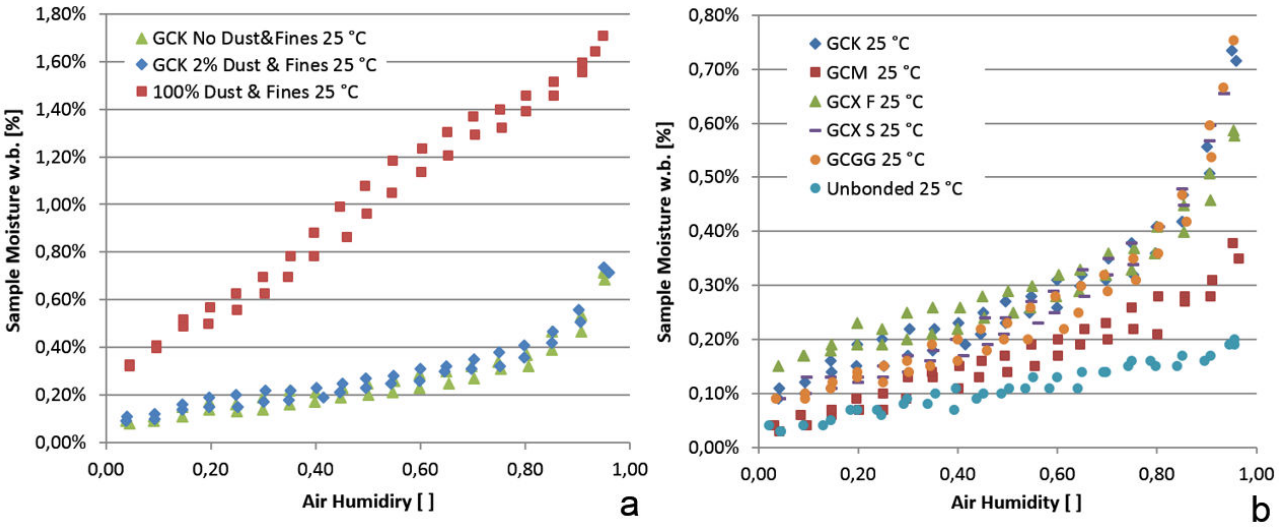

Figure 3.25 Sorption curves for a) dust, sand with 0% and 2% of dust and fines, b) sand with different binders and un-bonded sand.

3.5 - Moisture Diffusion Tests

In this section we present the results from the moisture diffusion tests. In this tests we investigate the effects of different test methodologies and process parameters on the moisture diffusion coefficients. Moisture diffusion coefficients determination is needed in order to calculate the moisture absorbed or released by moulds as a function of production time and dimensions.

3.5.1 - Manual Test Method Results

We start by looking at all the results obtained from the manual tests (Figure 3.26). The first large effect that we notice is the one of relative humidity. For example, in the tests carried out at 95% RH on GCM sand we have moisture coefficients values of about 1,00E-8 m^2/s, while for the same sand tested at 40% RH the moisture diffusion coefficient increases to around 2,40E-8 m^2/s.
The second effect that we see is the one of binder type. If we consider GCM sand at 40% RH the diffusion coefficient is around 2.40E-8 m^2/s while for GCK sand at 40% RH the diffusion coefficient drops to around 1.80E-8 m^2/s.

As with regard to compaction effect, in the range of density considered, there is a small effect for very low densities. For example GCK sand tested at 40% RH has diffusion coefficient of 1.2E-8 m^2/s at a density 1140 kg/m^3 while the other test samples are scattered around 1.00 E-8 m^2/s. For density

between 1250 kg/m^3 and 1550 kg/m^3 there seem to be no appreciable effect of density on the moisture diffusion coefficients values.

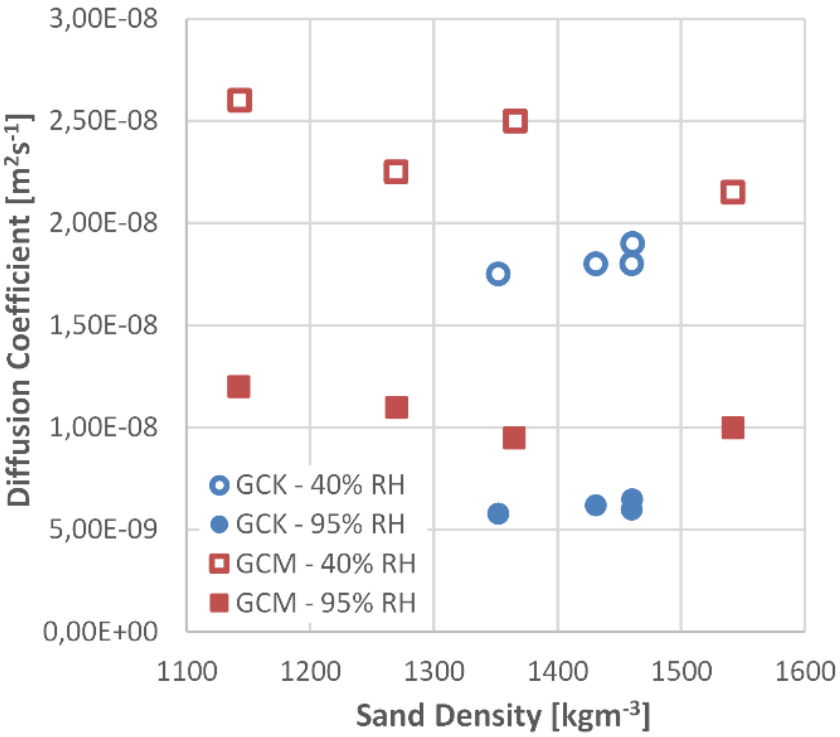

Figure 3.26 Density effect on moisture diffusion coefficient obtained with manual test method.

3.5.2 - Automatic Test Method Results

Figure 3.27 compares the results from the automatic tests and manual tests. With regard to the agreement between the results from the automatic test and the manual sorption tests, we see that there is good agreement for the tests at 40 % RH, but for the tests at 95% the manual tests are slightly overestimating the diffusion coefficients. This error is probably due to the fact that, since the moisture diffusion coefficients are not constant with relative humidity (as see confirmed by both tests), the value obtained from testing at 95% starting from a sample equilibrated at 5% will be influenced by the values of the diffusion coefficient at the intermediate relative humidities.

For both materials we see that the strong effect of relative humidity is confirmed also for the automatic tests. In particular, for relative humidity below 60% the diffusion coefficients show little variation, while there is sharp increase for humidity above 60%.
The binder effect is also shown clearly by the automatic tests.

If we compare the obtained values (4.00 E-9 m^2/s to 2.7E-8 m^2/s) to the ones available in literature [33] for somewhat similar ceramic material like concrete (5.0E-10 m^2/s to 1.2E-8 m^2/s), clay brick (1.3E-8 m^2/s to 1.4E-8 m^2/s) and sand (8.0E-8 m^2/s to 1.5E-7 m^2/s) we see that they are comparable.

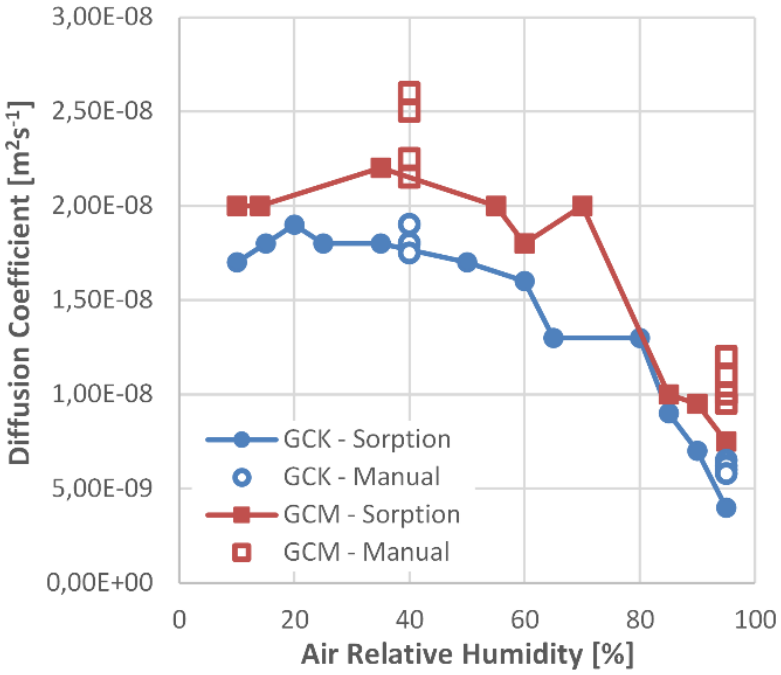

Figure 3.27 Effect of test method and air relative humidity on moisture diffusion coefficient of GCK and GCM furan sands.

Figure 3.28a shows the results obtained for different furan binder brands. We can see for example how some binders (like GCXS, GCGG and GCM) have a higher moisture diffusivity than other at low relative humidity value. On the other hand, for higher relative humidity value the differences between different binders behaviour becomes smaller.

It is also interesting to note how, for unbounded sand, we have the highest diffusion coefficient value (up to 3.1E-8 m^2/s) that decrease linearly for increasing relative humidity, while, for bonded sands, we have an nonlinear relation between diffusion coefficient values and relative humidity. These behaviours are in line with results found in section 3.4 where we show that sand moisture content increases linearly with relative humidity and is quite low, while the binder has a higher moisture content and a non-linear sorption curve.

With regard to the effect of dust content, in Figure 3.28b we see that pure dust has lower diffusion coefficients almost over the whole range of relative humidity values. Coherently with that, we see that the sample with 2% dust has slight lower diffusion coefficients than the one with no dust. This

is also in line with the fact that dust retains more moisture than bonded sand as shown in section 3.4.

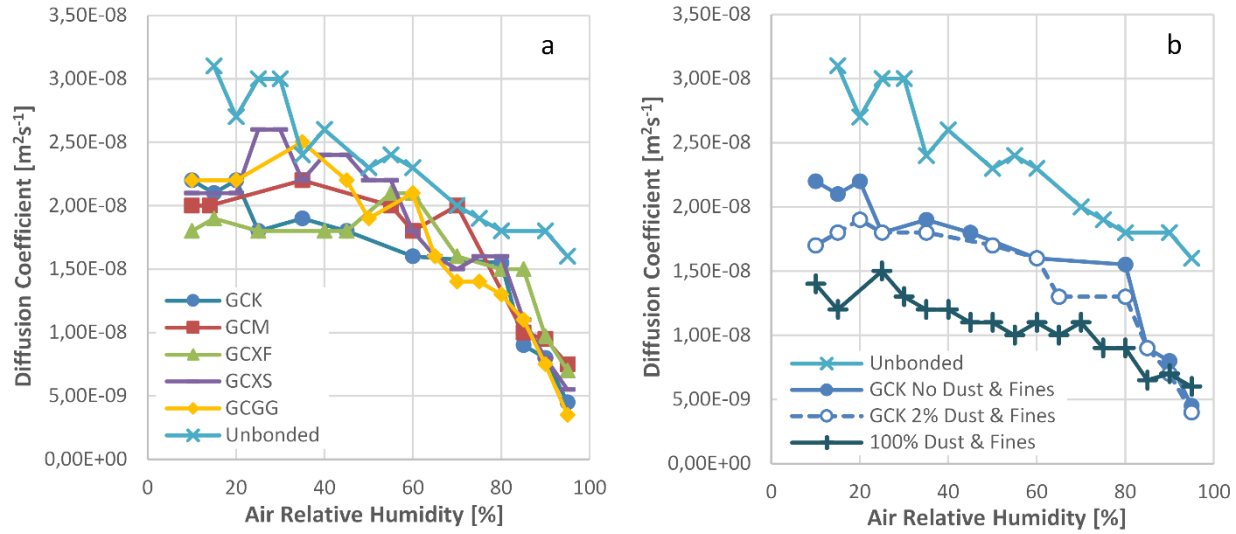

Figure 3.28 a) Effect of binder type and air relative humidity on moisture diffusion coefficient furan bonded sands. b) Effect of dust levels and air relative humidity on moisture diffusion coefficient of GCK furan bonded sand.

The effect of temperature in GCXF furan sand can be seen in Figure 3.29a. We see that an increase in temperature form 25 °C to 35 °C leads to an increase of the moisture diffusion coefficient for relative humidity values below 60%. A decrease in temperature from 25 °C to 15 °C does not have a significant effect of the diffusion coefficient.

Figure 3.29b shows how an increase in temperature from 25 °C to 35 °C causes an increase in moisture diffusion coefficients for water based foundry coatings. A decrease in temperature from 25 °C to 15 ° shows small decrease in the diffusion coefficient values. This is in line with what is typically found in literature and practical experience (increasing temperature will speed up moisture migration).

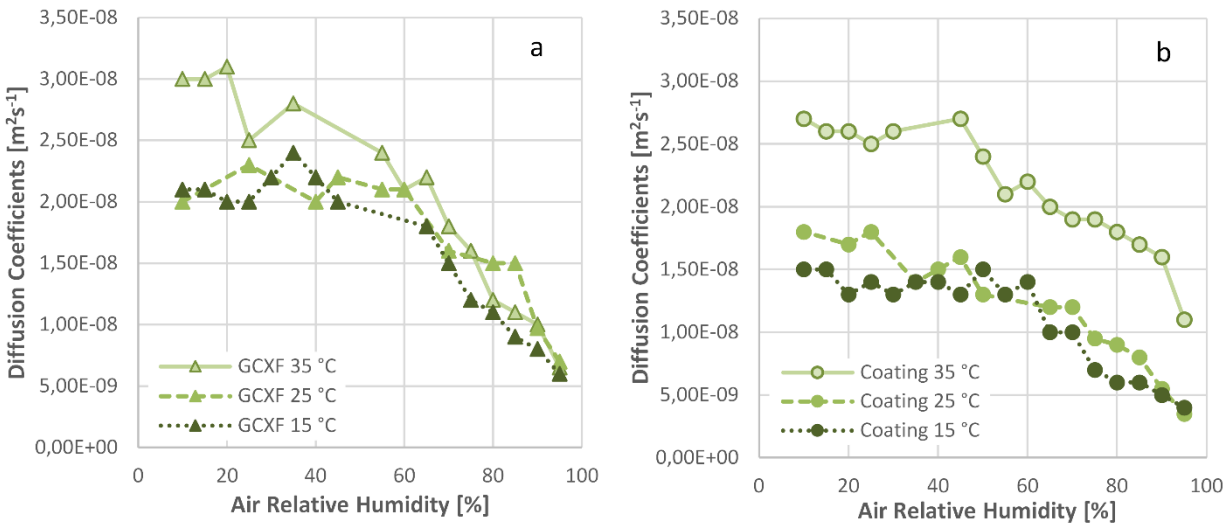

Figure 3.29 a) Effect of temperature and air relative humidity on moisture diffusion coefficient of GCXF furan bonded sand. b) Effect of temperature and air relative humidity on moisture diffusion coefficient of water based foundry coating.

3.5.3 - Possible Sources of Error

Figure 3.30a shows a typical fit of Eq.2.1.a and 2.1.b with results from manual sorption tests. We can see that there is no visible scatter, and that the solution approximates the experimental data well especially in the first part of the curve, while in the final part we have a small error. This error is most likely due to the fact that we are fitting a constant diffusion coefficient solution to a material that does not have constant diffusion coefficients.

Other possible error inherent to manual tests method can be subjected are due possible incorrect initial equilibration and lack of stability of test conditions. These will result in applying different boundary conditions to sample as compared to the one used in the mathematical model.
Figure 3.30b shows a typical fit of Eq.2.1.a and 2.1.b with results from automatic sorption tests. We can see that there is more scatter in these data. Possible cause for this is the fact that we are now using smaller samples and test steps (which decrees the quantity of adsorbed water therefore reducing the relative accuracy of the weight measurement) and adding/removing dry and humid air to control the chamber conditions (therefore perturbing the air around the sample and introducing noise in the weight measurement).

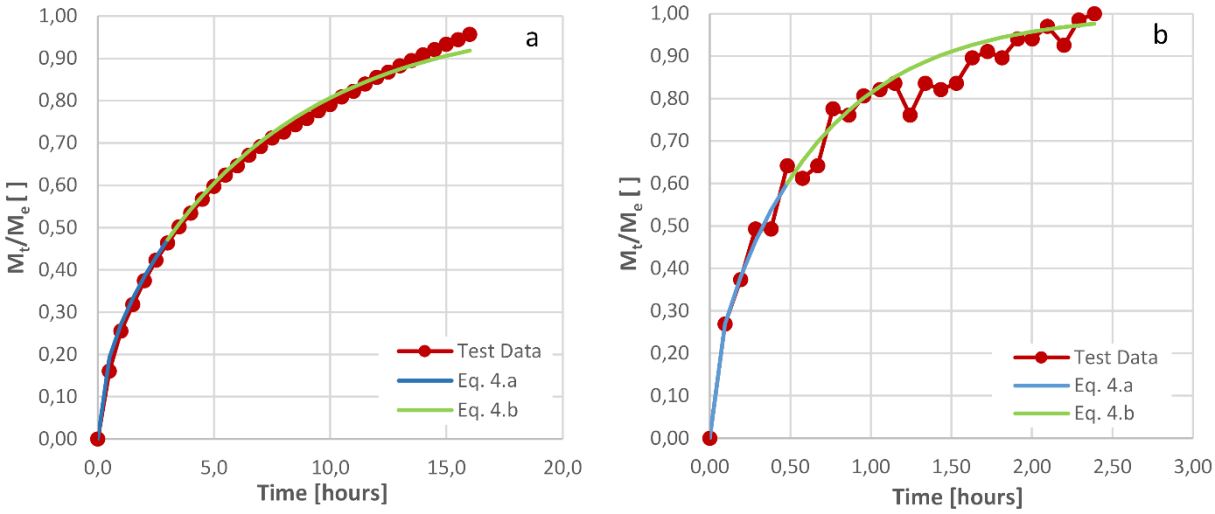

Figure 3.30 a) Typical fit results for a manual sorption test. b) Typical fit result for an automatic sorption test.

3.6 - Moisture Measurement Tests Results

3.6.1 - Moisture Tools Comparison Tests

In Figure 3.31we see the results from tests using Tool A with different wire configurations. We can see that tool A provides a full scale reading of 5% moisture at a resistance of 10 kOhm and that the minimum reading for short leads configuration is at 0.9% for a resistance of 100 GOhm. Long wires provide higher % reading for resistance levels above 80 GOhm. For example at 100 GOhm the configuration with standard long wires provide a reading of 0.22 % moisture (a difference of about 144%). Teflon wire significantly reduce the error by providing a reading of 0.12% at 100 GOhm (a difference of 33%).

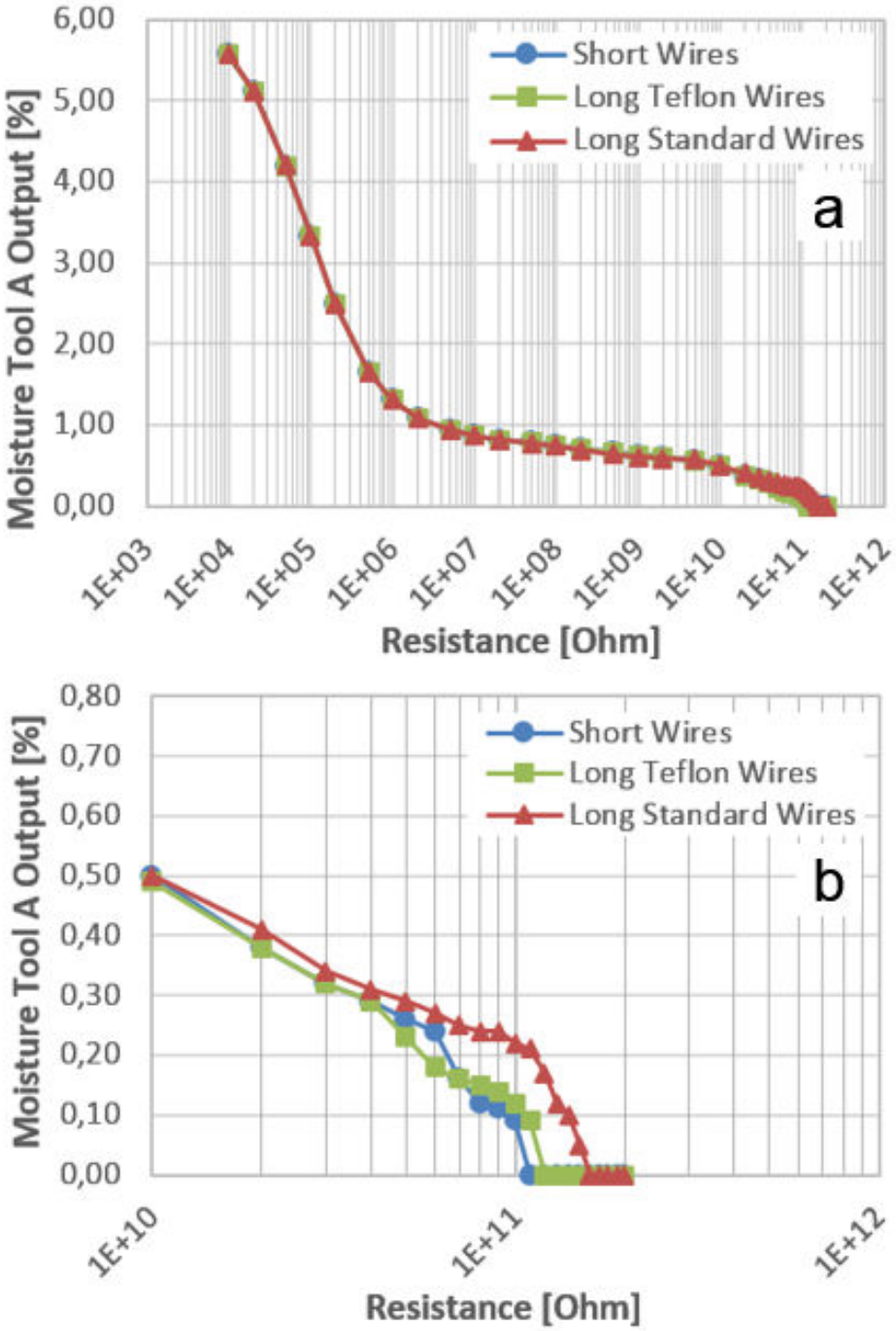

Figure 3.31 Moisture Tool A test results: a) complete range, b) close up on high resistance range.

Results from moisture tool B (Figure 3.32a) show that significant difference exists between setup with short and long wires (both standard and Teflon) already at 20 MOhm. For example at 500 MOhm the output for short wire setup is 8.2 V while for long Teflon wire setup is 9.42 V (a difference of 15%). The differences between readings are also visible at higher resistance values (Figure 3.32b). In particular we can see that the maximum measurable resistance is 110 GOhm with a short wire configuration. The range is then limited to 50 GOhm for long Teflon wire configuration.

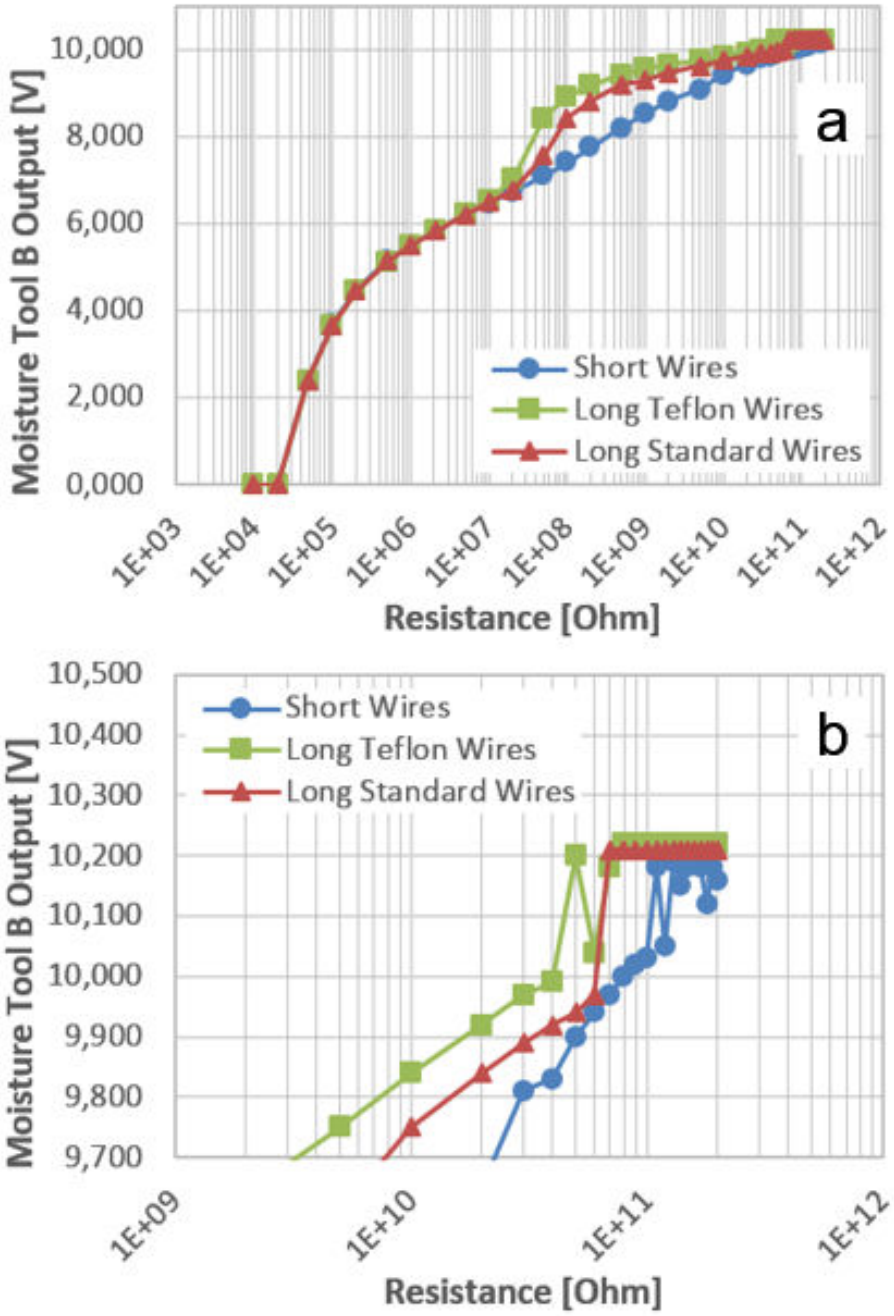

Figure 3.32 Moisture Tool B test results a) complete range, b) close up on high resistance range.

Regarding moisture tool C (Figure 3.33.a) we can see how there seem to be no significant difference between the three wiring configurations. Additionally, the response is logarithmic over the entire resistance range considered. In order to better visualize the results, Figure 3.33b shows the difference between the measured values and the expected voltage response and the nominal resistance values (details in supplement VII) . We can see how long standard wires have higher error at resistances above 30 GOhm, as this error is increasing with increasing resistance it might be due to leakage currents. On the other hand, long Teflon wires and short wires have a similar behavior

above 30 GOhm, and the deviation is smaller than 25mV. This might be related to differences in real resistor value compared to the nominal values (up to 10% as shown in Supplement VII).
From 100 MOhm to 2 GOhm the long Teflon wires measurements are affected by an error up 37 mV. This translates to a difference of only 2% considering the voltage output value of 1,665 V expected at 1 GOhm.
Tool C has therefore the most stable response and smaller error over the widest range considered.

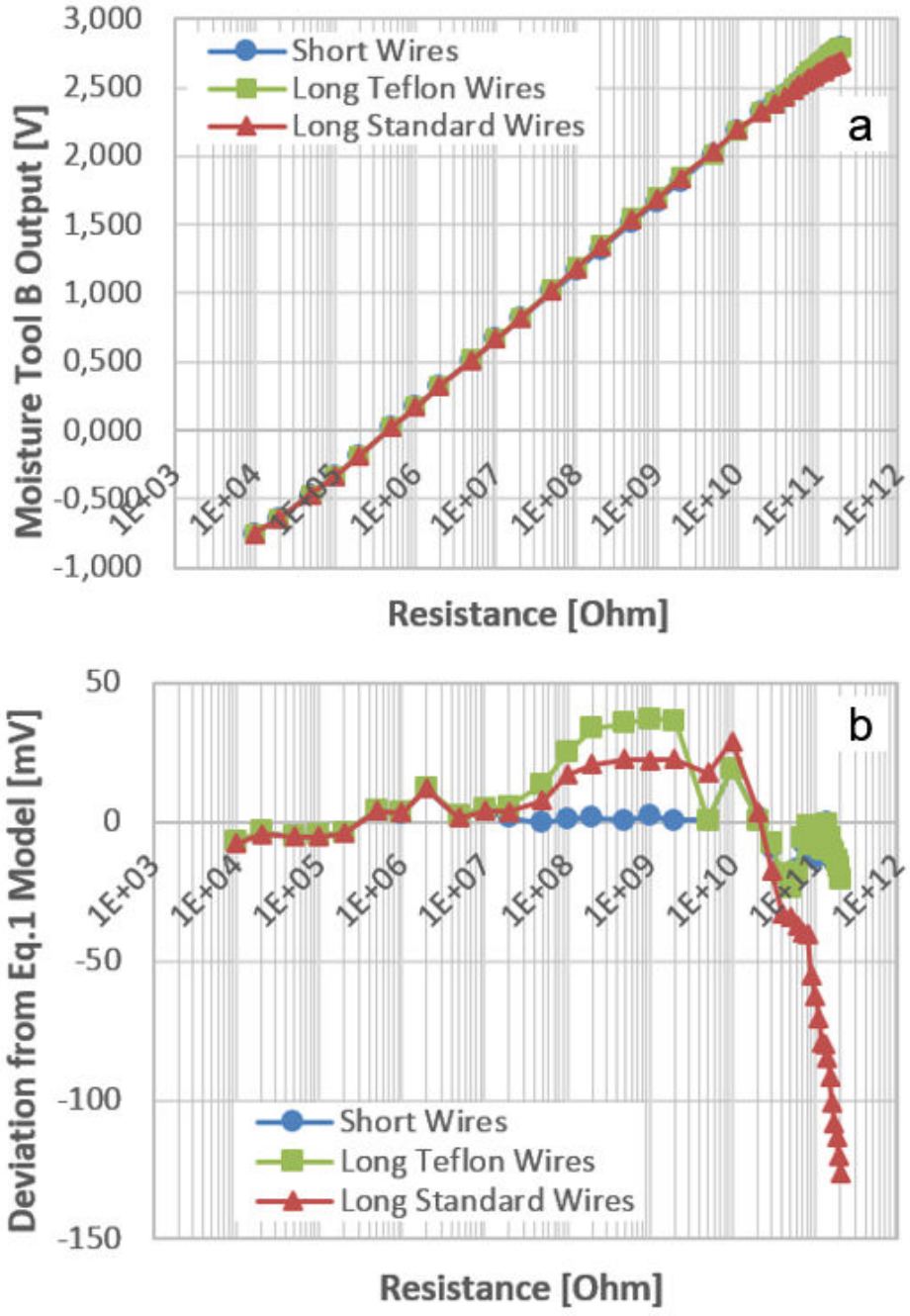

Figure 3.33 Moisture Tool C test results: a) complete range, b) deviation with respect to calculated nominal value.

3.6.2 - Moisture-Resistance Correlation Tests

In this section we report the results from the tests done in order to correlate the moisture content in the coating with its resistance. Figure 3.34 and Figure 3.35 show the results of five tested samples and the three curves fitted in order to obtain a moisture-resistance correlation.

From an overall point of view Figure 3.34, we can see that the correlation between moisture and resistance is strongly nonlinear. In particular, a marked increase in resistance occurs for moisture levels above 5%.

In order to best fit the moisture-resistance curve three different equations are used. Each equation is provided with the resistance range values in which it is applicable in Supplement VII. We can see how, up to 1.4 MOhm the use of a power law function (on a logarithmic scale) is needed to accommodate for the curvature of the curve, above this value a log-log law is used.

Regarding the accuracy, for moisture levels above 10% the typical scatter is +/- 3% in moisture. Between 5% and 10% moisture reading the typical scatter is within 2% and between 5% and 2% moisture is less than 1%. For moisture levels below two 2% (Fig 9.b) the data is typically scattered in the range of +/- 0.25%. Details can be found on Supplement VII.

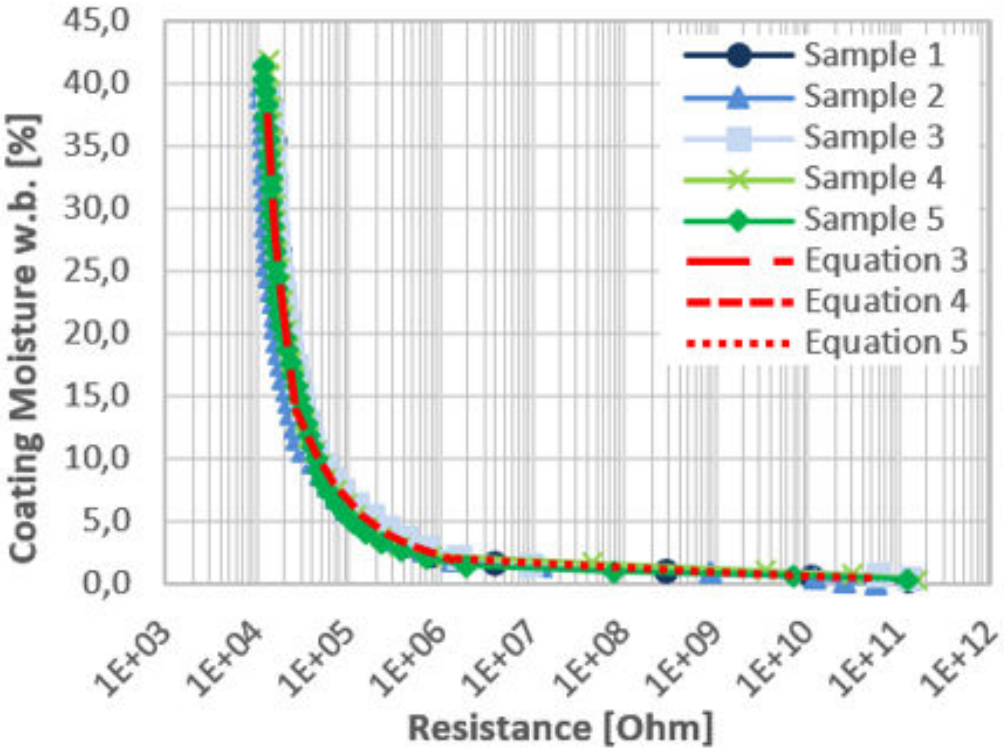

Figure 3.34 Moisture-Resistance calibration results: complete range.

As additional considerations for the accuracy of the experimental setup and representativeness of the tests, we can see that initial value of moisture in the coating is around 42%. This is in line with results obtained with automatic moisture analyzers for this coating mixture (section 3.1.4). Regarding final moisture of coating, since the samples are dried at 25 C and 50% RH, they do not reach 0% moisture level but an equilibrium moisture level of about 0.5%. Also this value is in line with results from sorption tests carried out in an automatic moisture analyzer for the same coating.

As final results, we show in Figure 3.35 a comparison between the moisture-resistance relationships of concrete (from Tool A tests) and foundry coating. We can see that on the whole moisture range, the coating has significantly higher resistance than concrete for the same moisture level. For example at 1% moisture concrete has a resistance of 3 MOhm, while foundry coating has 1 GOhm.

If moisture tools calibrated for concrete are to be used for assessing moisture in water based foundry coating it is important to be aware of this difference to avoid significant measurements errors. For example a reading of 5% on Tool A will correspond to a moisture of about 40% in the foundry coating.

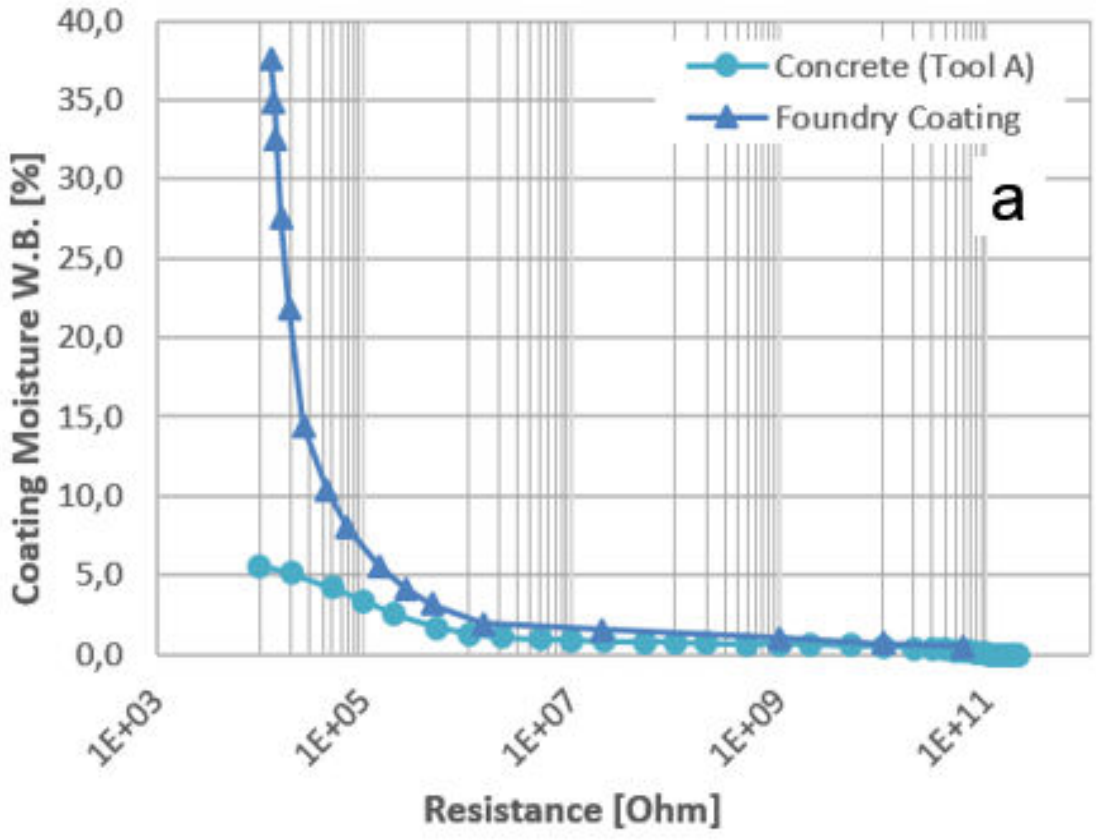

Figure 3.35 Moisture-Resistance relationship of concrete and foundry coating.

3.6.3 - Application to Large Moulds

Figure 3.36 shows how resistance moisture measurements on large size castings can be used to assess the effect of process changes like the changes in settings of drying cabinet. I this case we see the results from the measurement of a cold spot in a mould where changes in the air speed were done to with the air to reduce the drying time. It can be seen like Test 2 items (high a speed) have a drying time consistently shorter than test 1 items (standard air speed).

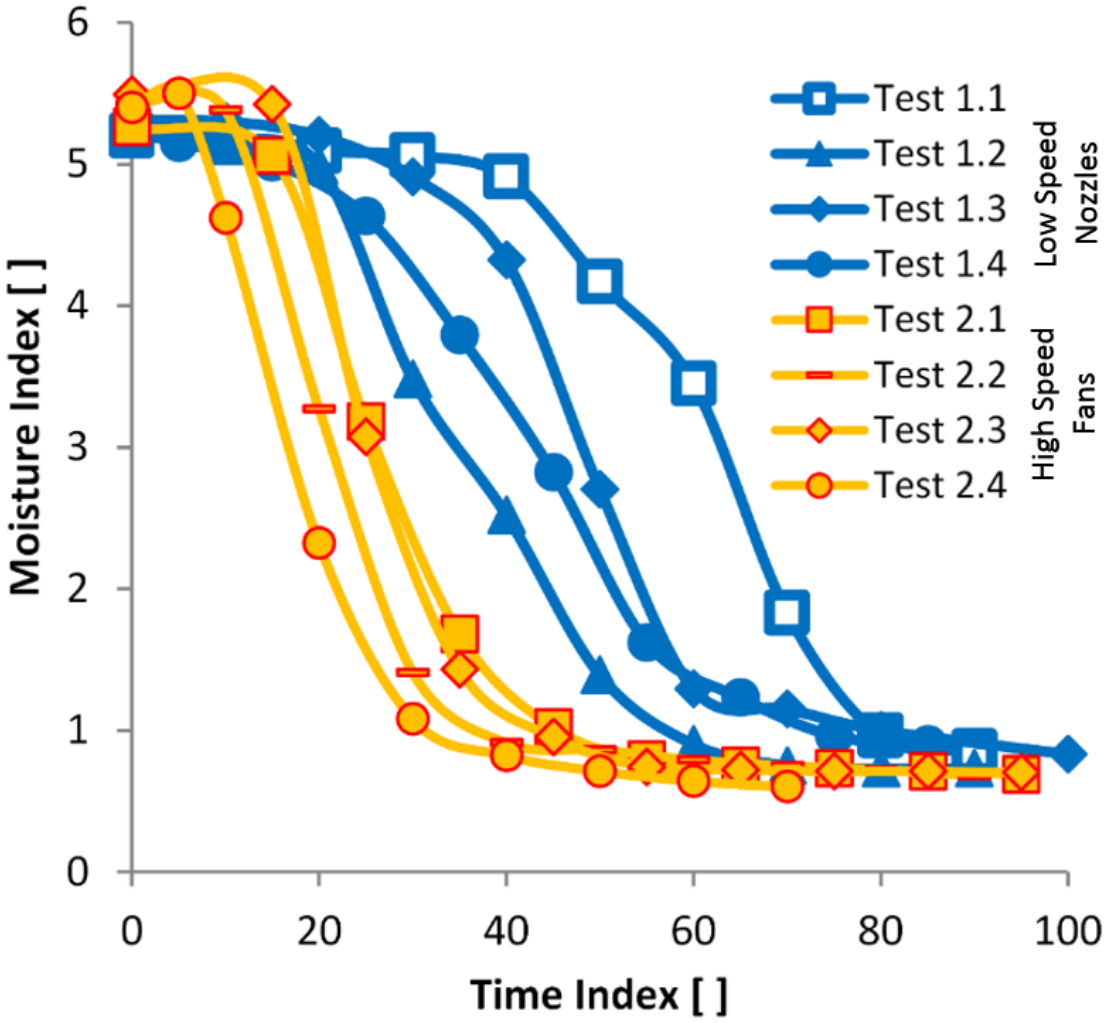

Figure 3.36 Moisture measurements carried out on production moulds with two different settings of drying cabinet were used. Test 2 items show a clear reduction of drying time compared to Test 1 items.

Figure 3.37 shows how moisture variation of the mould surface can be monitored through the complete lifetime of the mould. The effect of the drying process as well as the moisture pick up during the waiting time before assembly can clearly be seen. These measurements can therefore be used to compare differences between moulds and correlate them with possible defects.

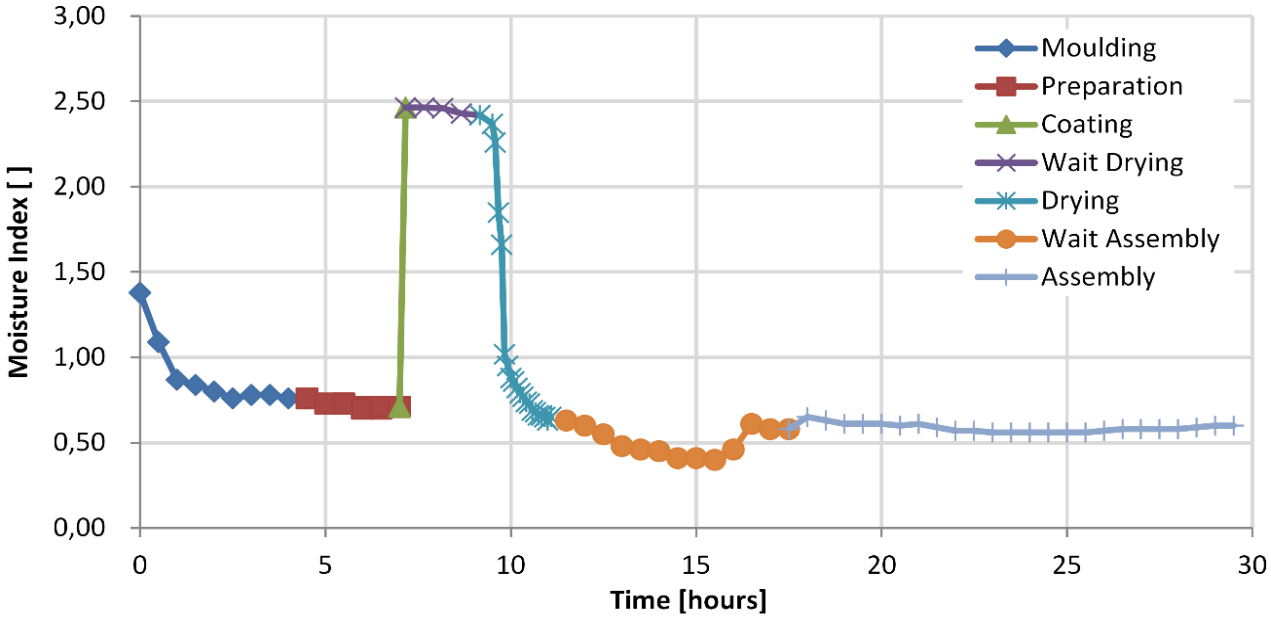

Figure 3.37 Example of process monitoring where moisture at the surface of the mould is measured at regular intervals in all the operations from moulding to assembly. The effect of the drying process can clearly be seen as well as the moisture pick up in during the waiting time before assembly.

3.6.4 - IR Methodology Results

Figure 3.38 shows a picture of a wind turbine hub mould taken with the infrared camera during the drying process. It can be seen how the corners are colder then the surrounding areas as well as some of the outer edges. It is therefore necessary to measure moisture in these areas in order to asses if the mould has been thoroughly dried.

Figure 3.38 Thermography of a mould coated with water based coating. Cold spots can be identified as the last to dry and final moisture measurement performed.

3.7 - Process Design and Simulations Results

3.7.1 - Drying Time Hand Calculation Method

With regard to drying time prediction Figure 3.39 shows how manual calculation method, described in section 2.8.1, can be used to predict drying time of moulds drying in a factory environment. Temperatures and relative humidities recorded in real production over a period of two years have been used to predict drying time of moulds drying in natural convection, low speed forced convection and high speed forced convection.

It can be seen that with natural convection drying time fluctuates from four to more than ten hours but with forced convection the drying time can be reduced to less than 6 hours. In this case it was

shown that just by applying few fans (limited investments) to force convection it was possible to satisfy the need of the production line in the whole year.

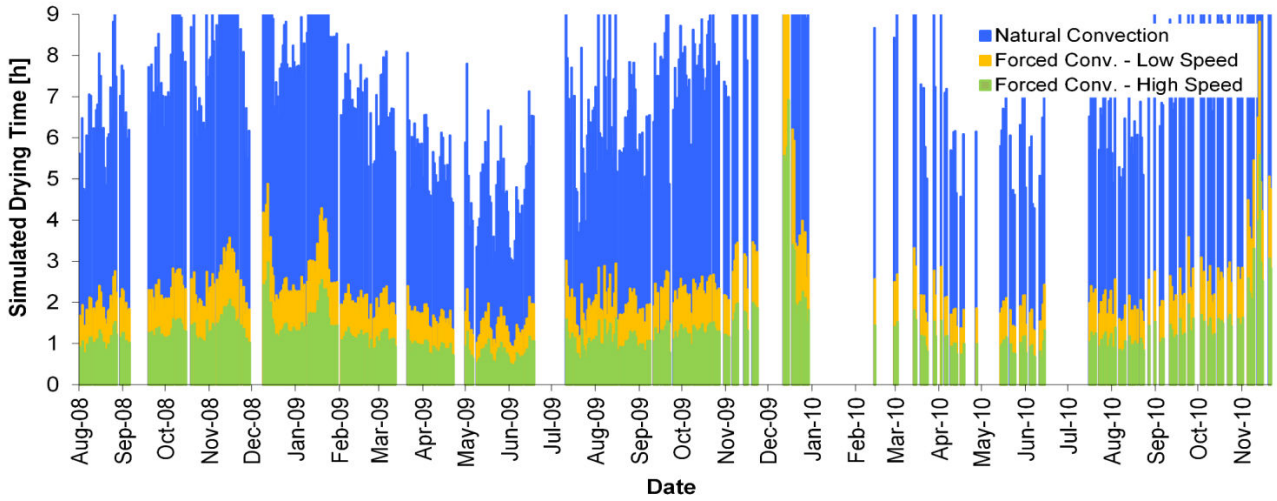

Figure 3.39 Drying time simulation of a mould drying at room conditions with natural convection and two different levels of forced convection. Historical temperature and relative humidity data of the specific geographic site were used.

3.7.2 - Drying Time Numerical Calculation Method

In Figure 3.40 we see an application of the numerical approach to calculate the drying time of a mould dried in a drying cabinet were different return air ratios were used to save energy needed for heating the air to 65 °C. We can see that for a return air ratio of 90 % the relative humidity in the cabinet increases due to the fact that the moisture evaporated form the mould is not completely expelled. Since the relative humidity is not constant the numerical methods is required for the solution.

The results show that as a consequence of the increased humidity level the drying time increases form 1 hour to 1.5 hours for a return air ratio of 90% but does not change significantly for a return air ratio of 50%. This means that it possible to save about 50% of the power needed to heat the air without significant changes to the process.

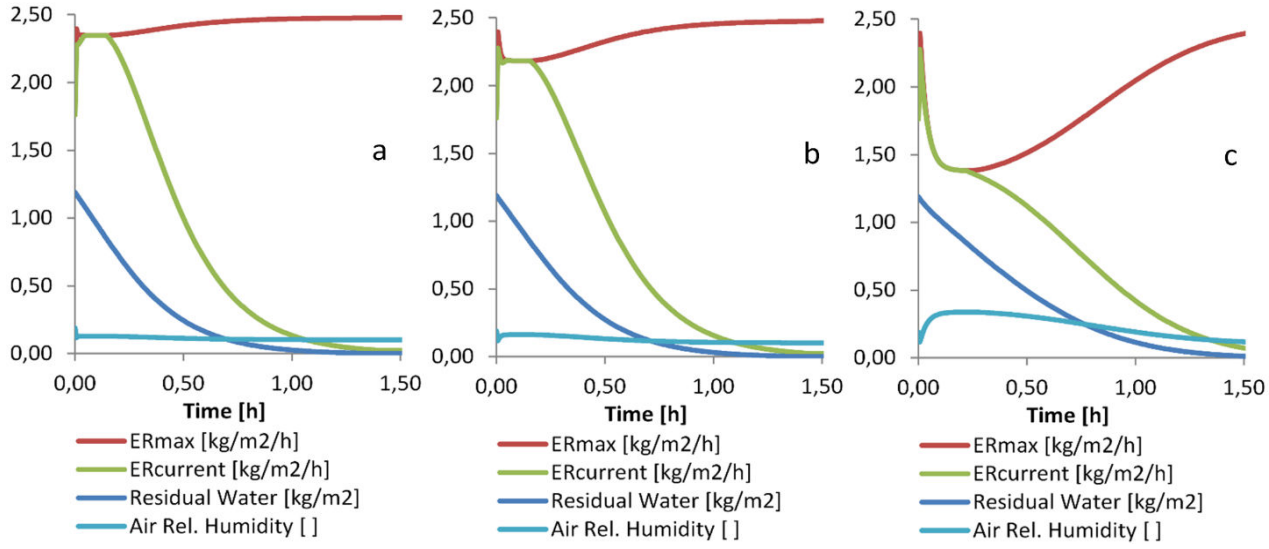

Figure 3.40 Simulations for a drying cabinet with different return air ratios a) 10%, b) 50% and c) 90%. It can be seen how at 90% return air ratio the evaporation rate drops due to an increase in relative humidity and the drying time (residual water <0.01 kg/m^2) increases from 1 hour t 1.5 hours.

3.7.3 - Residual Moisture Calculation

3.7.3.1 - Equilibrium Moisture

After the moulds are dried in a cabinet with low relative humidity and high temperature, they are brought back to environment conditions typically with lower temperature and higher relative humidity. This will cause the moulds to pick up moisture from the surrounding air.

A first estimation of the amount of water that a mould can adsorb is done using the sorption curves obtained in section 3.4. The equilibrium amount of water in a mould is obtained by using equation 2.8 described in section 2.8.3 and considering and M_t/M_e ratio of 1.

In Table 3.2 we see water amounts that are contained in 40 tons moulds for different binder types and relative humidity at equilibrium. It can be seen how water amount can vary from as low as 20 kg to as much as 272 kg. As consequence the risk of vapour and gas defects can be predicted.

Table 3.2 Water amount contained in 40 tons moulds for different binder types and relative humidity at equilibrium.

Binder Type	Air Relative Humidity [%]	Moisture [%]	Water Amount [kg] (40 tons mould)
GCK	10	0.11	44
GCK	50	0.25	100
GCK	90	0.68	272
GCM	10	0.05	20
GCM	50	0.15	60
GCM	90	0.30	120

3.7.3.2 - Time Effect

To take into account the effect of time we want to calculate the amount of moisture that can be picked up by a square sand block of 200 mm in thickness and 2000x2000mm side dimensions of 1120 kg initial mass M_i. The calculation will be performed for cores placed in an environment at 60 % or 90 % RH for 18 hours or 48 hours before usage.

The first step is to plot Eq. 2.1a and 2.1.b as function of time, using a thickness of 200 mm. Based on previous test results, we use for a relative humidity of 60% a moisture diffusion coefficient of 2.00E-8 m^2/s, while for relative humidity of 95% a diffusion coefficient of 8.50E-9 m^2/s.

Figure 3.41 shows how the cores will reach the equilibrium moisture in a longer time if placed in an environment at 90 % RH (dotted line) than compared to cores placed in an environment at 60% RH (continuous line). Now, based on the production times considered (18 and 48 hours) we can enter the graph and extract the ratios M_t/M_e between the adsorbed mass of water M_t at the considered production time t and the adsorbed mass of water at the equilibrium time M_e. The obtained values are reported in Table 3.3.

The next step, is to obtain the equilibrium moisture X_e at the considered relative humidity of the production environment, we will use the adsorption curve for typical GCK furan sand shown in Figure 3.25 and report the values in Table 3.3. It is important to notice that the equilibrium moisture value X_e at 95% RH than is much higher (0.70 %) than that at 60% RH (0.25 %).

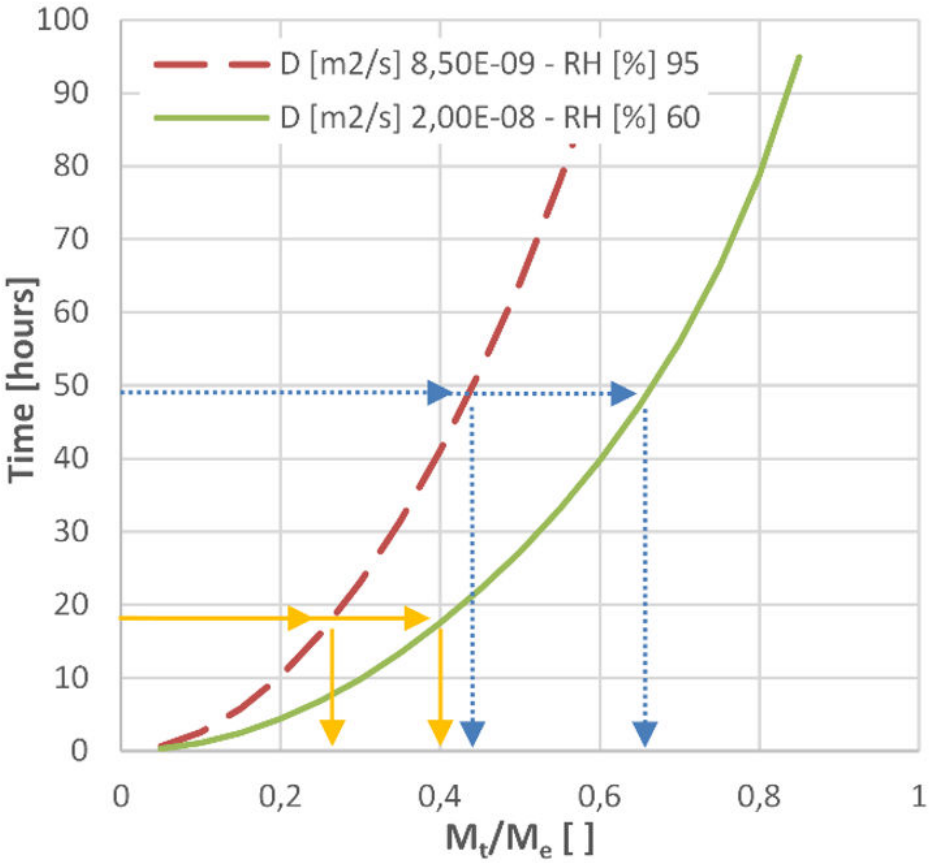

Figure 3.41 Adsorbed mass of water (Eq.2.1.a and Eq.2.1.b) for a core of 200 mm thickness in environments at 60% and 95% relative humidity.

Once we have obtained the M_t/M_e ratios and the equilibrium moistures X_e we can calculate the adsorbed mass of water M_t in the different situations for the considered cores and report the values in Table 3.3. The adsorbed mass M_t of water is simply calculated as shown in 2.8.3

By looking at the results in Table 3.3 we see how a core that is left in an environment at 60% RH for only 18 hours will adsorb 1.12 kg of water. The same core will adsorb 1.82 kg of water (63 % more) if left in the same environment for 48 hours. Similarly it will adsorb 1.96 kg of water (75 % more) if it was left for 18 hours at 95 % RH. The most water, 3.53 kg (216 % more), would be adsorbed for a core in 95 % RH environment for 48 hours.

We clearly notice that controlling production environment humidity to low levels and shortening the time between the completion of drying operation and use of the core can substantially reduce

the amount of water present in the moulds and core and therefore the risks of gas and vapour defects.

Even though the amounts of water involved in the calculation seem small we should recall that each kg of water will generate at least 1.7 m^3 of water vapour when the mould comes in contact with the melt and heats up to 100 °C.

Table 3.3 Summary of moisture pick-up parameters and adsorbed mass of water M_t for a core of dimensions 200x2000x200mm, initial mass M_i of 1120 kg placed in production in environments at 60% and 95% relative humidity for 18 hours and 48 hours.

		X_e [%]	M_e [kg]	M_t/M_e [ ]	M_t [kg]	M_t/M_e [ ]	M_t [kg]
				18 hours		48 hours	
RH [%]	60	0.25	2.8	0.40	1.12	0.65	1.82
	95	0.70	7.8	0.25	1.96	0.45	3.53

3.7.3.3 - Thickness Effect

Finally in Figure 3.42 we show the effect of time and thickness on the equilibration time of furan sand cores. It can be see how core with thickness of less than 50 mm will reach equilibrium (ratio of 1) in less than 24 hours. While large core can pick up more than 30% on the equilibrated moisture values in less 3 days. This shows that it is important to minimize storage time of cores after drying in high humidity environments.

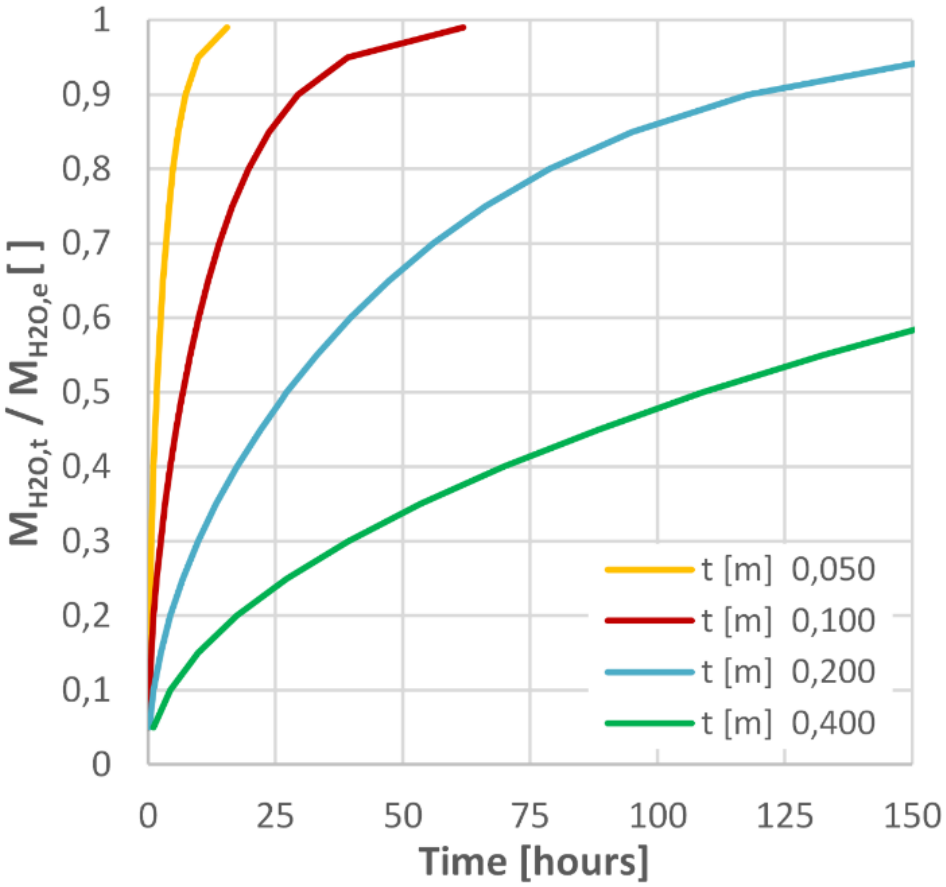

Figure 3.42 Effect of time and thickness on the equilibration time of furan sand cores. It can be see how core with thickness of less 50 mm will reach equilibrium in less than 24 hours.

3.7.4 - CFD Simulations Method

3.7.4.1 - Fan Selection

The first step in the CFD simulation is to evaluate the effect of one fan in order to estimate the number of fans needed for a given mould. In Figure 3.43 an evaluation of the fan can be done visually, by plotting the velocity contours as shown in for the fan. It can be see that for this specific fan, velocity drops level below 1 m/s before reaching the surface at 3500 mm downstream. As consequence we can see how the heat exchange coefficient field on the target surface is below 5 W/(m2K) as shown in Figure 3.44. Results for different fan models can be found in Supplement VIII.

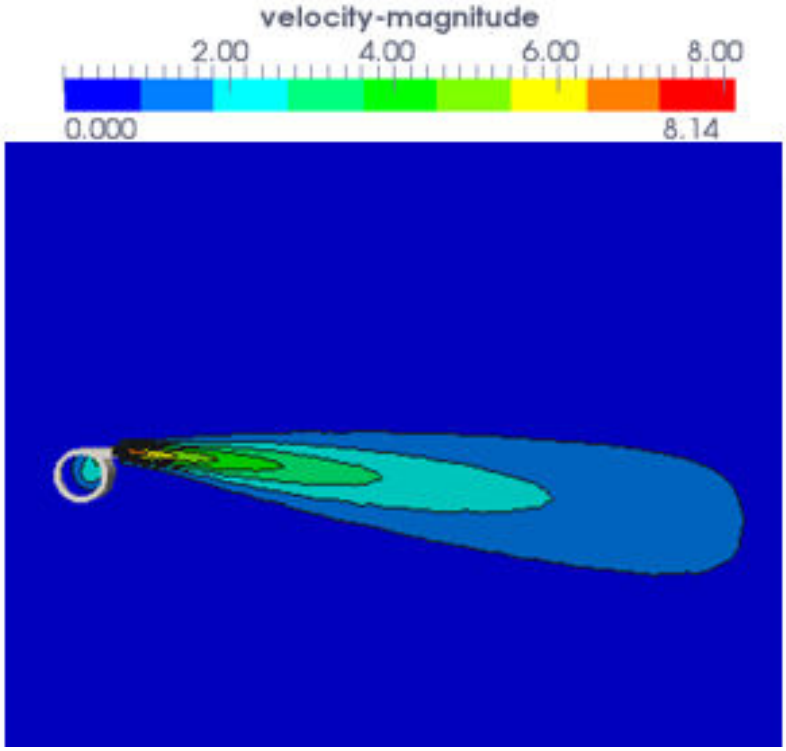

Figure 3.43 Velocity magnitude [m/s] contours over the central section plane for the fan TFV 10 S for a wall distance of 3500 mm.

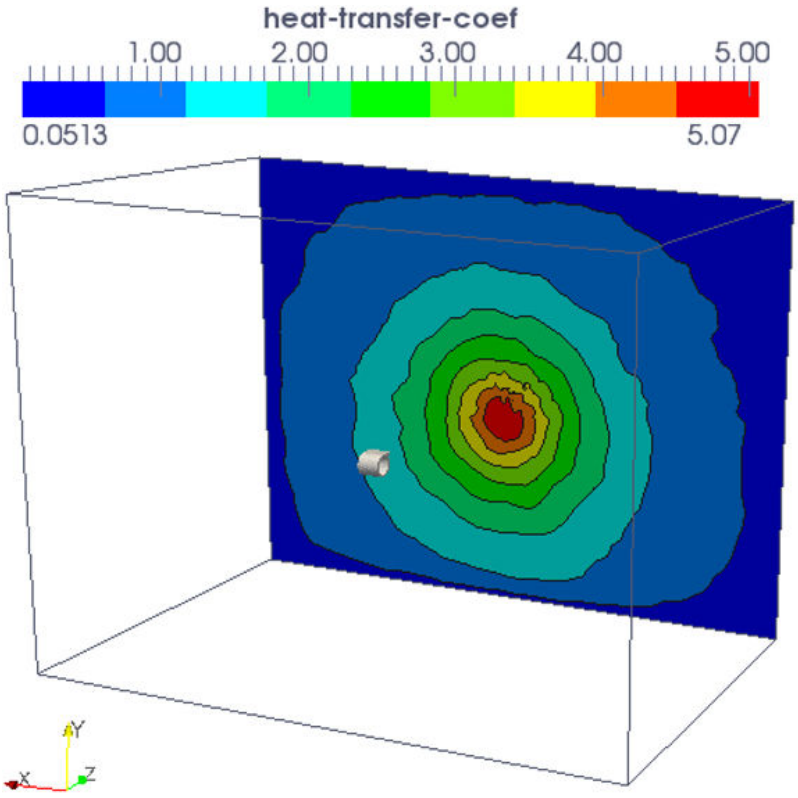

Figure 3.44 Convective heat transfer coefficient [W/(m²K)] distribution over isothermal surface for TFV 10 S fan for a wall distance of 3500 mm.

In order to compare the three different fans we plot the heat exchange coefficients on the x axis of the wall at the same y coordinate of the fan centre of mass (Figure 3.45). We can see how the TTV 4500 fans provides the highest heat exchange coefficient at a fraction of the power used by TFV 30 S. The TFV 10 S provides the smallest heat exchange coefficients.

Additionally, we notice that for all the distances form the surface, for the TTV 4500 provides and heat transfer coefficient higher then 10 W/(m^{2}K) (well above the typical values achievable by natural convection) on an approximately circular area of two meters in diameter.

Based on these results we choose the TTV 4500 for the mould simulations and decide to pre-dimension the number of require fans based on the area of the moulds and by the area where there is an heat transfer coefficient above 10 W/(m^{2}K).

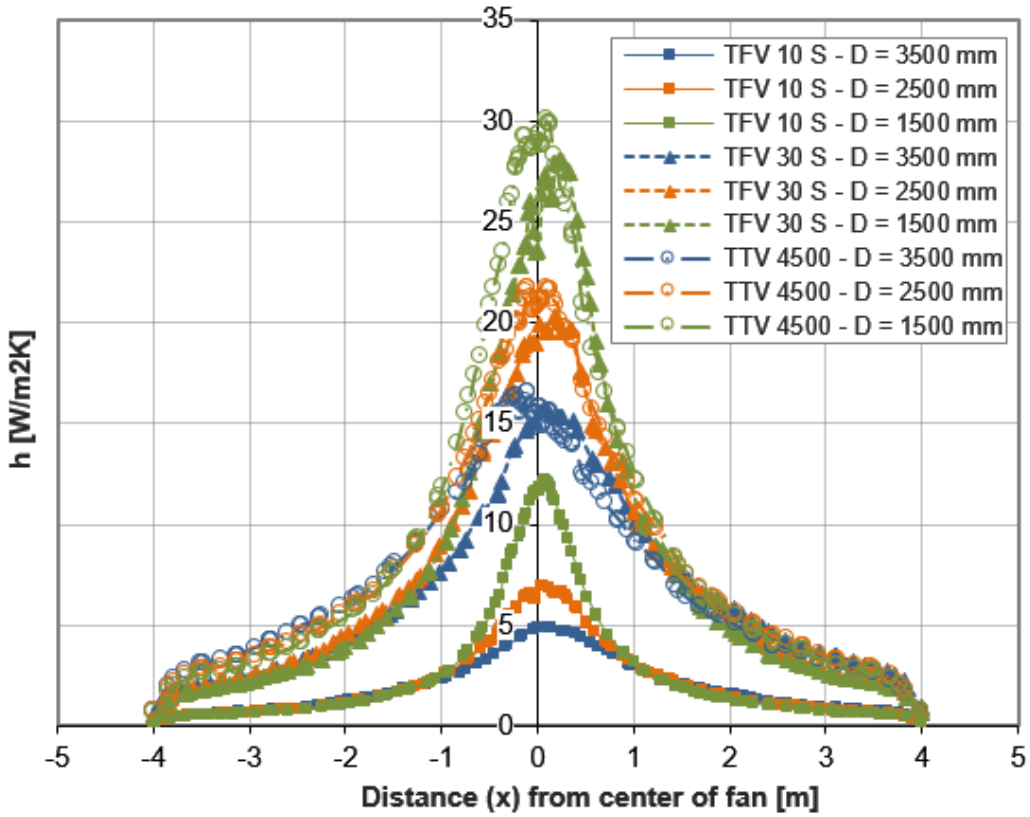

Figure 3.45 Convective heat transfer coefficient [W/(m^{2}K)] distribution for different fans and wall distances along the x axis.

3.7.4.2 - Wind Turbine Hub Mould Results

Figure 3.46 shows the optimal fan layout chosen for the hub mould consisting of three fans.

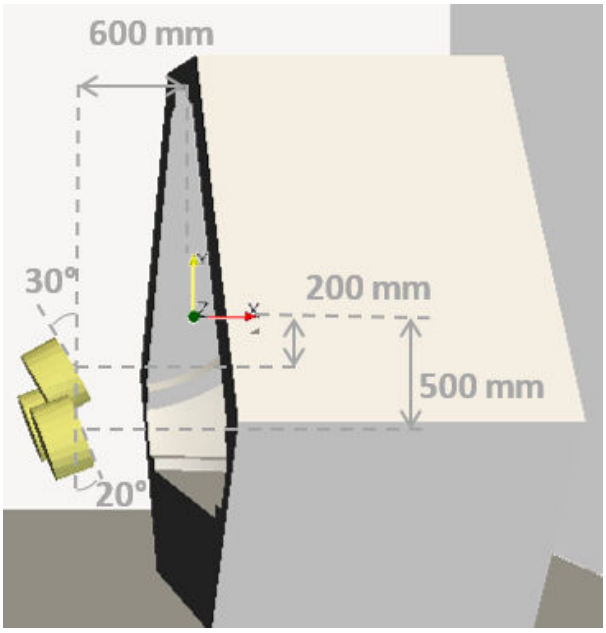

Figure 3.46 Optimal fan arrangement for the hub (side view).

Figure 3.47 shows how the air is channelled in the bottom section of the cavity and exits from the top, thus ensuring a steady value of air velocity to be maintained above the mould surface. This has beneficial effects over the average heat transfer coefficient which is thus increased with respect to other arrangements simulated.

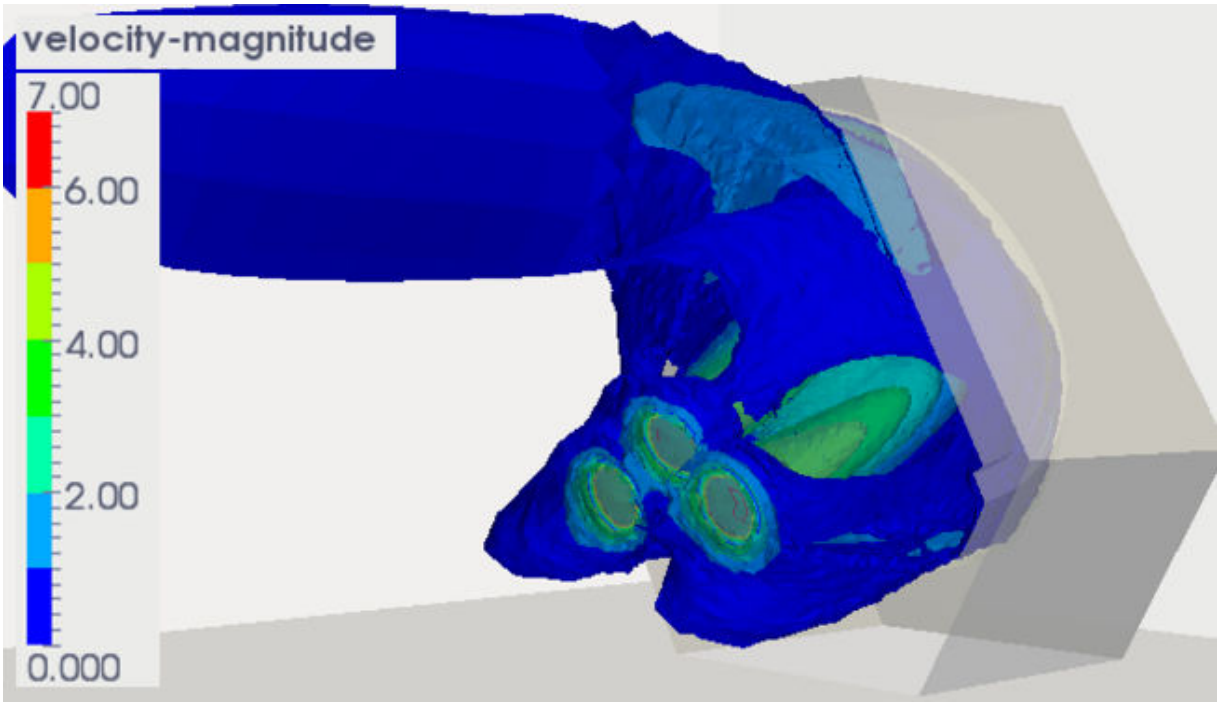

Figure 3.47 Velocity magnitude [m/s] isosurfaces. Air stream from the fans channelled in cavity.

Figure 3.48 shows the heat transfer coefficient distribution on the hub mould surface. It is possible to appreciate that the areas with the lowest value are localized near the corners. This observation allows to determine where localized moisture measurements should be done in real production.

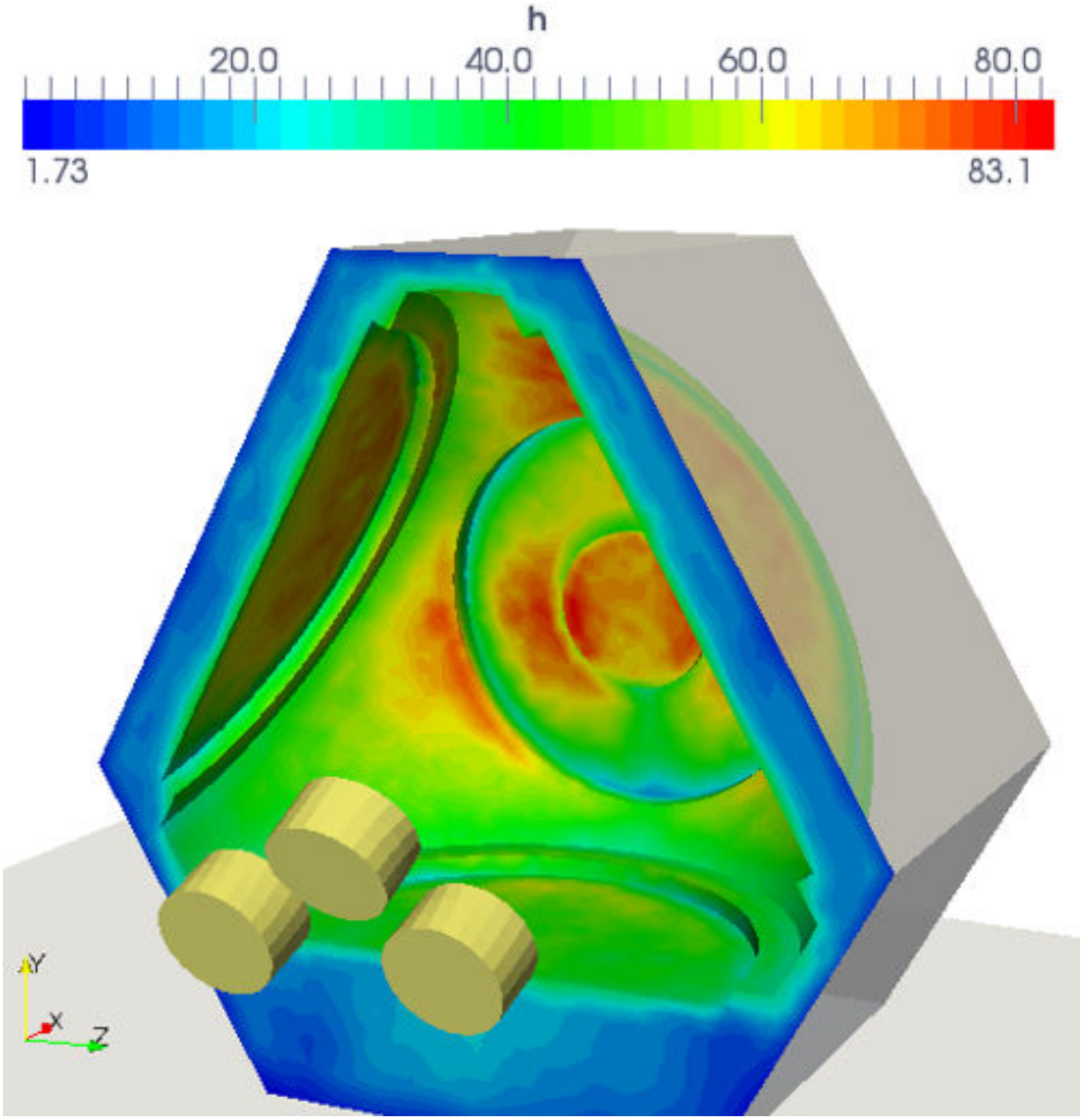

Figure 3.48 Convective heat transfer coeffient [W/(m^{2}K)] distribution on hub mould.

From Figure 3.49 we see that less than 2% of the total area of the mould is subjected to an heat transfer coefficient of less than 10 W/(m^{2}K).

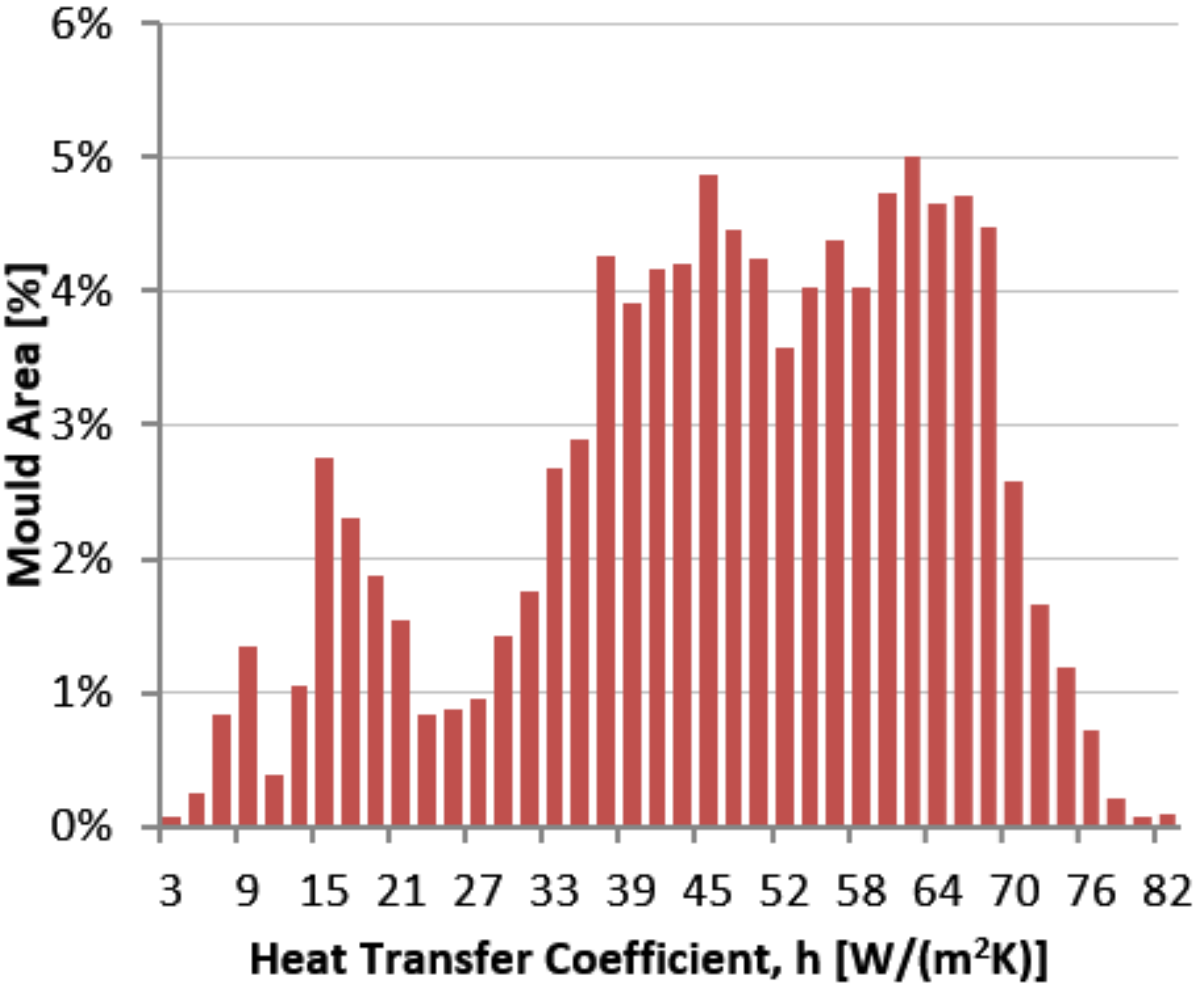

Figure 3.49 Histogram showing the distribution of the heat exchange coefficient on the hub mould surface.

3.7.4.4 - Main Foundation Mould Drying

The optimal fan arrangement for the main foundation moulds requires six fans due to the larger mould dimensions. In particular we it is important that the fans are never placed perpendicular to the mould wall in order to avoid formation of stagnation zones and therefore a reduction of the heat transfer coefficient. This is confirmed by Figure 3.50 where the jets exiting from the fans can be clearly seen.

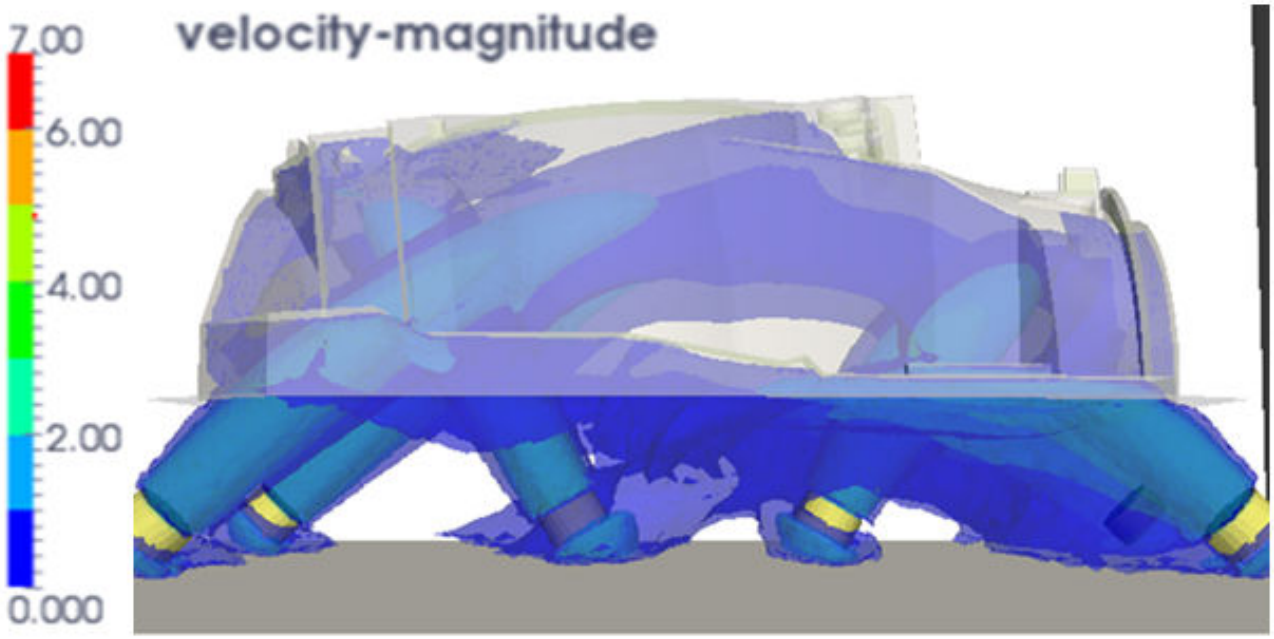

Figure 3.50 Velocity magnitude [m/s] isosurfaces. Air jets exiting from the fans are clearly visible below the drag.

The heat transfer coefficients obtained on the surface are concentrated in a lower range as compared to the hub. This means that the drying process of this mould will be necessary slower. However even for this case only less than 5% of the total area is subjected to heat exchange coefficients smaller than 5 W/(m^{2}K). These areas are clearly visible in dark blue in Figure 3.51 in correspondence of the top areas of the mould surface. Therefore it will be important to assess the moisture of these areas once the drying process is completed in order to ensure a complete drying and to avoid possible problems in quality.

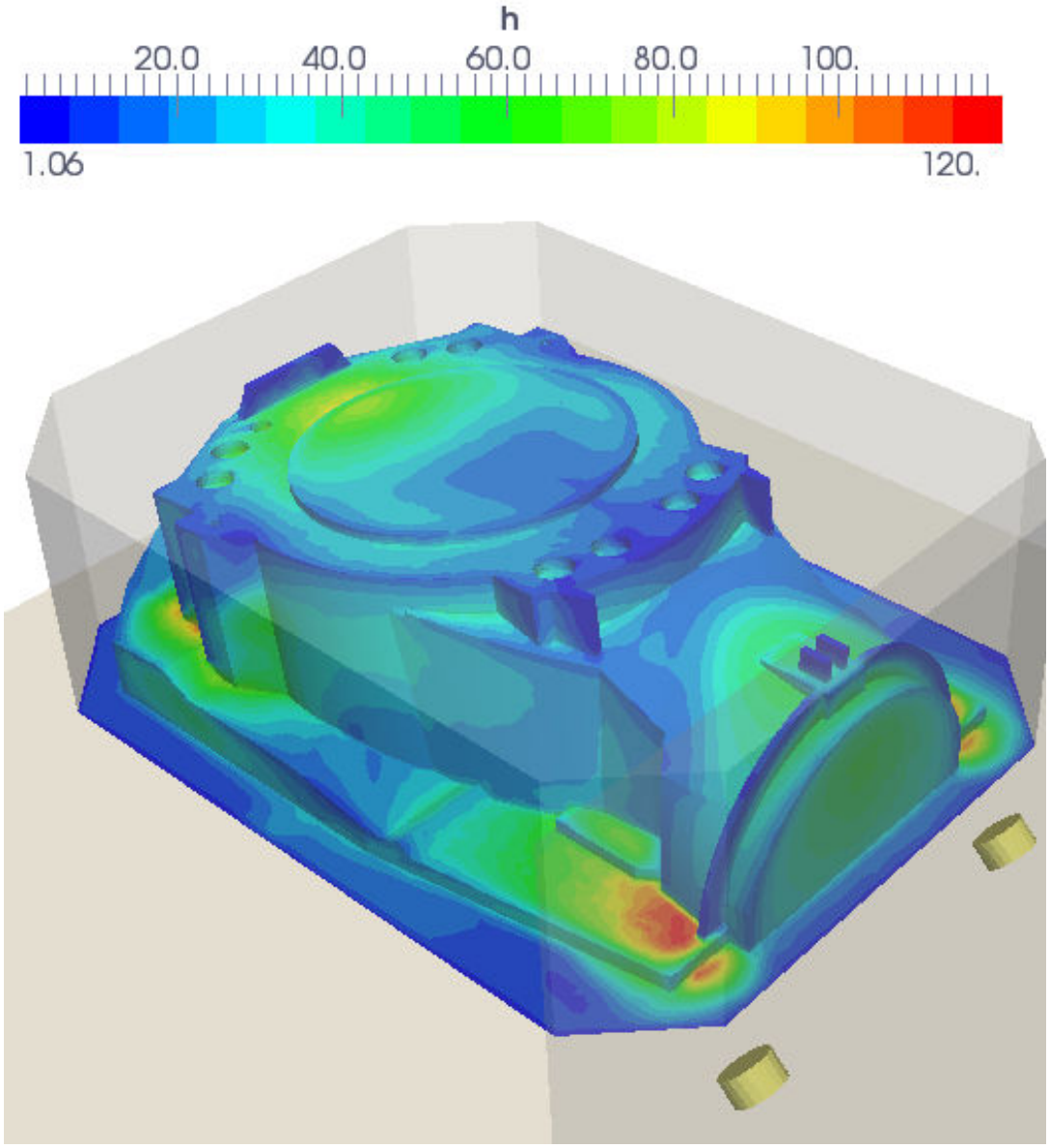

Figure 3.51 Convective heat transfer coeffient [W/(m²K)] distribution for the main foundation mould.

3.7.4.5 - Main Bearing House Mould Drying

The main bearing house requires two fans due to its smaller dimensions. Again the fans are positioned such that the air flow enters tangentially into the mould shape on one side and freely exits from the other as visualized in Figure 3.52.

In regards to heat transfer coefficients we see that the minimums are localized in the deeper pockets and cavities of the mould (Figure 3.53). Therefore these will be the areas to be checked for moisture residual after the drying process is completed.

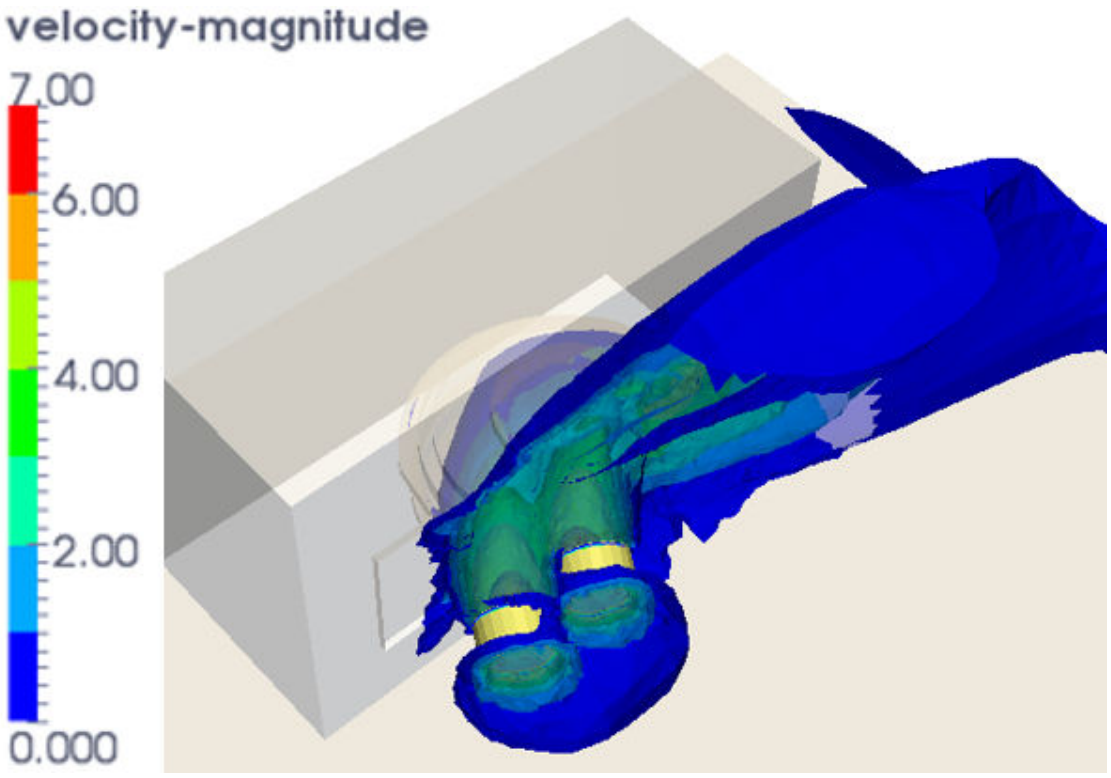

Figure 3.52 Velocity magnitude [m/s] isosurfaces. Air stream from the fans is channelled in the cavity.

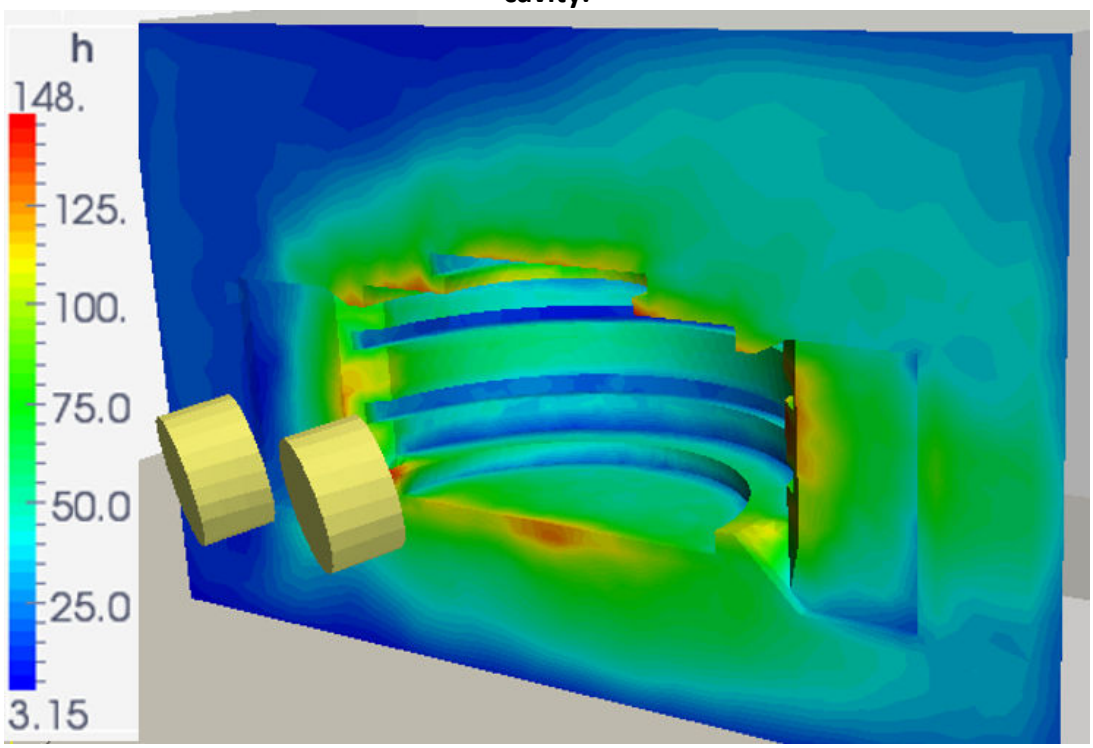

Figure 3.53 Convective heat transfer coeffient [W/(m^{2}K)] distribution for the main bearing house mould.

3.8 - Management of the Design Process

Table 3.4 shows how critical aspects differs between the classic the new design process applied to the optimization of mould design. For example, we can notice that 3D design competence, previously outsourced, is now handled in house to allow for better integration and communication. Additionally, overall competences of the staff were increased to be able to be able to use CAE tools in an advanced manner.

The level of innovation achieved is much higher since now the work on different tools is carried out in parallel and decision on design or interface changes are done based on a total cost evaluation, not just in respect to one production step.

Documentation process followed naturally and was speeded up by the in house availability of 3D models. Finally, the process helped to foster innovation by having a quantitative assessment of the ideas (based on calculation, simulation or tests) as compared to a qualitative assessment criteria that was often used previously.

Table 3.5 summarizes the main key performance indicators for a tool like a moulding box. It can be see how the steel amount used can be reduced in an optimized moulding box, but the percentage of custom plates increases drastically as well as the number of different BOM item. This results in a higher cost per kg of steel (due to increased amount of welds and custom plates) in the optimized moulding box but in a lower final total cost due to the material savings achieved.
Also we can see how sand usage quantity was drastically reduced, as well as the effect on the cost of the produced item.

Table 3.4 Comparison between the characteristics of a classic sequential design process and the new CAE integrated design process.

		Classic Sequential Design Process	New Integrated CAE Design Process
Design Process Characteristic	3D Design competence	Outsourced	In house
	Staff overall competences	Low-Medium	Medium-High
	Possibility of innovation	Low (design dependent on decisions made at previous steps)	High (design teams work in parallel and independently, but communicating often about interfaces changes)
	Interface design	Locked in initial stages	Locked when optimal solution reached
	Perceived need for communication between designers	Low	High
	Documentation system	Different and difficult to access	Standardized
	Idea selection criteria	Qualitative	Quantitative

Table 3.5 Overview of key performance indicators for the three different moulding boxes designs (values relative to standard moulding box).

		Standard Moulding Box	Moulding Box With Sand Saving	Optimized Moulding Box
Moulding Box Design KPI	Steel Amount [%]	100	120	70
	Welds Amount [%]	100	110	70
	# Custom plates # Square shape Plates [%]	5	15	75
	# of Different Items in BOM	25	40	80
	Sand Amount	100	80	55
	Moulding Box Cost	100	120	70
	Direct Savings on Casted Item [%]	0	2%	5%

4. Discussion

4.1 - Coating Properties Tests

Summarizing the results for the coating properties tests campaigns and in view of the stated objectives we can draw the following considerations:

- Coating viscosity is heavily affected by coating density, and to a minor degree by temperature. These variations can easily be measured with the rotational viscometer (the resolution and accuracy of the tool are smaller than the measured variation). With the Ford cup the small variations due to the temperature (0.5s to 1s) cannot be measured clearly due to the lower precision of this system. Also in case of manual measurements, density related variations might be affected by significant errors for the cup time method. The use of more accurate tools for measuring viscosity is therefore needed compared to what is currently used.
- Density of the coating is not dependent on temperature (from cup measured density results) however the Baume measurement method is varying with temperature and additionally it is characterized by low resolution. This suggests that Baume the stick can only be used as indication, and temperature compensation is needed for reducing the measurement errors. These findings are in line and confirm with what normally advised by the main foundry coating manufactures and suppliers [6,9].
- A slight difference in the coating batches properties is detected, but this is probably due to differences between the preparations of the test bottles. This suggests that the coating batches delivered to different factories do not have a substantial difference.
- The water content in the coating is heavily affected by density, even within the current control limits. This means that tight control of density is needed in order to achieve stable drying times.
- As density and viscosity are strongly correlated for a given coating (in agreement with [6]), we suggest that only one of these variables need to be closely monitored and controlled in production facilities. However the methods used for monitoring shall have a higher precision than the ones used today.
- Temperature has shown a much smaller effect on coating properties and it is therefore not needed a tight control of this parameter. As a consequence it has been eliminated from the coating layer properties test campaign. This finding is somewhat different from common

knowledge of the industry that coating viscosity is heavily affected by temperature [8]. For the considered coating and temperature ranges, we can conclude that temperature control systems are not needed, if the objective is to control coating properties. This finding can help to substantially reduce costs related to the control of temperature in production.

As a results of these findings, it is important to realize that both the Baume stick and the ford cup, traditionally used and described in [4,6,9], are only useful for rough estimation of coating properties, it therefore advised that coating properties are measured with more precise tools (such as in line density or viscosity meters). This is the first most important step to achieve control of the final coating layer properties and consequently improve control of surface quality, drying time and cost.

4.2 - Coating Layer Properties Test

Regarding coating layer properties tests we can summarize as follows:

- Sand compaction is critical for all the considered coating layer properties, typically a high compaction level will give more repeatable and uniform results. Direct consequences are that, if good sand mould compaction can be achieved, savings can be harvested from lower coating consumption, less energy required for drying, shorter drying time and more stable quality performance (due to repeatable coating layer properties). Additionally a better control of the coating layer can help to improve fatigue properties and life of the components by changing the microstructure of the skin of the cast part [3,7,13]. The most important contribution in this case has been to quantify the effect of compaction compared to already existing general knowledge that compaction is affecting the coating layer [9].
- Sand compaction level can be checked by measuring the density, since the sand density is only affected by the compaction level for a given sand recipe. This measurement could be easy to implement in a factory environment by taking samples from a real mould and then use the data to improve the moulding and compaction process. There is no reference, to the knowledge of the author, in literature of such a methodology for assessing mould sand density.
- The second most important property is, also in this case, coating density (in agreement with [9]). It affects heavily the coating penetration and the water thickness which determines energy and time required for drying. Additionally, coating water fraction in the coated layer has been found to be basically the same as the one in the prepared coating, it is therefore possible to directly predict the fraction of water in a coated layer if coating density is

monitored precisely. This second finding is typically not mentioned in the literature but it is extremely important from an industrial point of view in order to be able to correctly predict the energy required for the drying process and drying time.

- Both dipping time and gravity are relevant factors for coating thickness properties. In order to control these two factors it is important to design the coating process so as to avoid areas where coating is gathered for a long time compared to areas were coating is applied with only one quick pass. This is in agreement with most literature on coating rheology [8] but here quantification was provided for the specific foundry coating and moulding material combinations used in Global Castings factories.
- Finally, it is important to note that there are no significant differences between the two coating batches, from the two sand recipes considered and for the dust and fines quantity allowed in these experiments. This will allow experimenters to eliminate these variables from future experimental designs. Additionally it proves that the coatings supplied to the different factories are consistent and have uniform properties. It is important to note, that levels of dust outside the current specification will provide problems of sand strengths, however for coating testing purposes the elimination of dust as a variable is possible, if the level is below 2 %, without affecting coating layer test results.

If we look at the cost of the coating and drying process, an interesting finding is that adding water (lowering the density) to the coating (in an attempt to lower the consumption of purchased coating and therefore cost) will increase the wet thickness, the water content and the penetration (all these variables will increase drying time and energy required for drying, and therefore increase production cost). On the other hand, the dry thickness (which represents the consumption of purchased coating) is not affected by the coating density. This is somewhat is disagreement with common knowledge [8,9] that a coating with higher viscosity will provide a thicker coating layer. This statement is true for flat substrates where capillary suction between sand grains is not important and therefore viscosity helps the coating to adhere to the surface. But for porous substrates, like a furan sand mould, adding water lowers the viscosity and makes it easier for the coating to be absorbed by the voids in the sand. This results in final thicker coating layer.

In order to control the consumption of coating it is suggested to have a well compacted mould, this will substantially reduce the variation in dry thickness and therefore in coating consumption, additionally it will provide more uniform surface properties on the casting skin. Additionally when designing the mould and the coating process it important to avoid stagnation of coating to reduce the variations in coating thicknesses and penetration.

From a process control and stability point view we can summarize that:

- The relations between coating layer properties and coating variables are non-linear, it is therefore important to run trial laboratory tests before running serial production.
- The scatter (repeatability) of the coating process is not constant and can be controlled by choosing the right level of moulding and coating parameters.
- In particular to reduce scatter, the sand density should be above 1350 kg/m^3, the coating density maximized, the dipping time minimized and moulds should be coated facing downwards.
- It is possible to correlate the water thickness and coating penetration directly, independent of other variables and it is therefore possible to estimate water content in coated moulds just by simple penetration measurements. Such simple, easy to use, correlations have not been found in literature until now.

4.3 - Evaporation Rates Tests and Drying Time

In regards to evaporation rates and drying time we can say that:

- An experimental apparatus was designed, tested and built to carry out ad hoc evaporation tests
- Initial water thickness was found to heavily affect the drying behaviour for water based coating on furan bonded sand moulds. In particular, for initial water thicknesses higher than 1 kg/m^2, evaporation rates decrease and drying times increase in a non-linear fashion. The reason is that the main water transport phenomena for thin coating layers is evaporation from the surface to the air, while for thicker layers diffusion from the inner layer to the surface becomes the limiting phenomena. These findings are in agreement with traditional drying literature [22] and here we have now provided a quantitative measure of the effects for water based foundry coatings and furan sands.
- The ER_{max}/ER_{avg} ratio is also heavily affected by initial water thickness, and to some degree also by the air drying conditions. It is therefore important to use this information to correctly dimension drying equipment.
- Temperature measurement can be used to determine when surface is dry and for initial water thickness smaller than 1 mm this corresponds also a dry sample (for higher thickness there can still be moisture in the lower layers). This is a practical and low cost methodology measurement that could be easily implemented in factories.
- An empirical correlation between the average evaporation rates and important process parameters has been found and design maps have been generated for use in drying

equipment design. This knowledge was not present in literature to the knowledge of the author.

- Characteristic curves of the material have been obtained and found to be heavily dependent on initial water thickness, less on drying conditions and not dependent on initial coating density. This is in line with traditional drying literature ([21,22]) and characteristic curves were not available for these types of materials before.
- Finally it has been shown that it is possible to achieve a given drying times but it is necessary not only to control drying air conditions but also coating layer properties.

4.4 - Residual Moisture Levels

In regards to residual moisture levels:

- We have shown that automatic vapour sorption tests are useful to detect differences between factors affecting moisture and can help the foundry engineer to choose binders that have lower moisture levels. As a consequence this test could be used as an evaluation tool for new binding systems recipes and coatings to be introduced in production. This adds to the current literature knowledge since such materials were not tested in a vapour sorption analyser previously [21,22,32].
- Dust effect and temperature effect are not critical in the ranges currently allowed in the factories, it is therefore not critical to tightly control their values as soon are they are within current specification.
- Air humidity is a very important parameter, in particular when drying moulds at low air humidity it is possible to significantly reduce the drying time of the moulds. This is new knowledge compared to previous measured data in Global Castings facilities. The old sand moisture test procedure (where relative humidity was not taken in account for) can introduce significant errors in the measured moisture values and make impossible to detect even significant changes in moisture levels shown in this study.
- Binder type can heavily affect the moisture retention properties of the mould it is therefore important to choose binding systems that can reduce the amount of moisture in the sand to reduce the generated vapour and therefore the probability of gas defects. This data is not normally provided by suppliers so it is important to be aware of this new parameter for selection of binder systems.
- Due to the weak hysteresis effect between sorption and desorption curves, moisture lost during drying can be regained when moulds are stored for enough time in an open

environment at higher humidity. This might jeopardise the positive effects of expensive drying processes.

- The data obtained from this study can be used as basis for the design of dryers and to help define control limits for the drying of moulds and cores in the foundry industry.
- Simple calculation examples have been performed using the results from the experiments to show a possible use of this new test methodology. This is a new application field of application for automatic vapour sorption technique that was not investigated earlier [32].
- Coefficients of 3rd order polynomials fitted to sorption and desorption curves for the tested materials have been obtained.

4.5 - Moisture Diffusion

The main conclusions that we can draw from this section can be summarised as below:

- Two different tests methodologies (manual and automatic method) for testing water adsorption diffusion coefficients of foundry sands and coatings were compared, similar values of diffusion coefficients we obtained from both methodologies. This is critical knowledge needed for the simulation of moisture migration that previously was not available in literature [33-39] for this class of materials.
- Manual method has a lower cost and longer test times, but diffusion coefficients can be overestimated for relative humidities above 60 % for the tested sands, and, in general, whenever material will have a moisture diffusion coefficient which is a function of moisture content there will be some error.
- Automatic tests require the most expensive equipment, but it is possible to determine diffusion coefficients from 3 % to 95 % relative humidity in a short amount of time. The determination of moisture diffusion coefficients was not a feature available in the automatic sorption software [32] and it is therefore a new possible application for this testing methodology.
- Diffusion coefficients have been obtained for both furan sands and foundry coatings, these coefficients can be used in hand calculation as well as in 3D simulation software.
- Comparison with other ceramic materials available in literature [21,22] like concrete, clay and sand was carried out showing that foundry sands and coating have diffusion coefficients of similar order of magnitude.
- Sand density effect on moisture diffusion coefficient is minor for sand densities around 1100 kg/m^3 and not appreciable for densities between 1250 kg/m^3 and 1550 kg/m^3. This is an

important finding, because it means that there is no need to model density variation in a simulation software if the aim is to simulate moisture migration.

- Binder type can influence moisture diffusion coefficients so this could be used as a criteria for selecting binders when gas problems are encountered.
- Dust can decrease moisture diffusion coefficients but in the quantities smaller than 2% it does not play a major role.
- Temperature increase from 25 °C to 35 °C will increase moisture diffusion coefficients especially for coating. This is in line with what is typically described in literature for other materials (higher temperatures will increase the moisture diffusion coefficient [21,22]).
- A simple hand calculation methodology to estimate moisture content of foundry sand cores was introduced and applied to a real case.
- The tests and calculation example show that it is possible to lower moisture in cores and moulds by properly controlling time, relative humidity, binder type and temperature. This is normally not detailed in the literature for foundry material and has now been proven.

4.6 - Moisture Measurement

In regards to moisture measurement methodology we can say that:

- Moisture tool comparison tests have shown that different moisture tools can be used to measure moisture, but calibration is needed is good accuracy is required.
- A tools has been developed with increased accuracy in the low moisture range compared to the commercial tools [9]
- In order to minimize measurement error, when short wires cannot be used the choice should fall on Teflon insulated and shielded wires.
- A correlation between moisture and resistance of coating has been obtained and compared with the one for concrete showing that significant measurement errors can occur if concrete calibrated tools are used to measure moisture in foundry coatings and no correction is made. This is in line with literature about moisture measurement and sensor calibration [33-35], but no data was available for foundry coatings.
- Industrial application to large size mould has been successful and proven useful to monitor process variability. This application was not found in literature before.
- Infrared temperature measurements are proven useful to identify last spots to dry in large size mould. In these spots is therefore possible to carry out more precise moisture measurements with resistance based tools. This is in line with the methodology suggested

by suppliers for the use of infrared cameras but this has now been applied to foundry moulds.

4.7 - Calculation and Simulation Methods

In regards to process design and simulation tools for the preliminary dimensioning of drying processes as well as for the optimization have been described. In particular we developed:

- Simple hand calculation procedures for preliminary estimations of initial water content, drying time and residual moisture.
- Models to be used in numerical solvers for the optimization of drying processes.
- CFD simulations to reduce the risk and costs involved in the drying of large foundry moulds for wind turbines applications (to support the choice of fan model, layout and quality controls).

This reflects the iterative design approach described in [21,22] for the general design of driers, but it has been simplified and applied to the foundry industry.

4.8 - Management of the Design Process

A new design methodology that heavily relies on CAE tools as well as on improved management of the different systems and their interaction was implemented. The result was an increased capability to handle complex designs in an easy way and significant savings were achieved both in investment and variable costs. This is in line with literature that described the application of similar tool to other industries and with successful results [40-44].

5. Conclusions

5.1 Future Work at Global Castings

In regards to coating, a need for tight control of the properties has been identified. The use of more accurate tools for measuring viscosity is advised compared to what is currently used. Effect of coating type and possible temperature effects should be also taken in account by the new measuring system.

Coating layer properties variation can be significantly reduced by controlling sand compaction. This requires implementation of mould sand density measurement. High coating density should be used to reduce the effect of sand compaction variation, contact time and gravity. Test procedures developed in this work can be used to test new coatings to be implemented in the future to quantify control limits, non-linear behaviours and process stability issues. Simple penetration measurement should be used on normal basis as they are directly correlated to water amounts in the coating layer.

Evaporation rates can be controlled by controlling water thickness and air properties. To speed up drying rate and lower energy consumption coating thickness should be kept to less than 1 kg/m^2. Temperature measurements with infrared cameras can be used to find the last spot to dry.

A new methodology for residual moisture testing was developed with improved accuracy. Relative humidity has a large effect as well as binder type. A simple procedure for Global Castings would be to use an external lab to carry out these tests as done in this work.

Low cost methodology for diffusion coefficient determination has been developed. Test procedures have been developed and are ready to be used at global castings for new mould materials.

It is possible to quickly identify last areas to dry with infrared camera in production line and then locally assess moisture with resistance based tools. Accuracy such tools can be improved with calibration technique shown in this study and tools with increased measuring range developed in this study.

Drying calculation procedures have been developed and can be implemented in design procedures at Global Castings to reduce design time and drying operations costs.

A new process for the management of the design process has been used and substantial savings have been achieved. Full implementation of this process could substantially benefit Global Castings.

An overview table of the control methods developed and to be implemented at Global Castings as well as the developed design rules and calculation methods is presented in Table 5.1.

Table 5.1 Test methodology and design rules overview for properties affecting the drying of foundry moulds.

Investigated Area	New Lab. Tests	New Production Measurements	Design Rules	Prediction Method	Supplement.
Coating Properties	Rotational viscometer	In line sensors and real time control of density/viscosity	Tight control of coating density within specified range	Correlation between coating and viscosity at desired temperature	I
Coating Layer Properties	- Weight measurement - Penetration measurement	- Penetration measurement	Control dry and water thickness within specified range	Correlation between coating penetration and thickness	I,II
Drying Time	Evaporation rates tests	- Surface temperature - Surface moisture	Drying time and residual moisture below specified limit	Hand calculation 3D simulation	III,VIII,IX
Residual Moisture Levels	Adsorption/Desorption tests	- Moisture sensor	Keep moisture below a critical level	- Hand calculation - 3D simulation	IV,V
Moisture Diffusion	-Adsorption /desorption tests - Manual Method	- Moisture sensor	Keep moisture below a critical level	- Hand calculation - 3D simulation (diffusion coefficients)	VI
Moisture Measurement	-Moist vs resistance measurement	- Moist tool with new calibration	Correlate moisture with resistance	Experimental correlation moisture/resist.	VII

6. Bibliography

1 J. Campbell, R.A. Harding, 'Solidification Defects in Castings', Lecture 3207, The University of Birmingham, 4-8, 1994.

2 L. Elmquist, 'Defect formation in cast iron', Presentation, School of Engineering, Jonkoping University, Sweden, 2012.

3 B. Sarum, 'Ductile and Compacted Graphite Iron Casting Skin -Evaluation, Effect on Fatigue Strength and Elimination, B. Ohio State University', Ph.D Dissertation, 2013, Page 103-106.

4 U. C. Nwaogu, N. S. Tiedje, 'Foundry Coating Technology: A Review', Materials Sciences and Application, 2011, 2, 1143-1160.

5 U. C. Nwaogu, N.S. Tiedje, 'Influence of New Sol-Gel Refractory Coating on the Casting Properties of Cold Box and Furan Cores for Grey Cast Iron', Proceeding of 69th World Foundry Congress, October 16-20, 2010.

6 John Brown, 'Foseco Ferrous Foundryman's Handbook', Eleventh Edition, Butterworth Heinemann, 2000.

7 M. Swartzlander, 'Refractory Coatings: Making the Right Choice', Modern Casting, 1992.

8 A. A. Tracton, 'Coatings Technology Handbook', Third Edition.

9 N. Schutze, 'Control Limits for the Drying of Water Based Coatings', Foseco, Foundry Practice, Issue 255, June 2011.

10 L. Jamrozowicz, J. Zych, T. Snopkiewicz, 'The Research of Desiccation Rates Selected Protective Coating Used on Mould and Sand Cores', Archive of Foundry Engineering, Vol.13, 01/2013, 45-50.

11 Tom Penko, 'Ultra-Performance Core Coatings For Mass Iron Casting Production: Specialized Methods For Developing & Evaluating New Coating Technology', Foseco Metallurgical Inc.

12 U.C. Nwaogu, T. Poulsen, R.K. Stage, C. Bischoff, N.S. Tiedje, 'New sol–gel refractory coatings on chemically-bonded sand cores for foundry applications to improve casting surface quality', Surface and Coatings Technology, Volume 205, Issue 16, 15 May 2011, Pages 4035–4044.

13 U.C. Nwaogu, N.S. Tiedje, 'Using sol-gel component as additive to foundry coatings to improve casting quality', Journal of Cast Metals Research, 2012, 176-187.

14 'Improving Casting Quality through Optimized Coating Technology', Foseco.

15 M. Haanepen, F. Piekartz, 'Foundry Coating Composition', Patent EP2364798 B1, Foseco, 18 July 2012.

16 B. Sarum, 'Ductile and Compacted Graphite Iron Casting Skin - Evaluation, Effect on Fatigue Strength and Elimination', PhD Thesis, Ohio State University, Page 103-106.

17 J. Kollar, B. Schmitt, 'Decrease the Drying Time for Wash Coatings on Sand Molds and Cores', EPRI Center for Material Production, 1994.
18 IKO, 'Description of Casting Defects', Chapters 04,10,12, S&B Industrial Minerals.
19 A. Chojecki, J. Mocek, 'Effect of atmosphere in a foundry mould on casting surface quality', Archives of Foundry Engineering, Volume 12, Issue 1/2012, 13-18.
20 Elkem, 'Hydrogen Pinholes', Technical Information 30, Elkem Foundry Products, Rev. 1.2, 2007.
21 A.S. Mujumdar, 'Handbook of industrial drying', 3rd edition, Ch. 2, 2006.
22 A.S. Mujumdar, 'Handbook of industrial drying', 3rd edition, Ch. 1, 2006.
23 Gregor A. Scheffler, 'Introduction of a Drying Coefficient for Building Materials', Thermal Performance of the Exterior Envelopes of Whole Buildings XII International Conference, December 1-5, 2013
24 A. Siewiorek, R. Nowak, A. Chojecki, J. Mocek: 'Gas evolution rate from heated moulding sands bonded with organic binders', Archives of Foundry Engineering, ISSN (1897-3310), Volume 11, Issue 1/2011, 87 – 92
25 A.Starobin, C.W. Hirt, D. Goettsch, 'A Model for Binder Gas Generation and Transport in Sand Cores and Molds', Modeling of Casting, Welding, and Solidification Processes XII, TMS (The Minerals, Metals & Materials Society), 2009.
26 A.Starobin, T. Hirt, H. Lang, M. Rode, 'Core Drying Simulation and Validation', International Foundry Research 64 (2012) No. 1, 2-5.
27 P. Scarber, C.E. Bates, 'Simulation of Core Gas Production During Mold Fill', AFS, 2006.
28 N.Tiedje, R. Crepaz, T. Eggert, N. Bey: 'Emission of organic compounds from mould and core binders used for casting iron, aluminium and bronze in sand moulds', Journal of Environmental Science and Health, Part A, 45: 14, 1866 – 1876.
29 G. Samuels and C. Beckermann: 'Measurement of Gas Evolution from PUNB Bonded Sand as a Function of Temperature', University of Iowa, International Journal of Metal Casting, Spring 2012.
30 A. Shepherd: 'Understanding Emission Characteristics of a Foundry Sand Binder', Proceedings of The National Conference On Undergraduate Research (NCUR) 2012, Weber State University, Ogden, UT, March 29-31, 2012.
31 BCRA: 'Venting of mould and cores', BCIRA Broadsheet 188, 1980.
32 Decagon Devices: 'Vapor Sorption Analyzer', Operator's Manual, Ver.5, Ch. 2.
33 A.S. Mujumdar: 'Handbook of industrial drying', 3rd edition, Ch. 3-4, 2006.
34 I. Boulaoued, A. Mhimid. 'Determination of the diffusion coefficient of new insulators composed of vegetable fibers', Thermal Science, Year 2012, Vol. 16, No. 4, pp. 987-995.
35 J. Carmeliet, H. Hens, S. Roels, 'Determination of the Liquid Water Diffusivity from Transient Moisture Transfer Experiments', Journal of Thermal Env. & Bldg. Sci., Vol. 27, No. 4—April 2004.

36 JEDEC Solid State Technology Association, ‘Test Method for the Measurement of Moisture Diffusivity and Water Solubility in Organic Materials Used in Electronic Devices’, JESD22-A120A, January 2008.

37 D. Gaffner, ‘The Moment Method for Measuring Moisture Diffusivity of Porous Building Materials’, Bulding X, 2007 ASHRAE.

38 L. Hassini, S. Azzouz, R. Peczalski, A. Belghith, ‘Estimation of potato moisture diffusivity from convective drying kinetics with correction for shrinkage’, Journal of Food Engineering, Volume 79, Issue 1, March 2007, Pages 47–56.

39 M. Janz, ‘Methods of measuring the moisture diffusivity at high moisture levels’, Report TVBM-3076, University Of Lund, Lund Institute Of Technology, Division of Building Materials, Licentiate Thesis, Lund ,1997.

40 J. Mohammed, J. May, A. Alavi, ‘Application of Computer Aided Design (CAD) In Knowledge Based Engineering’, Proceedings of The 2008 IAJC-IJME International Conference, ISBN 978-1-60643-379-9.

41 F. Giesecke, A. Mitchell, H. Spencer, I. Hill, ‘Technical drawing’, Upper Saddle River, NJ,Prentice Hall, 2003.

42 K. T. Ulrich, S. D. Eppinger, ’Product Design and Development’, 2nd Edition, Irwin McGraw-Hill, 2000.

43 W. C. Kim, R. Mauborgne, ‘Fair Process: Managing in the Knowledge Economy’, Harvard Business Review, 2003.

44 P.S. Adler, A. Mendelabaum, V. Nguyen, E. Schwerer, ’Getting the Most out of Your Product Development Process’, Harvard Business Review, Reprint 96202.

45 X. Chen, S. Zhao, ‘Moisture Absorption and Diffusion Characterization of Molding Compound’, Transactions of the ASME, 460 / Vol. 127, December 2005.

46 E. Celik, I. Guven, and E. Madenci, ‘Experimental and Numerical Characterization of Non-Fickian Moisture Diffusion in Electronic Packages’, 1-4244-0985-3/07, IEEE, Electronic Components and Technology Conference, 2007.

Appendix A

Supplements

Supplement I

71st BILBAO 2014 WORLD FOUNDRY CONGRESS
Advanced Sustainable Foundry
19-21 May 2014 • Palacio Euskalduna, BILBAO

Critical Control Variables For The Coating Process Of Furan Bonded Sand With Water Based Foundry Coatings

G. L. Di Muoio
Global Castings A/S, Copenhagen, Denmark

N. Skat Tiedje
Technical University of Denmark, Copenhagen, Denmark

B. Budolph Johansen
Global Castings A/S, Copenhagen, Denmark

ABSTRACT

Water based coatings are used in the production of cast components with the objective of improving surface finish and reduce defects.

Drying time and coating layer properties are heavily dependent on the thickness of the applied layer. This paper summarizes the results of two sets of experiments designed to investigate the effect of different coating process variables on the coating layer properties.

The first series of experiments focuses on determining how coating properties, such as viscosity and density, are affected by temperature and water content, as well as to compare different methods for assessing such properties.

The second series of experiments has the objective to determine how coating layer thickness properties are affected by coating density, binder system type, gravity, dust levels, compaction and dipping time.

Data from the experiments were analyzed using ANOVA and results summarized in recommendations for the industry.

It is shown that water content is heavily affecting viscosity, while temperature might affect some measurements methods more than others. Coating viscosity, mould sand compaction, gravity and dipping time are instead critical for the control of the coating layer thickness and penetration.

Keywords: Water based foundry coating, furan mould, coating viscosity, coating thickness, binder system, gravity, compaction, dipping time.

INTRODUCTION

Foundry coatings are used to improve casting surface finish and therefore substantially reduce defects and quality related costs. Water has been introduced as a solvent in foundry coatings only in the latest years to eliminate the safety and health hazards as well as the environmental impact related to the use of organic solvents.

The introduction of water as a solvent has, however, introduced drying as an extra step in the process chain to dry the coatings and to avoid vapor related defects in the castings. From the production viewpoint there is a need to control drying time (to ensure a steady production flow) and coating layer properties (to ensure casting quality). Drying time and costs are heavily dependent on coating layer properties (such as water content and coating penetration)[1, 2] . Finally, coating layer properties can influence surface and veining defects in a casting[3-6].

For production of large castings (5-30 tons) flow coating, brush coating and spray coating can be used (dipping would be very unpractical). Flow coating is the most commonly used method as it leads to better and more uniform coating layer properties, as compared to spray and brush coating. It is therefore the focus of this study.

Even though flow coating is known to be a more stable process, there are still several variables that can affect the coating layer properties[7-9]. Another fundamental aspect in controlling the coating process is the ability to measure

and monitor the variables affecting the process (i.e. coating density, coating viscosity, mould properties, etc…) and to measure the properties of the resulting coating layer.

The first series of experiments has the objective to determine how coating properties such as viscosity and density are affected by temperature and water content as well as to compare different methods for assessing such properties. A review of the possible methods for assessing coating properties is presented by Nwaogu[10] and Tracton[11]. In this study, we chose to compare standard methods used in production, such as flow cup (equipped with a self-developed time measurement system) and Baume stick, against a laboratory rotational viscometer.

The second series of experiments has the objective to determine how coating layer properties are affected by process variables. In this paper, coating layer properties considered are: wet and dry coating thicknesses, coating layer water content/fraction, coating penetration and sand density. While process variables considered are: coating density, binder system type, gravity, dust levels, compaction and dipping time. Coating layer properties are calculated from weight variations of the test samples and also measured from pictures taken with a stereomicroscope. Commercially available tools for measurement of coating thickness (like wheel and comb) have not been used for mainly two reasons: first because these tools cannot measure the coating penetration into the sand (which can be significant, if not a major, part of the total coating layer as shown in Fig. 1 and described by Nwaogu et al.[5]), second because the samples would be damaged by removal of coating and it would have not been possible to carry out more accurate gravimetric analyses.

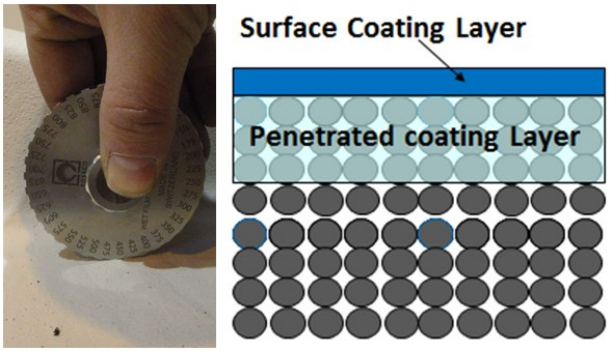

Fig. 1. Coating thickness measuring wheel (right), actual measured thickness (left).

Data from the two sets of experiments are analyzed using ANOVA and results summarized in recommendation for the industry.

EXPERIMENTAL METHOD

Based on the literature[1-5] and industrial experience a set of twelve variables that influence the coating layer properties has been identified. As shown in Fig. 2, coating properties, like viscosity and density, are known to be influenced by water content, temperature and coating type. While coating layer properties are influenced by coating properties as well as sand type, binder type, gravity effect, dust and fines levels, compaction level and contact time with coating. As a consequence, the two experimental campaigns presented in this paper are designed to study the effects of these variables on final coating layer properties. Additionally, results from the first campaign are used to determine how well the different measuring tools can detect the variation in the measured coating properties.

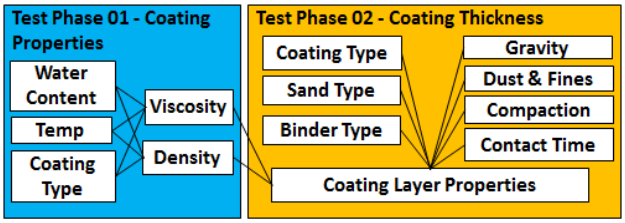

Fig. 2. Overview of properties affecting coating penetration and thickness.

COATING PROPERTIES TESTS

Design of Experiment

Of the many coating properties[10,11] that can be measured, density and viscosity are chosen since existing tools like Baume stick and DIN cup are measuring indirectly density and viscosity.

The main objectives of this first test campaign are to:

- determine in which measure different variables affect coating properties like viscosity and density
- check the sensibility and accuracy of different measuring methods for assessing coating properties
- quantify how water content in the coating is affected by coating density
- suggest which variables should be controlled in production

- eliminate non influent variables from next experimental campaign in order to reduce experimental effort

A full factorial plan (Table 1) is used to investigate how cup time, Baume reading and viscosity vary with temperature, density and coating batch (named also coating type). Additionally, for each of the coating batches, five runs were added at the central levels in order to create center composite designs to be used to assess the repeatability of the measurements.

Table 1. Factorial design for coating properties determination

Variable	Number of Levels	Level 1	Level 2	Level 3
Temp [C]	3	10	23	36
Density at 20 °C [kg/m^3]	3	1790	1908	2042
Coating Type	2	VCM	VCK	
Replicates	1			
Total Runs	18			

As for the choice of the temperature levels, 23 °C was used as this is the typical temperature at which coating should be used, 10 °C is temperature that the coating normally can reach during winter months in the factory and 36 °C is the temperature that can easily be reached in the summer months for some of the factories.

Density levels are calculated as correspondent density to Baume reading of 64 Bé, 69°Bé and 74 Bé at 23 °C using standard conversion in Eq. 1[12]. This is the range used by most of the factories to control the coating properties.

$$\rho_{coat} = \rho_{H2O} SG = \rho_{H2O} \frac{145}{145 - Be^o} \qquad \text{Eq. 1}$$

Six bottles of coating were prepared starting from two batches of coating (Foseco Zir 7320V) delivered to two different factories (VCM and VCK). The coating is typically delivered at a density of 103-110 °Bé. For each test density to be achieved the necessary quantity of coating and water were calculated, prepared and mixed in a container of known volume (1 liter) and the weight checked with a load cell of +/- 1.5 g accuracy. Adjustments were done until the density calculated from the measured volume of coating in the container and the measured weight were within an accuracy of +/- 10 kg/m^3 (at 23 °C).

For the tests at 10 °C the coating bottles were placed in a refrigerator for 12 hours, while for the tests at 36 °C a microwave oven was used. After cooling/heating the coating was remixed and temperature was measured with a temperature sensor with an accuracy of +/- 0.1°C.

Cup Time Measurement

In the industry, cup time measurement is typically done manually by immersing the cup in well stirred coating and timing with a stop watch the time it takes for the cup to empty. It has been reported by several factories that this method has low repeatability due do the presence of manual measurement, and it is therefore not easy to achieve the necessary strict control of coating properties.

In this study, in an attempt to improve the accuracy of this measurement, an experimental setup has been designed to reduce the time measurement error (Fig. 3). A sliding pin labelled “B” in figure C has been inserted in the flow cup “A” with an extension wire for its extraction. The weight of the cup is recorded via a load cell connected to a PC where the data is stored for subsequent processing.

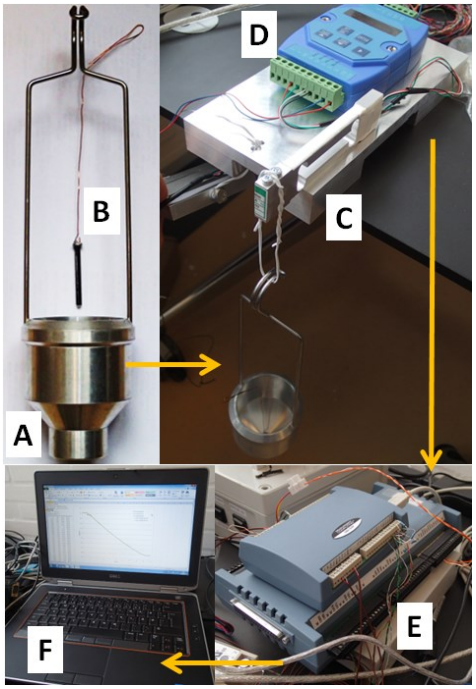

Fig. 3. Experimental setup for cup time measurement: a) 4mm flow cup, b) sliding pin, c)load cell, d) signal conditioner, e) acquisition card, f) computer.

In order to minimize measurement system errors, the load cell has an accuracy of +/- 0.12 grams and a full scale of 600 grams (while total weight of the cup and coating are below 500 g), and the data acquisition systems uses a sampling frequency of 100 Hz (cup times measured should be between 10 and 20 seconds).

After the acquisition, we plot the weight of the cup versus time and extract the cup time measurement from the curve (Fig. 4).

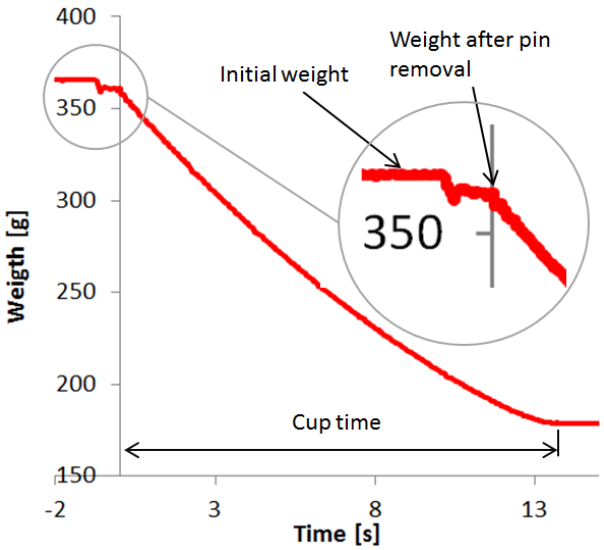

Fig. 4. Cup time measurement from acquired data.

Baumé Measurement

The Baumé measurements are taken as typically done in the industry. The coating is mixed thoroughly and allowed to settle for one minute. Then the Baumé stick is immersed in the coating, when there is no more movement, the reading is taken (Fig. 5).
The resolution of the Baumé stick used is 2°Bé, so it is not expected that this method will reveal small variations in density of the coating.

Cup Measured Density

In order check possible variation of density with temperature, for each cup tests, the density is calculated from the measured weight and the known cup volume.

Fig. 5. Baume measurement setup.

Viscosity Measurement

Viscosity is typically not measured directly in production, but it is known to be a critical parameter in coating performance[10, 11]. Typically for paints the viscosity should increase when shear rate decreases. In this way dripping of coating can be reduced after application.

In this study, we use an Elcometer 2300 RV rotational viscometer with a L3 spindle type (Fig. 6). With this setup is possible to measure viscosity with a resolution of 10mPas at any given rpm (rotation per minute). The maximum viscosity measurable is 400.000mPas at 0.3 RPM and 600mPas at 200 RPM. The accuracy of the measurement is +/-1% of the maximum viscosity measurable at a given RPM, in particular the accuracy is 6 mPas at 30 RMP and 40 mPas 200 RMP (see plots in the results section).

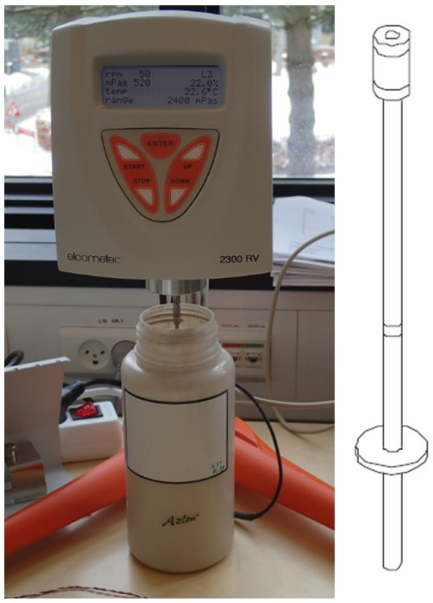

Fig. 6. Experimental setup for viscosity measurement

After preliminary trials it was chosen to run the tests at 30, 50, 60, 100, 200 RPM. This choice permits to reach a stable reading in 30 to 40 seconds (for the tested coatings) and faster test times. This allows for the coating container to only have negligible variation in temperature during the test (less than 3 °C).

Tests were initiated at 30 RPM and speed increased step by step up to 200 RPM, and then stepwise decreased again to 30 RPM. This procedure was repeated two times. For each spindle rotation speed, the viscosity measured to be used in the ANOVA is taken when the reading is stable, or at a maximum time of 60 seconds (especially for low speed and high solid content it is not easy to reach stable reading in short time) (Fig. 7).

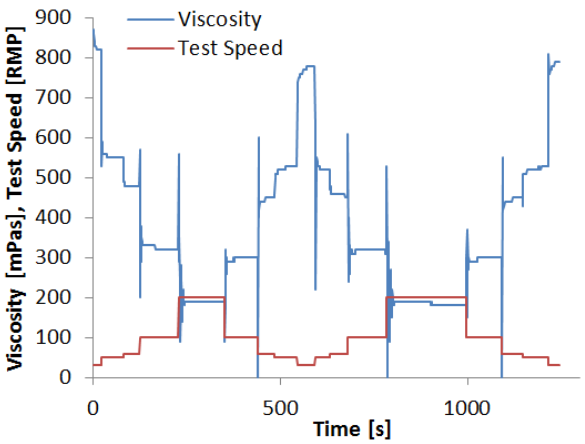

Fig. 7. Viscosity measurement at different rotational speeds.

Water Content Measurement

Coating water content is normally not measured in production. This property directly affects drying time, so it is important to understand how it varies with density.

For these tests, a MJ33 moisture analyzer from Mettler Toledo is used (Fig. 8).

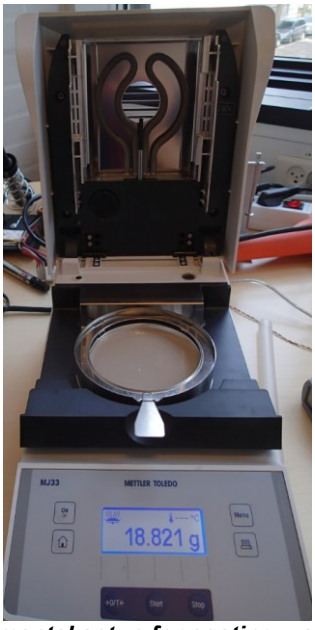

Fig. 8. Experimental setup for coating water content measurement.

A quantity of 15-20 grams of coating is placed in a container of known weight, and then the weight is measured while heat is applied to the sample at a temperature of 105 °C. The measurement stops when the weight variation is less than 1 mg over a period of 30 seconds.

The water content is then calculated as:

$$WaterContent = \frac{InitialWeight - FinalWeight}{InitialWeight} 100 \quad \text{Eq. 2}$$

COATING LAYER PROPERTIES TESTS

Design of Experiment

The main objectives of this second set of experiments are:

- To determine if and how different parameters known from literature and industry are affecting coating layer properties
- To suggest control strategies for the influent parameters in order to achieve repeatable coating and drying processes

The variables considered in these tests are: sand type, binder type, gravity effect, dust & fines level, compaction level, dipping time (time that the coating is in contact with the sand sample) and coating type.

Table 2 summarizes the variables and the levels used in this experimental campaign.

Sand type and binder type are combined to reflect the two furan based recipes used in the factories.
Dust and fines levels are chosen to be the minimum possible level (0.00 % dust and 0.10% fines) and the maximum allowed level in the factories (0.2 % dust and 2 % fines).
Low compaction is achieved by filling the test specimens without vibration and no compaction load applied while it cures. High compaction is achieved by applying a weight of 1 kg on a sample of 18 mm diameter. This will generate, in the compacted specimen, a pressure of 38 kPa, representative of the pressure present at the bottom of a mould with a height of about 2.5-3 m (assuming hydrostatic pressure distribution and a sand density of about 1450 kg/m^3).
Coating density levels are chosen to be the upper and lower boundaries of the current specification (1790 kg/m^3 and 2042 kg/m^3).
The variable "Coating type" indicates two different batches of the same commercial coating supplied to two different factories (VCM and VCK).
Dipping times are chosen as 2 seconds (to represent a single quick pass during flow coating process) and 2 minutes (to represent the area where the coating is gathered, that are inevitably formed during the coating of a large mould).

Gravity effect represents the fact the coated surface might be facing upwards or downwards and gravity might speed up or slow down the penetration on the coating in the sand surface of the mould.

All tests are carried out at temperature between 22 and 25 C.

Table 2. Variables for coating properties tests

Variable	Number of Levels	Level 1	Level 2
Sand Recipe	2	VCM HA 1%	VCK Dyn 1%
Dust & Fines	2	0.00%/0.10% Dust/Fines	0.20%/2.00% Dust/Fines
Compaction	2	High (1 kg weight)	Low (no weight)
Coating Density	2	1790	2042
Coating Type	2	VCM	VCK
Dipping Time	2	2	120
Gravity Effect	2	Sample facing up	Sample facing down
Full factorial runs	128		
Resolution VII fractional factorial runs	64		

When assessing coating layer properties, typically in literature the coating layer is divided in a top layer and an absorbed depth (Fig. 1)[8, 10].
Top layer is typically measured by a comb or wheel as a wet property. Absorbed layer is typically not measured in production. We are choosing not to measure top layer in order to avoid damaging the samples and to be able to carry out more accurate gravimetric analyses.

The response variables considered for this study are:

- Wet Coating Thickness (WCT) [kg/m^2]
- Dry Coating Thickness (DCT) [kg/m^2]
- Wet Coating Water Content/Thickness (WT) [kg/m^2]
- Coating Water Fraction (CWF) [%]
- Penetration depth [mm]
- Sand Density [kg/m^3]

Wet coating thickness is calculated from the weight variation in the sample before and after coating and from the area of the sample as in Eq.3. This property represents the quantity of material (solids+water) added to the coated surface.

$$WCT = \frac{SandWeight - WetCoatedSampleWeight}{SampleArea} \quad \text{Eq. 3}$$

Dry coating thickness indicates how much of the coating is still present on the surface after drying and is calculated as in Eq.4. This property represents how much solid material has been added to the surface and it is therefore a better indication of the final coating layer properties. Also cost of coating consumption is dependent on this quantity.

$$DCT = \frac{SandWeight - DryCoatedSampleWeight}{SampleArea} \quad \text{Eq. 4}$$

Water thickness is calculated from the difference between wet and dry coating thicknesses (Eq.5). This property heavily influences drying time and the energy required for the drying process.

$$WT = WCT - DCT \quad \text{Eq. 5}$$

Coating water fraction it is representative of the fraction of water in the coating absorbed by the sample (Eq. 6). This property is useful to understand, by comparison with the original water content of the coating (Eq. 2), if there is any adsorption of water from the coating to the sand sample.

$$DCT = \frac{WT}{WCT}100 \quad \text{Eq. 6}$$

Coating penetration is a measure of how deep the coating will penetrate in the coated surface and is measured from pictures taken with a stereo microscope. This property can affect drying time since drying front requires more time to reach deeper into the mould.

Sand density is calculated from the measured volume and weight of the tested specimens to verify if compaction has an effect on this parameter and therefore if it is possible to use density measurements to assess compaction of sand moulds.

In order to reduce the number of runs (for a full factorial we would need 128 runs) a factional factorial design is chosen. This design requires 64 runs and aliases only 6th order interactions with main effects. The full alias structure can be seen in Fig. 9.

Fractional Factorial Design

Factors:	7	Base Design:	7, 64	Resolution:	VII
Runs:	64	Replicates:	1	Fraction:	1/2
Blocks:	1	Center pts (total):	0		

Design Generators: G = ABCDEF

Alias Structure

I + ABCDEFG

A + BCDEFG	AB + CDEFG	ABC + DEFG	BCG + ADEF
B + ACDEFG	AC + BDEFG	ABD + CEFG	BDE + ACFG
C + ABDEFG	AD + BCEFG	ABE + CDFG	BDF + ACEG
D + ABCEFG	AE + BCDFG	ABF + CDEG	BDG + ACEF
E + ABCDFG	AF + BCDEG	ABG + CDEF	BEF + ACDG
F + ABCDEG	AG + BCDEF	ACD + BEFG	BEG + ACDF
G + ABCDEF	BC + ADEFG	ACE + BDFG	BFG + ACDE
	BD + ACEFG	ACF + BDEG	CDE + ABFG
	BE + ACDFG	ACG + BDEF	CDF + ABEG
	BF + ACDEG	ADE + BCFG	CDG + ABEF
	BG + ACDEF	ADF + BCEG	CEF + ABDG
	CD + ABEFG	ADG + BCEF	CEG + ABDF
	CE + ABDFG	AEF + BCDG	CFG + ABDE
	CF + ABDEG	AEG + BCDF	DEF + ABCG
	CG + ABDEF	AFG + BCDE	DEG + ABCF
	DE + ABCFG	BCD + AEFG	DFG + ABCE
	DF + ABCEG	BCE + ADFG	EFG + ABCD
	DG + ABCEF	BCF + ADEG	
	EF + ABCDG		
	EG + ABCDF		
	FG + ABCDE		

Fig. 9. Chosen fractional factorial design for coating thickness properties tests.

Test Procedure

The first step in the sample preparation procedure is to sieve the 1kg of sand from each of the two considered factories and place the content of each pan in separate containers (Fig. 10). Additionally 100 grams of filter dust is sieved in order to provide dust and fines needed to prepare the samples with high dust and fines levels.

Fig. 10. Sand from two different factories is sieved according to factory standard to eliminate dust and fines.

The sieved sand from each container is then weighed and mixed again (Fig. 11) in order to obtain four batches of 0.5 kg. Dust and fines is then added to two of these batches according to level 2 specified in Table 2 and the

other two batches will be added fines according to level 1 in Table 2.

Fig. 11. Sand weighing and mixing.

Cylindrical moulds of 18mm diam and 50mm depth are then filled with the sand from different batches and weights are applied to the mould where high level of compation is needed (Fig. 12).

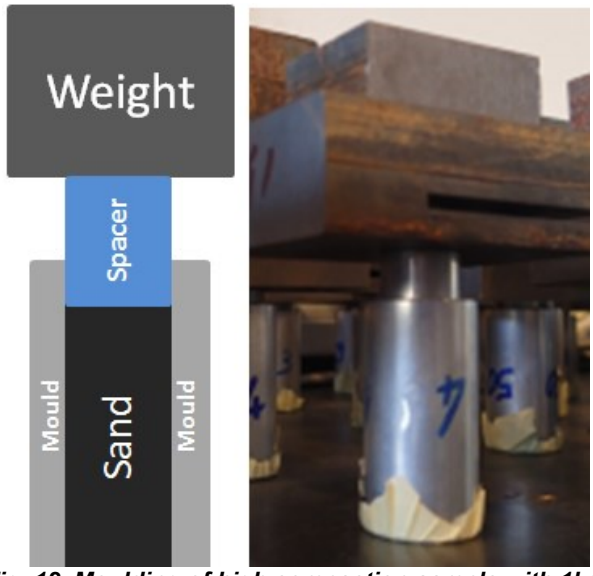

Fig. 12. Moulding of high compaction sample with 1kg weight.

Dimensions are taken (to calculate the volume of the sample) and weights of the sand mould are recorded for each mould (Fig. 13).
Weight measurements are carried out for the empty moulds, cured mould, freshly coated mould and the dry mould.

The coating of the mould is carried out either by immersion of the sample facing down in the coating or by placing on top of the sample a container that fits the moulds facing up and then pouring the coating in the container (Fig. 14).

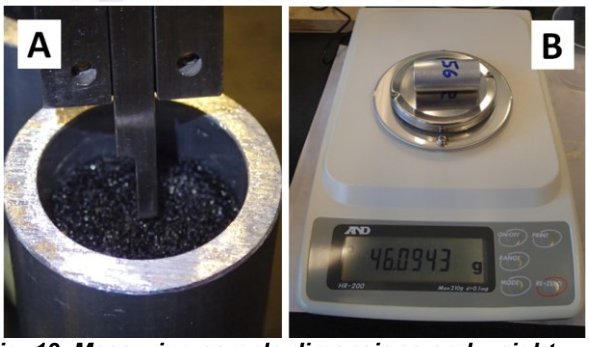

Fig. 13. Measuring sample dimensions and weight.

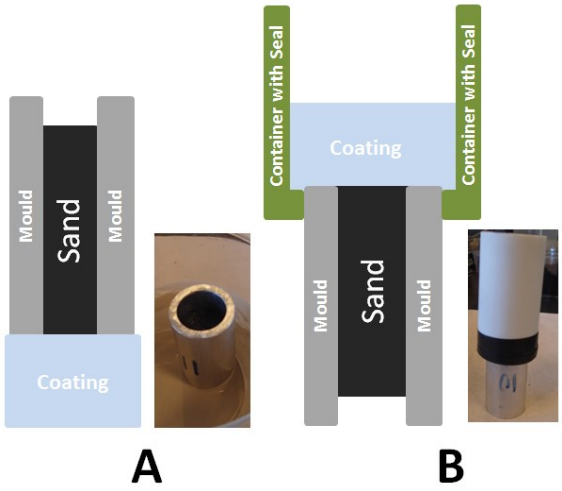

Fig. 14.Coating with: a) coated face down and b) coated face upwards

Then, the sides and top of the mould are cleaned from coating so that only the sand surface is coated (Fig. 15).

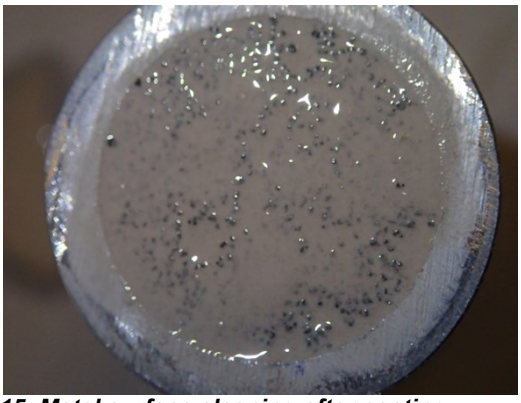

Fig. 15. Metal surface cleaning after coating

The samples are then dryed at 25 °C and 50% relative humidity for 1 week, to make sure the coating is dry (Fig. 16.).

Fig. 16. Samples drying in natural air at 25°C and 50% relative humidity for 1 week.

After the final weight measurement, the samples are extracted from the mould and ground along the length to obtain a flat surface (Fig. 17).

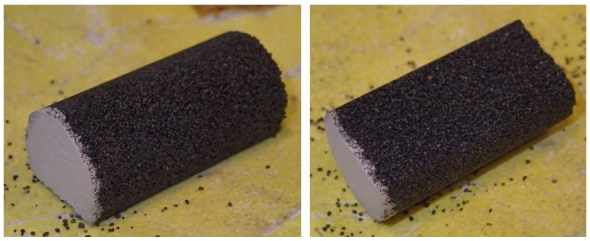

Fig. 17. Sample preparation for the microscope.

Images of the sample section are then taken with a stereomicroscope with an 8X magnification factor and saved (Fig. 18).

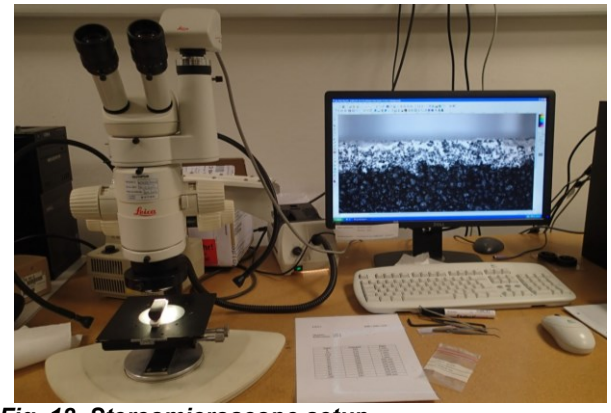

Fig. 18. Stereomicroscope setup.

Coating penetration depth measurements are then taken by analyzing each image in a photo editing software (Fig. 19).

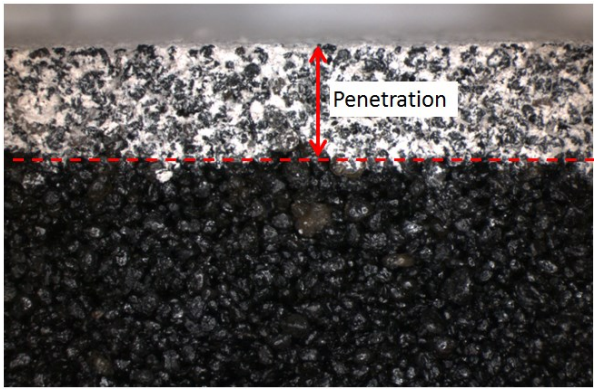

Fig. 19. Coating penetration measurement.

RESULTS

COATING PROPERTIES TESTS

Cup Time Tests Results

Results from the full factorial design for cup time, Baume and cup measured density are reported in Table 3. We can see how shortest cup times are obtained with the coating at 1790 kg/m^3, while the longest are obtained for the coating at 2042 kg/m^3.

Figure 20 shows the results of ANOVA where interactions up to the 3rd order are considered. Even though there are not enough degrees of freedom to compute the error and P-values, we can see from the adjusted sum of squares that density has by far the highest effect. Temperature and coating time have a very small effect and high order interaction have e a negligible effect.

ANOVA is repeated but eliminating all the non-relevant interactions except the one with the higher sum of squares value (Temp*Coating). Results shown in Fig. 21 confirm that coating density has an effect on cup time (P-value is zero), while temperature and coating seem not to have a relevant effect on cup time (P-value is 0.066 and 0.039 respectively).

Main effects plot (Fig. 22) graphically shows how cup time are increasing significantly with density but only have small fluctuation with respect of other variables.

It can also be noticed that when density decreases from 1908 kg/m^3 to 1790 kg/m^3, cup time decreases from about 13,5s to 12,5s. This difference might be difficult to measure with a manual cup time measurement.

Finally, in the main effect plot of density on cup time (Fig. 22), we can see that the relation between cup time and density is nonlinear.

Table 3. Full factorial resutls for cup time, Baume and cup measured density.

Factors			Responses		
Temp [°C]	Coating [ ]	Density [kg/m³]	Cup Time [s]	Baume [°Be]	Cup measured density [kg/m³]
10	VCM	1790	12,7	64	1718
10	VCM	1908	14,4	69	1891
10	VCM	2042	17,4	74	2074
10	VCK	1790	13,12	64	1790
10	VCK	1908	12,75	69	1956
10	VCK	2042	15,94	74	2046
23	VCM	1790	12,07	64	1750
23	VCM	1908	13,36	69	1885
23	VCM	2042	16,81	74	2024
23	VCK	1790	11,66	64	1749
23	VCK	1908	12,86	69	1907
23	VCK	2042	15,13	74	2036
36	VCM	1790	12,4	64	1761
36	VCM	1908	13,6	72	1865
36	VCM	2042	17,1	79	2007
36	VCK	1790	12,1	64	1761
36	VCK	1908	13,5	72	1913
36	VCK	2042	17,4	79	2032

Analysis of Variance for Cup Time [s], using Adjusted SS for Tests

Source	DF	Seq SS	Adj SS	Adj MS	F	P
Temp [C]	2	2,0725	2,0725	1,0362	**	
Coating [ ]	1	1,6080	1,6080	1,6080	**	
Density [kg/m3]	2	59,7847	59,7847	29,8924	**	
Temp [C]*Coating [ ]	2	0,7177	0,7177	0,3588	**	
Temp [C]*Density [kg/m3]	4	0,9616	0,9616	0,2404	**	
Coating [ ]*Density [kg/m3]	2	0,5940	0,5940	0,2970	**	
Temp [C]*Coating [ ]*Density [kg/m3]	4	1,3108	1,3108	0,3277	**	
Error	0	*	*	*		
Total	17	67,0493				

Fig. 20. ANOVA for cup time factorial design resutls with all effects included.

Analysis of Variance for Cup Time [s], using Adjusted SS for Tests

Source	DF	Seq SS	Adj SS	Adj MS	F	P
Temp [C]	2	2,0725	2,0725	1,0362	3,62	0,066
Coating [ ]	1	1,6080	1,6080	1,6080	5,61	0,039
Density [kg/m3]	2	59,7847	59,7847	29,8924	104,29	0,000
Temp [C]*Coating [ ]	2	0,7177	0,7177	0,3588	1,25	0,327
Error	10	2,8664	2,8664	0,2866		
Total	17	67,0493				

S = 0,535387 R-Sq = 95,72% R-Sq(adj) = 92,73%

Fig 21. ANOVA for cup time factorial design resutls with reduced number of effects.

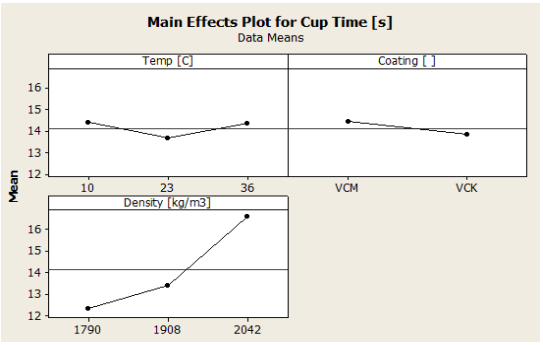

Fig. 22. Main effect plots for cuptime.

Table 4 reports results from the central composite design for cup time, Baume and cup measured density.

From figure 23, by looking at the P-values, we can see that density is still the most influent parameter on cup time. Coating type has a small effect (P-value of 0.002) this might be due also slight differences in the batches or in the preparation of the test container. Temperature does not seem to have an effect (P-value 0.694). Other interactions seem to have significant but very small effects.

Table 4. Center composite design results for cup time, Baume and cup measured density.

Factors			*Responses*		
Temp [°C]	Coating [ ]	Density [kg/m³]	Cup Time [s]	Baume [°Be]	Cup Measured Density [kg/m³]
10	VCM	1790	12,7	64	1718
10	VCK	1790	13,2	64	1790
10	VCM	2042	17,4	74	2074
10	VCK	2042	15,94	74	2046
36	VCM	1790	12,4	64	1761
36	VCK	1790	12,1	64	1761
36	VCM	2042	17,1	79	2007
36	VCK	2042	17,4	79	2032
23	VCM	1916	13,36	69	1885
23	VCK	1916	12,86	69	1907
23	VCM	1916	13,31	69	1916
23	VCK	1916	12,98	69	1914
23	VCM	1916	13,77	69	1880
23	VCK	1916	12,86	69	1923
23	VCM	1916	13,76	69	1927
23	VCK	1916	12,9	69	1936
23	VCM	1916	13,14	69	1896
23	VCK	1916	13,08	69	1924
23	VCM	1916	13,2	69	1898
23	VCK	1916	13,01	69	1925

Finally in Fig. 23 we can see that the P-value for curvature is zero, therefore it is confirmed that the relation between cup time and density is nonlinear.

Analysis of Variance for Cup Time [s] (coded units)

Source	DF	Seq SS	Adj SS	Adj MS	F	P
Main Effects	3	38,7522	38,7522	12,9174	291,84	0,000
Coating	1	0,7258	0,7258	0,7258	16,40	0,002
Density	1	38,0192	38,0192	38,0192	858,95	0,000
Temp	1	0,0072	0,0072	0,0072	0,16	0,694
2-Way Interactions	3	1,1656	1,1656	0,3885	8,78	0,003
Coating*Density	1	0,2312	0,2312	0,2312	5,22	0,043
Coating*Temp	1	0,1152	0,1152	0,1152	2,60	0,135
Density*Temp	1	0,8192	0,8192	0,8192	18,51	0,001
3-Way Interactions	1	0,8192	0,8192	0,8192	18,51	0,001
Coating*Density*Temp	1	0,8192	0,8192	0,8192	18,51	0,001
Curvature	1	12,1986	12,1986	12,1986	275,60	0,000
Residual Error	11	0,4869	0,4869	0,0443		
Lack of Fit	1	0,0663	0,0663	0,0663	1,58	0,238
Pure Error	10	0,4206	0,4206	0,0421		
Total	19	53,4225				

Fig. 23. ANOVA for cup time center composite design results with all effects included.

Baume Tests Results

Fig. 24 shows ANOVA analysis for Baume where the non relevant effects have not been considered in the model. It can be seen that density has the highest effect and temperature has a significant effect (P-value 0.007).

The main effect plot (Fig. 25) shows how how the baume reading increses when measuring at 36°C.

Analysis of Variance for Baume [Be], using Adjusted SS for Tests

Source	DF	Seq SS	Adj SS	Adj MS	F	P
Temp [C]	2	28,444	28,444	14,222	8,42	0,007
Coating [ ]	1	0,000	0,000	0,000	0,00	1,000
Density [kg/m3]	2	408,444	408,444	204,222	120,92	0,000
Temp [C]*Coating [ ]	2	0,000	0,000	0,000	0,00	1,000
Error	10	16,889	16,889	1,689		
Total	17	453,778				

S = 1,29957 R-Sq = 96,28% R-Sq(adj) = 93,67%

Fig. 24. ANOVA for Baume factorial design results with results with reduced number of effects.

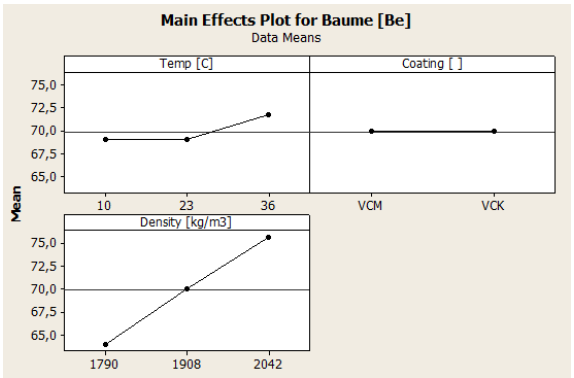

Fig. 25. Main effect plots for Baume.

The ANOVA of the central composite design for Baume tests (Fig. 26) shows that it is still not possible to calculate a total error even though center runs have been added. This problem is due to the lack in variation in the data (due low resolution of the Baume stick) and not in the lack of degrees of freedom. However, from the analysis of the sum of square we can see that the density has the highest effect, while temperature and interactions of second order have a minor effect.

Analysis of Variance for Baume [Be] (coded units)

Source	DF	Seq SS	Adj SS	Adj MS	F	P
Main Effects	3	325,000	325,000	108,333	*	*
Coating	1	0,000	0,000	0,000	*	*
Density	1	312,500	312,500	312,500	*	*
Temp	1	12,500	12,500	12,500	*	*
2-Way Interactions	3	12,500	12,500	4,167	*	*
Coating*Density	1	0,000	0,000	0,000	*	*
Coating*Temp	1	0,000	0,000	0,000	*	*
Density*Temp	1	12,500	12,500	12,500	*	*
3-Way Interactions	1	0,000	0,000	0,000	*	*
Coating*Density*Temp	1	0,000	0,000	0,000	*	*
Curvature	1	7,500	7,500	7,500	*	*
Residual Error	11	0,000	0,000	0,000		
Lack of Fit	1	0,000	0,000	0,000		
Pure Error	10	0,000	0,000	0,000		
Total	19	345,000				

Fig. 26. ANOVA for Baume central composite design results with all effects included.

Cup Measured Density Tests Results

The analysis of cup measured density (Fig 27) shows that coating density (at 23°C) is the variable with the highest effect on the cup measured density (P-value is zero). While temperature effect seems not to be affecting density since the P-value is 0.118. Coating type has a small effect (P-value 0.009). This might be due to small differences in preparation of the batches.

Analysis of Variance for Density measured cup [kg/m3] (coded units)

Source	DF	Seq SS	Adj SS	Adj MS	F	P
Main Effects	3	161812	161812	53937	276,57	0,000
Coating	1	1921	1921	1921	9,85	0,009
Density	1	159330	159330	159330	816,99	0,000
Temp	1	561	561	561	2,88	0,118
2-Way Interactions	3	1876	1876	625	3,21	0,066
Coating*Density	1	703	703	703	3,61	0,084
Coating*Temp	1	45	45	45	0,23	0,640
Density*Temp	1	1128	1128	1128	5,78	0,035
3-Way Interactions	1	1953	1953	1953	10,01	0,009
Coating*Density*Temp	1	1953	1953	1953	10,01	0,009
Curvature	1	725	725	725	3,72	0,080
Residual Error	11	2145	2145	195		
Lack of Fit	1	18	18	18	0,09	0,775
Pure Error	10	2127	2127	213		
Total	19	168512				

Fig. 27. ANOVA for cup measured density center composite design results with all effects included.

Rotational Viscosity Tests Results

Fig 28 reports the results from the rotational viscosity tests for all the considered coating at 23 °C. It can be seen that test speed does have an effect on absolute value (the higher the speed the lower the viscosity) but it does not change the curves shape compared to each other.
It also can be noticed that the higher the density of the coating the higher the viscosity.

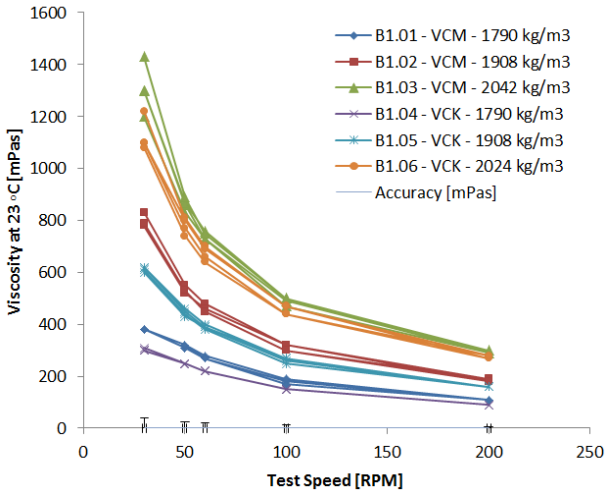

Fig. 28. Viscosity tests results at 23 °C for different coating batches and densities.

Figure 29 shows the viscosity test resutls for VCM coating with a density of 1908 kg/m^3 at the three different test temperatues. It can bee seen that temperature does not appear to influence the viscosity in the range investigated here.

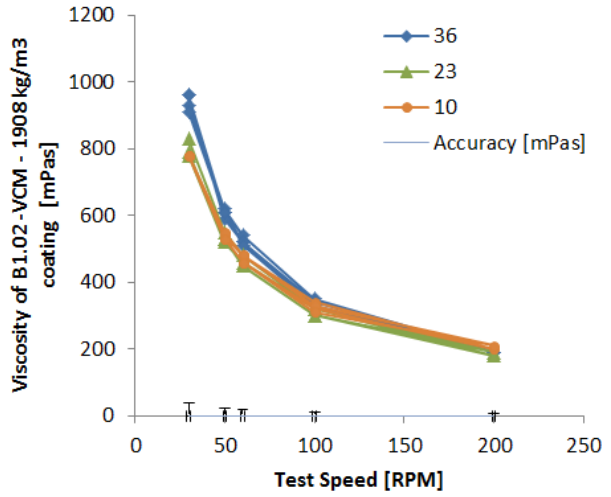

Fig. 29. Viscosity tests results for VCM coating with a density of 1908 kg/m^3.

ANOVA was performed for the full factorial considering as responses the viscosities at each test speed. Figure 30 shows the results for test speeds of 30, 100 and 200 RPM where the non-relevant interactions have been disregarded. It can be seen that, for all the test speeds, density is the factor with higher effect. Also coating density and temperature are significant (P-values are 0.001 and 0.000). The influence of temperature is however small compared to that of density. Interactions considered in the analysis are either non relevant (P-value above 0.05) or with a very small effect.

A

Analysis of Variance for mu_30_1, using Adjusted SS for Tests

Source	DF	Seq SS	Adj SS	Adj MS	F	P
Temp [C]	2	344100	344100	172050	30,04	0,001
Coating [ ]	1	40139	40139	40139	7,01	0,038
Density [kg/m3]	2	2880300	2880300	1440150	251,43	0,000
Temp [C]*Coating [ ]	2	38544	38544	19272	3,36	0,105
Temp [C]*Density [kg/m3]	4	107600	107600	26900	4,70	0,046
Error	6	34367	34367	5728		
Total	17	3445050				

B

Analysis of Variance for mu_100_1, using Adjusted SS for Tests

Source	DF	Seq SS	Adj SS	Adj MS	F	P
Temp [C]	2	19744	19744	9872	38,63	0,000
Coating [ ]	1	3472	3472	3472	13,59	0,010
Density [kg/m3]	2	356344	356344	178172	697,20	0,000
Temp [C]*Coating [ ]	2	6144	6144	3072	12,02	0,008
Temp [C]*Density [kg/m3]	4	3856	3856	964	3,77	0,072
Error	6	1533	1533	256		
Total	17	391094				

C

Analysis of Variance for mu_200_1, using Adjusted SS for Tests

Source	DF	Seq SS	Adj SS	Adj MS	F	P
Temp [C]	2	3811	3811	1906	31,18	0,001
Coating [ ]	1	800	800	800	13,09	0,011
Density [kg/m3]	2	118878	118878	59439	972,64	0,000
Temp [C]*Coating [ ]	2	1633	1633	817	13,36	0,006
Temp [C]*Density [kg/m3]	4	1556	1556	389	6,36	0,024
Error	6	367	367	61		
Total	17	127044				

Fig. 30. ANOVA for rotational viscosity factorial design results. Test speed of 30, 100 and 200 RPM. Non relevant interactions disregarded.

Figure 31 and 32 provide a visual representation of the effects. It can bee seen how at 30 RMP viscosity varies from 480 to 760 mPas for a change in density from 1790 kg/m^3 to 1908 kg/m^3. At 200 RMP viscosity varies from 120 to 180 mPas for a change in density from 1790 kg/m^3 to 1908 kg/m^3.

Also, we can notice that temperature does have a small effect on viscosity that cannot be detected so clearly by the other instruments.

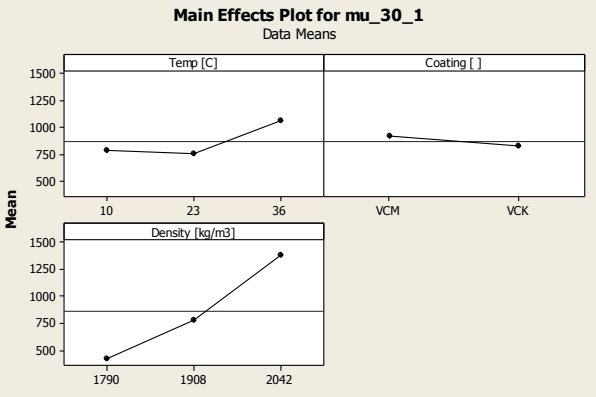

Fig. 31. Main effect plots for rotational viscosity full factorial tests at 30 RMP.

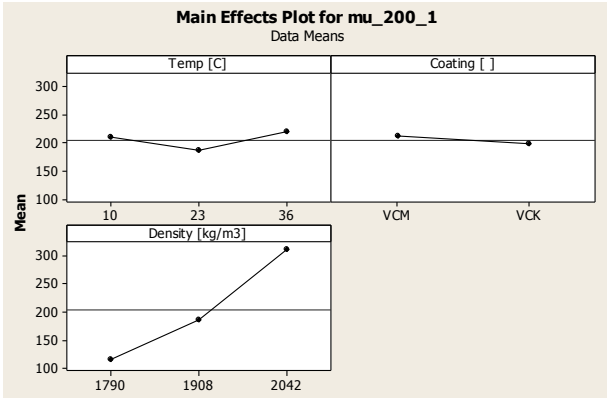

Fig. 32. Main effect plots for rotational viscosity full factorial tests at 200 RMP.

Results for the other speeds are similar to the one shown, but omitted due to lack of space.

Water Content Tests Results

Water content result are reported in figures 33 and 34. We can see that for both coating batches we have a water content of about 43% for a density of 1790 kg/m^3, 38% for a density of 1908 kg/m^3 and 34 % for a density of 2042 kg/m^3.

Also from figure 34 we note that coating batch has a small effect on moisture content.

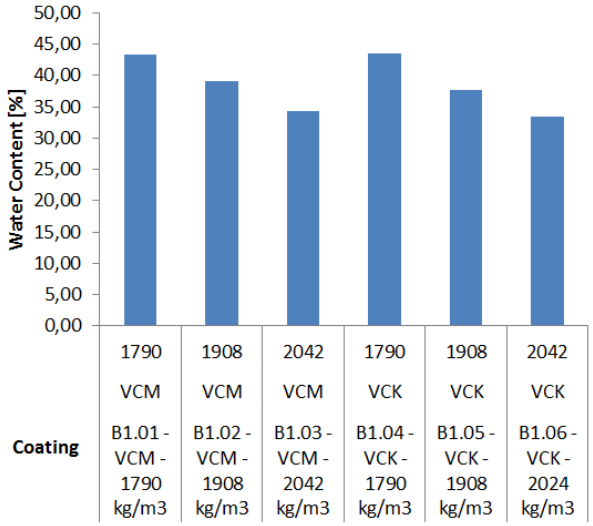

Fig. 33. Moisture content results for different coatings.

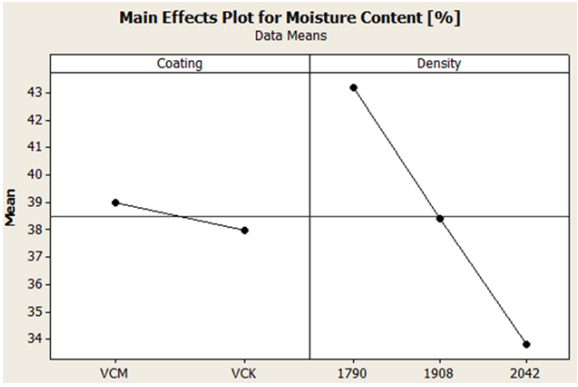

Fig. 34. Main effects plot for moisture content tests.

COATING THICKNESS

Raw data for coating thickness properties tests are not reported due to lack of space. ANOVA has been performed considering interaction up to the 3rd order in the statistical model and results are reported as Pareto charts of the effects (to visualize critical parameters) and box plots (to visualize entity of effects and scatter of the data).

From figures 35 and 36 we can notice that for wet coating thickness and dry coating thickness the most relevant effect is sand compaction followed by dipping time and gravity effect. Second order interactions have smaller effects.

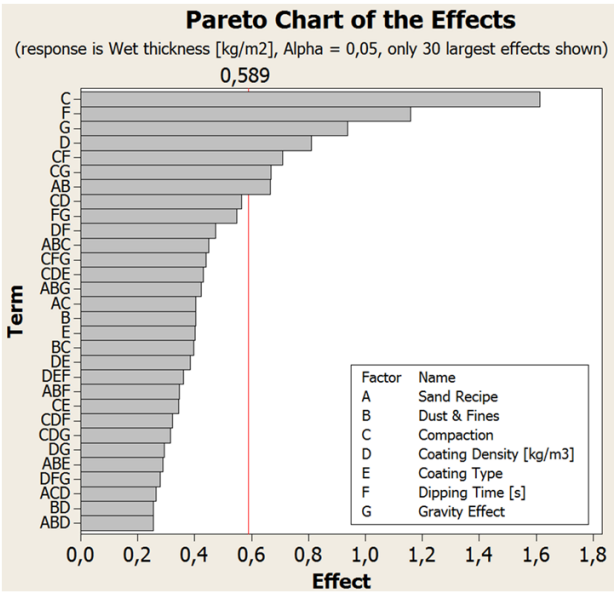

Fig. 35. Pareto chart of effects for wet coating thickness (up to 3rd order interection inlcuded).

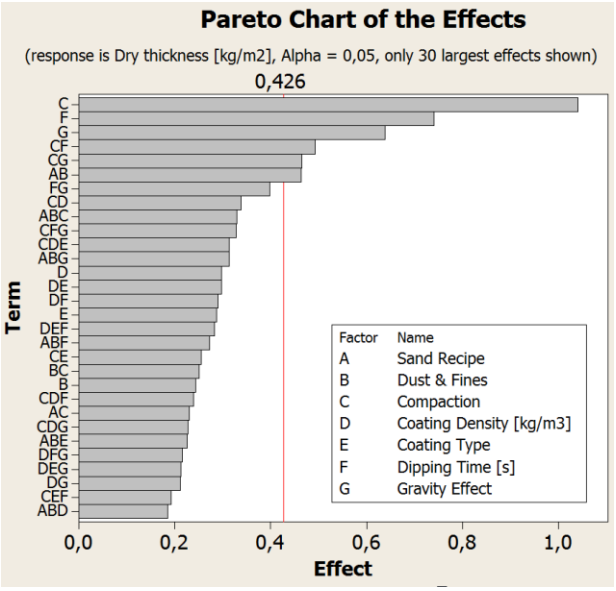

Fig. 36. Pareto chart of effects for dry coating thickness (up to 3rd order interection inlcuded).

From figure 37 we can see how the main effects relevant for the dry coating thickenss affect this variable. In particular low compaction generate a larger variation compared to high compaction. For high compaction dry thickness is typically between 0.8 kg/m^2 and 1.5 kg/m^2, while for low compaction is above 1.2 kg/m^2. The worst combination is for low compaction, 120s dipping time and with sample facing up, in this case dry coating thickness varies from about 1.5 kg/m^2 to more than 6 kg/m^2.

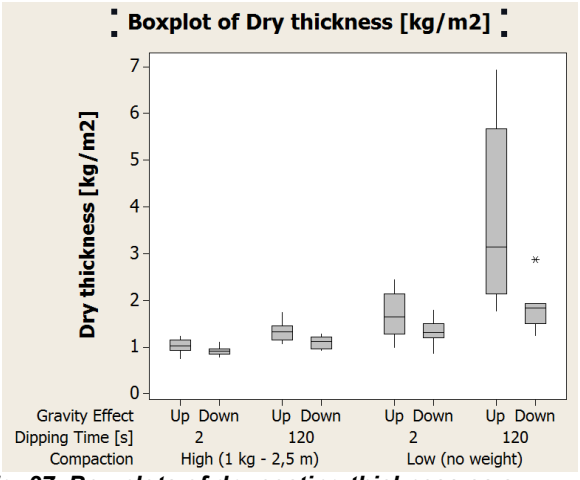

Fig. 37. Box plots of dry coating thickness as a function of most relevant effects.

From the pareto chart of effects for water coating thickness (Fig. 38) we see that, additionally to compaction, coating density and dipping time, also gravity effect is relevant.

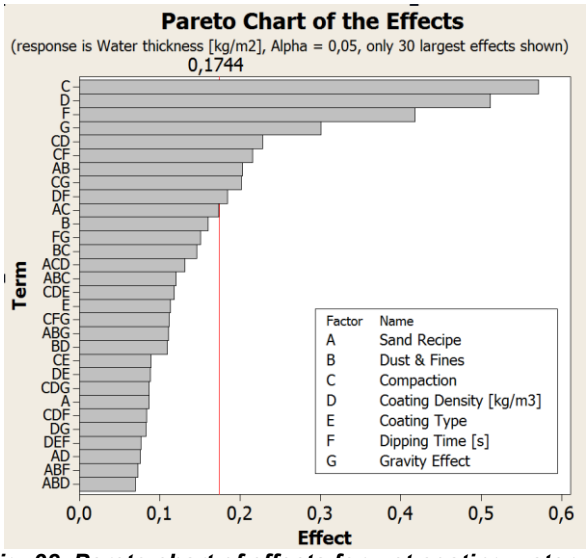

Fig. 38. Pareto chart of effects for wet coating water content/thickness (up to 3rd order interection inlcuded).

In figure 39 we see that, when other levels are kept constant, samples facing up always have a higher water thickness. Also we can see that water thickness can vary from less than 0.5 kg/m^3 to more than 3 kg/m^2 depending on the levels chosen.

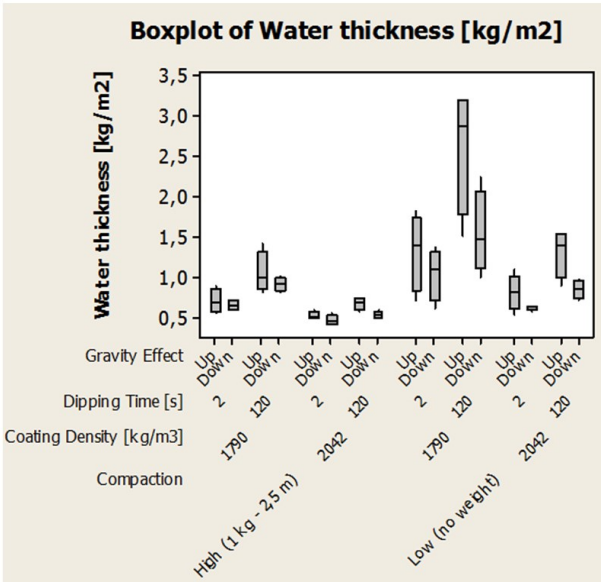

Fig. 39. Box plots of dry water thickness as a function of most relevant effects.

With respect to coating water fraction, Fig. 40 shows that coating density is by far the most important factor for this response.

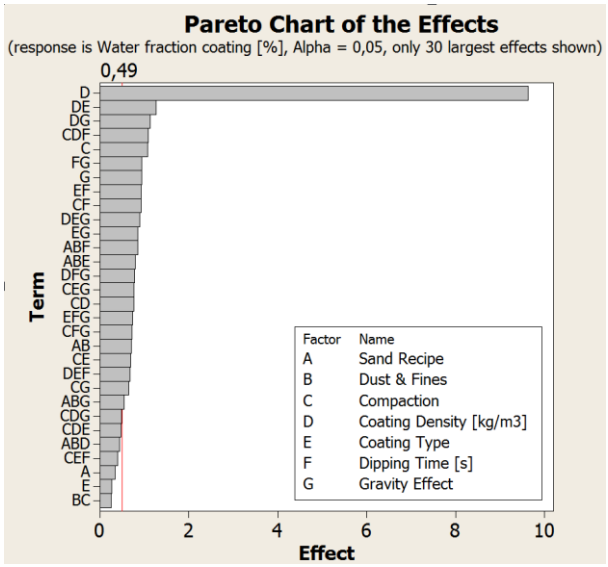

Fig. 40. Pareto chart of effects for coating water fraction (up to 3rd order interection inlcuded).

Fig. 41 shows that for a coating density of 1790 kg/m^3 the water fraction data are scattered around a value of 43% and for a coating density of 2042 kg/m^3 the value are scattered around a value of 33 %.

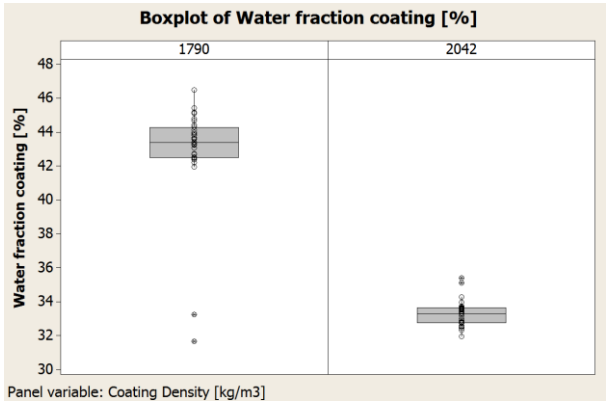

Fig. 41. Box plots of coating water fraction as a function of most relevant effects.

For coating penetration (Fig. 42) the most important effects are coating density, compaction and dipping time.

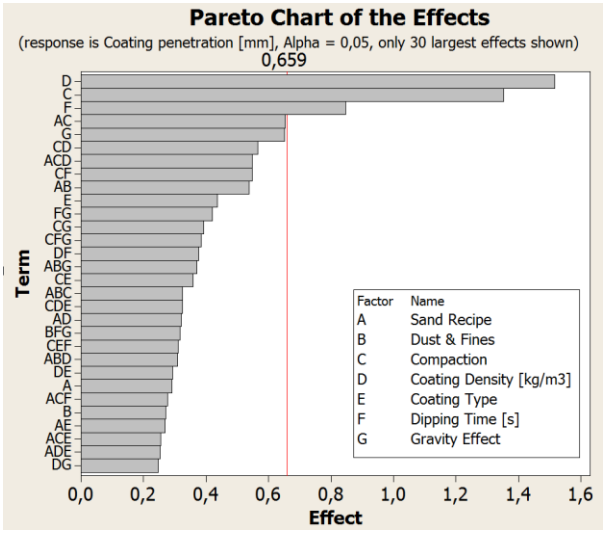

Fig. 42. Pareto chart of effects for coating penetration (up to 3rd order interection inlcuded).

From figure 43 we can see that coating penetration is comprised between 1.5 and 3 mm for a coating density of 2042 kg/m^3, while it can reach more than 6 mm for a coating density of 1790 kg/m^3.

Figure 44 shows microscope pictures of samples coated with coating density of 2042 kg/m^3, high sand compaction and 2 seconds dipping time versus samples coated with coating density of 1790 kg/m^3, low sand compaction and 120 seconds dipping time. Not only we can see the clear difference in penetrationd depth, but also there is a clear difference in uniformity of the layer. In particular the high compaction samples (Fig. 44 A and B) have quite uniform coating penetration, while the low compaction (Fig. 44 C & D) samples have a non uniform coating penetration.

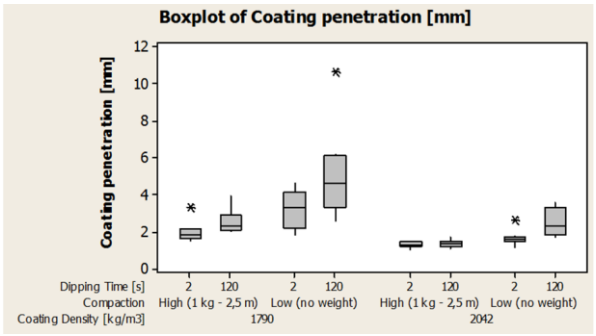

Fig. 43. Box plots of coating penetration as a function of most relevant effects.

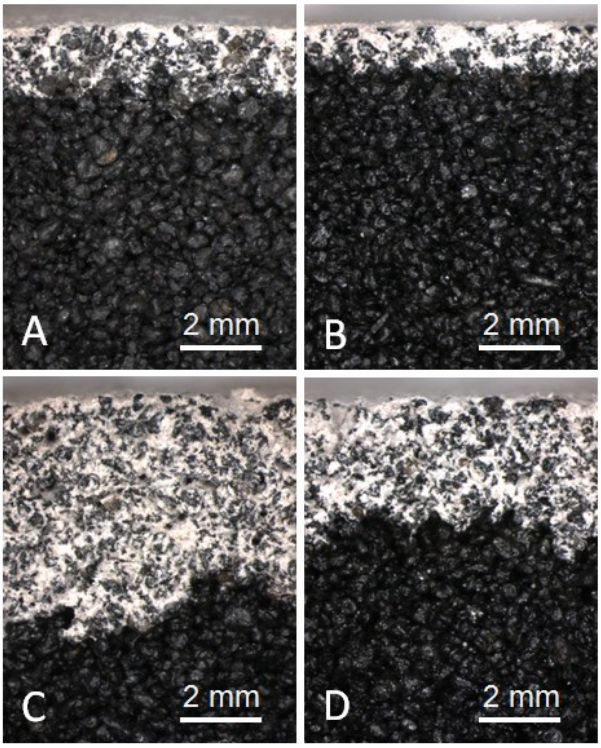

Fig. 44. Coating penetration pictures for samples with coating density of 2042 kg/m^3, high sand compaction coated for 2 seconds facing up(A) and down (B). Samples with coating density of 1790 kg/m^3, low sand compaction coated for 120 seconds facing up (C) and down (D).

From Fig 45 we can see that sand density is heavily affected by sand compaction and sand type.

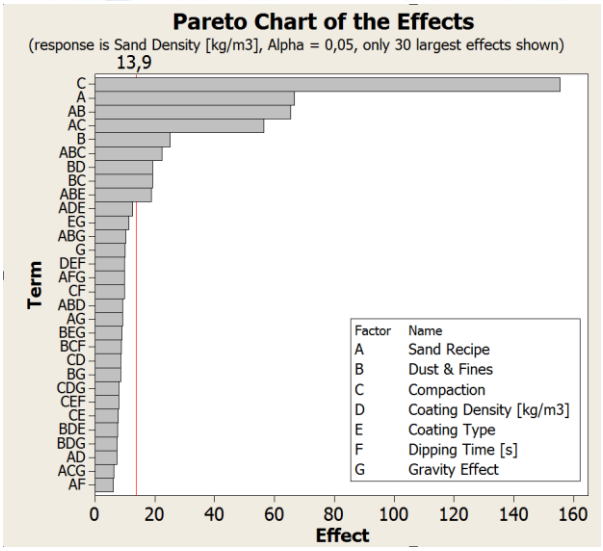

Fig. 45. Pareto chart of effects for sand density (up to 3rd order interection inlcuded).

In figure 46 we can see that sand densities between 1400 kg/m^3 and 1550 kg/m^3 are achieved with high compaction. With low compaction sand density achieved are between 1150 kg/m^3 and 1400 kg/m^3.

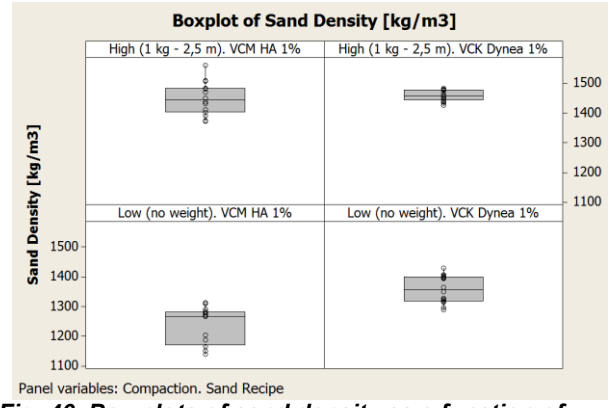

Fig. 46. Box plots of sand density as a function of most relevant effects.

In Table 5, a summary of the main effects relevant for each coating thickness property is provided. We can see that compaction is critical for all the properties. Coating density is critical for control of coating penetration and water fraction. Dipping time and gravity are relevant for the other coating properties. Finally, the considered sand recipes and coating batch do not have an effect of the thickness properties.

Table 5. Summary of main effects that are relevant for each coating layer property. Lowest numbers used to indicate the largest effects.

	Wet Coat. Thick. [kg/m^2]	Dry Coat. Thick. [kg/m^2]	Water Thick. [kg/m^2]	Coat. Water Fract. [%]	Penetration [mm]	Sand Den. [kg/m^3]
Sand Recipe						2
Dust & Fines			(5)			
Comp.	1	1	1	(2)	2	1
Coating Density	4		2	1	1	
Coating Type						
Dipping Time	2	2	3		3	
Gravity	3	3	4		(4)	

DISCUSSION

COATING PROPERTIES TESTS

Summarizing the results described in the previous section and in view of the stated objectives for this set of tests we can draw the following considerations:

- Coating viscosity is heavily affected by coating density, and to a minor degree by temperature. These variations can easily be measured with the rotational viscometer (the resolution and accuracy of the tool are smaller than the measured variation). With the Ford cup the small variations due to the temperature (0.5s to 1s) cannot be measured clearly due to the lower precision of this system. Also in case of manual measurements, density related variations might be affected by significant errors for the cup time method. The use of more accurate tools for measuring viscosity is therefore needed compared to what is currently used.
- Density of the coating is not dependent on temperature (from cup measured density results) however the Baume measurement method is varying with temperature and additionally it is characterized by low resolution. This suggests that Baume the stick can only be used as indication, and temperature compensation is needed for reducing the measurement errors.
- A slight difference in the coating batches properties is detected, but this is probably due to differences between the preparation of the test bottles. This suggests that the coating batches delivered to different factories do not have a substantial difference.
- The water content in the coating is heavily affected by density, even within the current control limits. This means that tight control of density is needed in order to achieve stable drying times.
- As density and viscosity are strongly correlated for a given coating, we suggest that only one of these variables need to be closely monitored and controlled in production facilities. However the methods used for monitoring shall have a higher precision than the ones used today.
- Temperature has shown a much smaller effect on coating properties and it is therefore not needed a tight control of this parameter. As a consequence it has been eliminated from the coating layer properties test campaign. This finding is somewhat different from common knowledge of the industry that coating viscosity is heavily affected by temperature. For the considered coating and temperature ranges, we can conclude that temperature control systems are not needed, if the objective is to control coating properties.

As a results of these findings, it is important to realize that both the Baume stick and the ford cup are only useful for rough estimation of coating properties, it therefore advised that coating properties are measured with more precise tools (such as in line density or viscosity meters). This is the first most important step to achieve control of the final coating layer properties and consequently improve control of surface quality, drying time and cost.

COATING LAYER PROPERTIES TESTS

Regarding coating layer properties tests we can summarize as follows:

- Sand compaction is critical for all the considered coating layer properties, typically a high compaction level will give more repeatable and uniform results. Direct consequences are that, if good sand mould compaction can be achieved, savings can be harvested from lower coating consumption, less energy required for drying, shorter drying time and more stable quality performance (due to repeatable coating layer properties). Additionally a better control of the coating layer can help to improve fatigue properties and life of the components by changing the microstructure of the skin of the cast part[9].

- Sand compaction level can be checked by measuring the density, since the sand density is only affected by the compaction level for a given sand recipe. This measurement could be easy to implement in a factory environment by taking samples from a real mould and then use the data to improve the moulding and compaction process.
- The second most important property is, also in this case, coating density. It affects heavily the coating penetration and the water thickness which determines energy and time required for drying. Additionally, coating water fraction in the coated layer has been found to be basically the same as the one in the prepared coating, it is therefore possible to directly predict the fraction of water in a coated layer if coating density is monitored precisely.
- Both dipping time and gravity are relevant factors for coating thickness properties. In order to control these two factors it is important to design the coating process so as to avoid areas where coating is gathered for a long time compared to areas were coating is applied with only one quick pass.
- Finally, it is important to note that there are no significant differences between the two coating batches, from the two sand recipes considered and for the dust and fines quantity allowed in these experiments. This will allow experimenters to eliminate these variables from future experimental designs. Additionally it proves that the coatings supplied to the different factories are consistent and have uniform properties.

If we look at the cost of the coating and drying process, an interesting finding is that adding water (lowering the density) to the coating (in an attempt to lower the consumption of purchased coating and therefore cost) will increase the wet thickness, the water content and the penetration (all these variables will increase drying time and energy required for drying, and therefore increase production cost). On the other hand, the dry thickness (which represents the consumption of purchased coating) is not affected by the coating density.
In order to control the consumption of coating it is suggested to have a well compacted mould, this will substantially reduce the variation in dry thickness and therefore in coating consumption, additionally it will provide more uniform surface properties on the casting skin. Additionally when designing the mould and the coating process it important to avoid stagnation of coating to reduce the variations in coating thicknesses and penetration.

CONCLUSION

Two test campaigns have been designed to better understand the effect of different process variables on the coating layer properties for furan bonded sand coated with water based coatings.

Results show that coating viscosity is strictly correlated to density and affects heavily coating layer properties. Temperature has only a small effect on viscosity but not on density.

Cup time and Baumé measurement methods have shown to have low repeatability or sensibility and it is therefore advised to improve the accuracy of current coating monitoring methods.

Process variables critical for the layer properties are also sand compaction, dipping time and gravity. All these variables need to be controlled in order to achieve stability in coating layer properties, energy required for drying and drying time.

ACKNOWLEDGMENTS

This work was financed by Global Castings A/S, the Danish Agency for Science, Technology and Innovation (DASTI) and the Technical University of Denmark (DTU).

REFERENCES

1. Control Limits for the Drying of Water Based Coatings, N. Schutze, Foseco, Foundry Practice, Issue 255, June 2011.
2. The Research of Desiccation Rates Selected Protective Coating Used on Mould and Sand Cores, L. Jamrozowicz, J. Zych, T. Snopkiewicz, Archive of Foundry Engineering, Vol.13, 01/2013, 45-50.
3. Ultra-Performance Core Coatings For Mass Iron Casting Production: Specialized Methods For Developing & Evaluating New Coating Technology, Tom Penko, Foseco Metallurgical Inc.
4. Influence of New Sol-Gel Refractory Coating on the Casting Properties of Cold Box and Furan Cores for Grey Cast Iron, U. C. Nwaogu, N.S. Tiedje, Proceeding of 69th World Foundry Congress, October 16-20, 2010.
5. New sol–gel refractory coatings on chemically-bonded sand cores for foundry applications to improve casting surface quality, U.C. Nwaogu, T.

Poulsen, R.K. Stage, C. Bischoff, N.S. Tiedje, Surface and Coatings Technology, Volume 205, Issue 16, 15 May 2011, Pages 4035–4044.

6. Using sol-gel component as additive to foundry coatings to improve casting quality, U.C. Nwaogu, N.S. Tiedje, Journal of Cast Metals Research, 2012, 176-187.
7. Improving Casting Quality through Optimized Coating Technology, Foseco.
8. Foundry Coating Composition, Patent EP2364798 B1, M. Haanepen, F. Piekartz, Foseco, 18 July 2012.
9. Ductile and Compacted Graphite Iron Casting Skin - Evaluation, Effect on Fatigue Strength and Elimination, B. Sarum, PhD Thesis, Ohio State University, Page 103-106.
10. Foundry Coating Technology: A Review, U. C. Nwaogu, N. S. Tiedje, Materials Sciences and Application, 2011, 2, 1143-1160.
11. Coatings Technology Handbook, Third Edition, Arthur A. Tracton, Ch. 1-3.
12. 'Perry's Chemical Engineers' Handbook (7th Edition)', McGraw-Hill, 2008. Table 1-12 (page 1-20).

Supplement II

Achieving Control of Coating Process in your Foundry

G.L. Di Muoio [a]*, N.S. Tiedje [b]
[a]* Castings Technology, Global Castings A/S, 373N Diplomvej, Lyngby, 2800, Denmark
[b] Mechanical Engineering, Technical University of Denmark, Building 427, room 306b, Kgs. Lyngby, 2800, Denmark

Received Jan 2015; accepted in revised form Feb 2015

Abstract

Achieving control of coating thickness in foundry moulds is needed in order to guarantee uniform properties of the mould but also to achieve control of drying time. Since drying time of water based coatings is heavily dependent on the amount of water present in the coating layer, a stable coating process is prerequisite for a stable drying process. In this study, we analyse the effect of different variables on the coating layer properties. We start by considering four critical variables identified in a previous study such as sand compaction, coating density, dipping time and gravity and then we add centre points to the original experimental plans to identify possible non-linear effects and variation in process stability. Finally, we investigate the relation between coating penetration (a variable that is relatively simple to measure in production) and other coating layer thickness properties (relevant for the drying process design). Correlations are found and equations are provided. In particular it is found that water thickness can be directly correlated to penetration with a simple linear equation and without the need to account for other variables.

Keywords: Innovative Foundry Technologies and Materials, Quality Management, Coating Process Control, Sand Compaction, Coating Penetration.

1. Introduction

Since the introduction of water based foundry coatings in the recent years, controlling drying time has become an important issue for many foundries [1]. Coating thickness stability in foundry moulds is needed in order to guarantee uniform properties of the mould. This allows to reach control of drying time [1,2] (by limiting the amount of water deposited on the mould) but also to improve casting quality by reducing the chance of moisture related defects and improving surface quality [3,4].

For a given sand recipe the most important parameters for the control of coating thickness properties are compaction, coating density, dipping time and gravity effects [5]. In this study we investigate the effect of these variables on the different coating properties and their influence on process stability.

Finally we look for correlations between coating penetration (a variable that can be simply be measured in production) and other coating layer thickness properties. Correlations are found and equations provided. In particular it is found that water thickness can be directly correlated to penetration with a simple linear equation.

2. Methods

For this study we consider a cylindrical mould filled with sand and compacted with an aluminium spacer on which different pressure levels are applied in order to achieve different levels of compaction (Figure 1). The compacted and cured samples are then coated by dipping method using different process parameters (Table 1)

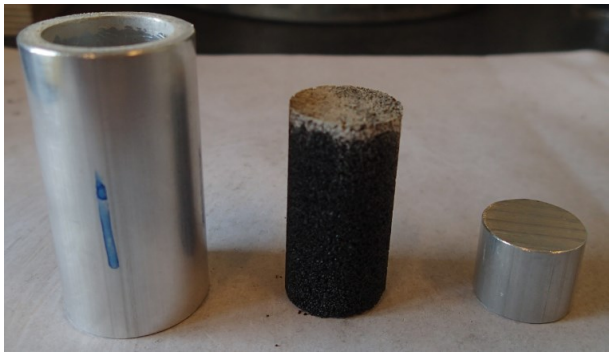

Figure 1. Pictures of cylindrical mould (right), coated sand sample (centre) and aluminium spacer used for compaction (left).

In Table 1 we can see the different levels used for each variable. Compaction levels are obtained by applying to the mould a pressure calculated by multiplying a standard sand density of 1300 kg/m^2 by the depth of the mould. For this study we choose a pressure equivalent to that under a column of sand 0.2 m, 1.25 m and 2.5 m high. Such pressures are considered representative for large foundry moulds.
Coating density is chosen to represent the minimum, maximum and centre of the specification used in the factories. Dipping times are chosen to represent four cases: a fast pass (2 s), normal pass (5 s), slow pass (15s) and a pool of coating gathering in a cavity of the mould (120 s). Gravity is represented by dipping the sample facing up or down.

Table 1. Variables considered in this study and correspondent levels used.

	Level 1	Level 2	Level 3	Level 4
Compaction	Low (0.2 m)	Medium (1.25 m)	High (2.5 m)	
Coating Density [kg/m3]	1790	1908	2042	
Dipping Time [s]	2	5	15	120
Gravity	Up	Down		

The response variables considered in this study are: sand density [kg/m^3] (varied density is achieved by compacting sand under different pressures, i.e. compaction level), water thickness [kg/m^2] (represents the amount of water per square meter of mould), wet thickness [kg/m^2] (the total amount of coating deposited on the surface of the mould), dry thickness [kg/m^2] (amount of refractory material deposited in the mould) and coating penetration [mm] (depth reached by the coating layer). The experimental methods are described in full detail in [5]. To estimate the general variation in the experiments several "centre point experiments" were carried out under the following conditions: medium compaction, coating density of 1908 kg/m3, dipping time of 5 seconds and sample facing down.

3. Results

3.1. Main Effects

The first results (Figure 2) show the effect of sand depth (and relative compaction pressure) on the achieved sand density. In the figure we can see that the function is non-linear. In particular sand density decreases significantly for low sand depths and the scatter increases substantially. It is therefore important for small moulds (depth lower than 1 m) to make sure that manual compaction methods and vibration are used.

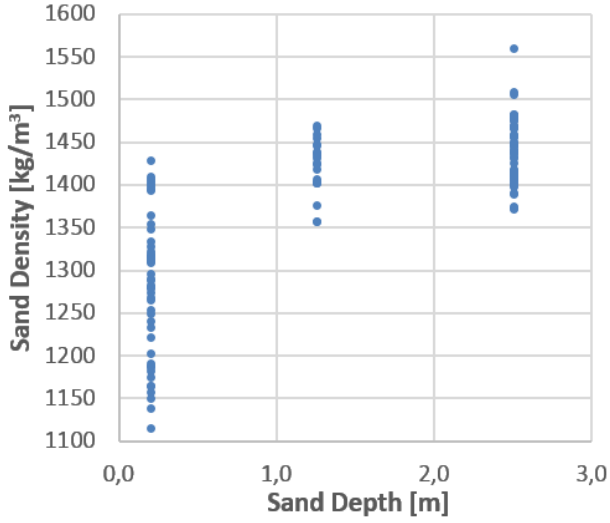

Figure 2. Sand density of samples as a function of mould depth.

Figure 3 shows how water thickness depends heavily on the sand density and scatter increases substantially for sand densities below 1350 kg/m^3.

The effect of coating density is shown in Figure 4. In this case we see that the scatter in water thickness decreases as the coating density increases. It appears that there is a threshold density above which the scatter is reduced by a factor of 3. The threshold is near a coating density of 2042 kg/m^3.

The effect of time is represented in Figure 5. Again we see a strong non-linear correlation where water thickness increases substantially with dipping time as well as scatter does. It is therefore important to coat samples with fast passes and avoid pools of coating that will increase substantially the water thickness layer.

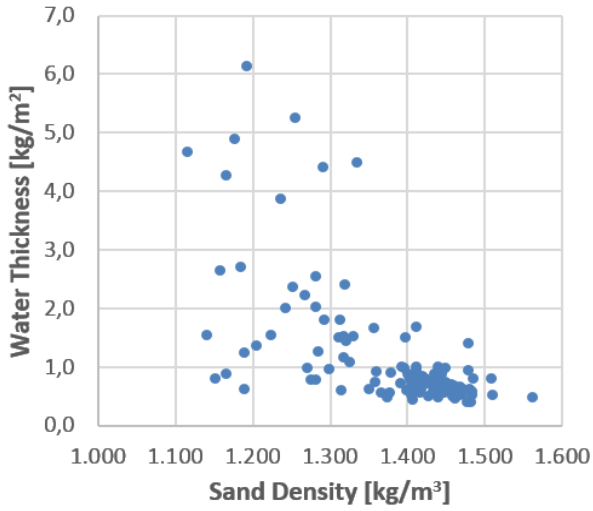

Figure 3. Water thickness as a function of sand density.

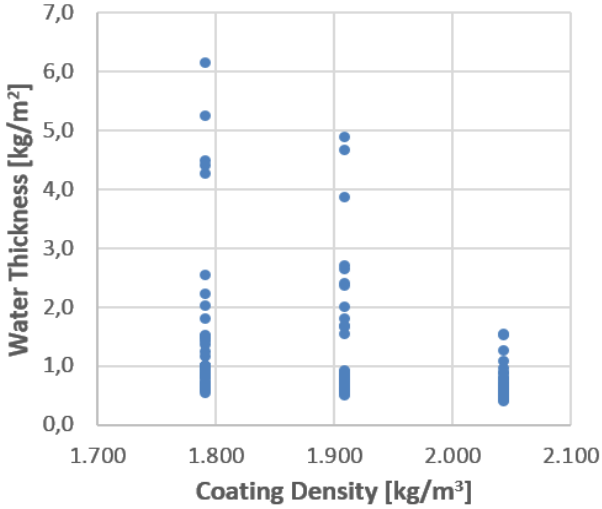

Figure 4. Water thickness as a function of coating density.

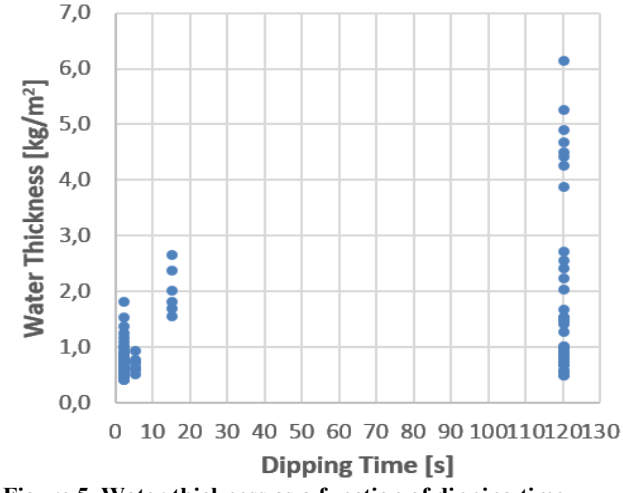

Figure 5. Water thickness as a function of dipping time.

Finally in Figure 6 we can see that for samples facing down, where the coating is applied against gravity, the variation in water thickness is much smaller than for samples coated facing upwards.

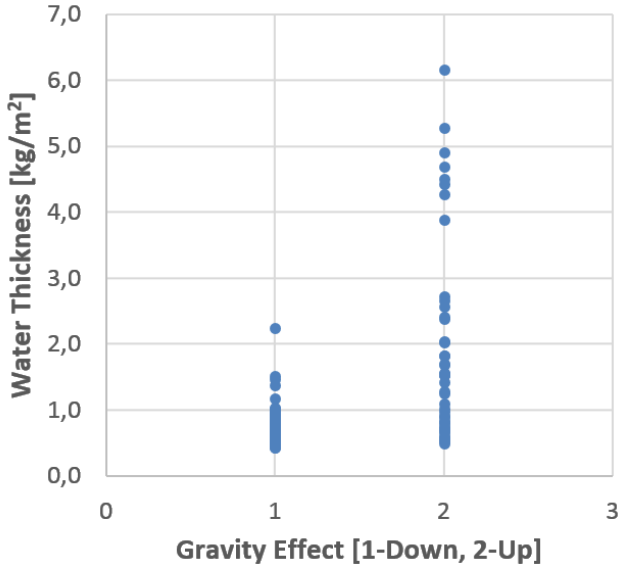

Figure 6. Water thickness as a function of gravity effect.

3.1. Process Control

To investigate the stability of the process, Figure 7 shows the water thickness of several samples coated with the centre point levels of the process parameters (medium compaction, coating density of 1908 kg/m^3, dipping time of 5 seconds and sample facing down). We can see how there is a limited amount of scatter and that is possible to control the coating thickness between 0.65 and 0.85 kg/m^2.

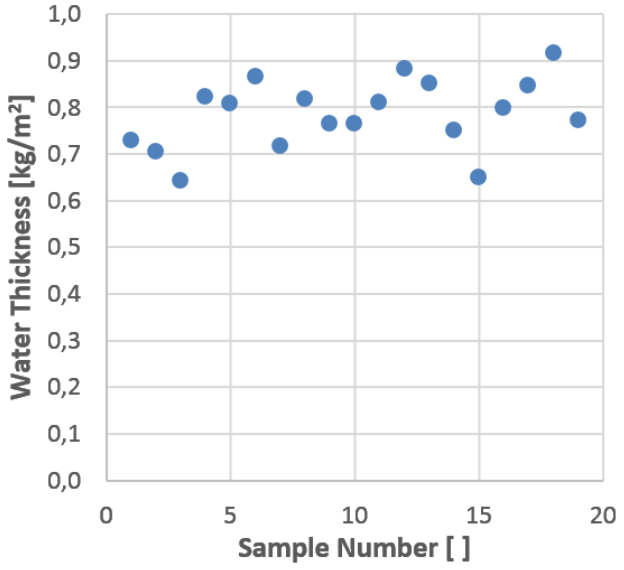

Figure 7. Water thickness of sample coated with the same coating conditions (medium compaction, coating density of 1908 kg/m3, dipping time of 5 seconds and sample facing down).

3.1. Correlations

In Figure 8 we can see coating layer moisture cannot be correlated to coating penetration but is a clear relation to coating density. Therefore we will not provide a correlation between coating layer moisture and penetration.

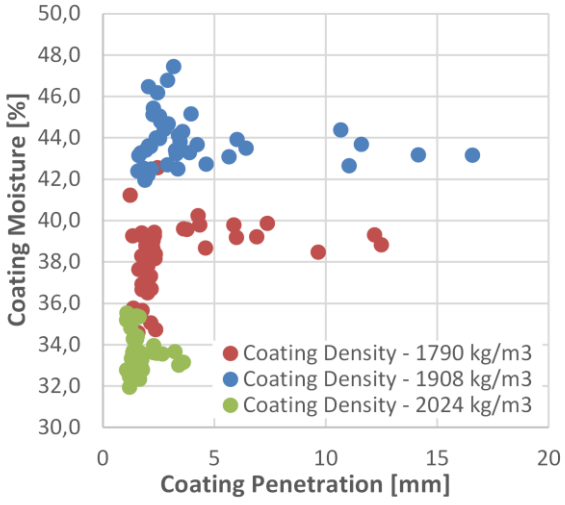

Figure 8. Coating moisture as function of coating penetration.

Figures 9.a to 9.c show correlations between different coating thickness properties and coating penetration. We can see that, especially for dry thickness (Figure 9.a) and wet thickness (Figure 9.b) the correlation is heavily dependent on the coating density values. On the other hand, very interestingly, for the water thickness (Figure 9.c) there is little dependence of coating penetration on coating density.

Based on the above finding, in order to provide an even simpler correlation for the designers, in Figure 10 we perform a fit of all the data (including the three different coating densities) using a linear function. We obtain a coefficient of correlation of 0.98 % for the below correlation:

Water Thickness [kg/m^2] = 0.3866 x Coat. Penetration [mm]

With this equation it will be possible to estimate the amount of water to be dried on a foundry mould or core just by performing a simple penetration measurement and independently of other variables affecting the coating process for thicknesses up to 17 mm.

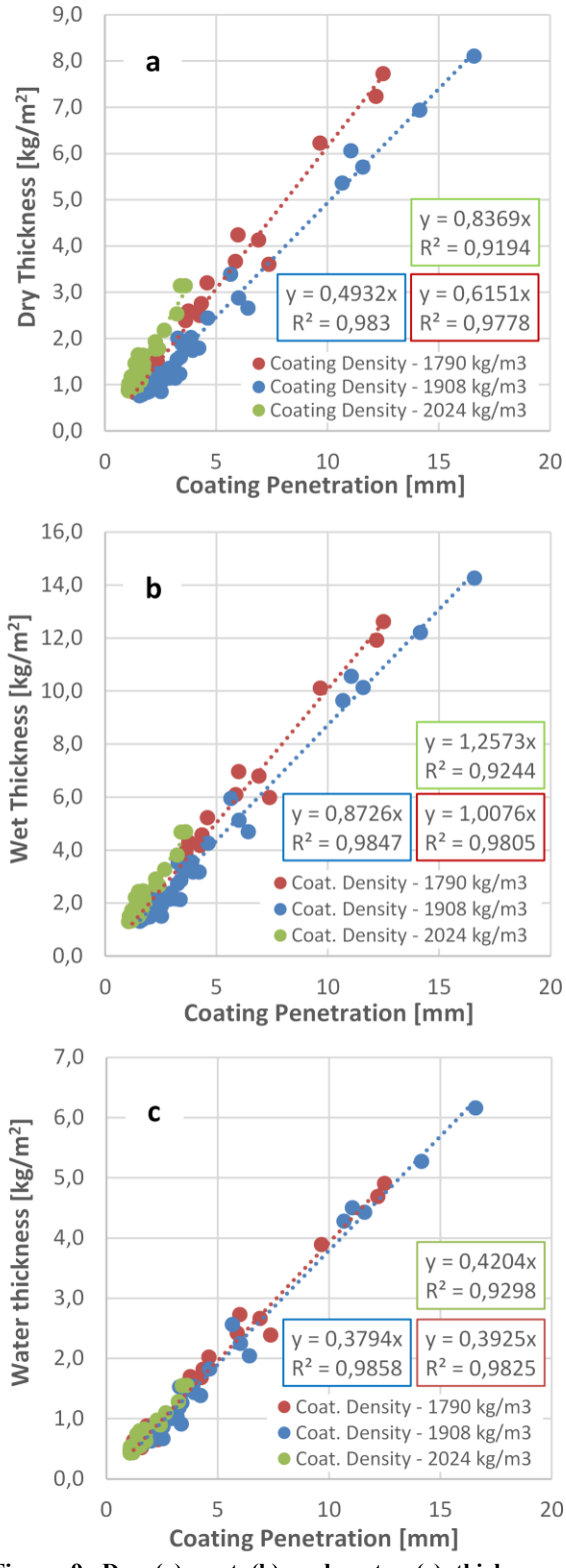

Figure 9. Dry (a), wet (b) and water (c) thicknesses as a function of penetration with respective correlations.

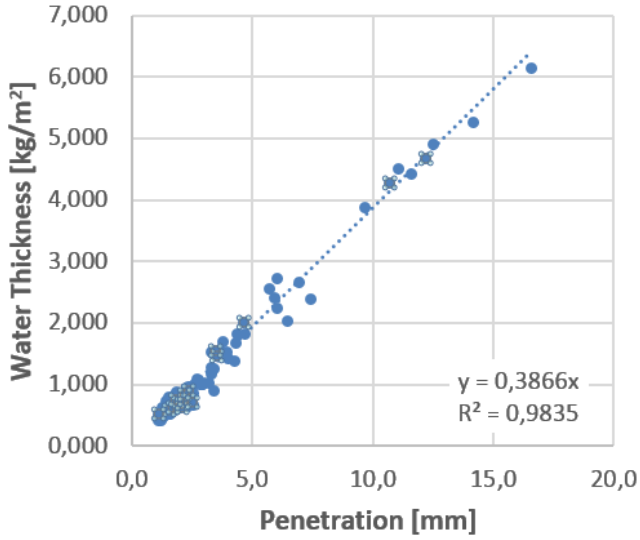

Figure 10. Water thickness as a function of penetration with overall correlation.

4. Conclusions

From the experiments and analysis performed in this study we can conclude that:

- The relations between coating layer properties and coating variables are non-linear
- The scatter (repeatability) of the coating process is not constant and can be controlled by choosing the right level of moulding and coating parameters
- In particular to reduce scatter, the sand density should be above 1350 kg/m^3, the coating density maximized, the dipping time minimized and moulds should be coated facing downwards
- It is possible to correlate directly the water thickness and coating penetration independently of other variables and therefore it is possible to estimate water content in coated moulds just by simple penetration measurements.

Acknowledgements

This work was financed by Global Castings A/S, the Danish Agency for Science, Technology and Innovation (DASTI) and the Technical University of Denmark (DTU).

References

[1] Control Limits for the Drying of Water Based Coatings, N. Schutze, Foseco, Foundry Practice, Issue 255, June 2011.

[2] L. Jamrozowicz, J. Zych, T. Snopkiewicz. (2013). The Research of Desiccation Rates Selected Protective Coating Used on Mould and Sand Cores. *Archive of Foundry Engineering*, Vol.13, 01/2013, 45-50.

[3] J. Jakubski, S. Dobosz, P. Jelinek. (2005). The influence of the protective coating type on thermal deformation of casting cores. *Archives of Foundry Engineering*, Year 2005, Volume 5, № 15.

[4] B. Sarum. (2013). Ductile and Compacted Graphite Iron Casting Skin -Evaluation, Effect on Fatigue Strength and Elimination, B. Ohio State University, Page 103-106.

[5] G.L. Di Muoio, N. Skat Tiedje, B. Budolph Johansen. (2014). Critical control variables for the coating of furan bonded sand with water based foundry coating. World foundry congress, 19-21 May 2014. Bilbao, Spain.

Supplement III

Evaporation Rates of Water Based Foundry Coatings on Furan Bonded Sands

Giovanni Luca **Di Muoio***,

Global Castings A/S, Copenhagen, Denmark

Niels Skat **Tiedje,**

Technical University of Denmark, Copenhagen, Denmark

*Corresponding author: gidmu@globalcastings.com, M: +45 6180 9266, Global Castings A/S, 373 N Diplomvej, Lyngby, 2800,

Evaporation rates of water based foundry coatings are needed in order to estimate drying times and correctly dimension drying equipment used in foundries. It this study we measure and analyse the evaporation rates of a water based foundry coating applied to furan bonded sand moulds.

An experimental setup is built to be able to dry the coated samples with air conditions similar to the ones used in full scale factory equipment. The effects of different coating layer thicknesses and air drying conditions are investigated.

Weight variation and surface temperature of the sample are measured and used to calculate drying rates and other parameters needed to understand the drying behaviour.

A model for calculating average evaporation rates is provided for use in drying equipment design. Characteristic drying curves are analysed and it is found that they are heavily affected by coating thickness, while drying conditions have only a minor effect.

150 words

Keywords

Evaporation rate, drying of foundry moulds, furan sand, water based foundry coating, process control

List of Symbols

A_{sample} coated area of sample [m^2]

$CT_{dry,\ coat}$ thickness of dry coating [kg/m^2]

CT_{water} thickness of water [kg/m^2]

$CT_{wet,coat}$ thickness of wet coating [kg/m^2]

ER_{avg} average water evaporation rate [kg/m^2/h]

ER water evaporation rate [kg/m^2/h]

$MC_{W.B.}$ moisture of coating layer on wet basis [%]

t_{dry} drying time [hours]

W_{dry} weight of coated sample after drying [g]

W_{water} weight of water in the coating layer [g]

W_{wet} weight of coated sample after coating [g]

$W_{dry,\ coat}$ weight of dry coating [g]

$W_{wet,coat}$ weight of wet coating [g]

W_{sand} weight of sample before coating [g]

1 – Introduction

Water based foundry coatings are use in the production of large furan sand moulds to improve the surface quality of the cast parts. Typically water based coatings contain more than 30% of water [1] at the time of application. Drying of moulds is needed in order to reduce the moisture of the coating to a minimum and to lower the risk of vapour and gas defects [2-7].

In the foundry industry, moulds are normally dried in forced air convection ovens (Figure 1) or in ambient conditions depending on the needed drying time. Drying times, however, are heavily influenced by the type of coating used, the initial amount of water in the coating layer and the conditions of the drying air (Figure 2). [8-10]

A proper understanding of the drying behaviour of water based coatings can help to correctly dimension drying equipment, therefore helping to reduce investment cost, power usage and risk of vapour defects which finally lowers the cost of the produced castings.

In the drying industry it is common practice to characterize materials drying behaviour with laboratory tests where the sample is dried while the water loss is monitored by measuring the weight variation of the sample [11]. From the weight measurement is then possible to obtain important drying properties such as evaporation rates and characteristic drying curves [12,13].

In this study, we obtain evaporation rates and drying characteristics of a water based coating used in Global Castings production facilities. An experimental setup, specifically built to test the drying

of water based coatings applied to furan sands, is used to perform the drying in controlled conditions. In addition to weight, the surface temperature of the dried mould is measured in order to better understand the surface drying behaviour of this material.

The effect of different coating thicknesses as well as the effect of different air conditions (air speed, humidity and temperature) are investigated. Evaporation rates and characteristic curves are obtained and presented. It is found that evaporation rates are affected both by initial coating thickness and air conditions, while characteristic curves are mainly affected by coating thickness.

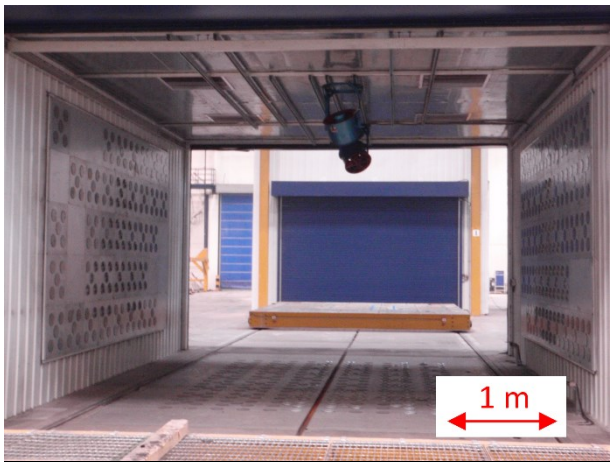

Figure 1. Example of drying cabinet normally used for drying water based foundry coatings.

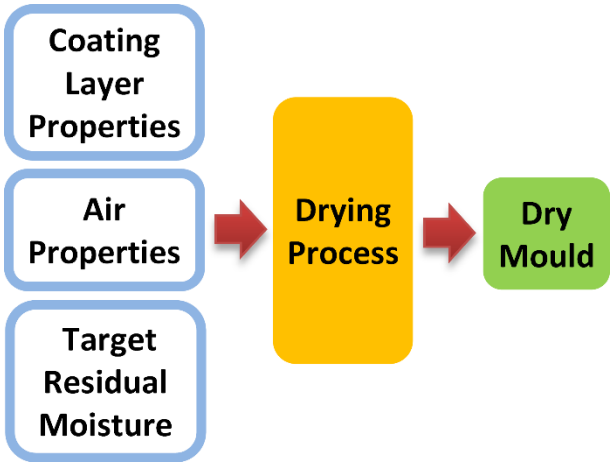

Figure 2. Drying process parameters.

2 - Methods

In order to obtain the evaporation rates and drying characteristics we start by preparing the sand samples. Water based coating is then applied and drying process started. The data obtained from the tests is then analysed and presented.

2.1 – Sample preparation

Sand samples (Figure 3) are prepared with same binder and sand used in the productions facilities. Cylindrical moulds of 25 mm diameter and 50 mm height are used. The mould material (PVC-U) is chosen for its good resistance to acids and solvents, to minimize moisture adsorption and maximize thermal insulation on the sides of the specimen. This is done to minimize possible errors coming from weight variations of the mould. After curing, each sample is coated right before the drying process is started. A more detailed description of the sample preparation can be found in [1]. The weight of the sample is measured before coating, after coating and after drying on a precision laboratory scale with +/- 0.1 mg accuracy.

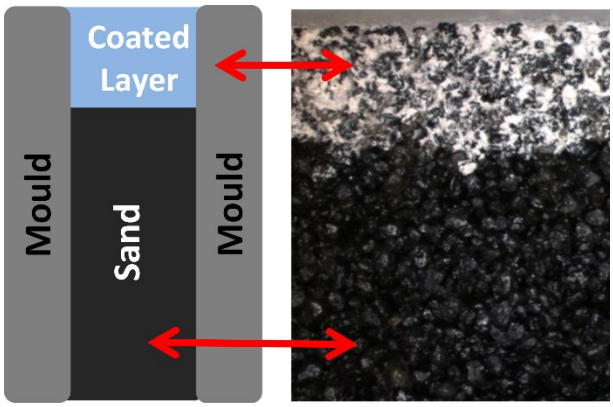

Figure 3. Coated furan sand mould used in the drying tests.

2.2 – Drying Setup

The drying operation is performed in a specially designed experimental setup (Figure 4). Air speed, humidity and temperature are measured as well as sample weight and surface temperature. All the data from the sensors are transferred from the acquisitions card to a computer. Then, a program developed in the data acquisition software DasyLab stores the data for subsequent analysis and provides real time feedback to control to the heaters, the humid air supply and dry air supply. In this way is possible to maintain the desired drying conditions within an accuracy of +/- 0.1 m/s for the air speed, +/- 2 °C for the temperature and +/- 3 % for the relative humidity. In regards to the measurement of surface temperature of the sample, a non-contact infrared sensor is used in order to avoid possible effects of contact on the weight measurement.

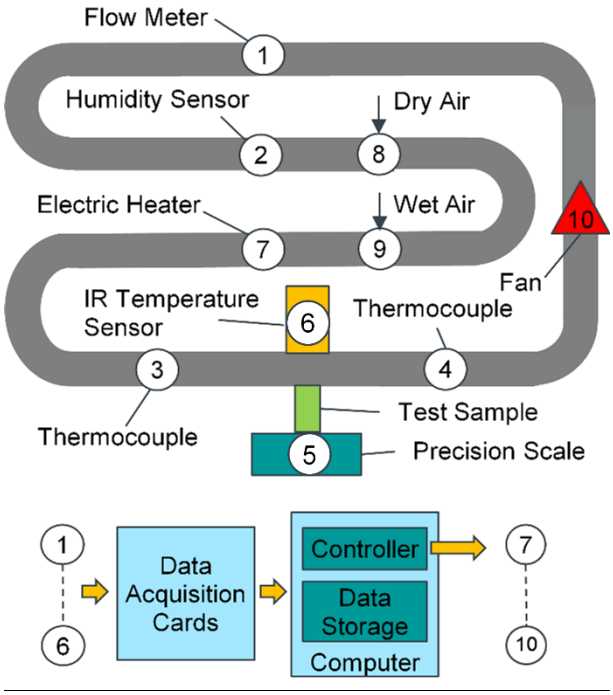

Figure 4. Experimental setup used for the drying tests.

2.3 - Experimental Plan – Thickness Effect

In order to determine the effect of the coating layer thickness on the drying behaviour, the coating parameters levels are chosen according to Table 1. The ranges (maximum and minimum levels) of the each parameter is chosen to be representative of the highest and lowest limits allowed by the factory specifications. Additionally, centre points are added to represent the target of the specification and to ensure that the experimental data can be used to obtain a non-linear response surface. More details about the levels used and sample preparation can be found in [1]. For each coating conditions 6 samples are produced for a total of 36 sample.

Air speed levels are chosen as 0.8 m/s, 1.5 m/s and 2.5 m/s (AS1, AS2 and AS3 Table 2). These values will provide, in the test duct used for the tests, similar values of heat transfer coefficients to the ones achieved in the factory. In particular AS1 replicates values normally achieved by natural convection, AS3 represents values obtained with forced convection and AS2 provides a centre point for the experimental plan.

In regards to drying air conditions, we choose the values of low relative humidity at 30 °C, 50 °C and 70 °C (levels AC1, AC4, AC7 in Table 3) normally achievable in production. The temperatures are chosen to represent drying conditions typically used in the factories considered. Low relative humidities are chosen for these tests to limit the drying time (especially for samples with high coating thickness) and to isolate the effect of thickness.

For each set of drying conditions (AC1-AS1, AC4-AS2 and AC7-AS3) two samples coated with the same coating conditions are dried. In this way an experimental plan of 3 (air conditions) x 6 (coating conditions) is replicated two times and provides a total of 36 runs.

Table 1. Coating parameters levels used to achieve different coating layer thicknesses.

Coating Thickness Level	Sand Comp.	Coating Density [kg/m^3]	Gravity Effect	Dipping Time [s]
CT1	High	2042	Down	2
CT2	Med	1908	Down	5
CT3	Low	1790	Up	120
CT4	Low	1908	Up	120
CT5	Low	1908	Up	15
CT6	High	1790	Down	2

Table 2. Air Speed levels used in the drying tests.

Air Speed Levels	Air Speed [m/s]	Heat Exchange Coeff. [W/m^{2}K]
AS1	0,8	3,5-4
AS2	1,5	7,5-8
AS3	2,5	13-15

2.4 - Experimental Plan – Air Properties Effect

To determine the effects of different air conditions we now choose only one coating level (CT2 in Table 1) that is the centre point of the specification values used in the factory.

A total of 9 air conditions levels are used (Table 3) that are representative of drying conditions normally achievable in foundry environment and drying cabinets. As shown in Figure 5 we can see that relative humidity conditions are normally limited by low limits that are determined by the typical minimum air humidity present in the ambient air (assuming 100% of fresh air is supplied to the drying cabinet) and by maximum limit where risk of condensation in the drying becomes high due to the increased dew point (this can happen especially when air is recirculated in the drying cabinet to reduce energy losses).

Each of the air drying conditions is tested at the three air speed levels described in Table 2 for a total of 27 runs.

Table 3. Air temperature and humidity levels used in the drying tests.

Air Conditions Levels	Temperature [C]	Dew Point [C]	Relative Humidity [%]
AC1	30	4	20
AC2	30	18	50
AC3	30	26	80
AC4	50	10	10
AC5	50	25	25
AC6	50	32	40
AC7	70	10	5
AC8	70	25	10
AC9	70	40	23

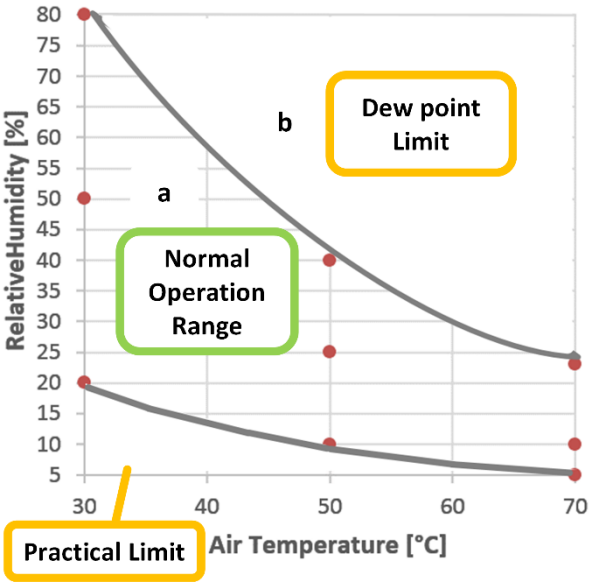

Figure 5. Design space limits for air temperature and humidity.

2.5 - Data Analysis

In order to understand how water is removed from the sample, the mould weight is recorded before coating and the uncoated sand weight is obtained (W_{sand}). Right after coating, the sample is weighted again (W_{wet}) and the weight of wet coating layer is calculated ($W_{wet,coat}$) as:

$W_{wet,coat}$ [g] = W_{wet} - W_{sand} Eq.1

After drying is completed the sample weight becomes constant and this weight is defined as W_{dry}. It is then possible to calculate the weight of the removed water during the drying process (W_{water}) and of the final dry coating layer ($W_{dry,\ coat}$) as:

W_{water} [g] = W_{wet} - W_{dry} Eq.2

$W_{dry,\ coat}$ [g] = W_{dry}-W_{sand} Eq.3

It is important to note that, in order to eliminate weight measurement errors induced by the air movement over the sample, initial and final weights are recorded on the scale with no air flow. The weight recorded during drying (with air flow) is then corrected (moved slightly up or down) so that the initial and final weight measurement are the same as the one recorded with no air flow (Figure 6) and then used to calculate all relevant properties (water thickness, moisture, etc..).

Coating thicknesses of wet coating, water and dry coating can be simply calculated by dividing the relevant weight by the sample surface area, so we have:

$CT_{wet,coat}$ [kg/m^2] = $W_{wet,coat}$ / A_{sample} Eq.4

CT_{water} [kg/m^2] = W_{water} / A_{sample} Eq.5

$CT_{dry,\ coat}$ [kg/m^2] = $W_{dry,coat}$ / A_{sample} Eq.6

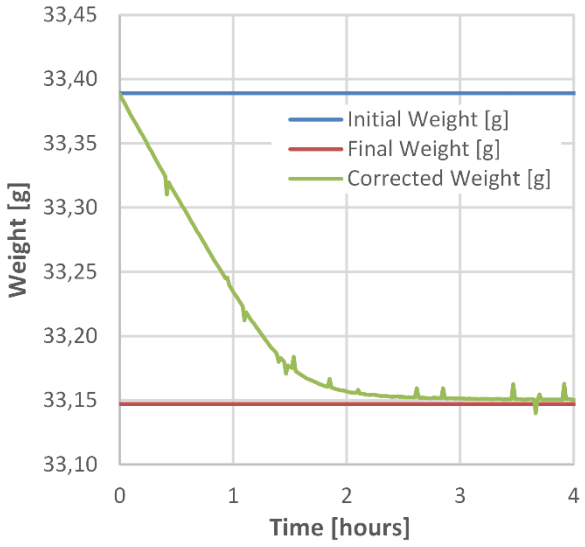

Figure 6. Coated sample weight variation during drying.

Another important property that is used to define the drying time is the coating layer moisture calculated in wet basis ($MC_{W.B.}$) as:

$MC_{W.B.}$ = W_{water} / $W_{wet,coat}$ x 100 Eq.7

The moisture present in the coating layer can be calculated and plotted as function of time (Figure 7.a). The drying time is then defined as the time at which we reach a moisture of 1%.

The average evaporation rate is then calculated as:

ERavg [kg/m2/h] = $CT_{water,\ initial}$ / t_{dry} Eq.8

It is also possible to calculate the evaporation rate at each instant during the drying by deriving the weight with respect to time:

ER [kg/m2/h] = dCT_{water}/dt Eq.9

The maximum evaporation rate ER_{max} is obtained as shown in Figure 7.b. ER_{avg} and ER_{max} are important parameters used to design drying equipment.

Finally, we plot the surface temperature of the sample as a function of time (Figure 7.c), and define t_1 as the time at which the surface water of the sample is being evaporated at a constant temperature (initial plateau of the curve), and t_2 the time at which the surface temperature of the sample reached the second higher plateau but more moisture can be present in lower layers. By comparing t_1, t_2 and t_{dry} we can calculate the proportion of time where water evaporated is coming from the surface (t_1/t_{dry}) or from the layer below the surface ($(t_{dry}-t_2)/t_{dry}$).

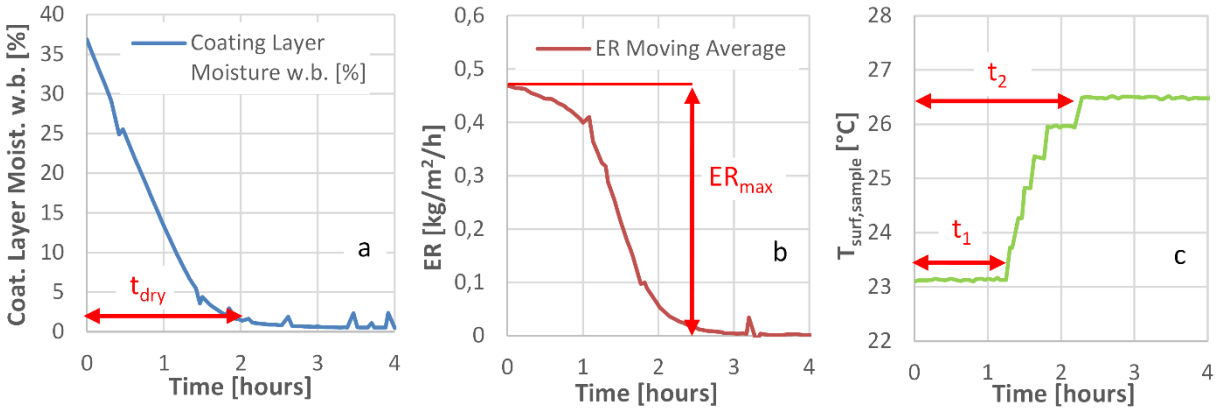

Figure 7. Drying parameters used in this study: a) drying time, b) maximum evaporation rate and c) surface temperature transition times.

Characteristic curves are used to describe the evaporation rate as a function of the coating moisture. These curve can help to understand changes in material behaviour that are needed when designing a dryer. In order to obtain these curves, we plot the ratio between the evaporation rate and the maximum evaporation rate (ER/ER_{max}) versus the coating layer moisture divided by the initial moisture (Figure 8).

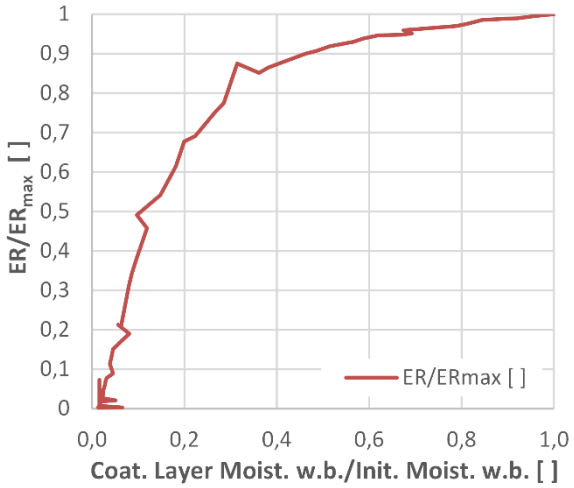

Figure 8. Example of characteristic drying curve of furan sand sample coated with water based foundry coating.

3 – Results and Discussion

3.1 Thickness Effect

In order to understand the effect of coating layer thickness, we plot the average evaporation rates as a function the initial coating layer water thickness. If we look at the results for drying conditions AC1 and AS1 (Figure 9), we can see that the average evaporations rate is clearly a function of the initial water thickness. In particular ER_{avg} seems to be constant for initial water thicknesses below 1 kg/m^2 and it drops significantly (almost to 35% of the original value) for water thicknesses above 4 kg/m^2.

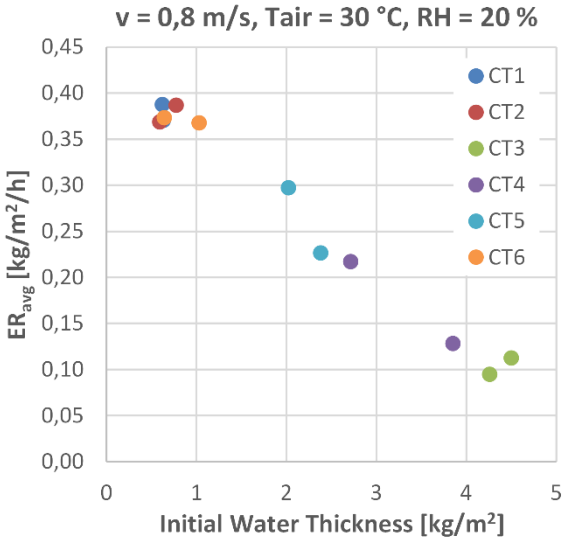

Figure 9. Average evaporation rates as a function of initial water thickness for air condition AC1.

Figure 10.a shows the effect of drying conditions and water thickness on the average evaporation rate. We can see that for all the drying conditions ER_{avg} is constant for initial water thicknesses below 1 kg/m^2. If we look at the evaporation rate values, we see that the thickness effect varies for the different air conditions. In particular, from the AC7 to AC1 the evaporation rate increases from 0.38 kg/m^2/h to 1.2 kg/m^2/h (about 300% increase) for initial thicknesses below 1 kg/m^2, while for thicknesses above 4 kg/m^2 the increase is only from 0.10 kg/m^2/h to 0.2 kg/m^2/h (about 200% increase). These results confirm that it is extremely important to control the coating layer thickness in order to achieve control of the drying time.

The effect of the evaporation rate variation on the drying time can be seen in Figure 10.b and 10.c. We can see that the drying time increases linearly with the initial water thicknesses for value below 1 kg/m^2, this reflects the fact that a linear increase initial water to be evaporated and a constant drying rate will provide a linear increase in drying time. On the other hand, for thicknesses above 1 kg/m^2 the drying time increases more than linearly with increases of initial water thickness. This is because not only there is more water to be evaporated but also because the evaporation rate is decreasing. We can therefore conclude that to minimize drying time a water coating thickness below 1 kg/m^2 should be used.

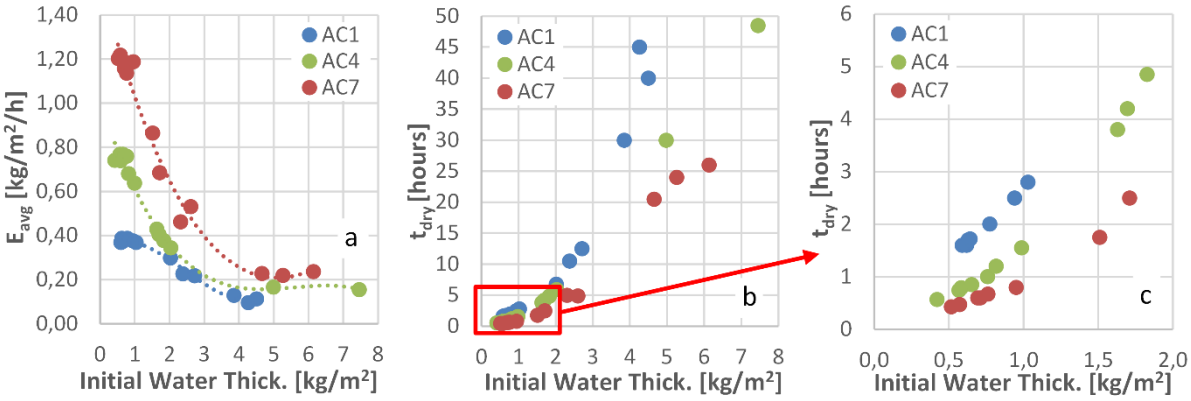

Figure 10. Effect of air conditions and initial water thickness on average evaporation rate (a) and drying time (b). Figure 10.c is an enlargement of the curve shown in Fig 10.b.

In Figure 11.a we can see that the ER_{max}/ER_{avg} ratio is typically between 2 and 3 for initial water thicknesses below 1 kg/m^2 while it increases up to 14 for initial water thicknesses of 6 kg/m^2. This means that driers dimensioned on ER_{max} in order to avoid problems with condensation will have to be significantly over dimensioned if coating thicknesses exceeding 1 kg/m^2 are to be dried.

Figure 11.b and 11.c we see that for samples with less than 1 kg/m^2 of initial water thickness the ratio t_1/t_{dry} is comprised between 0.20 (for AC7) and 0.40 (for AC1), therefore for at least 20% of drying time evaporation from the surface to the air is the driving phenomena. For higher water thicknesses the t_1/t_{dry} ratio drops to less than 0.05 therefore, in this case, for most of the drying time diffusion from the inner layers is the driving phenomena. This is confirmed by that fact that at the same time the $(t_{dry}-t_2)/t_{dry}$ ratio increases from 0.20 to 0.90.

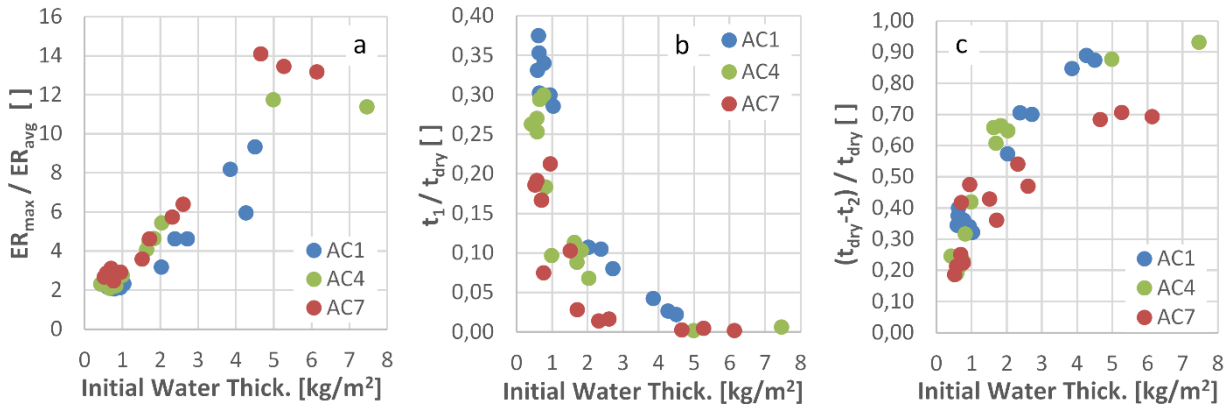

Figure 11. Effect of air conditions and initial water thickness on ER_{max}/ER_{avg} ratio (a) and surface temperature transition times (b and c).

The above results can be summarised by stating that the initial coating thickness is the main factor determining the evaporation rate, and therefore drying time, of water based coated furan sand moulds. In particular, for low initial water thicknesses, evaporation from the surface to the air is determining the evaporation rate. In this case, it is mainly the combination of temperature, humidity and velocity that controls the drying time. While for samples with higher thicknesses, diffusion of water from the inner layers of the samples to the surface is the determining phenomena. For high initial water thicknesses, evaporation is slower and air conditions effect is less relevant than for low initial water thicknesses.

3.1 Effect of Air Properties

Figures 12 show the average evaporation rates for the tests where air properties are dried. We can clearly see that increasing air speed and temperature will increase evaporation rate, while increasing relative humidity decreases the evaporation rate. In particular, we can see that there is a non-linear the relation between relative humidity and evaporation rate, especially for the higher values. Additionally we note that, by varying air drying conditions in the considered range is possible to achieve variations of average evaporation rates from 0.1 to 1.2 kg/m^2/h (1200 % increase), this confirms that a good control of air drying conditions is critical to controlling evaporation rates and therefore the drying time.

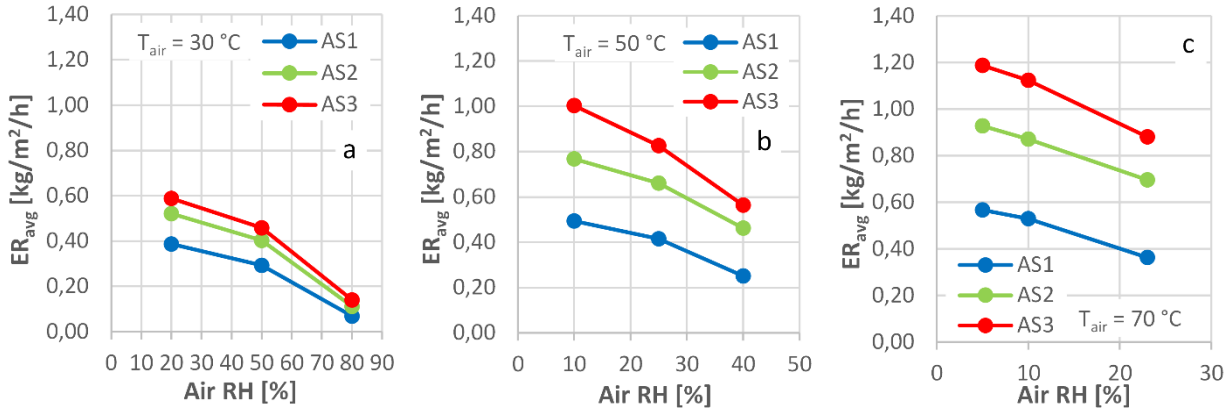

Figure 12. Average evaporation rates results at 30 °C (a), 50 °C (b) and 70 °C (c).

Figure 13 shows that the ER_{max}/ER_{avg} ratio varies between 1.4 and 3.0. It is therefore necessary to over dimension the drier power from 40% to 300% compared to the average power needed depending on the drying conditions used. In particular low relative humidity gives higher ER_{max}/ER_{avg} ratios.

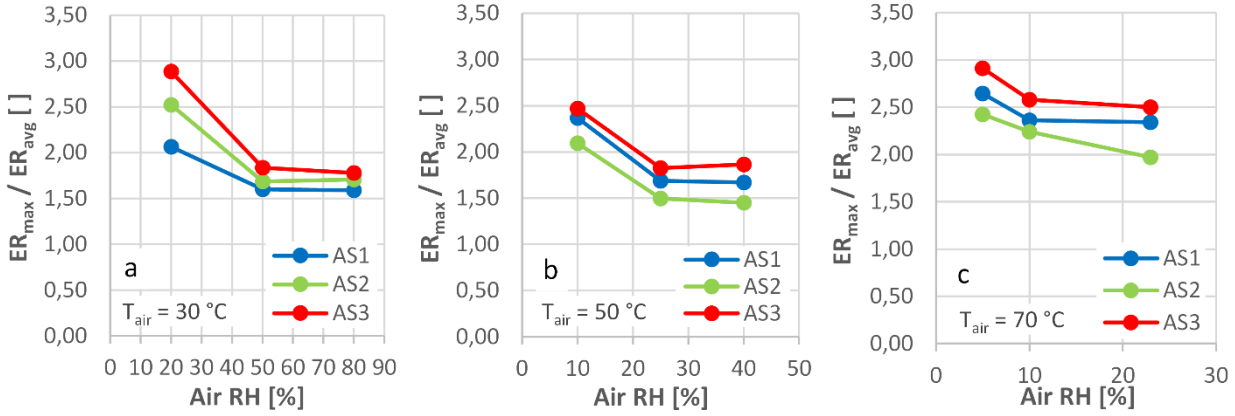

Figure 13. ER_{max}/ER_{max} ratio results at 30 °C (a), 50 °C (b) and 70 °C (c).

In order to provide a useful tool for the drying process and equipment design the experimental data has been fitted with a second order polynomial (Eq.10) where V_{air} is expressed in m/s, T_{air} in °C and RH in %. The coefficient of determination obtained is 99.31 %.

The polynomial is then used to build design maps that drying process designers can use a simple tool (Figure 14).

$$ER_{avg} = -0.556 + 0{,}4022\,V_{air} + 0{,}02264\,T_{air} + 0{,}01611\,RH - 0{,}1031\,V_{air}^2 - 0{,}000178\,T_{air}^2 - 0{,}000085\,RH^2 + 0{,}004368\,V_{air}T_{air} - 0{,}001980\,V_{air}\,RH - 0{,}000371T_{air}\,RH \quad \text{Eq.10}$$

$$R^2 = 99.31\%$$

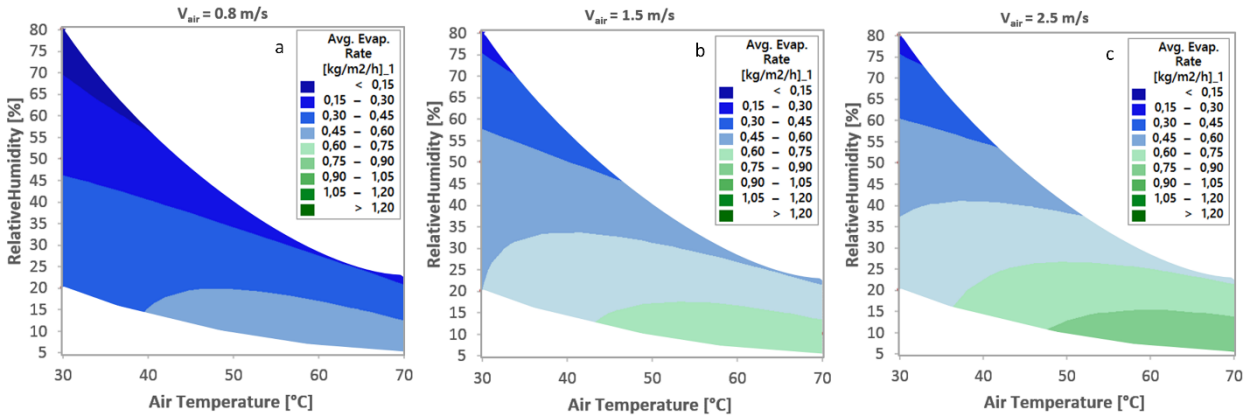

Figure 14. Average evaporation rates design maps for air speeds of 0.8 m/s (a), 1.5 m/s (b) and 2.5 m/s (c).

As a final check, we plot surface temperature of the samples during the initial drying stage ($T_{surf,min}$) versus the wet bulb temperature of the air used for the drying. As we can see (Figure 15) there is good overall agreement except for low and high wet bulb temperature situations. For low wet bulb temperatures (Figure 15.a) the sample is drying at higher temperature, this is because initial temperature of the sample (25 °C) is above the wet bulb temperature (16 °C). For high wet bulb temperature (Figure 15.c) the sample is drying at lower temperature, this is because initial temperature of the sample (25 °C) is significantly below the wet bulb temperature (45 °C).

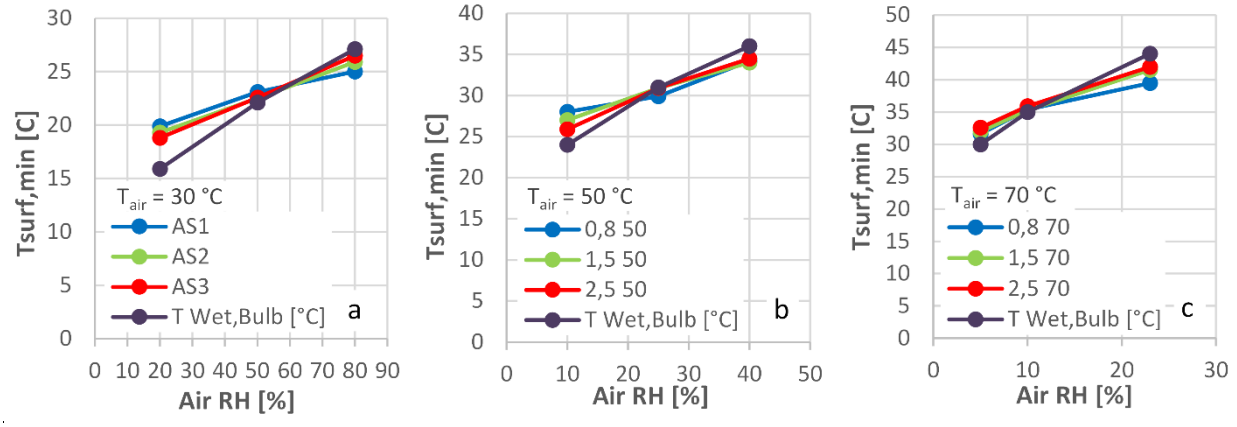

Figure 15. Initial surface temperature results for drying at 30 °C (a), 50 °C (b) and 70 °C (c) versus air wet bulb temperature.

Characteristic curves

In this last result section we analyse the effect of initial water thickness and drying conditions on the characteristic drying curves.

In Figure 16.a we can see how for increasing initial water thicknesses the shape of the curve is heavily affected. Coating density does not have significant effect on the curves shape (Figure 16.b) Air conditions seem to have minor effects (Figure 16.c), especially in the initial stages of drying (moisture ratio above 0.9) when the evaporation rate has its maximum. Also, in air conditions

effect curves the noise is more visible since supply of dry and wet are was used more frequently and the high levels of air speed were used.

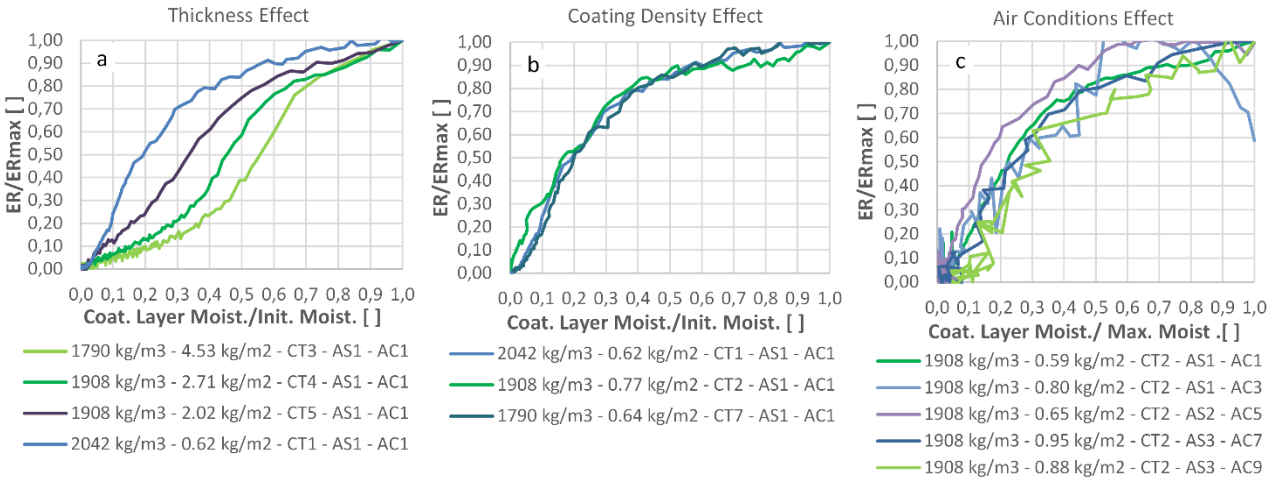

Figure 16. Effect of coating thickness (a), density (b) and drying condition (c) on the characteristic drying curves.

4 - Conclusions

The main conclusions that we can draw from this study can be summarised as below:

- Initial water thickness heavily effects the drying behaviour for water based coating on furan bonded sand moulds. In particular, for initial water thicknesses higher than 1 kg/m^2, evaporation rates decrease and drying times increase in a non-linear fashion. The reason is that the main water transport phenomena for thin coating layers is evaporation from the surface to the air, while for thicker layers diffusion from the inner layer to the surface becomes the limiting phenomena.
- The ER_{max}/ER_{avg} ratio is also heavily affected by initial water thickness, and to some degree also by the air drying conditions. It is therefore important to use this information to correctly dimension drying equipment.
- Temperature measurement can be used to determine when surface is dry and for initial water thickness smaller than 1 mm this corresponds also a dry sample (for higher thickness there can still be moisture in the lower layers). This is a practical and low cost methodology measurement that could be easily implemented in factories.
- An empirical correlation between the average evaporation rates and important process parameters has been found and design maps have been generated for use in drying equipment design.

- Characteristic curves of the material have been obtained and found to be heavily dependent on initial water thickness, less from drying conditions and not dependent from initial coating density.
- Finally it has been shown that it is possible to achieve a given drying times but it is necessary not only to control drying air conditions but also coating layer properties.

5 - Acknowledgments

This work was financed by Global Castings A/S, the Danish Agency for Science, Technology and Innovation (DASTI) and the Technical University of Denmark (DTU).

6 - References

1 - G.L. Di Muoio, N. Skat Tiedje and B. Budolph Johansen: 'Critical Control Variables For The Coating Process Of Furan Bonded Sand', 71st World Foundry Congress, 19-21 May 2014, Bilbao

2 - J. Campbell, R.A. Harding: 'Solidification Defects in Castings', Lecture 3207, The University of Birmingham, 4-8, 1994.

3 - L. Elmquist: 'Defect formation in cast iron', Presentation, School of Engineering, Jonkoping University, Sweden, 2012.

4 - IKO: 'Description of Casting Defects', Chapters 04,10,12, S&B Industrial Minerals

5 - A. Chojecki*, J. Mocek: 'Effect of atmosphere in a foundry mould on casting surface quality', Archives of Foundry Engineering, Volume 12, Issue 1/2012, 13-18.

6 - D - Elkem: 'Hydrogen Pinholes', Technical Information 30, Elkem Foundry Products, Rev. 1.2, 2007.

7 - G.L. Di Muoio, N. Skat Tiedje and B. Budolph Johansen: 'Automatic vapour sorption analysis as new methodology for assessing moisture content of water based foundry coating and furan sands', 10th International Symposium on the Science and Processing of Cast Iron – SPCI10, 2014 November, Argentina, Mar de Plata.

8 - N. Schutze: 'Control Limits for the Drying of Water Based Coatings', Foseco, Foundry Practice, Issue 255, June 2011.

9 - J. Kollar, B. Schmitt: 'Decrease the Drying Time for Wash Coatings on Sand Molds and Cores', EPRI Center for Material Production, 1994.

10 - L. Jamrozowicz, J. Zych, T. Snopkiewicz: 'The Research of Desiccation Rates Selected Protective Coating Used on Mould and Sand Cores', Archive of Foundry Engineering, Vol.13, 01/2013, 45-50.

11 - A.S. Mujumdar: 'Handbook of industrial drying', 3rd edition, Ch. 2, 2006.

12 - A.S. Mujumdar: 'Handbook of industrial drying', 3rd edition, Ch. 1, 2006.

13 - Gregor A. Scheffler: 'Introduction of a Drying Coefficient for Building Materials', Thermal Performance of the Exterior Envelopes of Whole Buildings XII International Conference, December 1-5, 2013

Figure Captions

Figure 1. Example of drying cabinet normally used for drying water based foundry coatings.

Figure 2. Drying process parameters.

Figure 3. Coated furan sand mould used in the drying tests.

Figure 4. Experimental setup used for the drying tests.

Figure 5. Design space limits for air temperature and humidity.

Figure 6. Coated sample weight variation during drying.

Figure 7. Drying parameters used in this study: a) drying time, b) maximum evaporation rate and c) surface temperature transition times.

Figure 8. Example of characteristic drying curve of furan sand sample coated with water based foundry coating.

Figure 9. Average evaporation rates as a function of initial water thickness for air condition AC1.

Figure 10. Effect of air conditions and initial water thickness on average evaporation rate (a) and drying time (b and c).

Figure 11. Effect of air conditions and initial water thickness on ER_{max}/ER_{avg} ratio (a) and surface temperature transition times (b and c).

Figure 12. Average evaporation rates results at 30 °C (a), 50 °C (b) and 70 °C (c).

Figure 13. ER_{max}/ER_{max} ratio results at 30 °C (a), 50 °C (b) and 70 °C (c).

Figure 14. Average evaporation rates design maps for air speeds of 0.8 m/s (a), 1.5 m/s (b) and 2.5 m/s (c).

Figure 15. Initial surface temperature results for drying at 30 °C (a), 50 °C (b) and 70 °C (c) versus air wet bulb temperature.

Figure 16. Effect of coating thickness (a), density (b) and drying condition (c) on the characteristic drying curves.

Table Captions

Table 1. Coating parameters levels used to achieve different coating layer thicknesses.

Table 2. Air Speed levels used in the drying tests.

Table 3. Air temperature and humidity levels used in the drying tests.

Supplement IV

19th International Drying Symposium (IDS 2014)
Lyon, France, August 24-27, 2014

INVESTIGATION OF MOISTURE LEVELS IN WATER BASED FOUNDRY COATING AND FURAN SANDS USING AN AUTOMATIC VAPOR SORPTION ANALYZER

G.L. Di Muoio[1,2]*, N. Skat Tiedje[2] and B. Budolph Johansen[1]

[1]*Casting Technology Department, Global Castings A/S*
373N Diplomvej, Kgs. Lyngby, 2800, Denmark

[2]*Department of Mechanical Engineering, Technical University of Denmark*
Building 427S, room 306b, Kgs. Lyngby, 2800, Denmark

**Corresponding author: Tel.: +45 6180 9266, E-mail: gidmu@globalcastings.com*

Abstract: Vapor generated by moulding materials during the casting process can cause defects in cast items that increase the cost of the components and eventually lead to scrapping the parts. This study investigates how equilibrium moisture content varies in foundry coating and in different furan based binding systems. Results show that highest effects are given by relative humidity and binder type. They can cause moisture level variations from 0.1% to about 0.8%. Temperature and dust levels play and a minor role. Additionally, it is shown that there is not a large difference between sorption and desorption curves for the materials considered.

Keywords: Moisture, furan sand, foundry coating, automatic gravimetric sorption analysis, sorption/desorption curves, drying process control.

INTRODUCTION

When cast parts are produced, the molten metal in contact with the mould causes the production of gases that can lead to defects and scrapped items.[1,2,3] Gas defects can be correlated directly to vapor generated by the mould and coating material (Fig.1) due to high level of residual moisture.[4,5,6] Moisture is present in furan sand as product of the binder and catalyst reaction but its amount can change over time.[5] Literature shows that simulation software used to predict gas related defects need to be calibrated with experimental data for the specific moulding material in order to improve prediction accuracy.[7,8,9] Other studies shows that gas evolution rates can vary for different materials.[10,11]

All the current studies, however, focus on different classes of binding systems and foundry materials but do not provide information about the influence of parameters such as temperature, air humidity and dust levels and about different brands of furan binders used in Global Castings production facilities.

In this study the objective is to identify how the moisture content in foundry coating and in sands bonded with different brands of furan binders are affected by relative humidity, temperature and dust levels (Fig. 2).

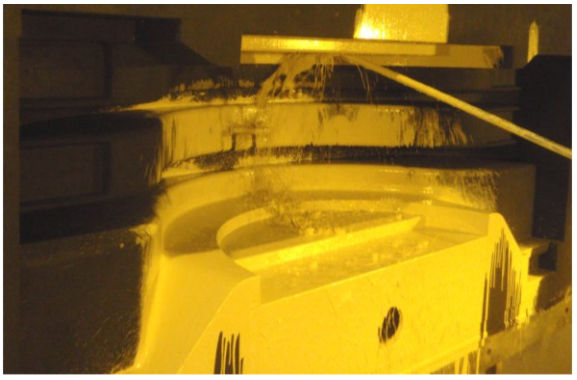

Fig. 1: Furan sand mould coated with water based foundry coating.

In order to do this, we use an automatic vapor sorption analyzer to determine the equilibrium sorption/desorption curves of the considered materials. The reason for choosing an automatic moisture analyzer are: a shorter test time (due to the use of a small sample), the increased precision in weight measurement (due to eliminating manual handling operations of the samples during the tests) and easy and precise control of temperature and humidity.

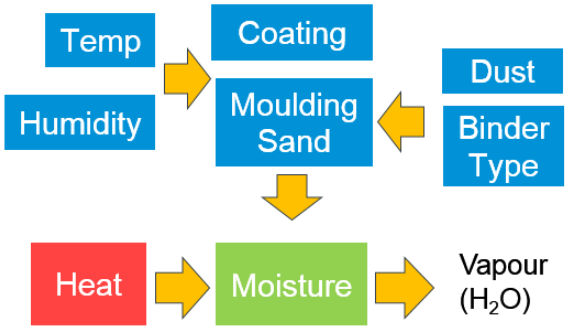

Fig. 2: Parameters affecting vapor generation in a castings process.

Sorption/desorption curves are typically used in other industries (such as food, wood, paper) to help design and optimize drying processes [12], to provide limits for production processes control and monitoring, to predict shelf life [13], to study possible moisture migration between materials [12,13] and to estimate material properties.[14] These curves are a property of the material and show how its moisture levels vary as a function of relative humidity at a given temperature. In particular they will show the minimum possible level of moisture achievable in given environmental conditions for a given material.

Sorption curves are normally not used in the foundry industry but are thought to be relevant by the authors for the following reasons:

- to understand which parameters have the highest effect on moisture levels in the considered material and therefore on the generation of water vapor and the risk of gas defects
- to create a set of data that can be used for the design and control of driers of furan moulds and foundry coatings
- to support foundry engineers making the right choices when optimizing the production and drying process of coated furan sand moulds.

METHODS

Design of Experiment

In order to investigate the effect of different variables, the experimental plan described in Table 1 was designed. First, the effect of temperature on the two main classes of materials is studied (coating and GCX F sand). Then the effect of dust levels (no dust and 2% dust) and different binder system brands (GCX S, GCM and GCGG) are investigated. Finally pure dust and un-bonded sand were tested to provide baselines for comparison.

The temperature levels were chosen as the minimum (15°C), typical (25°C) and maximum (35°C) sand temperature allowed in the production facilities. Similarly, dust levels representing the maximum allowed (2%) and the minimum possibly achievable levels. The binders brands are the same as used in the considered production facilities.

Table 1: Overview of Experimental Plan.

Material	Temperature [°C]		
	15	25	35
Coating	X	X	X
GCX F sand	X	X	X
GCK sand No Dust		X	
GCK sand 2% Dust		X	
GCX S sand		X	
GCM sand		X	
GCGG sand		X	
Pure Dust		X	
Un-bonded Sand		X	

Experimental Procedure

For the bonded sand, the sample preparation started by mixing of sand, binder and catalyst, followed by curing for one week at 23-25 °C and 45-50% RH and finally manual crushing (Fig.3a) (for easier handling during tests). Binder addition was 1% of sand weight and catalyst addition was 40% of binder weight. The coating samples were obtained by drying liquid coating (typically containing an initial moisture of about 40% on wet basis) at same conditions and time used for the sand samples and then manually crushing the dry coating into powder (Fig.3b). Pure dust and un-bonded sand were taken directly from filter bags and silos in the factory and then let equilibrate at the same temperature and humidity conditions as described for the other samples.

After sample preparation and equilibration at 23-25 °C and 45-50% RH for a week, a sample of each type was tested in an MJ33 automatic moisture analyzer with an accuracy of 0.05%. The automatic moisture analyzer was set to dry the sample at a temperature of 105 °C. The wet basis moisture (calculated as in Eq.1) values obtained are needed as input in the automatic vapor sorption analyzer to compute the sample moisture values during the sorption tests since it is not possible for the automatic moisture analyzer to dry the samples at 105 °C.

$$InitialMoist_{w.b.} = \frac{InitialWeight - DryWeight}{InitialWeight} 100 \quad (1)$$

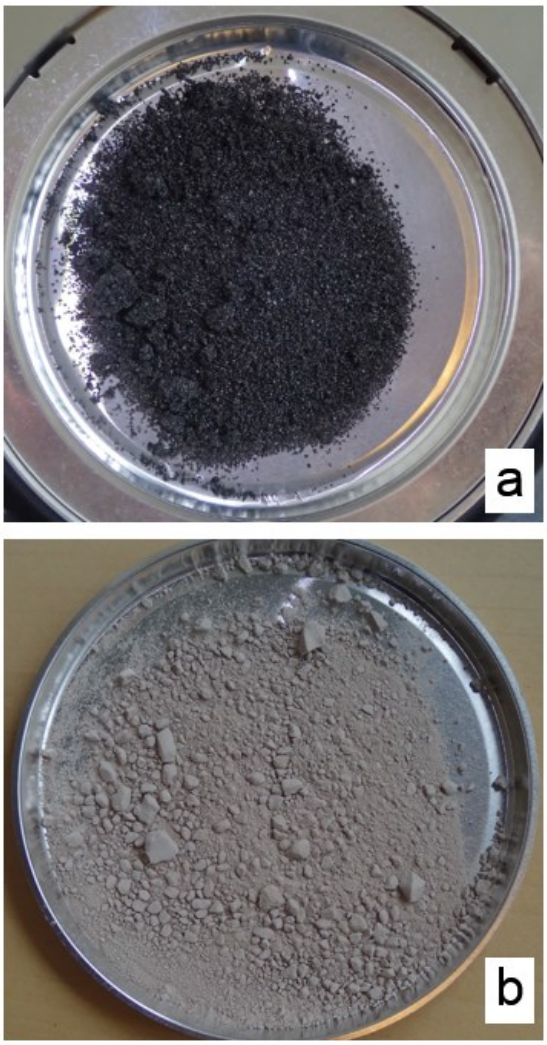

Fig. 3: Materials preparation: a) crushed sand and b) crushed coating.

The AquaLab automatic vapor sorption analyzer used for this study (Fig. 4) is equipped with a precision scale with +/- 0.1 mg accuracy, a dew point sensor with 0.5 % RH accuracy and infrared sensor for temperature control. The moisture level can be controlled by supplying either wet air or dry air.

The sorption/desorption tests were carried out by loading a sample of about 10-12g in the automatic sorption analyzer and inputting the initial moisture of the sample at 23-25 °C and 45-50% RH from the previous tests. After sealing the cover, the machine will start recording weight variation and changing temperature and relative humidity according to the test plan.

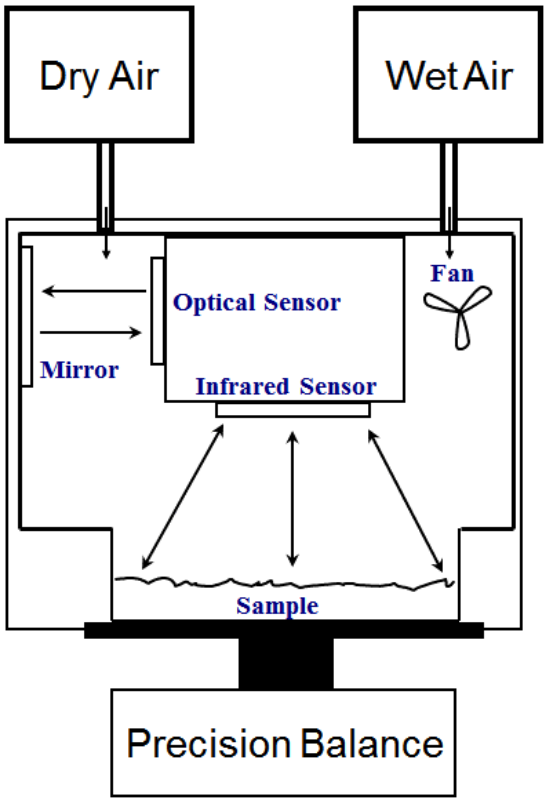

Fig. 4: Automatic moisture analyzer schematic.

In order to obtain the sorption/desorption curves, the temperature is held constant at either 15 °C, 25 °C or 35°C while the moisture is changed stepwise in 5% increments. The current moisture content of the sample is calculated as:

$$CurrentMoist_{w.b.} = \frac{CurrentWeight - DryWeight}{CurrentWeight} 100 \quad (2)$$

Where dry weight is calculated from the initial moisture and weight as:

$$DryWeight = InitialWeight\left(1 - \frac{InitialMoist_{w.b.}}{100}\right) \quad (3)$$

During the test, at each imposed air humidity level, the moisture level in the sample is calculated using Eq.2. If the variation in moisture is less than 0.02% in one hour, the sample is considered equilibrated and the air humidity can be changed to the value required by the next step (Fig.5a).

Each test begins at 50% RH and the air humidity is increased stepwise up to 95% to initialize the sample, then the desorption phase starts (humidity is decreased step wise to 5% RH) and finally the adsorption phase is carried out (humidity is increased stepwise to 95% RH) as shown in Fig. 5b. In order to obtain the final sorption curve, the moisture level of each equilibrium point is plotted versus the air humidity. Sorption curves are plotted in the results section without the initialization steps.

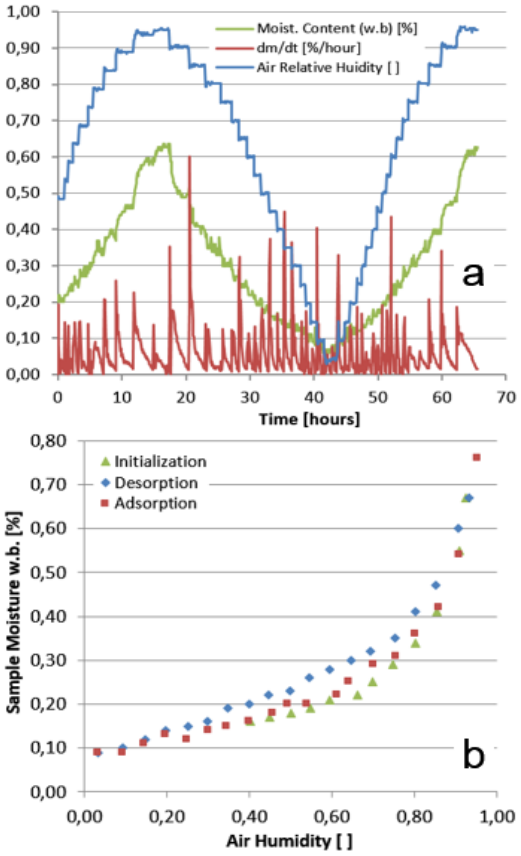

Fig. 5: Example of: a) Sorption tests data, b) equilibrated points.

RESULTS AND DISCUSSION

Table 2 summarizes the results of the initial moisture tests carried out on the equilibrated samples at 23-27 °C and 45-55% relative humidity.

We can see that pure filter dust has the highest initial moisture level (0.71%), un-bonded sand has the lowest moisture level (0.11%) and all the bonded sands have initial moisture levels between 0.17% and 0.24%.

Table 2: Initial sample moisture after and equilibration at 23-25 °C and 45-55% RH for a week.

Material	**Init. Moist. w.b. [%]**	**Material**	**Init. Moist. w.b. [%]**
Coating	0.20	GCX S	0.17
GCX F	0.24	GCM	0.18
GCK No Dust	0.21	GCGG	0.17
GCK 2% Dust	0.23	Un-bonded Sand	0.11
Pure Dust	0.71		

Figure 6a and 6b show the sorption curves respectively for GCX F furan bonded sand and for foundry coating at 15 °C, 25 °C and 35 °C. It can be seen that, for both materials, temperature does not have a significant effect. On the other hand, air humidity has a major effect. For both materials, moisture can be as low as 0.1% at 5% RH and become as high as 0.6% at 95% RH. Even though the absolute values seem small, we need to notice that from 0.10 % to 0.60% there is a variation of 600%. It is therefore important to be aware of this variation when designing the drying process, factory environment conditions and venting channels in the moulds.

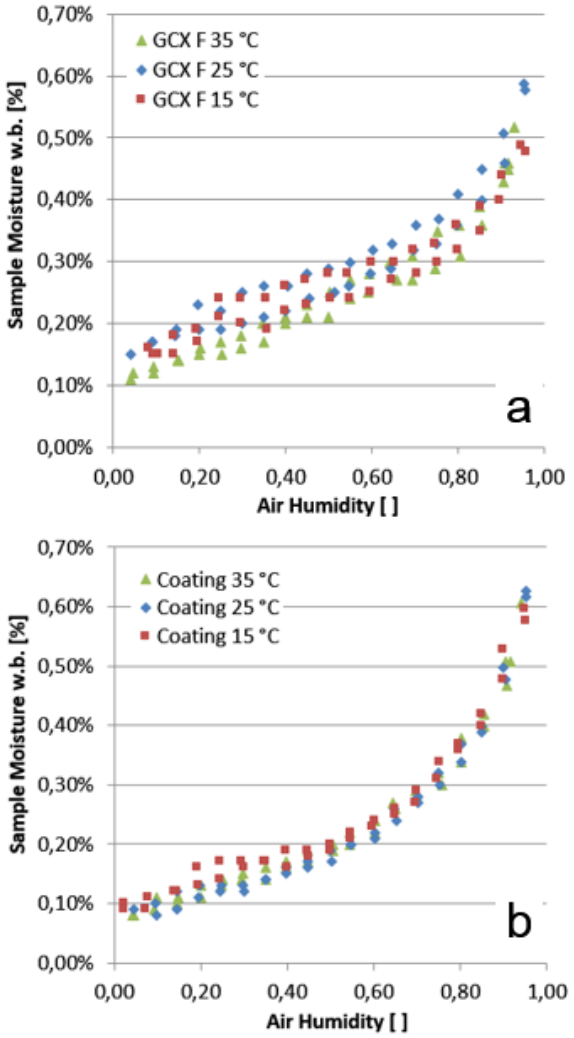

Fig. 6: Sorption curves at 15 °C, 25 °C and 35 °C for a) sand and b) coating.

Another important conclusion is that the hysteretic behavior between adsorption and desorption is fairly limited especially for the coating. For the moulding sand, where there is slightly more hysteresis, the difference between sorption and desorption curve is typically less than 0.05% in moisture.

Figure 7a shows that the effect of a 2% dust addition causes a small increase in moisture levels, for

example from 0.20% to 0.24% at 50% relative humidity. However, pure dust can contain from 0.30% to 1.70% moisture, it is therefore important to reduce dust segregation in silos to avoid lumps of dust in the moulds.

Figure 7b shows a comparison between different binder types and un-bonded sand. It can be seen that un-bonded sand has the smallest moisture content (between 0.04% and 0.20%), it has no hysteresis between adsorption and desorption and moisture value is a linear function of air humidity.

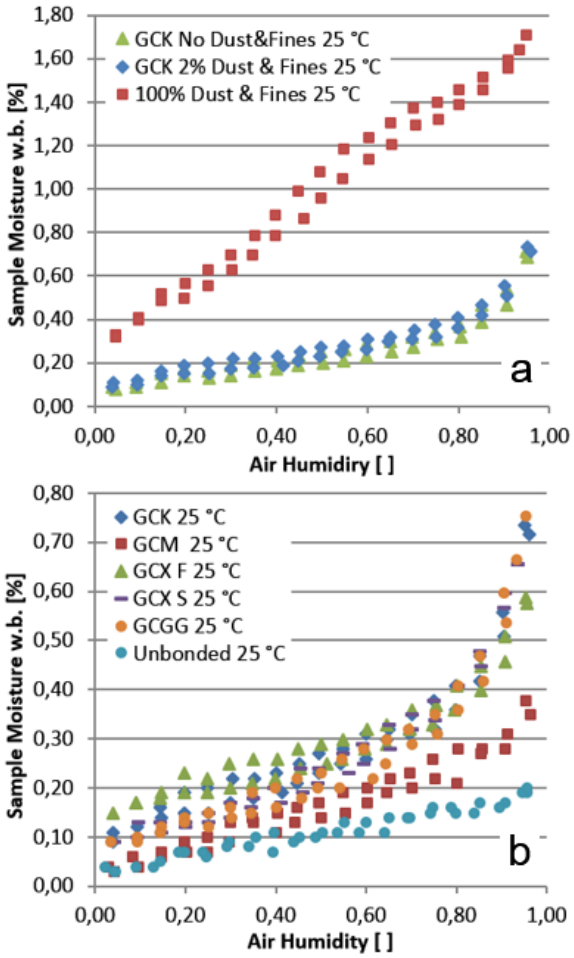

Fig. 7: Sorption curves for a) dust, sand with 0% and 2% of dust and fine, b) sand with different binders and un-bonded sand.

When adding binder the behavior becomes non-linear and the moisture level increases up to 4 times that of the un-bonded sand. Also we can see that a binder like GCM can has significantly lower moisture levels than the other binders, and it could therefore be used in moulds that are more prone to gas defects.

CONCLUSIONS

We can summarize the main finding as follows:

- We have shown that automatic vapor sorption tests are useful to detect differences between different factors affecting moisture and can help the foundry engineer to choose binders that have lower moisture levels
- Dust effects and temperature effects are not critical in the ranges currently allowed in the factories
- Air humidity is a very important parameter. In particular, drying at low air humidity can significantly reduce the moisture in the moulds
- Due to the weak hysteresis effect between the sorption and desorption curves, moisture lost during drying can be regained when moulds are stored for enough time in an open environment at higher humidity. This might jeopardize the positive effects of expensive drying processes.
- The data provided can be used as basis for the design of dryers and to help define control limits for the drying of moulds and cores in the foundry industry.

ACKNOWLEDGEMENTS

This work was financed by Global Castings A/S, the Danish Agency for Science, Technology and Innovation (DASTI) and the Technical University of Denmark (DTU). LabCell Ltd. provided support in executing the tests on the automatic vapor sorption analyzer.

REFERENCES

1. Campbell, J.; Harding, R.A. Solidification Defects in Castings. Lecture 3207, The University of Birmingham, 1994; 4-8.
2. Elmquist, L. Defect formation in cast iron. Presentation, School of Engineering, Jonkoping University, Sweden, 2012.
3. IKO. Description of Casting Defects; Chapters 4,10,12, S&B Industrial Minerals.
4. Chojecki, A.; Mocek J. Effect of atmosphere in a foundry mould on casting surface quality. Archives of Foundry Engineering, 2012, Volume 12, Issue 1, 13-18.
5. Elkem. Hydrogen Pinholes. Technical Information 30, Elkem Foundry Products, Rev. 1.2, 2007.
6. Siewiorek, A.; Nowak, R.; Chojecki, A.; Mocek J. Gas evolution rate from heated moulding sands bonded with organic binders. Archives of Foundry Engineering, 2011, ISSN (1897-3310), Volume 11, Issue 1, 87 – 92.
7. Starobin, A.; Hirt, C.W.; Goettsch, D. A Model for Binder Gas Generation and Transport in Sand Cores and Molds. Modeling of Casting, Welding, and Solidification Processes XII,

TMS (The Minerals, Metals & Materials Society), 2009.

8. Starobin, A.; Hirt, T.; Lang, H.; Rode, M. Core Drying Simulation and Validation, International Foundry Research 64 (2012) No. 1, 2-5.

9. Scarber, P.; Bates C.E. Simulation of Core Gas Production During Mold Fill. AFS, 2006.

10. Tiedje, N.; Crepaz, R.; Eggert, T.; Bey N. Emission of organic compounds from mould and core binders used for casting iron, aluminium and bronze in sand moulds. Journal of Environmental Science and Health, Part A, 45: 14, 1866 - 1876.

11. Samuels G.; Beckermann C. Measurement of Gas Evolution from PUNB Bonded Sand as a Function of Temperature. University of Iowa, International Journal of Metal Casting, Spring 2012.

12. Mujumdar, A.S. In Handbook of industrial drying, 3rd edition, 2006; Ch. 1-2.

13. Decagon Devices. Vapor Sorption Analyzer Operator's Manual; Ver.5, Ch. 2-3.

14. Bogucka J.; Grabiec-Mizera T. Evaluation of structure of concrete porosity on the basis of adsorption process. Poznan University of Technology, DS 11-956/07.

Supplement V

Automatic vapour sorption analysis as new methodology for assessing moisture content of water based foundry coating and furan sands

G.L. Di Muoio[1,2]*, N. Skat Tiedje[2] and B. Budolph Johansen[1]
[1]Global Castings A/S, Copenhagen, Denmark
[2]Technical University of Denmark, Copenhagen, Denmark

Gas generated during the casting process can cause defects that increase the cost of the components and possibly lead to scrapping the parts. Gases are produced during evaporation of water and by decomposition of organic materials present in the foundry coating and in the moulding sand.

This study investigates how equilibrium water content varies in foundry coating and in different furan based binding systems with the objective to determine what variables are critical for material moisture process control. The influence of relative humidity, temperature, dust levels and binder type are investigated.

Results show that highest effects are given by relative humidity and binder type. They can cause moisture level variations from 0.1% to about 0.8%. Temperature and dust levels play a minor role. Hysteresis effects between sorption and desorption curves are limited. Finally, the sorption curves are fitted with 3rd order polynomial equations.

Keywords: Water based coating, furan sand, automatic sorption analysis, sorption/desorption curves, drying process control, moisture control.

Introduction

When cast parts are produced, the molten metal in contact with the mould causes the production of gases that can lead to defects and scrapped items (Fig 1.a). Possible gas related defects are: hydrogen pin holes, blow holes, cracks and explosive penetrations.[1,2,3] These gases are composed by a mixture of water vapour, decomposition products of the coating and moulding materials and from gases dissolved in the molten iron.[1,2] Gas defects can be correlated directly to vapour generated in the mould and coating material due to a high level of residual moisture.[3,4,5] In particular for furan sands, water vapour is a significant component of the gases generated during the decomposition.[6] Moisture is present in furan sand as product of the binder and catalyst reaction but its amount can change over time.[5] Literature shows that gas defects probability can be predicted by simulation if models are calibrated with experimental data for the specific binding system used.[7,8,9] Other studies show that gas evolution rates can vary for different materials.[10,11,12,13]

All the current studies however focus on different classes of binding system and foundry material but do not provide information about the influence of parameters such as temperature, air humidity and dust levels and about different brands of furan binders used in Global Castings production facilities.

In this study the objective is to identify how the moisture contents in foundry coating and in sands bonded with different brands of furan binders (Fig.1.b) are affected by relative humidity, temperature and dust levels (Fig.1.c). In order to do this, we use an automatic vapour sorption analyser to determine the equilibrium sorption/desorption curves of the considered materials. The reason for choosing an automatic moisture analyser are: a shorter test time (due to the use of a small sample), the increased precision in weight measurement (due to eliminating manual handing operations of the samples during the tests) and easy and precise control of temperature and humidity.

Sorption/desorption curves are typically used in other industries (such as food, wood, paper) to design and optimise drying processes (by knowing the initial moisture and final moisture achievable at the drier's air humidity and temperature levels)[14], to provide limits for production processes control and monitoring, to predict shelf life by knowing what moisture level a material will reach in an environment at a given air humidity (i.e. shelf life prediction in food packaging depends on moisture content)[15] or to predict possible moisture migration between different materials.[14,15] These curves are a property of the material and show how its moisture levels vary as a function of relative humidity at a given temperature. In particular they will show the minimum possible level of moisture achievable in given environmental conditions for a given material.

These test are normally not used in the foundry industry but are thought to be relevant by the authors for the following reasons:

- to understand which parameters have the highest effect on moisture levels in the considered material and therefore on the generation of water vapour and the risk of gas defects

* Corresponding author, email: gidmu@globalcastings.com

- to create a set of data that can be used for the design and control of driers of furan moulds and foundry coatings
- to support foundry engineers making the right choices when optimizing the production and drying process of coated furan sand moulds.
- to provide a new methodology for testing foundry coatings and binding systems

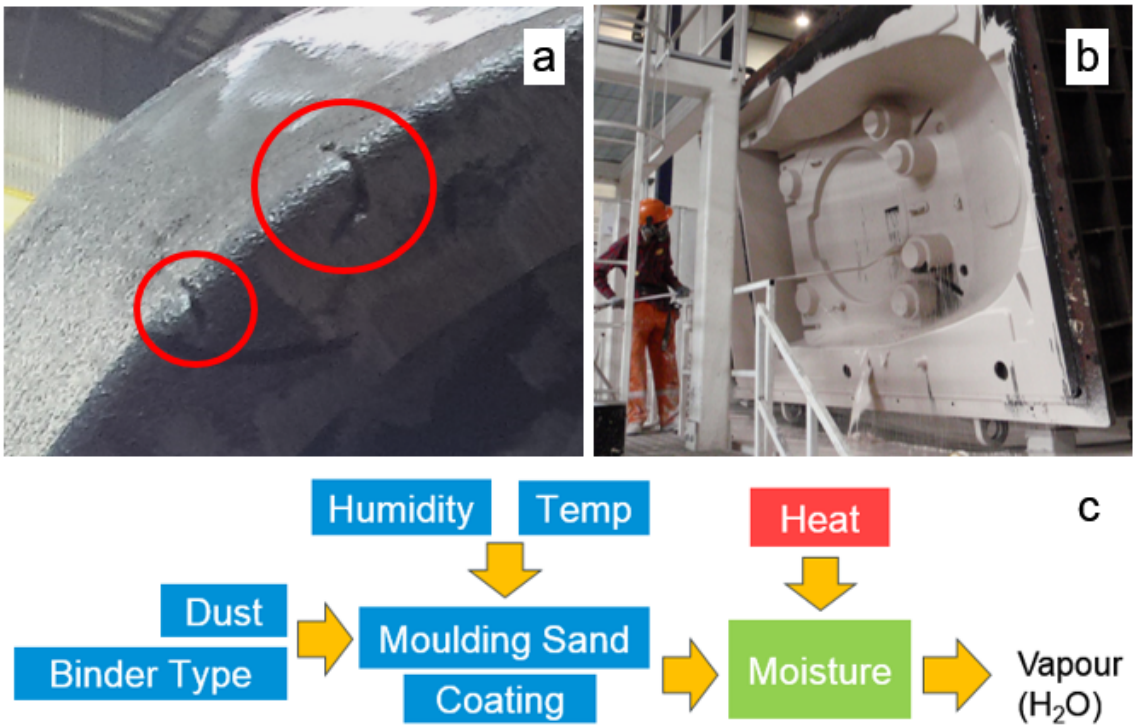

Fig.1: a) Example of moisture related casting defect, b) coating process of furan bonded sand mould, c) parameters affecting vapour generation in a castings process.

Experimental Procedure

In order to investigate the effect of different variables, the experimental plan described in Table 1 was designed. First, the effect of temperature on the two main classes of material is studied (coating and GCX F sand). Then the effect of dust levels are investigated (no dust and 2% dust) and different binder system brands (GCX S, GCM and GCGG). Finally pure dust and un-bonded sand were tested to provide baselines for comparison.

Table 1: Overview of Experimental Plan.

Material	Temperature [°C]		
	15	25	35
Coating	X	X	X
GCX F	X	X	X
GCK No Dust		X	
GCK 2% Dust		X	
GCX S		X	
GCM		X	
GCGG		X	
Pure Dust		X	
Un-bonded Sand		X	

The temperature levels were chosen as the minimum (15°C), typical (25°C) and maximum (35°C) temperature allowed in the produciton facilities. Similarly, dust levels representing the maximum allowed (2%) and the minimum (0%) possibly achievable levels were used. The binder brands are the same as used in the considered produciton facilities.

For the bonded sand, the sample preparation started by mixing of sand, binder and catalyst (Fig.2a), followed by curing for one week at 23-25 °C and 45-50% RH and finally manual crushing (Fig.2b) (for easier handling during tests).

Binder addition was 1% of sand weight and catalyst addition was 40% of binder weight. The coating samples were obtained by drying the liquid coating (typically containing an initial moisture of about 40% on wet basis) at same conditions and time used for the sand samples and then manually crushing the dry coating into powder (Fig.2c). Pure dust and un-bonded sand were taken directly from filter bags and silos in the factory and then let equilibrate at the same temperature and humidity conditions as described for the other samples.

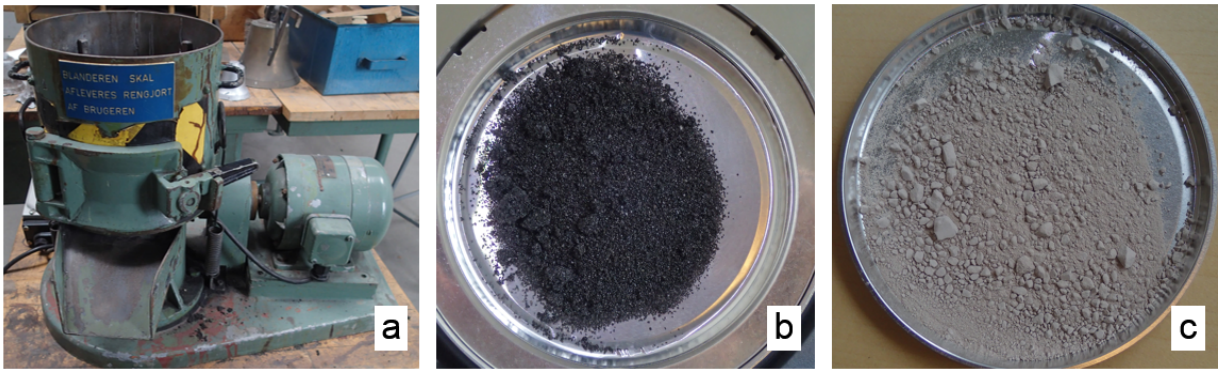

Fig.2: Materials preparation: a) mixing, b) crushed sand and c) crushed coating.

After sample preparation and equlibration at 23-25 °C and 45-50% RH for a week, a sample of each type was tested in an automatic moisture analyzer (Fig.3.a) with an accuracy of 0.05%. The automatic moisture analyzer was set to dry the sample at a temperature of 105 °C. The wet basis moisture (calculated as in equation (1)) values obtained are needed as input in the automatic vapor sorption analyser to compute the sample moisture values during the sorption tests since it is not possible for the automatic moisture analyzer to dry the samples at 105 °C.

$$InitialMoisture_{w.b.} = \frac{InitialWeight - DryWeight}{InitialWeight} 100 \quad (1)$$

The automatic vapor sorption analyser used for this study (Fig.3.c) is equipped with a precision scale with +/- 0.1 mg accuracy, a dew point sensor with 0.5 % RH accuracy and infrared sensor for temperature control. The moisture level can be controlled by supplying either wet air or dry air.

The sorption/desorption tests were carried out by loading a sample of about 10-12g in the automatic sorption analyzer and inputting the initial moisture of the sample at 23-25 °C and 45-50% RH (Fig.3.b) from the previous tests. After sealing the cover, the machine will start recording weight variation and changing temperature and relative humidity according to the test plan.

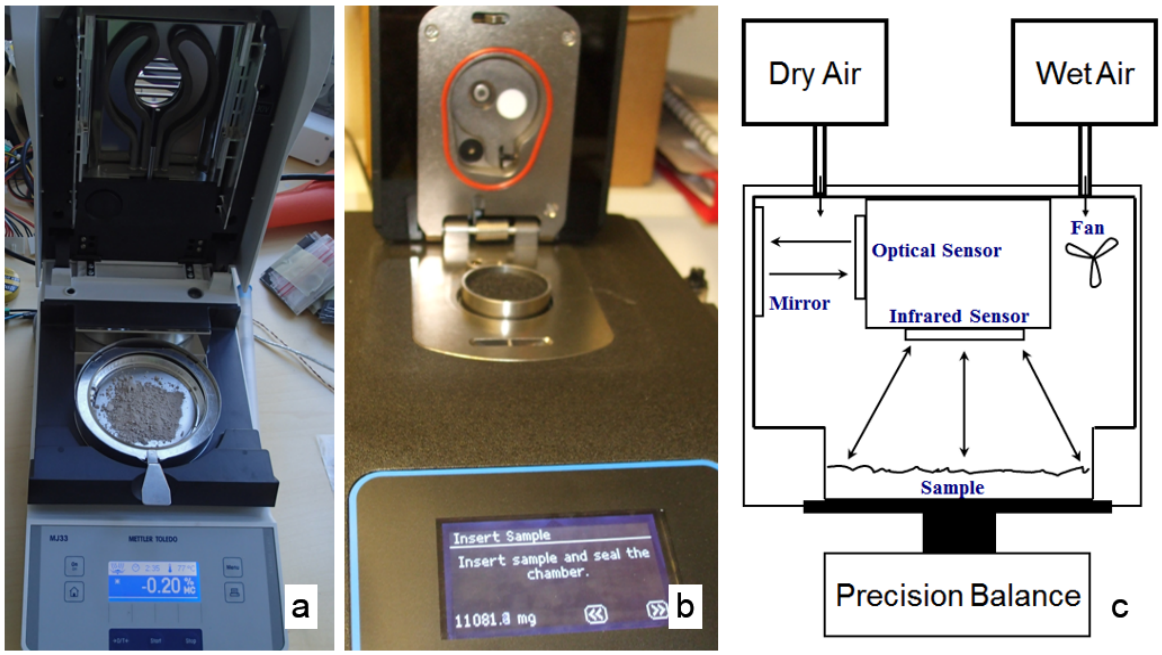

Fig.3: Test Setup: a) initial moisture level measurement, b) automatic vapour sorption analyser and c) schematic.

In order to abtain the sorption/desorption curves, the temperature is held constant at either 15 °C, 25 °C or 35°C while the air humidity is changed stepwise in 5% increments. The current moisture content of the sample is calculated as:

$$CurrentMoisture_{w.b.} = \frac{CurrentWeight - DryWeight}{CurrentWeight} 100 \quad (2)$$

Where dry weight is calculated from the initial moisture and weight as:

$$DryWeight = InitialWeight\left(1 - \frac{InitialMoisture_{w.b.}}{100}\right) \quad (3)$$

During the test, at each imposed air humidity level, the moisture level in the sample is calculated using equation (2). If the variation in moisture is less then 0.02% in one hour, the sample is considered equilibrated and the air humidity can be changed to the value required by the next step (Fig.4a).

Each test begins at 50% RH and the air humidity is incresed stepwise up to 95% to initialise the sample (Fig.4b), then the desorption phase starts (humidity is decresed step wise to 5% RH) and finally the adsorption phase is carried out (humidity is increased stepwise to 95% RH). In order to obtain the final sorption curve, the moisture level of each equilibrium point is plotted versus the air humidity. Sorption curves are plotted in the results section without the initialization steps.

Finally, 3rd degree polynomial equations are fitted to the experimentally obtained sorption and desorption curves (Fig.4c and equation (4)). The curves coefficients are reported in the result section for each material, as well as the coefficient of determination R^2 used to check how well the model fits the data (R^2 values close to 1 represent a good fit between the curve and the data).

$$MaterialMoisture_{w.b.} = a_0 + a_1\frac{RH_{air}}{100} + a_2\left(\frac{RH_{air}}{100}\right)^2 + a_3\left(\frac{RH_{air}}{100}\right)^3 \quad (4)$$

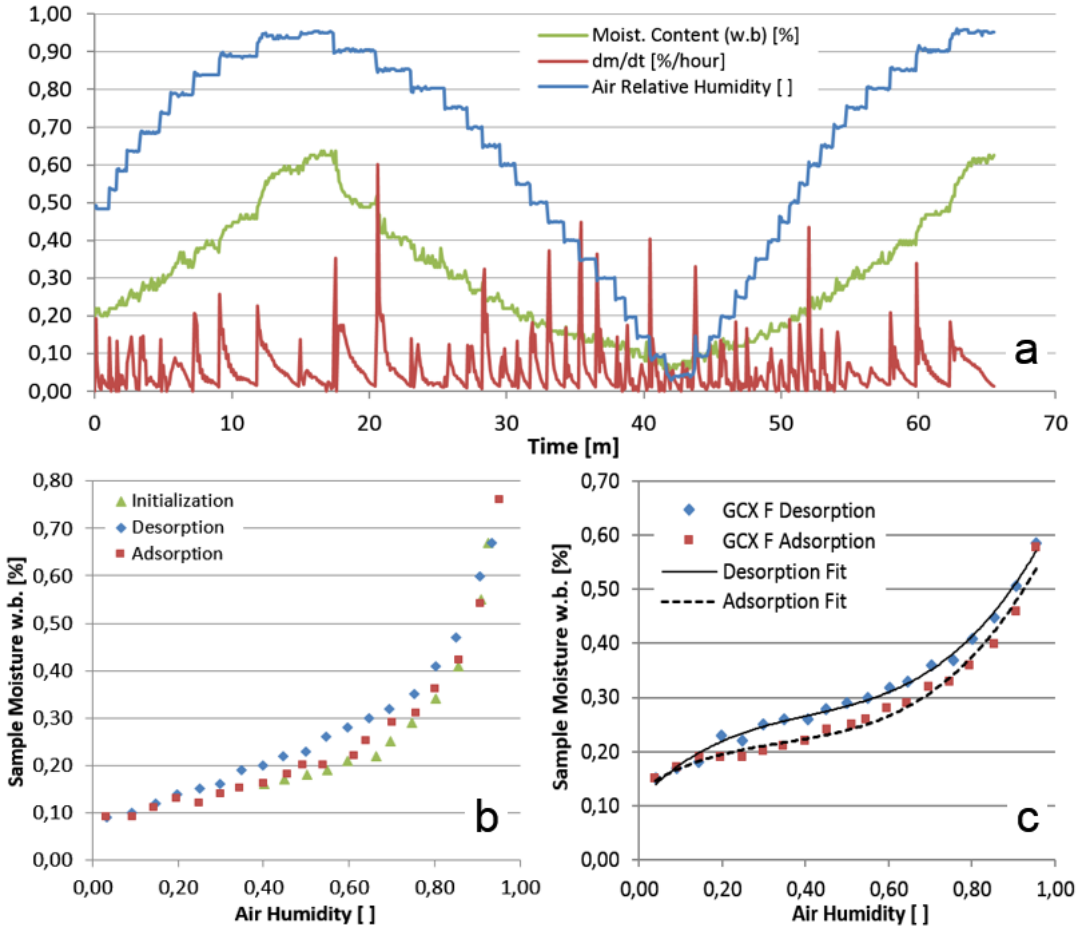

Fig.4: Example of: a) Sorption tests data, b) equilibrated points, c) fitted curves.

Results and Discussion

Table 2 summarises the results of the initial moisture tests carried out on the equilibrated samples at 23-27 °C and 45-55% relative humidity. We can see that pure filter dust has the higher initial moisture level (0.71%), un-bonded sand has the lowest moisture level (0.11%) and all the bonded sands have initial moisture levels between 0.17% and 0.24%.

Table 2: Initial sample moisture after and equilibration at 23-25 °C and 45-50% RH for a week.

Material	Initial Moisture w.b. [%]
Coating	0.20
GCX F	0.24
GCK No Dust	0.21
GCK 2% Dust	0.23
Pure Dust	0.71

Material	Initial Moisture w.b. [%]
GCX S	0.17
GCM	0.18
GCGG	0.17
Un-bonded Sand	0.11

Figures 5a and 5b show the sorption curves respectively for GCX F furan bonded sand and for foundry coating at 15 °C, 25 °C and 35 °C. It can be seen that, for both materials, temperature does not have a significant effect. On the other hand, air humidity has a major effect. For both materials, moisture can be as low as 0.1% at 5% RH and become as high as 0.6% at 95% RH. Even though the absolute values seem small, we need to notice that from 0.10 % to 0.60% there is a variation of 600%. Additionally, large amounts of moulding sands are used in each mould. For example a 40 tons mould might contain as low as 40 kg of water at 0.1% moisture (if dried at 5% RH for enough time) or as much 240 kg of water at 0.6 % moisture (if stored for enough time at 95% RH). It is therefore important to be aware of this variation when designing the drying process, factory environment conditions and venting channels in the moulds.

Another important conclusion is that the hysteretic behaviour between adsorption and desorption is fairly limited especially for the coating. For the moulding sand, where there is slightly more hysteresis, the difference between sorption and desorption curve is typically less than 0.05% in moisture.

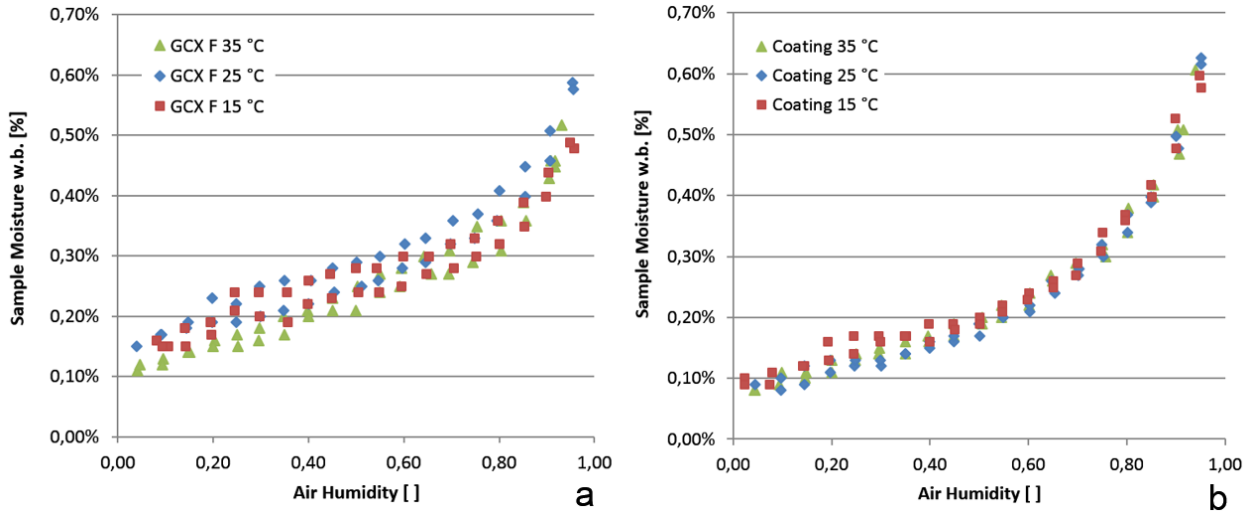

Fig.5: Sorption curves at 15 °C, 25 °C and 35 °C for a) sand and b) coating.

Figure 6a shows that the effect of a 2% dust addition causes a small increase in moisture levels, for example from 0.20% to 0.24% at 50% relative humidity. However, pure dust can contain from 0.30% to 1.70% moisture. It is therefore important to reduce dust segregation in silos to avoid lumps of dust in the moulds.

Figure 6b shows a comparison between moulding sands bonded with different binder types and un-bonded sand. It can be seen that un-bonded sand has the smallest moisture content (between 0.04% and 0.20%), it has no hysteresis between adsorption and desorption and moisture value is a linear function of air humidity. When adding binder the behaviour becomes nonlinear and the moisture level increases up to 4 times that of the un-bonded sand. This is a confirmation of the hydrophilic nature of furan binding systems.

Also we can see that a binder like GCM has significantly lower moisture level compared to the other binders, and it could therefore be used in moulds that are more prone to gas defects. For example, considering a 40 ton mould at 90 % RH where GCM binder is used, it will have a moisture of 0.30 % and therefore a water content of 120 kg. On the other hand if GCK or GCGG binders are used, the same mould will have a moisture content of about 0.55 % at 90% RH,

which translates to a water content of 220 kg (almost double the one of VCM binder). Finally, the highest moisture content is 0.75%, given by GCGG binder at 95% RH, this translates in a quantity of 300 kg of water for a 40 tons mould.

These results show that different amounts and brands of furan binders can have different performance with respect to moisture content. Sorption tests can help to quantify these performances and to choose the right material recipe.

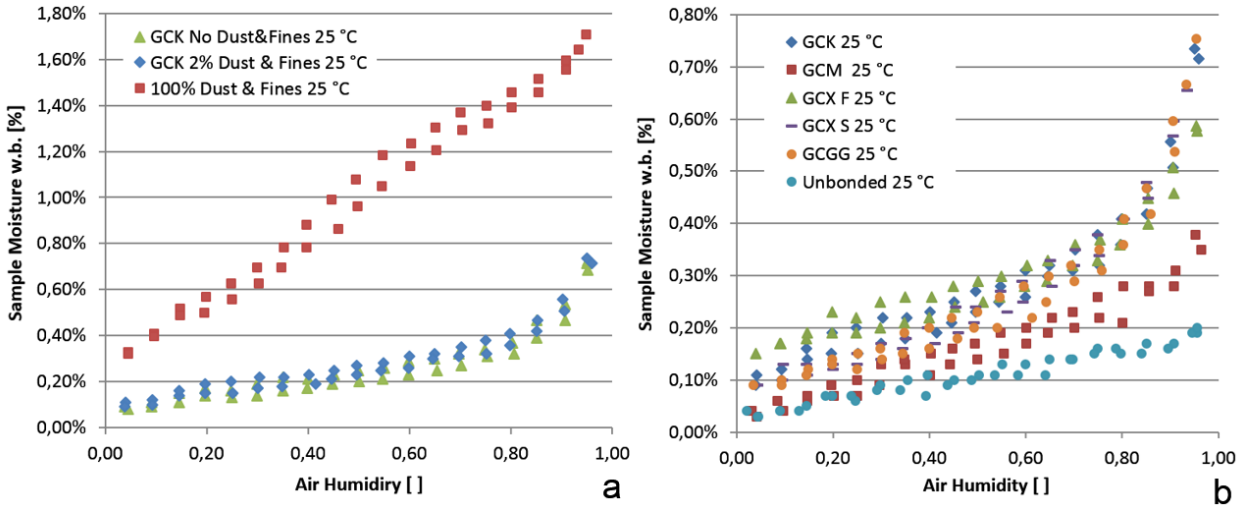

Fig.6: Sorption curves for a) dust, sand with 0% and 2% of dust and fines, b) sand with different binders and un-bonded sand.

Table 2 reports the coefficients of the 3rd degree polynomials used to fit the experimental sorption curves of the different materials as well as the coefficient of determination R^2. Coefficients are provided for the desorption and the sorption of each material tested but not for the different test temperature and dust levels since these two parameters were found to have little influence on the curves. Additionally, it was chosen to provide the same coefficients for the desorption and sorption curves of coating and un-bonded sand since hysteresis was found to be negligible. Finally, we can see that for un-bonded sand a_3 and a_2 coefficients have a value of 0 since its behaviour can simply be described by a linear curve.

As a final check, we can see that all the curves have good fit since R^2 values are always above 0.95 and above 0.97 for most of the curves.

Table 2: Coefficient of 3rd order polynomials fitted to sorption and desorption curves for furan bonded sands and foundry coating with corresponding coefficients of determination R^2

	Desorption					**Sorption**				
	a_3	**a_2**	**a_1**	**a_0**	**R^2**	**a_3**	**a_2**	**a_1**	**a_0**	**R^2**
Coating	1.5094	-1.4926	0.6256	0.0444	0.9869	1.5094	-1.4926	0.6256	0.0444	0.9869
GCK	2.1500	-2.5702	1.1754	0.0402	0.9807	2.0139	-2.3105	1.003	0.0371	0.9687
GCM	0.3853	-0.4522	0.4298	0.0215	0.9867	0.4665	-0.5090	0.3853	0.0168	0.9775
GCX F	1.2690	-1.5475	0.8048	0.1099	0.9932	1.0985	-1.1412	0.5195	0.1275	0.9831
GCX S	1.3006	-1.2949	0.6960	0.0484	0.9893	1.3734	-1.1971	0.5098	0.0683	0.9895
GCGG	1.6866	-1.7783	0.8256	0.0425	0.9882	2.2606	-2.4140	0.9222	0.320	0.9692
Un-bonded	0	0	0.1616	0.0284	0.9562	0	0	0.1616	0.0284	0.9562
Pure Dust	-0.6240	0.6183	1.4406	0.2623	0.9951	-0.8065	1.3640	0.8244	0.2958	0.9964

Conclusions

To summarise the main conclusions of the study we can say that:

1. We have shown that automatic vapour sorption tests are useful to detect differences between factors affecting moisture and can help the foundry engineer to choose binders that have lower moisture levels. As a consequence

these tests could be used as an evaluation tool for new binding systems recipes and coatings to be introduced in production.

2. Dust effect and temperature effect are not critical in the ranges currently allowed in the factories, it is therefore not critical to tightly control their values as soon are they are within current specification.
3. Air humidity is a very important parameter, in particular drying at low air humidity can significantly reduce the moisture in the moulds
4. Binder type can heavily affect the moisture retention properties of the mould. It is therefore important to choose binding systems that can reduce the amount of moisture in the sand to reduce the generated vapour and therefore the probability of gas defects
5. Due to the weak hysteresis effect between sorption and desorption curves, moisture lost during drying can be regained when moulds are stored for enough time in an open environment at higher humidity. This might jeopardise the positive effects of expensive drying processes.
6. The data obtained from this study can be used as basis for the design of dryers and to help define control limits for the drying of moulds and cores in the foundry industry.
7. Simple calculation examples have been performed using the results from the experiments to show a possible use of this new test methodology
8. Coefficients of 3rd order polynomials fitted to sorption and desorption curves for the tested materials have been obtained.

References

1. J. Campbell, R.A. Harding: 'Solidification Defects in Castings', Lecture 3207, The University of Birmingham, 4-8, 1994.
2. L. Elmquist: 'Defect formation in cast iron', Presentation, School of Engineering, Jonkoping University, Sweden, 2012.
3. IKO: 'Description of Casting Defects', Chapters 04,10,12, S&B Industrial Minerals
4. A. Chojecki*, J. Mocek: 'Effect of atmosphere in a foundry mould on casting surface quality', Archives of Foundry Engineering, Volume 12, Issue 1/2012, 13-18.
5. D - Elkem: 'Hydrogen Pinholes', Technical Information 30, Elkem Foundry Products, Rev. 1.2, 2007.
6. A. Siewiorek, R. Nowak, A. Chojecki, J. Mocek: 'Gas evolution rate from heated moulding sands bonded with organic binders', Archives of Foundry Engineering, ISSN (1897-3310), Volume 11, Issue 1/2011, 87 – 92.
7. A.Starobin, C.W. Hirt, D. Goettsch: 'A Model for Binder Gas Generation and Transport in Sand Cores and Molds', Modeling of Casting, Welding, and Solidification Processes XII, TMS (The Minerals, Metals & Materials Society), 2009.
8. A.Starobin, T. Hirt, H. Lang, M. Rode: 'Core Drying Simulation and Validation', International Foundry Research 64 (2012) No. 1, 2-5.
9. P. Scarber, C.E. Bates: 'Simulation of Core Gas Production During Mold Fill', AFS, 2006.
10. N.Tiedje, R. Crepaz, T. Eggert, N. Bey: 'Emission of organic compounds from mould and core binders used for casting iron, aluminium and bronze in sand moulds', Journal of Environmental Science and Health, Part A, 45: 14, 1866 – 1876.
11. G. Samuels and C. Beckermann: 'Measurement of Gas Evolution from PUNB Bonded Sand as a Function of Temperature', University of Iowa, International Journal of Metal Casting, Spring 2012.
12. A. Shepherd: 'Understanding Emission Characteristics of a Foundry Sand Binder', Proceedings of The National Conference On Undergraduate Research (NCUR) 2012, Weber State University, Ogden, UT, March 29-31, 2012.
13. BCRA: 'Venting of mould and cores', BCIRA Broadsheet 188, 1980.
14. A.S. Mujumdar: 'Handbook of industrial drying', 3rd edition, Ch. 1-2, 2006.
15. Decagon Devices: 'Vapor Sorption Analyzer', Operator's Manual, Ver.5, Ch. 2.

Acknowledgement

This work was financed by Global Castings A/S, the Danish Agency for Science, Technology and Innovation (DASTI) and the Technical University of Denmark (DTU). LabCell Ltd. provided support in executing the tests on the AquaLab automatic vapour sorption analyser.

Supplement VI

Moisture Diffusion Coefficients Determination of Furan Bonded Sands and Water Based Foundry Coatings

Giovanni Luca **Di Muoio***,

Global Castings A/S, Copenhagen, Denmark

Niels Skat **Tiedje,**

Technical University of Denmark, Copenhagen, Denmark

*Corresponding author: gidmu@globalcastings.com, M: +45 6180 9266, Global Castings A/S, 373 N Diplomvej, Lyngby, 2800,

Moisture content in furan bonded sand and water based coatings can be one of the main causes for gas related defects in large cast iron parts. Moisture diffusion coefficients for these materials are needed to precisely predict the possible moisture levels in foundry moulds. In this study, we first compare two different experimental methods that can be used to determine moisture diffusion coefficients. Then, we determine diffusion coefficients for water based coatings and for different types of furan binders and we investigate the effects of compaction, dust levels and temperature. Finally, we provide an example on how it is possible to apply this knowledge to estimate moisture variation in a sand mould during production.

Keywords

Moisture diffusion coefficients, furan sand, water based foundry coating, vapour sorption analysis, core drying.

List of Symbols

D diffusion coefficient [m^2 s^{-1}]

L thickness of the sample [m]

M_t adsorbed mass of water at time t [kg]

M_e adsorbed mass of water at equilibrium [kg]

t time [s]

x space [m]

X moisture [ ]

X_i initial moisture content [%]

X_e moisture content at equilibrium [ ]

X_t moisture content at time t [ ]

X* nondimensional moisture [ ]

1 – Introduction

Residual moisture in moulds and foundry coatings can be responsible for generating gases that lead to the formation of different kinds of defects such as hydrogen pin holes, blow holes, cracks and explosive penetrations (as shown in figure 1) [1-3]. These defects can lead to non-conformities or, eventually, to a scraped casting and therefore and to an increase in production cost. Moisture present in moulds and core is an important contributor to the generation of gases (and related defects) during the pouring of liquid metal [3-5].

Foundry moulding and coating materials contain moisture and they can adsorb or release it in different amounts and at different speeds. The equilibrium moisture levels and the effects of different factors, such as dust amount, binder type and temperature, for different furan sands and foundry coating have been investigated in [6].

With regard to the adsorption rate of moisture, the critical parameter needed to model this behaviour is the moisture diffusion coefficient [7]. Such coefficient, typically obtained from laboratory tests, is needed in order to predict more precisely how the moisture distribution in a mould changes when conditions in the surrounding environment are varying. For example, foundry cores and moulds are exposed to a varying environment for different time after drying in a drying cabinet at low RH and high temp (figure 2).

In the drying industry moisture diffusion coefficients are used to design driers used mainly in food and wood industry [7]. Determining the coefficients is done with different methods in different industries [7-13]. Data for moisture diffusivity coefficients is available for general classes of materials (like wood, milk, paper, sand, etc…) [7] but not for materials used in the foundry industry like furan sands and water based coatings.

Literature shows that the moisture diffusion coefficient can be affected by many factors (like temperature and moisture) [7] and also by methods used to obtain and analyse the data [8].

In this study, we present results from gravimetric moisture adsorption tests on which an analytical solution of the diffusion equation is fitted. The objective to estimate moisture diffusion coefficients and the effect of different factors on the moisture diffusion of furan bonded sands and of water based coatings. The variables investigated in this study are sand compaction, air relative humidity, temperature, dust content and binder type. Two possible test methods are compared and evaluated.

Finally, an example of how it is possible to use these coefficient for the estimation of moisture in a foundry moulds is provided.

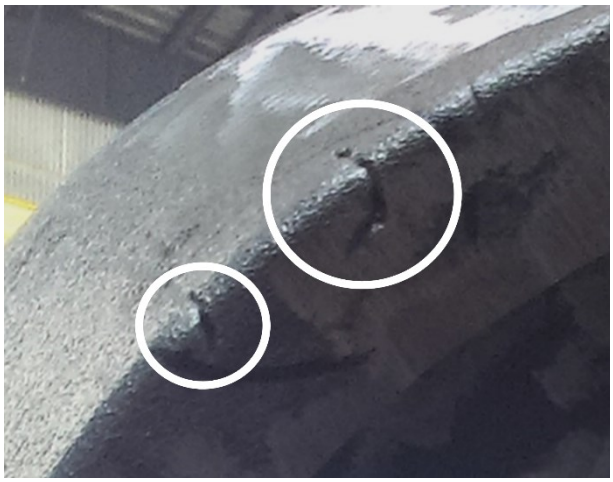

Figure 1. Example of Moisture Related Defect.

Operation	Moulding	Drying	Assembly
Temp Relative Humidity	15-35 °C 30-95%	70-90 °C 2-10%	15-35 °C 30-95%

Figure 2. Production process steps for a furan sand mould coated with water based coating and correspondent ranges of environment conditions.

2 - Methods

Two different methods were used to run moisture adsorption tests. A manual method, in which a simple (but slow), low cost equipment is used and an automatic test methodology (Automatic Vapour Sorption Analysis) where more costly (but faster) equipment is used. In this way, it will be possible not only to determine the diffusion coefficient, but also to compare the results from the two methods and give recommendations to the foundry industry on which test methods to use to estimate moisture diffusion coefficients.

2.1 - Manual Tests

In the manual tests method furan sand samples are moulded in a cylindrical mould of 18 mm diameter and 50 mm depth.

In order to represent the possible ranges of density of a real production mould, some mould are left un-compacted, while on the others a 1 kg weight is added right after filling as shown in figure 3 (more details on the preparation and compaction procedure can be found in [14]). In this way, it will be possible to achieve different sand density of the samples and to determine the possible effect on the moisture diffusion coefficients.

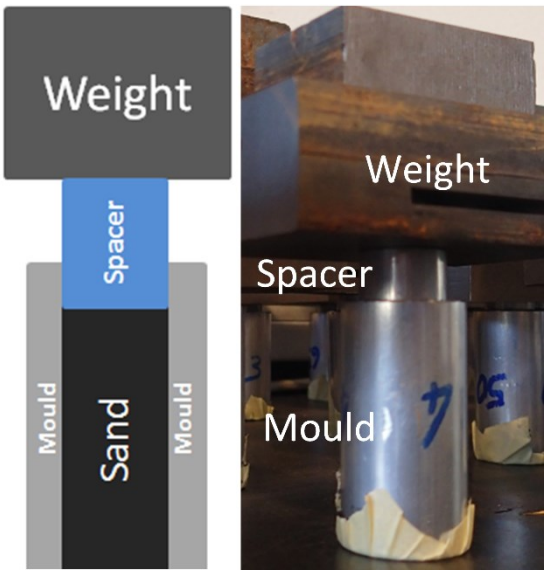

Figure 3. Sample Preparation for manual adsorption tests.

Samples are cured for 48 hours at room conditions (23-25 °C and 35-45% RH), followed by a period of equilibration of 48 hours where samples are placed in a sealed container where silica gel is used to keep air relative humidity at 5-7%. In this way, we equilibrate the moisture of the sample to replicate the situation of a mould which has been through a drying step as shown in figure 2.

After equilibration at 5 % RH, the sample is placed on a precision scale connected to computer that records weight changes. The air around the sample will be either at laboratory conditions (23-25 °C and 35-45% RH) or near saturation (23-25 °C and 95% RH). In order to achieve the 95% RH test condition, a water soaked cloth is added on the wall of the sample chamber (figure 4).

This procedure is aiming at reproducing the process of a mould taken out from a drying step and placed in environment where the humidity can vary from 30 to 95% RH (as shown in figure 2). However due to limitations of the manual method, only the two above described values of relative humidity are used in these experiments.

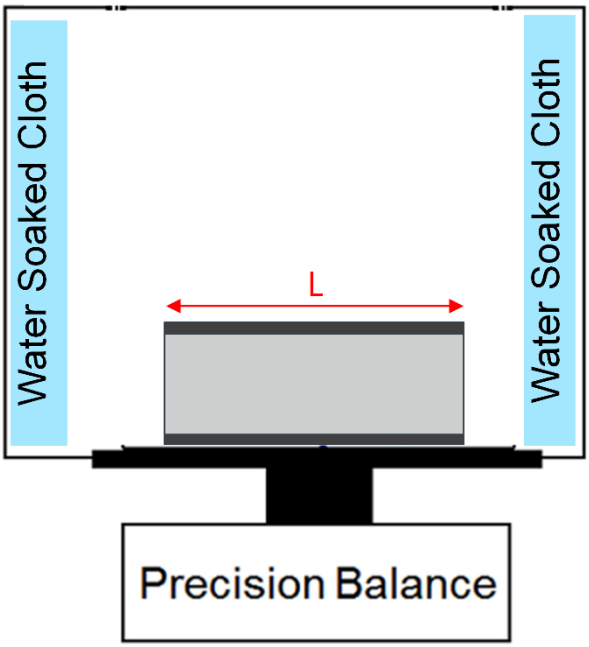

Figure 4. Schematic test setup for manual sorption tests.

The experimental plan for manual tests can be summarised as in Table 1 where two possible sand binder recipes (GCK and GCM) were tested at two humidity levels.

The plan is repeated for low and high compaction sample and replicated two times, for a total of 16 runs.

Table 1. Overview of experimental plan for manual sorption tests.

Material	Temperature [°C]	
	25	
	Relative Humidity [%]	
	40	95
GCK	X	X
GCM	X	X

The sample moisture can be calculated from the weight variation (Eq.1) and is defined on wet basis as common practice in foundry industry:

$$X(t)_{w.b.} = \frac{CurrentWeight - DryWeight}{CurrentWeight} 100 \quad \text{Eq.1}$$

The dry weight is obtained by drying the sample at 105 °C for 30 minutes.

2.2 - Automatic Tests

For the automatic tests method, an AquaLab automatic vapour sorption analyser is used. The cured sand samples and dry coating samples are crushed, since it is only possible to test granular material in such equipment, as shown in figure 5.

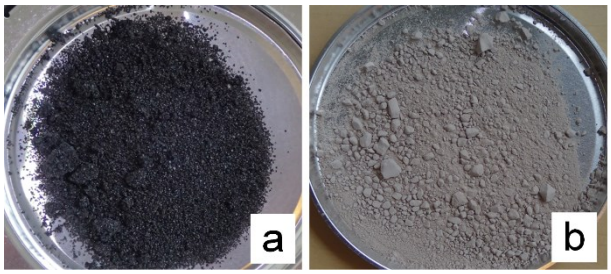

Figure 5. Sample preparation for automatic vapour sorption tests.

Then, the samples are placed in the automatic sorption analyser (Figure 6) and the initial moisture value (obtained from preliminary tests) is entered. The equipment, then, starts to record weight variation as air humidity is varied stepwise from 3 to 95% RH. In this way it is possible to test the full range of environmental condition to which a sand mould can be subjected in a real factory.

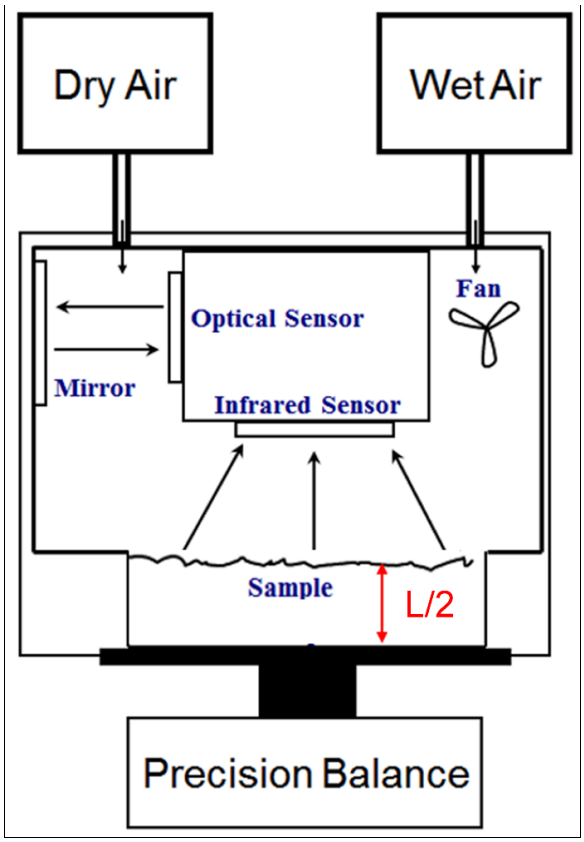

Figure 6. Test setup schematic for automatic sorption tests.

Figure 7 shows a typical data output from an automatic sorption test run. At each test step the relative humidity is kept constant until the mass variation of the sample is less than 0.2% per hour. At this point the sample is considered to be in equilibrium and the next step starts. More details on the automatic test procedure can be found in [6].

Moisture is calculated on wet basis using Eq. 1 as for the manual tests.

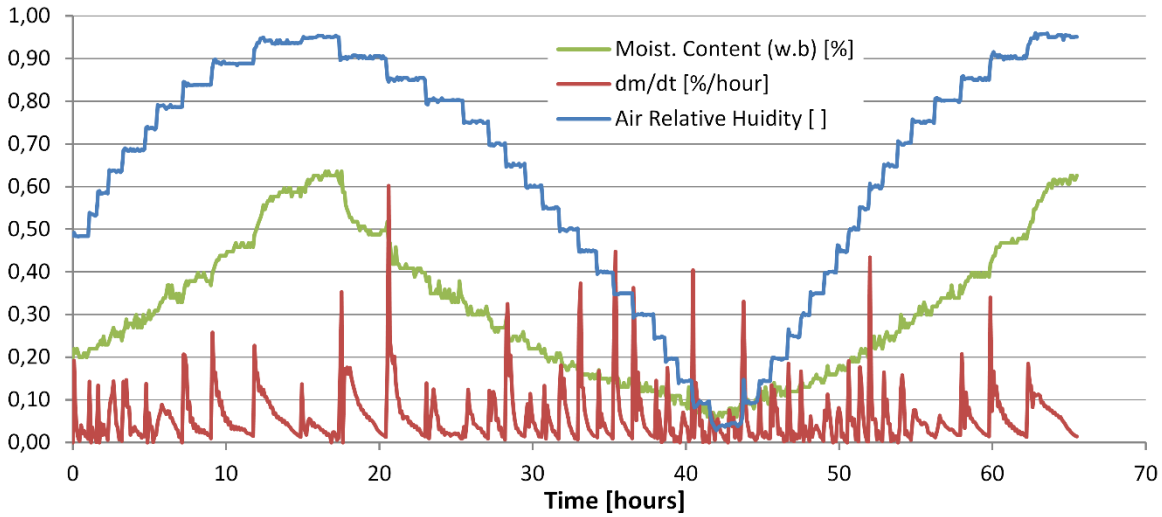

Figure 7. Typical data output from and automatic sorption test run.

Figure 8 shows a typical adsorption/desorption curve, illustrating the equilibrated weight of the sample at different relative humidity during the initialization cycle and during the desorption and adsorption cycle.

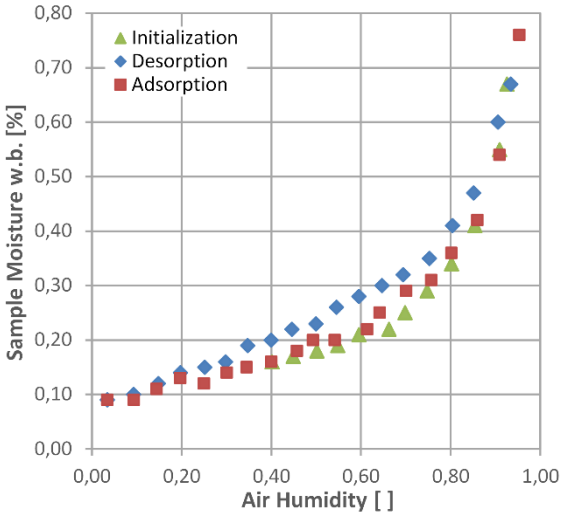

Figure 8. Typical adsorption/desorption curve for furan sand.

The experimental plan for the automatic tests is summarised in Table 2. Tests are carried out at 15 °C, 25 °C and 35 °C for coating and GCX F furan sand. Then at 25 °C we test effect of dust amount (0 and 2%) and different brands of furan binders. Pure dust and un-bonded sand are also tested to provide basis for comparison. A total of thirteen sorption tests is carried out.

Table 2. Overview of experimental plan for automatic vapour sorption tests.

Material	Temperature [°C]		
	15	25	35
Coating	X	X	X
GCX F	X	X	X
GCK No Dust		X	
GCK 2% Dust		X	
GCX S		X	
GCM		X	
GCGG		X	
Pure Dust		X	
Un-bonded Sand		X	

2.3 – Diffusion Coefficients Determination

In order to obtain diffusion coefficients from the test data, approximated solutions of the diffusion equation are fitted to the measured weight curves.

The moisture diffusion equation (Eq. 2a) is solved with boundary conditions representative of the one used in the tests [8,15,16].

$$\frac{\partial X}{\partial t} = D\frac{\partial^2 X}{\partial t^2} \qquad \text{Eq. 2a}$$

Initial condition:

$$X(x,0) = X_i \qquad \text{Eq. 2.b}$$

Boundary conditions on the air side

$$X(0,t) = X_f \qquad \text{Eq.2c}$$

Boundary condition the other air side (manual tests):

$$X(L,t) = X_f \qquad \text{Eq2.d}$$

Boundary Condition at bottom of sample holder (automatic tests):

$$\left(\frac{\partial X}{\partial x}\right)_{x=\frac{L}{2}} = 0 \qquad \text{Eq. 2.e}$$

The next step involves a change of variables to normalise the moisture content as follows:

$$X^* = \frac{X - X_i}{X_e - X_i} \qquad \text{Eq.3}$$

In this way, for a sample moisture of $X = X_i$ the normalised moisture X^* will have a value of zero. On the other hand, for a sample moisture of $X = X_e$ the normalised moisture value X^* will be 1.

For the manual sorption tests, nondimensionalization is applied so that for each test initial moisture X_i is equal to the equilibrated moisture at 5% RH and the final moisture X_e is the equilibrated moisture value reached at the specific test relative humidity (40% or 95% RH).

For the automatic sorption test, the nondimensionalization is carried out for each test step (time for which the relative humidity is kept constant). The initial moisture X_i is the initial moisture of the sample at the specific test step and the final moisture X_e is the final equilibrated moisture at the specific test step. In this way it is possible to obtain a diffusion coefficient for each value of relative humidity used in test steps.

The full form of the analytical solution of the moisture distribution for the above problem is reported in several works [10,15,16]. An integration of the analytical solution of the moisture distribution over the thickness of the test sample is carried out to obtain the mass of the sample.

Finally, the solution is expressed in a ratio between the adsorbed mass of water by the sample at the time t (M_t) and the equilibrated mass of the sample M_e and approximated as below [15,16]:

$$\frac{M_t}{M_e} = \frac{4}{L}\sqrt{\frac{Dt}{\pi}} \qquad \text{for } \frac{M_t}{M_e} < 0.5 \quad \text{Eq.4a}$$

$$\frac{M_t}{M_e} = 1 - \frac{8}{\pi^2}\exp\left(-\frac{\pi^2 D}{L^2}t\right) \text{ for } \frac{M_t}{M_e} > 0.5 \quad \text{Eq.4b}$$

Where D is the diffusion coefficient and L the thickness of the sample as shown in figures 4 and 6.

Both approximations of the solution must fit experimental data in the correspondent range of M_t/M_e using the same diffusion coefficient (Figure 9).

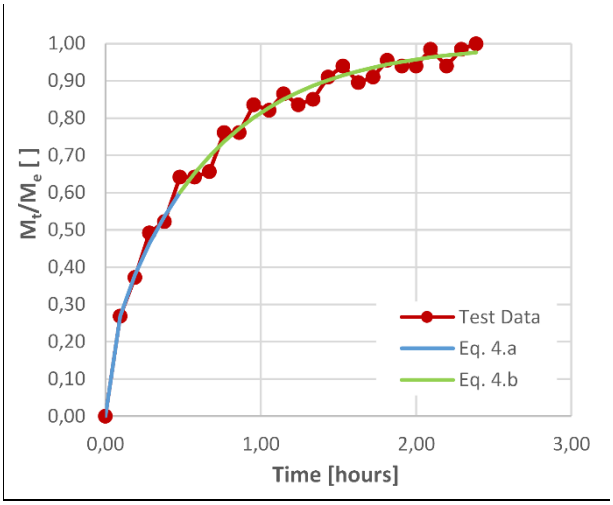

Figure 9. Example of experimental data fitted with the two approximated solutions Eq.4a and Eq4.b.

3 - Results and Discussion

In the following sections first we present the diffusion coefficients obtained from the different tests, then we show how we use them to estimate the moisture in a foundry mould.

3.1 - Diffusion coefficients

We start by looking at all the results obtained from the manual tests (Figure 10).

The first large effect that we notice is the one of relative humidity. For example, in the tests carried out at 95% RH on GCM sand we have moisture coefficients values of about 1,00E-8 m^2/s, while for the same sand tested at 40% RH the moisture diffusion coefficient increases to around 2,40E-8 m^2/s.

The second effect that we see is the one of binder type. If we consider GCM sand at 40% RH the diffusion coefficient is around 2.40E-8 m^2/s while for GCK sand at 40% RH the diffusion coefficient drops to around 1.80E-8 m^2/s.

As in regard to compaction effect, in the range of density considered there is a small effect for very low densities. For example GCK sand tested at 40% RH has diffusion coefficient of 1.2E-8 m^2/s at a density 1140 kg/m^3 while the other test samples are scattered around 1.00 E-8 m^2/s. For density between 1250 kg/m^3 and 1550 kg/m^3 there seem to be no appreciable effect of density on the moisture diffusion coefficients values.

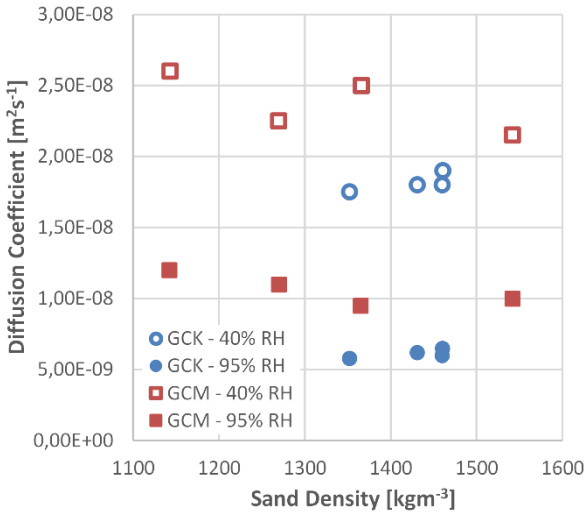

Figure 10. Density effect on moisture diffusion coefficient obtained with manual test method.

Figure 11 compares the results from automatic tests and manual tests.

As in regards to the agreement between the results from automatic and sorption tests, we see that there good agreement for the tests at 40 % RH, but for the tests at 95% the manual tests slight overestimating the diffusion coefficients. This error is probably due to the fact that, since the moisture diffusion coefficients are not constant with relative humidity (as see confirmed by both tests), the value obtained from testing at 95% starting from a sample equilibrated at 5% will be influenced by the values of the diffusion coefficient at the intermediate relative humidifies.

For both materials we see that the strong effect of relative humidity is confirmed also for the automatic tests. In particular, for relative humidity below 60% the diffusion coefficients show little variation, while there is sharp increase for humidity above 60%.

The binder effect is also shown clearly by the automatic tests.

If we compare the obtained values (4.00 E-9 m^2/s to 2.7E-8 m^2/s) to the ones available in literature [7] for somewhat similar ceramic material like concrete (5.0E-10 m^2/s to 1.2E-8 m^2/s), clay brick (1.3E-8 m^2/s to 1.4E-8 m^2/s) and sand (8.0E-8 m^2/s to 1.5E-7 m^2/s) we see that they are comparable.

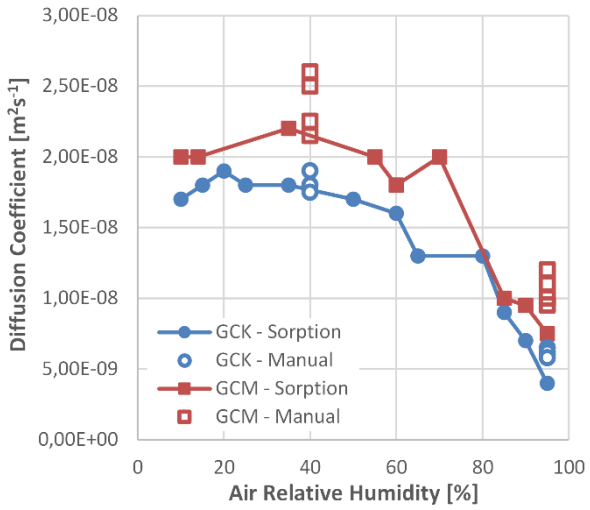

Figure 11. Effect of test method and air relative humidity on moisture diffusion coefficient of GCK and GCM furan sands.

Figure 12.a shows the results obtained for different furan binder brands. We can see for example how some binders (like GCXS, GCGG and GCM) have a higher moisture diffusivity than other at low relative humidity value. On the other hand, for higher relative humidity value the differences between different binders behaviour becomes smaller.

It is also interesting to note how. for unbounded sand, we have the highest diffusion coefficients value (up to 3.1E-8 m^2/s) that decrease linearly for increasing relative humidity, while, for bonded sands, we have an nonlinear relation between diffusion coefficient values and relative humidity. These behaviours are in line with results found in [6] where we show that sand moisture content increases linearly with relative humidity and is quite low, while binder have a higher moisture content and a non-linear sorption curve.

With regard to the effect of dust content, in Figure 12.b we see that pure dust has lower diffusion coefficients almost over the whole range of relative humidity values. Coherently with that, we see that the sample with 2% dust has slight lower diffusion coefficients that the one with no dust. This is also in line with the fact dust has retains more moisture than bonded sand [6].

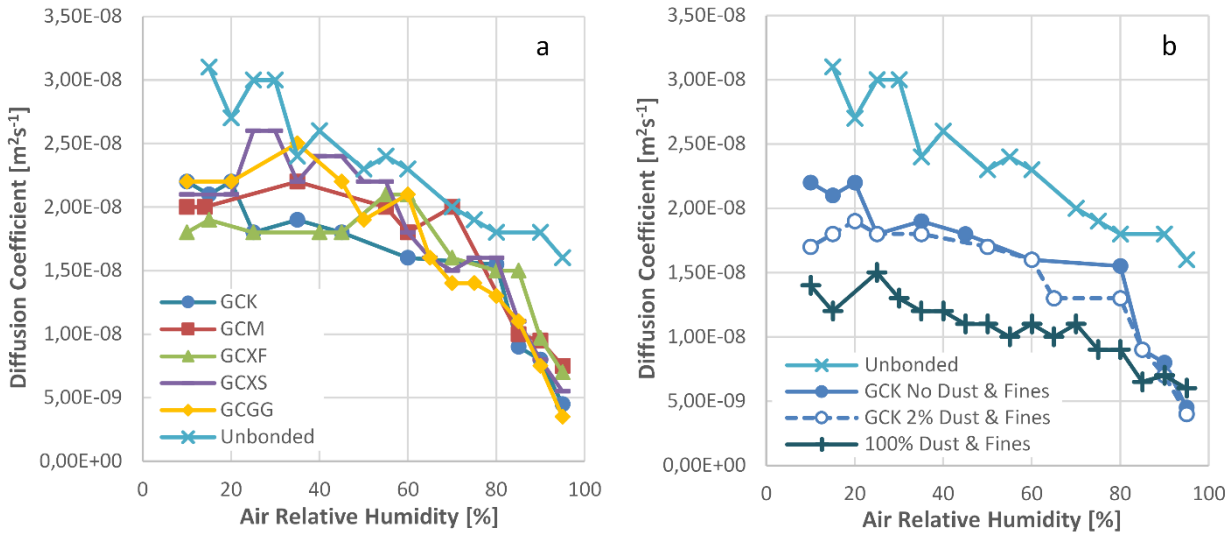

Figure 12. a) Effect of binder type and air relative humidity on moisture diffusion coefficient furan bonded sands. b) Effect of dust levels and air relative humidity on moisture diffusion coefficient of GCK furan bonded sand.

The effect of temperature in GCXF furan sand can be seen in Figure 13.a. We see that an increase in temperature form 25 °C to 35 °C leads to an increase of the moisture diffusion coefficient for relative humidity values below 60%. A decrease in temperature from 25 °C to 15 °C does not have a significant effect of the diffusion coefficient.

Figure 13.b shows how an increase in temperature from 25 °C to 35 °C causes an increase in moisture diffusion coefficients for water based foundry coatings. A decrease in temperature from 25 °C to 15 ° shows small decrease in the diffusion coefficient values. This is in line with what is typically found in literature and practical experience (increasing temperature will speed up moisture migration).

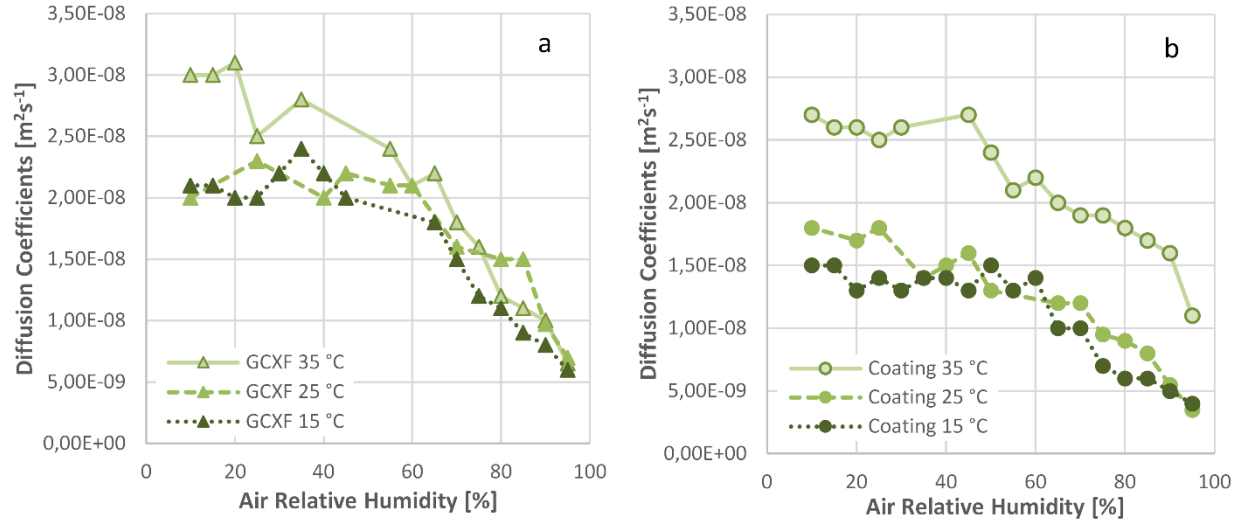

Figure 13. a) Effect of temperature and air relative humidity on moisture diffusion coefficient of GCXF furan bonded sand. b) Effect of temperature and air relative humidity on moisture diffusion coefficient of water based foundry coating.

Picture 14.a shows a typical fit of Eq.4.a and 4.b with results from manual sorption tests. We can see that there is no visible scatter, and that the solution approximates the experimental data well especially in the first part of the curve, while in the final part we have a small error. This error is most likely due to the fact that we are fitting a constant diffusion coefficient solution to a material that does not have constant diffusion coefficients.

Other possible error inherent to manual tests method can be subjected are due possible incorrect initial equilibration and lack of stability of test conditions. These will result in applying different boundary conditions to sample as compared to the one used in the mathematical model.

Picture 14.b shows a typical fit of Eq.4.a and 4.b with results from automatic sorption tests. We can see that there is more scatter in these data. Possible cause for this is the fact that we are now using smaller samples and test steps (which decrees the quantity of adsorbed water therefore reducing the relative accuracy of the weight measurement) and adding/removing dry and humid air to control the chamber conditions (therefore perturbing the air around the sample and introducing noise in the weight measurement).

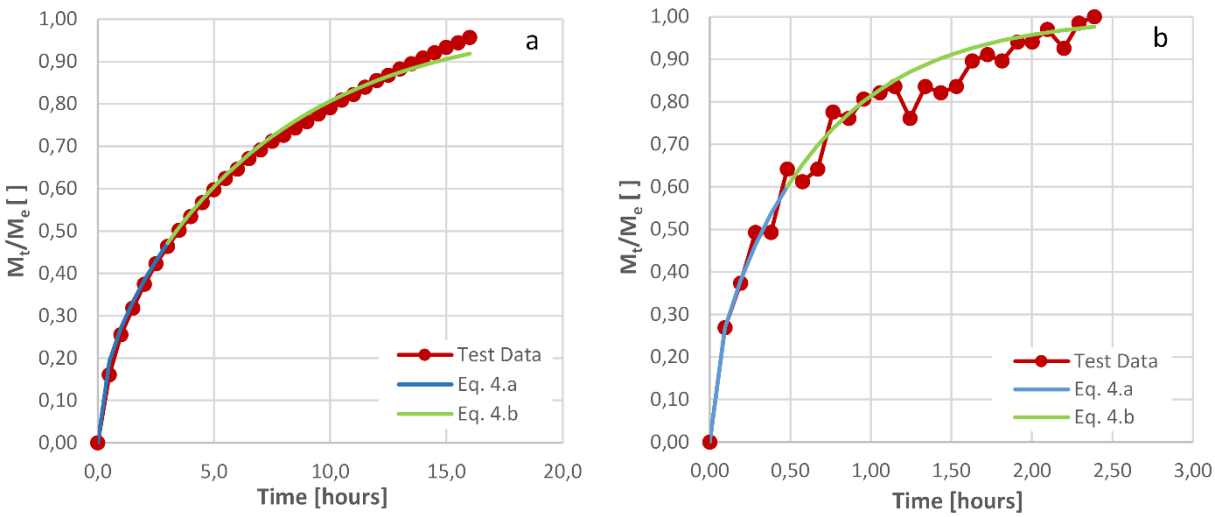

Figure 14. a) Typical fit results for a manual sorption test. b) Typical fit result for an automatic sorption test.

3.2 – Application Example

In order to provide a practical example, we want to show how to calculate the amount of moisture that can be picked up by a square sand block of 200 mm in thickness and 2000x2000mm side

dimensions of 1120 kg initial mass M_i. The calculation will per performed for cores placed in an environment at 60 % or 90 % RH for 48 hours or 18 hours before usage.

The first step is to plot Eq. 4a and 4.b as function of time, using a thickness of 200 mm. Based on previous test results, we use for a relative humidity of 60% a moisture diffusion coefficient of 2.00E-8 m^2/s, while for relative humidity of 95% a diffusion coefficient of 8.50E-9 m^2/s.

Figure 15 shows how the cores will reach the equilibrium moisture at a lower speed if placed in an environment at 90 % RH (dotted line) than compared to cores placed in an environment at 60% RH (continuous line). Now, based on the production times considered (18 and 48 hours) we can enter the graph and extract the ratios M_t/M_e between the adsorbed mass of water M_t at the considered production time t and the adsorbed mass of water at the equilibrium time M_e. The obtained values are reported in Table 3.

The next step, is to obtain the equilibrium moisture X_e at the considered relative humidity of the production environment, we will use the adsorption curve for generic furan sand shown in Figure 8 and report the values in Table 3. It is important to notice that equilibrium moisture value X_e at 95% RH than is much higher (0.70 %) than that at 60% RH (0.25 %).

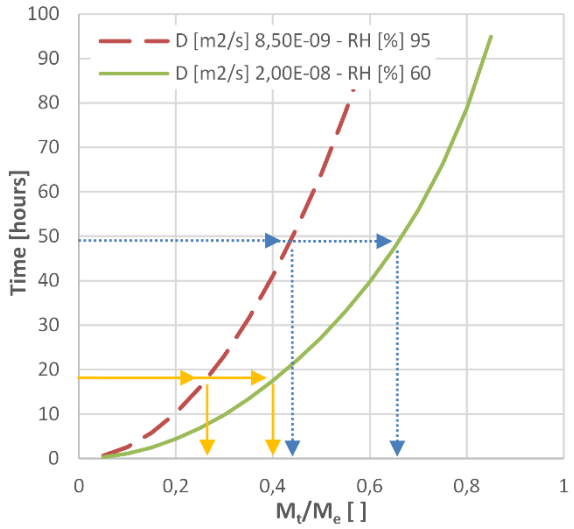

Figure 15. Adsorbed mass of water (Eq.4.a and Eq.4.b) for a core of 200 mm thickness in environments at 60% and 95% relative humidity.

Once we have obtained the M_t/M_e ratios and the equilibrium moistures X_e we can calculate the adsorbed mass of water M_t in the different situations for the considered cores and report the values in Table 3.

The adsorbed mass M_t of water is simply calculated as:

$$M_t = M_e \frac{M_t}{M_e} = M_i X_e \frac{M_t}{M_e} \quad \text{Eq. 5}$$

By looking at the results in Table 3 we see how a core that is left in an environment at 60% RH for only 18 hours will adsorb 1.12 kg of water. The same core will adsorb 1.82 kg of water (63 % more)

if left in the same environment for 48 hours. Similarly it will adsorb 1.96 kg of water (75 % more) if it was left for 18 hours at 95 % RH. The most water, 3.53 kg (216 % more), would be adsorbed for a core in 95 % RH environment for 48 hours.

We clearly notice that controlling production environment humidity to low levels and shortening the time between the completion of drying operation and use of core can substantially reduce the amount of water present in the moulds and core and therefore the risks of gas and vapour defects.

Even though the amounts of water involved in the calculation seem small we should recall that each kg of water will generate at least 1.7 m^3 of water vapour when it will come in contact with the melt and heat up to 100 °C.

Table 3. Summary of moisture pick-up parameters and adsorbed mass of water M_t for a core of dimensions 200x2000x200mm, initial mass M_i of 1120 kg placed in production in environments at 60% and 95% relative humidity for 18 hours and 48 hours.

		X_e [%]	M_e [kg]	M_t/M_e [ ]	M_t [kg]	M_t/M_e [ ]	M_t [kg]
				18 hours		48 hours	
RH [%]	60	0.25	2.8	0.40	1.12	0.65	1.82
	95	0.70	7.8	0.25	1.96	0.45	3.53

4 - Conclusions

The main conclusions that we can draw from this study can be summarised as below:

- Two different tests methodologies (manual and automatic method) for testing water adsorption diffusion coefficients of foundry sands and coatings were compared, similar values of diffusion coefficients we obtained from both methodologies
- Manual method has a lower cost and longer test times, but diffusion coefficients can be overestimated for relative humidities above 60 % for the tested sands, and ,in general, whenever material will have a moisture diffusion coefficient which is a function of moisture content there will be some error
- Automatic tests require the most expensive equipment, but it is possible to determine diffusion coefficients from 3 % to 95 % relative humidity in short amount of time
- Diffusion coefficients have been obtained for both furan sands and foundry coatings, these coefficients can be used in hand calculation as well as in 3D simulation software
- Comparison with other ceramic materials available in literature (like concrete, clay and sand) was carried out showing that foundry sands and coating have diffusion coefficients of similar order of magnitude
- Sand density effect on moisture diffusion coefficient is minor for sand densities around 1100 kg/m^3 and not appreciable for densities between 1250 kg/m^3 and 1550 kg/m^3
- Binder type can influence moisture diffusion coefficients so this could be used as a criteria for selecting binders when gas problems are encountered

- Dust can decrease moisture diffusion coefficients but in the quantities smaller than 2% it does not play a major role
- Temperature increase from 25 °C to 35 °C will increase moisture diffusion coefficients especially for coating
- A simple hand calculation methodology to estimate moisture content of foundry sand cores was introduced and applied to a real case
- The tests and calculation example show that it is possible to lower moisture in cores and moulds by properly controlling time, relative humidity, binder type and temperature

5 - Acknowledgments

This work was financed by Global Castings A/S, the Danish Agency for Science, Technology and Innovation (DASTI) and the Technical University of Denmark (DTU). LabCell Ltd. provided support in executing the tests on the automatic vapour sorption analyser.

6 - References

1 - J. Campbell, R.A. Harding: 'Solidification Defects in Castings', Lecture 3207, The University of Birmingham, 4-8, 1994.

2 - L. Elmquist: 'Defect formation in cast iron', Presentation, School of Engineering, Jonkoping University, Sweden, 2012.

3 - IKO: 'Description of Casting Defects', Chapters 04,10,12, S&B Industrial Minerals

4 - A. Chojecki*, J. Mocek: 'Effect of atmosphere in a foundry mould on casting surface quality', Archives of Foundry Engineering, Volume 12, Issue 1/2012, 13-18.

5 - D - Elkem: 'Hydrogen Pinholes', Technical Information 30, Elkem Foundry Products, Rev. 1.2, 2007.

6 - G.L. Di Muoio, N. Skat Tiedje and B. Budolph Johansen: 'Automatic vapour sorption analysis as new methodology for assessing moisture content of water based foundry coating and furan sands', 10th International Symposium on the Science and Processing of Cast Iron – SPCI10, 2014 November, Argentina, Mar de Plata.

7 - A.S. Mujumdar: 'Handbook of industrial drying', 3rd edition, Ch. 3-4, 2006.

8 - I. Boulaoued, Abdallah Mhimid: 'Determination of the diffusion coefficient of new insulators composed of vegetable fibers', Thermal Science, Year 2012, Vol. 16, No. 4, pp. 987-995.

9 - J. Carmeliet,* H. Hens, S. Roels: 'Determination of the Liquid Water Diffusivity from Transient Moisture Transfer Experiments', Journal of Thermal Env. & Bldg. Sci., Vol. 27, No. 4—April 2004.

10 - JEDEC Solid State Technology Association: 'Test Method for the Measurement of Moisture Diffusivity and Water Solubility in Organic Materials Used in Electronic Devices', JESD22-A120A, January 2008.

11 - D. Gaffner: 'The Moment Method for Measuring Moisture Diffusivity of Porous Building Materials', Bulding X, 2007 ASHRAE.

12 - L. Hassini, S. Azzouz, R. Peczalski, A. Belghith: 'Estimation of potato moisture diffusivity from convective drying kinetics with correction for shrinkage', Journal of Food Engineering, Volume 79, Issue 1, March 2007, Pages 47–56.

13 - M. Janz: 'Methods of measuring the moisture diffusivity at high moisture levels', Report TVBM-3076, University Of Lund, Lund Institute Of Technology, Division of Building Materials, Licentiate Thesis, Lund ,1997.

14 - G. L. Di Muoio, N. Skat Tiedje, B. Budolph Johansen: 'Critical Control Variables For The Coating Process Of Furan Bonded Sand With Water Based Foundry Coatings', 71st World Foundry Congress, Bilbao, May 2014.

15 - X. Chen, S. Zhao: 'Moisture Absorption and Diffusion Characterization of Molding Compound', Transactions of the ASME, 460 / Vol. 127, December 2005.

16 - E. Celik, I. Guven, and E. Madenci: 'Experimental and Numerical Characterization of Non-Fickian Moisture Diffusion in Electronic Packages', 1-4244-0985-3/07, IEEE, Electronic Components and Technology Conference, 2007.

Figure Captions

Figure 1. Example of Moisture Related Defect.

Figure 2. Production process steps for a furan sand mould coated with water based coating and correspondent ranges of environment conditions.

Figure 3. Sample Preparation for manual adsorption tests.

Figure 4. Schematic test setup for manual sorption tests.

Figure 5. Sample preparation for automatic vapour sorption tests.

Figure 6. Test setup schematic for automatic sorption tests.

Figure 7. Typical data output from and automatic sorption test run.

Figure 8. Typical adsorption/desorption curve for furan sand.

Figure 9. Example of experimental data fitted with the two approximated solutions Eq.4a and Eq4.b.

Figure 10. Density effect on moisture diffusion coefficient obtained with manual test method.

Figure 11. Effect of test method and air relative humidity on moisture diffusion coefficient of GCK and GCM furan sands.

Figure 12. a) Effect of binder type and air relative humidity on moisture diffusion coefficient furan bonded sands. b) Effect of dust levels and air relative humidity on moisture diffusion coefficient of GCK furan bonded sand.

Figure 13. a) Effect of temperature and air relative humidity on moisture diffusion coefficient of GCXF furan bonded sand. b) Effect of temperature and air relative humidity on moisture diffusion coefficient of water based foundry coating.

Figure 14. a) Typical fit results for a manual sorption test. b) Typical fit result for an automatic sorption test.

Figure 15. Adsorbed mass of water (Eq.4.a and Eq.4.b) for a core of 200 mm thickness in environments at 60% and 95% relative humidity.

Table Captions

Table 1. Overview of experimental plan for manual sorption tests.

Table 2. Overview of experimental plan for automatic vapour sorption tests.

Table 3. Summary of moisture pick-up parameters and adsorbed mass of water M_t for a core of dimensions 200x2000x200mm, initial mass M_i of 1120 kg placed in production in environments at 60% and 95% relative humidity for 18 hours and 48 hours.

Supplement VII

19th International Drying Symposium (IDS 2014)
Lyon, France, August 24-27, 2014

MEASUREMENT OF MOISTURE IN FOUNDRY COATINGS USING RESISTANCE BASED MEASURING DEVICES

G.L. Di Muoio[1,2]*, N. Skat Tiedje[2] and B. Budolph Johansen[1]

[1]Casting Technology Department, Global Castings A/S
373N Diplomvej, Kgs. Lyngby, 2800, Denmark

[2]Department of Mechanical Engineering, Technical University of Denmark
Building 427S, room 306b, Kgs. Lyngby, 2800, Denmark

**Corresponding author: Tel.: +45 6180 9266, E-mail: gidmu@globalcastings.com*

Abstract: Water based foundry coatings require monitoring of the drying process in order to ensure that the correct level of residual moisture is reached and the risk of moisture related defects in the castings is minimized. In this study, the performance of a self-developed moisture measuring device and two commercial tools calibrated for concrete are compared. The stability of the output for different wire types and cable lengths is evaluated and a calibration of the self-developed tool is performed by comparing gravimetric moisture measurements with resistance measurements. A correlation between moisture and resistance for the considered foundry coating is presented.

Keywords: Water based foundry coating, resistance based moisture measurement, moisture-resistance correlation, moisture measuring device, drying process monitoring

INTRODUCTION

Foundry coatings are used to increase surface quality of the final casted parts and lower production cost. [1,2] In recent years, water based coatings have been introduced in the foundry industry as a substitute for alcohol based coatings to eliminate health and safety hazards.[3] However, water based coatings require monitoring of the drying process in order to ensure that the correct level of residual moisture is reached. This is because excessive moisture in the coating can cause gas related defects in the castings and possibly lead to scrapped parts.[4,5,6]

In the drying industry, moisture can be measured indirectly by measuring changes in electrical properties.[7,8,9] There are several factors that can affect the measurement accuracy (such as transducer design, leakage currents, electrode shape, material moisture uniformity, etc.)[10] and the correlation between the considered electrical property of the material and moisture is different from one material to another. A tool providing a measure of coating moisture on a relative scale is used by Schultze [3]. But there are no commercial moisture measuring tools that are specifically calibrated for foundry coatings.

In this paper, we compare the performance of a self-developed resistance based moisture measuring device versus two commercial tools calibrated for concrete and wood. The performance of the tools are compared using a bank of resistors in the range from 10 kOhm to 200 GOhm. The stability of the output for different wire types (standard copper wire and Teflon insulated and shielded wire) and cable length is evaluated at different resistance levels. This is done in order to determine which setup can provide the most accurate results in a factory installation. Additionally, a calibration of the self-developed tool is performed by comparing gravimetric moisture measurements with resistance measurements.

Results show that the self-developed tool provides the most stable readings over the whole range of resistances considered and that Teflon insulated wires with shielding shall be used to avoid losing accuracy. Finally, a correlation between moisture and resistance for the considered foundry coating is presented.

METHODS

In this study we present two sets of tests: in the first set we compare the performance of commercial tools with a self-developed and built device (Fig. 1). In the second set of tests we want to obtain a correlation between the moisture in the considered foundry coating and the measured resistance.

Moisture tool Comparison Tests

The tool choice is based on different capabilities of the tools. Tool A (Fig. 1.a) can provide moisture reading for concrete and has been used in some of Global Castings production facilities to give indications on the moisture level of the considered coating. However, it was found to significantly loose accuracy when extension wires were used to reach hard to measure locations of parts, and it seemed to have a significant error for readings above 1% due to different properties of concrete and the considered coating. Additionally, Tool A can only provide visual output so that no automatic logging is possible by connecting to a data acquisition system. The only advantages of Tool A are that it is battery powered and is rugged for industrial use.

Tool B (Fig. 1.b) provides an analogue voltage signal from 0 to 10 V, is calibrated for wood and it requires an external power supply. The hope is that it could be used also for foundry coatings if its performance is good in the relevant range.

Tool C (Fig. 1.c) is a prototype transducer designed to have a nominal voltage response V_{out} that can be converted to a resistance R_{meas} using Eq. 1. It is powered by and external power supply.

$$R_{meas} = 468000 \cdot 10^{2V_{out}} - 5060 \qquad (1)$$

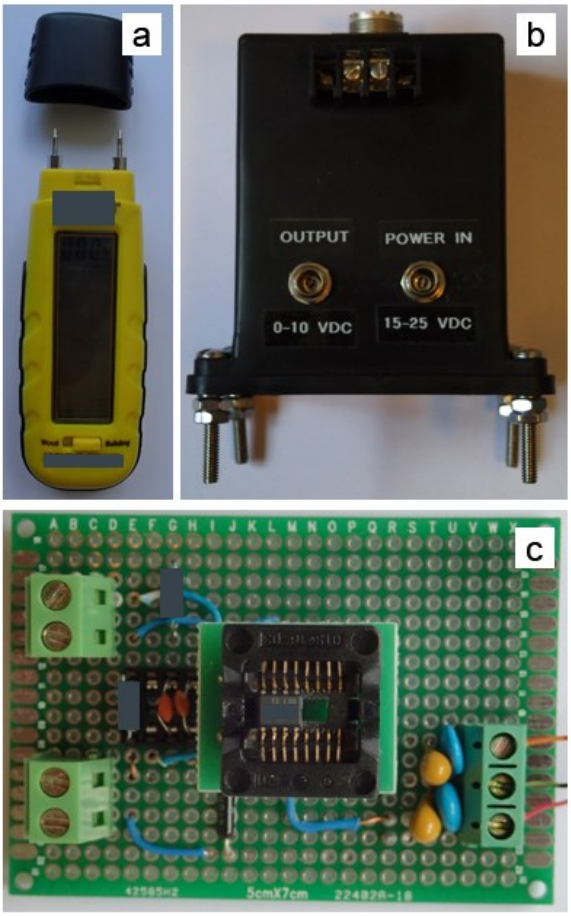

Fig. 1. Transducers used in the performance comparison a) Tool A, b) Tool B and c) Tool C.

The transducers are tested using a bank of resistors ranging from 10 kOhm to 200 GOhm. Table 1 provides a full list of the resistors used and their tolerances.

The objectives of the tests are to determine if the tools can provide stable and meaningful reading across the considered resistance range. Three test configuration were used: 30 cm wire (to minimize leakage currents) to be used as a reference or best case, 15 m standard wires (used in production environment to do measurements in hard to reach areas) and 15 m Teflon wires (expected to reduce the effect of leakage currents).

Table 1. Resistors used for the tool performance comparison and respective tolerances

Resistor [Ohm]	Tolerance [%]	Resistor [Ohm]	Tolerance [%]
10 x 10^3	1	20 x 10^9	10
20 x 10^3	1	30 x 10^9	10
50 x 10^3	1	40 x 10^9	10
100 x 10^3	1	50 x 10^9	10
200 x 10^3	1	60 x 10^9	10
500 x 10^3	1	70 x 10^9	10
1 x 10^6	1	80 x 10^9	10
2 x 10^6	1	90 x 10^9	10
5 x 10^6	1	100 x 10^9	1
10 x 10^6	1	110 x 10^9	2
20 x 10^6	1	120 x 10^9	3
50 x 10^6	1	130 x 10^9	3
100 x 10^6	1	140 x 10^9	5
200 x 10^6	2	150 x 10^9	6
500 x 10^6	1	160 x 10^9	7
1 x 10^9	1	170 x 10^9	8
2 x 10^9	2	180 x 10^9	9
5 x 10^9	1	190 x 10^9	10
10 x 10^9	10	200 x 10^9	11

Fig. 2 shows a schematic of the test setup for the moisture tools comparison tests.

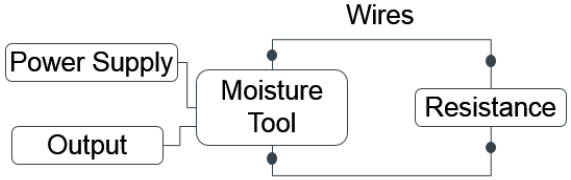

Fig. 2. Schematic of experimental setup for moisture tool comparison tests.

Moisture-Resistance Correlation Tests

In order to obtain a correlation between moisture in the coating and resistance we have designed a Teflon sample holder (Fig. 3) that can accommodate two

electrodes and provide support for a layer of coating of 1mm thickness. The electrodes are spaced 15mm from each other and Teflon was chosen for its high resistivity and its low sensitivity to moisture in order to minimize leakage currents.

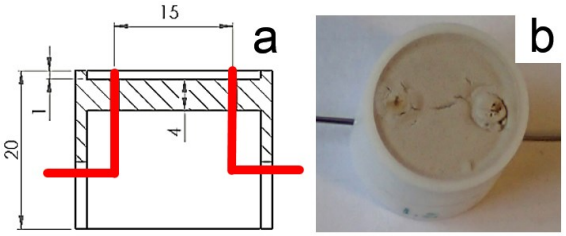

Fig. 3. a) Coating sample holder with electrodes and b) with coating.

The coated sample holder is placed on a scale with 0.1 mg accuracy and connected to a computer and a data logging software. The coated surface of the sample is facing upwards and inserted by few millimeters in an air duct where air at 45-55% RH and 24-26 C is supplied at a speed of 1 m/s. This provides similar drying conditions for all the tests. The electrodes are connected to the moisture tool C by flexible copper wires, as shown in Fig. 4, to minimize any weight measurement errors.

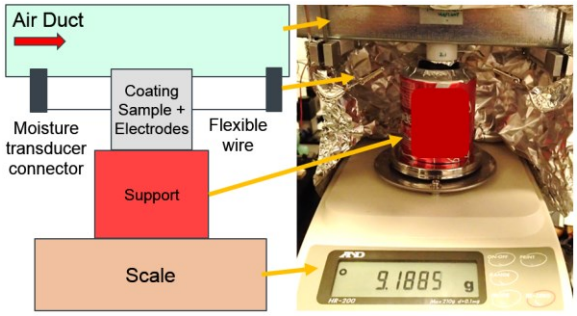

Fig. 4. Experimental apparatus for logging of weight and resistance during drying.

The moisture in the coating layer $U_{\%}$ is calculated from the logged weigth on a wet basis as:

$$U_{\%} = \frac{LoggedWeight - FinalWeight}{InitialWeight} 100 \qquad (2)$$

and then it is plotted versus the resistance R calculated from the logged voltage using Eq.1.

The above described method is used to simplify the measurement of a non-equilibrium moisture condition of the coating being dried. The advantages of such a setup is shorter test speed and increased accuracy due to minimal handling of the coating sample.

RESULTS AND DISCUSSION

Moisture tool Comparison Tests

In Fig. 5 we see the results of tool A from tests with different wire configurations. We can see that tool A provides a full scale reading of 5% moisture at a resistance of 10 kOhm and that the minimum reading for short leads configuration is at 0.9% for a resistance of 100 GOhm. Long wires provide higher % reading for resistance levels above 80 GOhm. For example at 100 GOhm the configuration with standard long wires provide a reading of 0.22 % moisture (a difference of about 144%). Teflon wire significantly reduce the error by providing a reading of 0.12% at 100 GOhm (a difference of 33%).

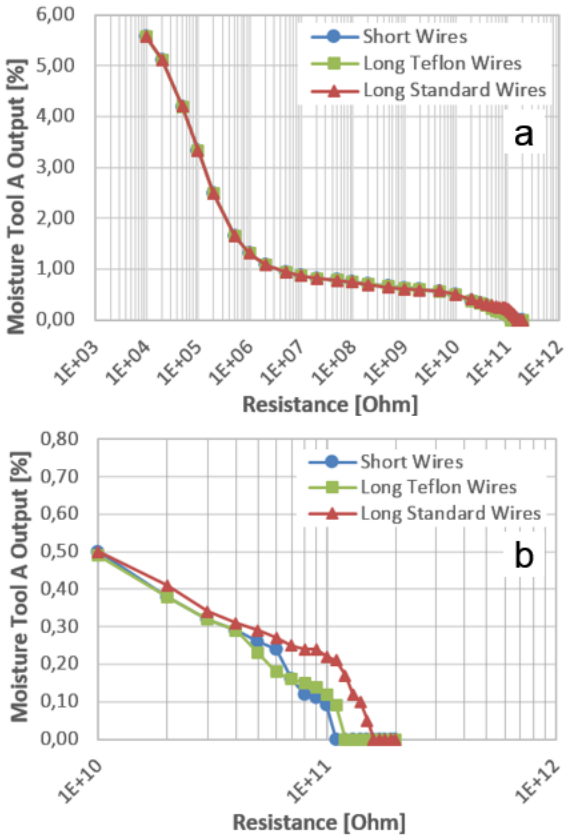

Fig. 5. Moisture Tool A test results: a) complete range, b) close up on high resistance range.

Results from moisture tool B (Fig. 6.a) show that significant difference exists between setup with short and long wires (both standard and Teflon) already at 20 MOhm. For example at 500 MOhm the output for short wire setup is 8.2 V while for long Teflon wire setup is 9.42 V (a difference of 15%). The differences between readings are also visible at higher resistance values (Fig. 6.b). In particular we can see that the maximum measurable resistance is 110 GOhm with a short wire configuration. The range is then limited to 50 GOhm for long Teflon wire configuration.

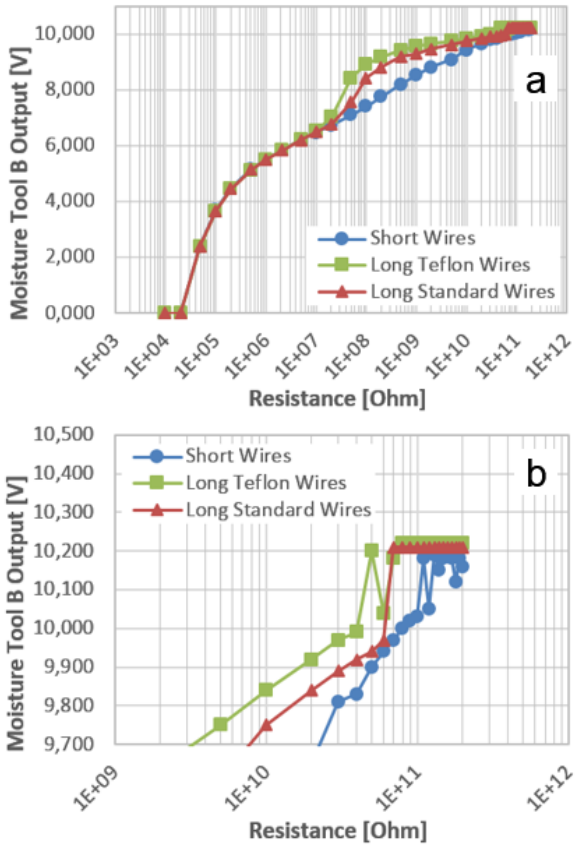

Fig. 6 Moisture Tool B test results a) complete range, b) close up on high resistance range.

Regarding moisture tool C (Fig. 7.a) we can see how there seem to be no significant difference between the three wiring configurations. Additionally, the response is logarithmic over the entire resistance range considered. In order to better visualize the results, Fig. 7b shows the difference between the measured values and the expected voltage response calculated using Eq.1 and the nominal resistance values of Table 1. We can see how long standard wires have higher error at resistances above 30 GOhm, as this error is increasing with increasing resistance it might be due to leakage currents. On the other hand, long Teflon wires and short wires have a similar behavior above 30 GOhm, and the deviation is smaller than 25mV from Eq. 1. This might be related to differences in real resistor value compared to the nominal values (up to 10% as shown in Table 1).

From 100 MOhm to 2 GOhm the long Teflon wires measurements are affected by an error up 37 mV. This translates to a difference of only 2% considering the voltage output value of 1,665 V expected at 1 GOhm.

Tool C has therefore the most stable response and smaller error over the widest range considered.

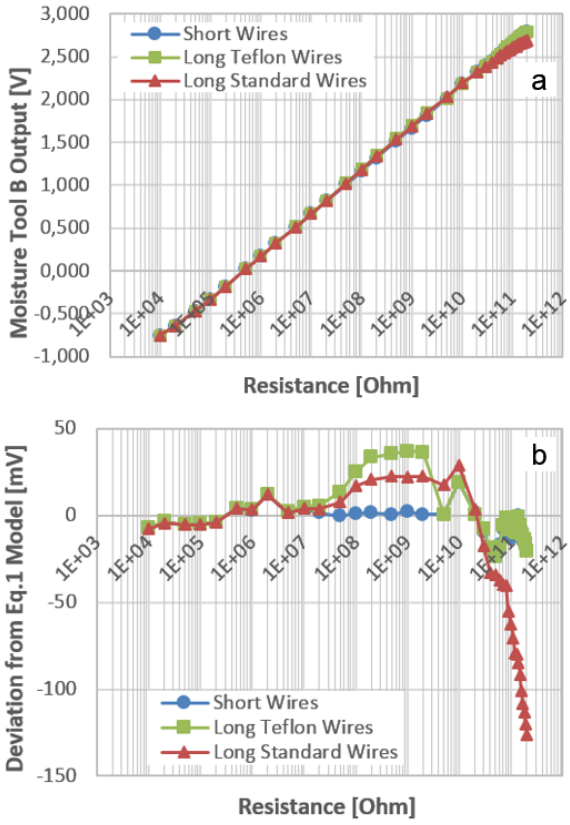

Fig. 7. Moisture Tool C test results: a) complete range, b) deviation with respect to Eq. 1.

Moisture-Resistance Correlation Tests

In this section we report the results from the tests done in order to correlate the moisture content in the coating with its resistance. Figure 8 and 9 show the results of five tested samples and the three curves fitted in order to obtain a moisture-resistance correlation.

From an overall in view Fig. 8, we can see that the correlation between moisture and resistance is strongly nonlinear. In particular, a marked increase in resistance occurs for moisture levels above 5%.

In order to best fit the moisture-resistance curve three different equations are used (Eq.3-5). Each equation is provided with the resistance range values in which it is applicable. We can see how, up to 1.4 MOhm the use of power law (on a logarithmic scale) is needed to accommodate for the curvature of the curve, above this value a log-log law is used.

Regarding the accuracy of the relationship, we can see in (Fig 9.a) that the scatter of the data increases as the moisture level increases. For moisture levels above 10% the typical scatter is +/- 3% in moisture. Between 5% and 10% moisture reading the typical scatter is within 2% and between 5% and 2% moisture is less than 1%. For moisture levels below two 2% (Fig 9.b) the data is typically scattered in the range of +/- 0.25%.

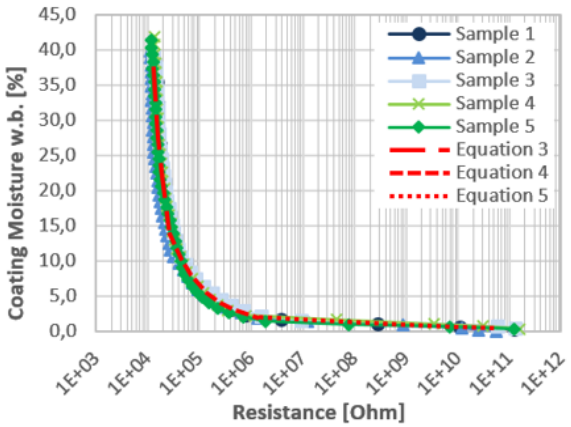

Fig. 8. Moisture-Resistance calibration results: complete range.

$$U_{\%} = \begin{cases} 5 \cdot 10^{9} \cdot (\log_{10}(R))^{-13,24} \\ for \quad 12,8 \cdot 10^{3} \le R \le 26 \cdot 10^{3}, \quad (3) \\ 108534 \cdot (\log_{10}(R))^{-6,03} \\ for \quad 26 \cdot 10^{3} < R \le 1,4 \cdot 10^{6}, \quad (4) \\ 5,9837 \cdot \log_{10}(\log_{10}(R)) + 6,7014 \\ for \quad 1,4 \cdot 10^{6} < R \le 60 \cdot 10^{9}, \quad (5) \end{cases}$$

As additional considerations for the accuracy of the experimental setup and representativeness of the tests, we can see that initial value of moisture in the coating is around 42%. This is in line with results obtained with automatic moisture analyzers for this coating mixture.[11] Regarding final moisture of coating, since the samples are dried at 25 C and 50% RH, they do not reach 0% moisture level but an equilibrium moisture level of about 0.5%. Also this value is in line with results from sorption tests carried out in an automatic moisture analyzer for the same coating.[12]

As final results, we show in Fig. 10 a comparison between the moisture-resistance relationships of concrete (from Tool A tests) and foundry coating. We can see that on the whole moisture range, the coating has significantly higher resistance than concrete for the same moisture level. For example at 1% moisture concrete has a resistance of 3 MOhm, while foundry coating has 1 GOhm.

If moisture tools calibrated for concrete are to be used for assessing moisture in water based foundry coating it is important to be aware of this difference to avoid significant measurements errors. For example a reading of 5% on Tool A will correspond to a moisture of about 40% in the foundry coating.

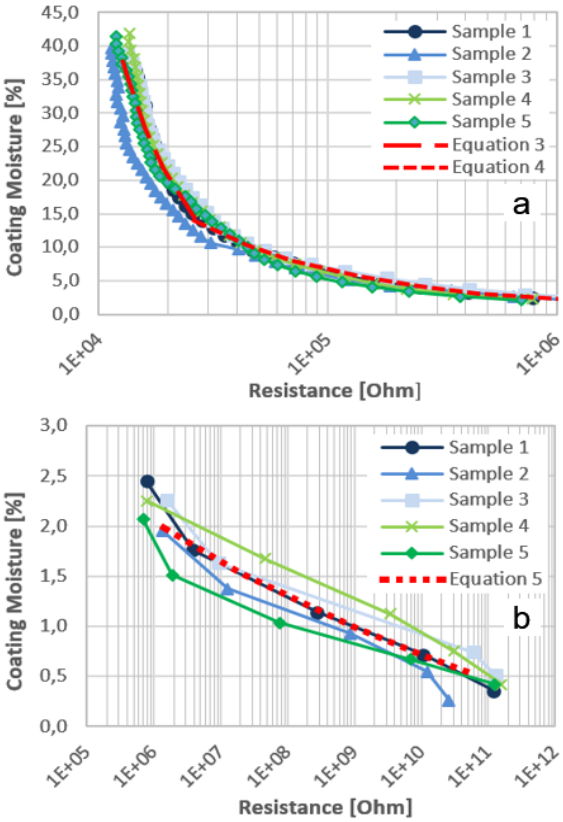

Fig. 9. Moisture-Resistance calibration results: a) close up on range up to 1 MOhm, b) close up on range above 1 MOhm.

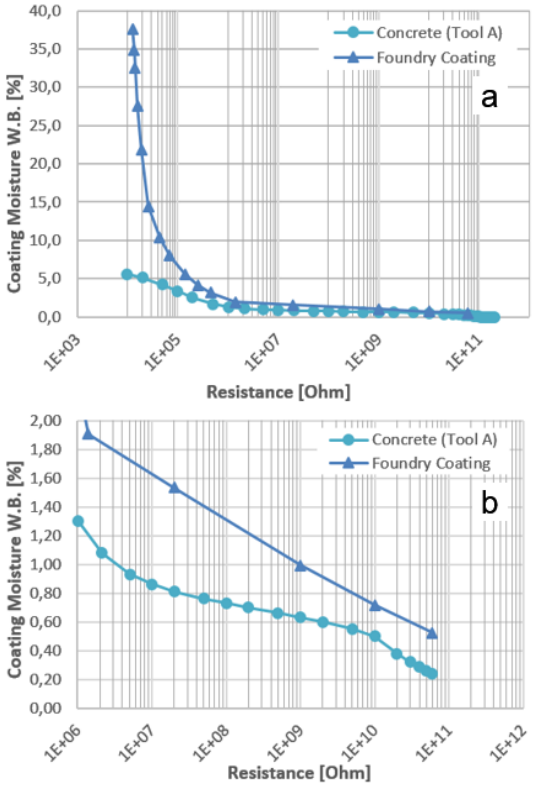

Fig. 10. Moisture-Resistance relationship of concrete and foundry coating: a) complete range, b) close up on range above 1 MOhm.

CONCLUSIONS

Moisture tool comparison tests have shown that moisture Tool C provides the most stable results on widest range of resistance considered (10 kOhm to 200 GOhm) and the lowest error.

In order to minimize measurement error, when short wires cannot be used the choice should fall on Teflon insulated and shielded wires.

A correlation between moisture and resistance of coating has been obtained and compared with the one for concrete showing that significant measurement errors can occur if concrete calibrated tools are used to measure moisture in foundry coatings and no correction is made.

ACKNOWLEDGEMENTS

This work was financed by Global Castings A/S, the Danish Agency for Science, Technology and Innovation (DASTI) and the Technical University of Denmark (DTU). P. Albicocco provided support during the moisture transducer development.

REFERENCES

1. Penko T. Ultra-Performance Core Coatings For Mass Iron Casting Production: Specialized Methods For Developing & Evaluating New Coating Technology. Foseco Metallurgical Inc.
2. Nwaogu U. C.; Tiedje N.S. Influence of New Sol-Gel Refractory Coating on the Casting Properties of Cold Box and Furan Cores for Grey Cast Iron. In Proceeding of 69th World Foundry Congress, October 16-20, 2010.
3. Schutze N. Control Limits for the Drying of Water Based Coatings. Foseco, Foundry Practice, Issue 255, June 2011.
4. Chojecki A.; Mocek J. Effect of atmosphere in a foundry mould on casting surface quality. In Archives of Foundry Engineering, 20012, Volume 12, Issue 1, 13-18.
5. Elkem; Hydrogen Pinholes. In Technical Information 30, Elkem Foundry Products, Rev. 1.2, 2007.
6. IKO; Description of Casting Defects. Chapters 04,10,12, S&B Industrial Minerals.
7. Day, R. D. Cure Monitoring: Micro-dielectric Techniques. In Coating Technology Handbook, 3rd Edition, Chapter 13; Arthur A. Tracton,, CRC Press, 2006.
8. Laurens, S.; Arliguie, G. Non-destructive evaluation of concrete moisture by GPR technique: experimental study and direct modeling. In International Symposium of Non-Destructive Testing in Civil Engineering 2003 (NDT-CE 2003).
9. Brameshuber, W.; Raupach, M. Non destructive Determination of the Water-Content in the Concrete Cover using Multiring-Electrode. In International Symposium of Non-Destructive Testing in Civil Engineering 2003 (NDT-CE 2003).
10. Ressel, J.B. Fundamentals of Wood Moisture Content Measurement; University of Hamburg, Department of Wood Science, 2006.
11. Di Muoio, G.; Tiedje, N. S.; Johansen, B. B. Critical control variables for the coating process of furan bonded sand with water based foundry coating. In Proceedings of World Foundry Congress, Bilbao, Spain, May 18-22, 2014.
12. Di Muoio, G.; Tiedje, N. S.; Johansen, B. B. Investigation of moisture levels in water based foundry coating and furan sands using an automatic vapor sorption analyzer. Proceedings of International Drying Symposium, Lyon, France, August 24-27, 2014.

Supplement VIII

RESEARCH ARTICLE OPEN ACCESS

CFD Study for the Optimization of the Drying Process of Foundry Moulds used in the Production of Wind Turbine Components

Giovanni Luca Di Muoio*, Alessandro Della Rocca**, Niels Skat Tiedje***
*Casting Technology, Global Castings A/S, Lyngby, Denmark
** MOX, Department of Mathematics, Politecnico di Milano, Milano, Italy
*** Mechanical Engineering Department, Technical University of Denmark, Lyngby, Denmark

ABSTRACT
In order to drive down the cost of wind turbine cast components, the optimization of each production step is necessary. In particular, foundry moulds used for the production of cast components undergo a process of drying needed to avoid quality problems in the final parts. In order to reduce drying times forced convection by the use of fans is needed. In this work we perform Computational Fluid Dynamic studies with the aim to optimize the drying process for mould geometries typically used for the production of wind turbine components. Representative geometries are modelled in a 3D software, imported in a fluid flow solver and complete Navier-Stokes equations coupled with energy transport equations are solved. Velocity profiles from shop floor measurements are used as boundary conditions for the problem. Finally surface heat exchange coefficients are determined and results analyzed. Results show that it is possible to use this methodology to optimize the drying process, and determine areas of the moulds that are more difficult to dry than others. Optimal fan arrangement for typical geometries are also provided.

Keywords **–** CFD Simulation, Drying, Foundry Moulds, Wind Turbine Components, Quality, CAE

I. INTRODUCTION

In order for wind turbines to become more and more competitive there is a need to lower cost by optimizing production times and quality [1]. Drying of coated sand moulds is a time consuming, as well as energy and capital intensive process. CFD simulations can be used as a tool to decrease the design time and lower the possible risk and costs related to the start- up of drying operations [2,3].

In this study we consider the case of moulds coated with water based foundry coatings [4,5] dried with forced air convection obtained by fans. The heat transfer coefficient (dependent on the air speed and temperature) plays a major role in the removal of water and therefore in the reduction of drying times [6,7].

Given the large dimensions of the moulds to be dried (typically above 3000x3000x3000mm) it is important to choose a fan layout that minimize the areas with low heat exchange coefficients and help to determine the area that will be the last to dry so that quality checks can be done with higher certainty [8].

The goals of this work can therefore be summarized as follows:

- Asses different fans types with CFD simulations
- Propose an optimal fan layout typical for wind turbine components moulds
- Determine areas that are difficult to dry in typical wind turbine component moulds
- Perform a qualitative validation for the use CFD methodology

II. METHODS

2.1 Fan Selection

The first step of the optimization consists in comparing the performances of different fans (Table 1) with the objective to choose a fan model to be used in the subsequent mould drying simulations.

CFD simulations of each fan model were carried out to compare the performance and make a preliminary selection. A representative test chamber of dimensions 8000x6000x5000 mm was used and the fans were placed at three different distances (1500, 2500, 3500 mm) from a surface at constant temperature. The test chamber was chosen in order to minimize the effect of walls on the enclosed flow field.

The incompressible Navier-Stokes equations and the energy equation are solved in a pressure-based segregated solver of SIMPLE type, with standard under relaxation of inner iterations. The buoyancy effects of the natural convection are accounted for by the Boussinesq approximation in the negative z direction. The turbulence model selected is the standard k-ω (k-omega) with wall functions. The boundary conditions in terms of the velocity field were obtained after technical data from the data sheets of the different fans. A fixed temperature increment is applied between inlet and

outlet sections of the fan, in order to trigger the heat transfer effects on the target wall. This temperature difference allows to calculate heat transfer coefficient maps on the target wall, as in Figure B.

The simulations were run in order to compare the performances of three different fan models reported in Table A and to determine the effects of the distance between the fan and the target wall for each model.

Table 1. Fan models considered in this study.

	TFV 10 S	TFV 30 S	TTV 4500
Air flow rate max [m³/h]	525	3500	4500
Air pressure max [Pa]	80	500	80
Power input [kW]	0.1	1.2	0.23
Dimensions [mm x mm x mm]	300 x 275 x 330	545 x 515 x 490	210 x 510 x 510

2.2 Moulds Drying

For the mould drying simulations we start by modeling three representative geometries, namely hub, main foundation and main bearing house in a 3D software. These geometries are then imported into a fluid flow solver where complete Navier-Stokes equations coupled with energy transport equations are solved. Moisture transfer and evaporation are not modelled in order to reduce the modelling effort and reduce the overall computational time, while velocity field and heat exchange coefficient are used to evaluate the effectiveness of different fan layouts.

For the simulation we choose chamber dimensions big enough (typically 10x10x7m) to have a far field stagnation velocity smaller than 1 m/s (as in an ordinary room with still air) [9]. The typical number of mixed cells (tetrahedral, pyramids, hexahedral) in the simulation is around 1.000.000, with a dimensions refined towards the impinging jet and on the target surface. The heat transfer coefficient is computed by assigning a fixed temperature to the target surface and heating up the air with a $\Delta T = 5°$ C as the ambient air flows through the fan.

A qualitative validation of the results is done by comparing the results for the hub with a picture take by infrared camera (moulds areas with higher surface temperatures represent areas with higher heat exchange coefficients).

III. RESULTS

3.1 Fan Selection

A first qualitative evaluation of the fans can be done visually, by comparing the velocity contours as shown in Fig. 1 for the fan TFV 10 S and a wall distance of 3500 mm. It can be seen that, for this specific fan, the velocity drops to below 1 m/s before reaching the surface at 3500 mm distance.

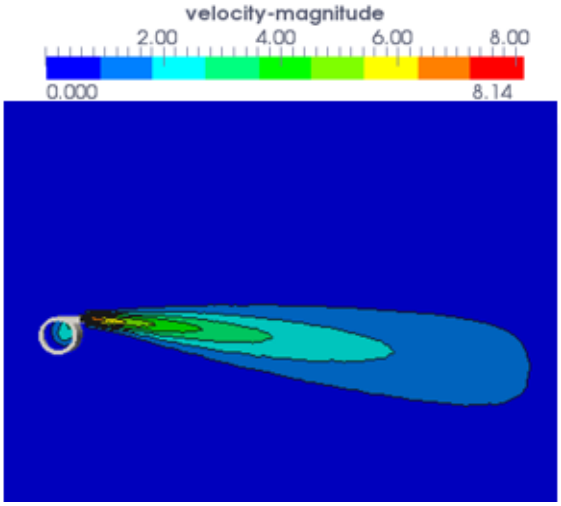

Figure 1. Velocity magnitude [m/s] contours over the central section plane for the fan TFV 10 S for a wall distance of 3500 mm.

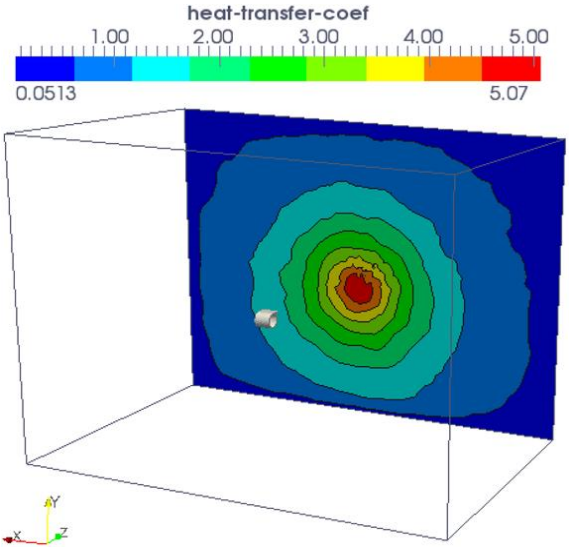

Figure 2. Convective heat transfer coefficient [W/(m²K)] distribution over isothermal surface for TFV 10 S fan for a wall distance of 3500 mm.

As consequence we can see how the heat exchange coefficient field on the target surface is below 5 W/(m²K) as shown in Fig. 2.

In order to compare the three different fans we plot the heat exchange coefficients on the x axis of the wall at the same y coordinate of the fan center of mass (Fig. 3). We can see how the TTV 4500 fans provides the highest heat exchange coefficient at a fraction of the power used by TFV 30 S. The TFV

10 S provides the smallest heat exchange coefficients.

Additionally, we notice that for all the distances form the surface, the TTV 4500 provides a heat transfer coefficient higher then 10 W/(m^{2}K) (well above the typical values achievable by natural convection [10]) on an approximately circular area of two meters in diameter.

Based on these results we choose the TTV 4500 for the mould simulations and decide to pre-dimension the number of required fans based on the area of the moulds and the area spanned by a heat transfer coefficient above 10 W/(m^{2}K).

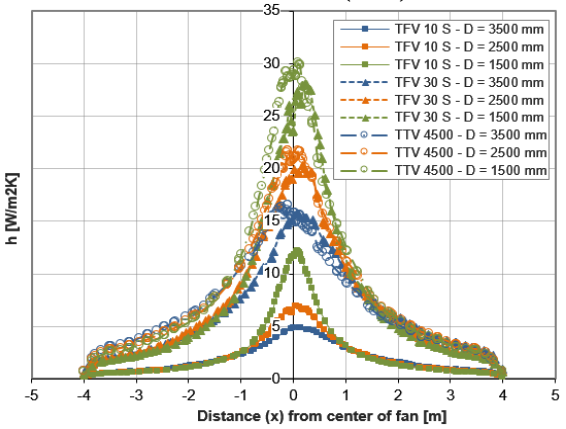

Figure 3. Convective heat transfer coefficient [W/(m^{2}K)] distribution for different fans and wall distances along the x axis.

3.2 Hub Mould Drying

Figures 4 and 5 show the optimal fan layout chosen for the hub mould using three fans.

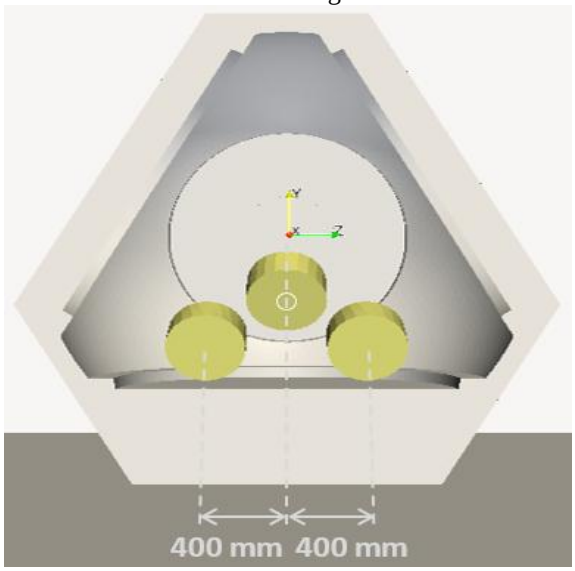

Figure 4. Optimal fan arrangement for the hub (front view).

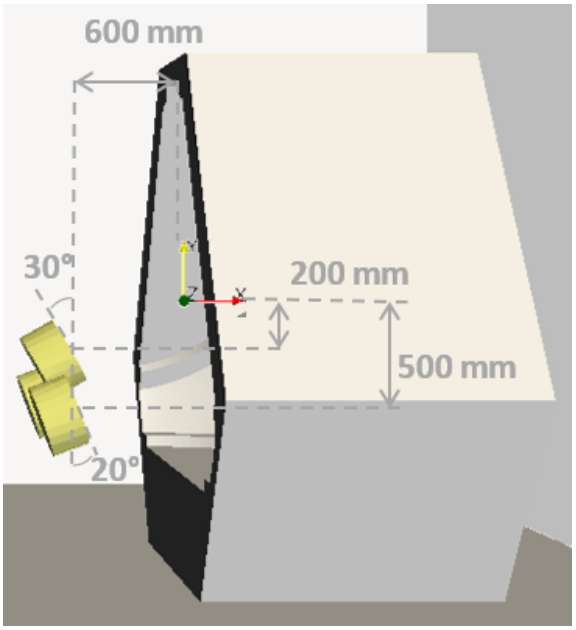

Figure 5. Optimal fan arrangement for the hub (side view).

Figure 6 shows how air is channelled in the bottom section of the cavity and exits from the top, thus ensuring a steady air velocity to be maintained above the mould surface. This has beneficial effects on the average heat transfer coefficient which is thus increased with respect to other arrangements simulated.

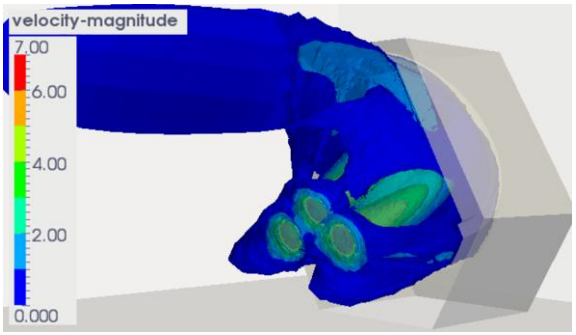

Figure 6. Velocity magnitude [m/s] isosurfaces. Air stream from the fans is channeled in cavity.

Figure 7 shows the heat transfer coefficient distribution on the mould surface. It is possible to appreciate that the areas with the lowest values are localized near the corners. This observation allows to determine where localized moisture measurements should be done in real production.

From Figure 8 we see that less than 2% of the total area of the mould is subjected to a heat transfer coefficient of less than 10 W/(m^{2}K).

In Figure 9 we see a surface temperature measurement done with infratred camera. The areas near corners have lower temperature due to lower heat exchange coefficient as shown by the simulation.

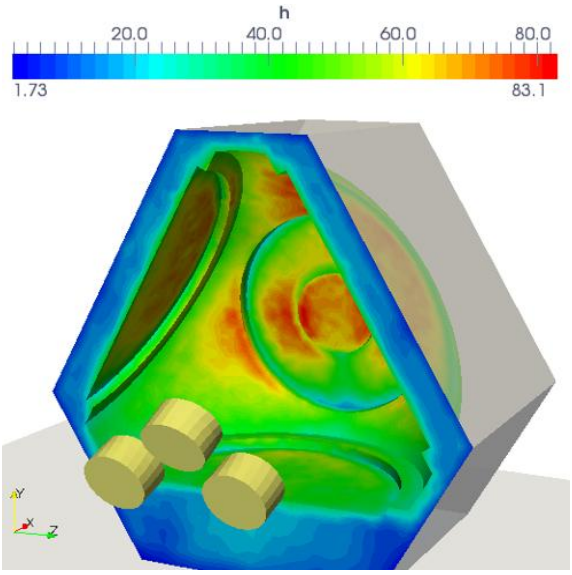

Figure 7. Convective heat transfer coeffient [W/(m^{2}K)] distribution on hub mould.

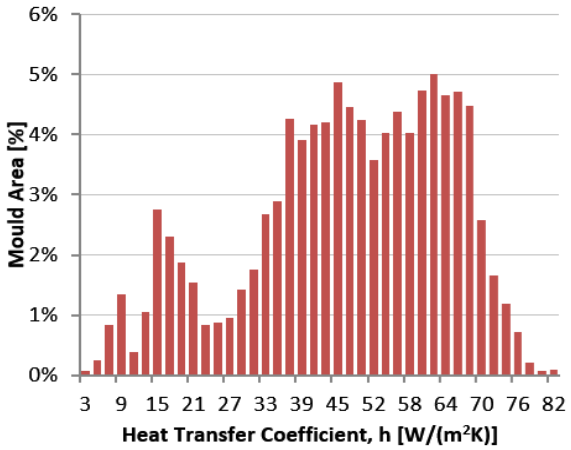

Figure 8. Histogram showing the distribution of the heat exchange coefficient on the hub mould surface.

Figure 9. Hub mould surface temperature measurement done with infratred camera. Areas near corners have lower temperatures due to lower heat exchange coefficient as shown by simulation.

3.3 Main Foundation Mould Drying

The optimal fan arrangement for the main foundation moulds requires six fans due to the larger mould dimensions. In particular we see that the fans are never placed perpendicular to the mould wall (Figure 10) in order to avoid formation of stagnation zones and therefore a reduction of the heat transfer coefficient. This is confirmed by Figure 11 where the jets exiting from the fans can be clearly seen.

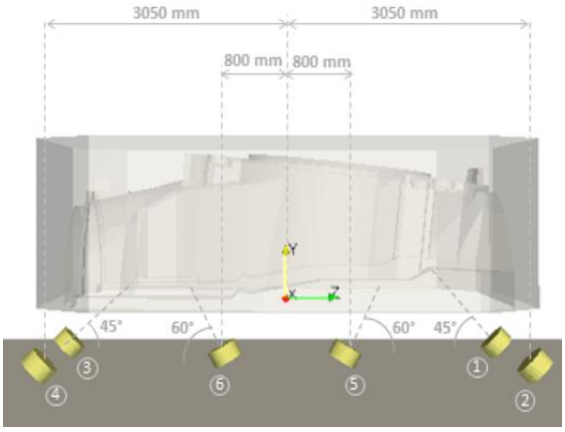

Figure 10. Optimal fan arrangement for main foundation mould.

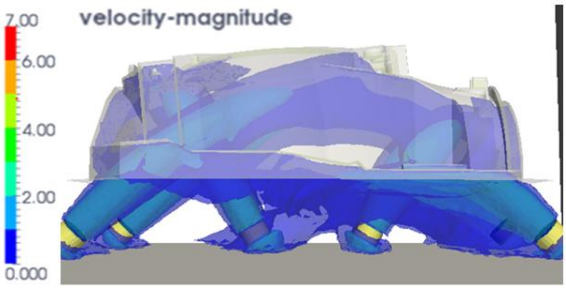

Figure 11. Velocity magnitude [m/s] isosurfaces. Air jets exiting from the fans are clearly visible below the drag.

The heat transfer coefficients obtained on the surface are concentrated in a lower range as compared to the hub (Figure 12). This means that the drying process of this mould will be necessary slower. However even for this case only less than 5% of the total area is subjected to heat exchange coefficients smaller than 5 W/(m^{2}K). These areas are clearly visible in dark blue in Figure 13 in correspondence of the top areas of the mould surface. Therefore it will be important to assess the moisture of these areas once the drying process is completed in order to ensure a complete drying and to avoid possible problems in quality.

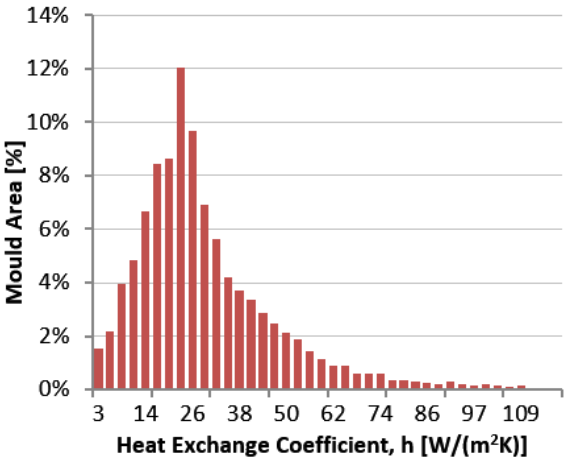

Figure 12. Histogram showing the distribution of the heat exchange coefficient on the main foundation mould surface.

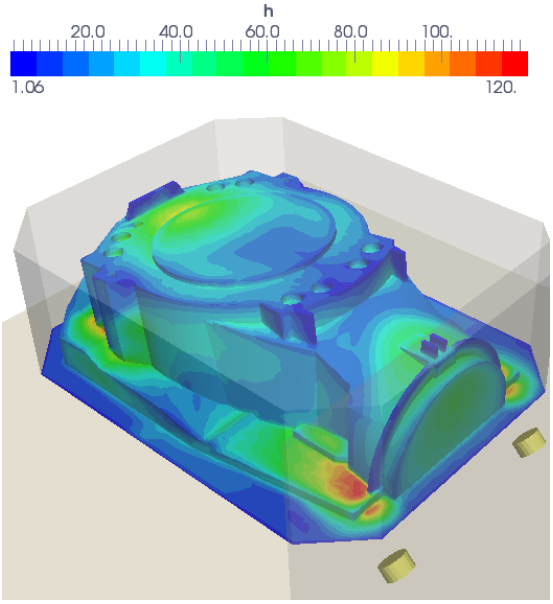

Figure 13. Convective heat transfer coeffient [W/(m^{2}K)] distribution for the main foundation mould.

3.4 Main Bearing House Mould Drying

The main bearing house requires two fans due to its smaller dimensions (Figure 14). Again the fans are positioned such that the air flow enters tangentially into the mould shape on one side and freely exits from the other as visualized in Figure 15.

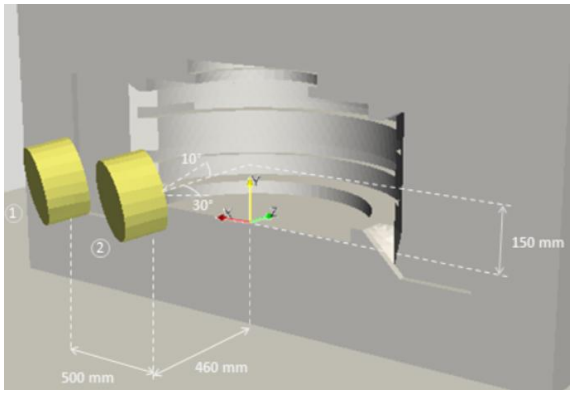

Figure 14. Optimal fan arrangement for main bearing house mould.

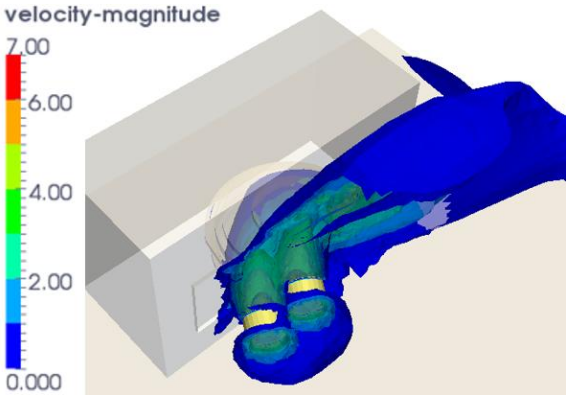

Figure 15. Velocity magnitude [m/s] isosurfaces. Air stream from the fans is channeled in the cavity.

With regard to heat transfer coefficients we see that the areas with minimum heat transfer coefficient are localized in the deeper pockets and cavities of the mould (Figure 16). Therefore these will be the areas to be checked for residual moisture after the drying process is completed.

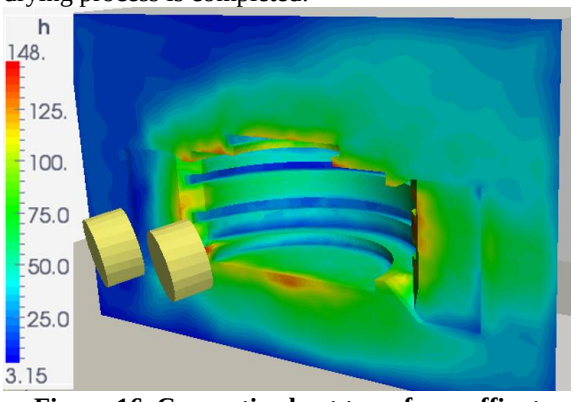

Figure 16. Convective heat transfer coeffient [W/(m^{2}K)] distribution for the main bearing house mould.

A final check of the heat transfer coefficient distribution (Figure 17) shows that only less than 0.5% of the mould area is subjected to a heat transfer

coefficient smaller than 5 W/(m^{2}K). Also the overall distribution has higher values than the one of the other moulds previuosly analyzed. This suggests that the drying times for this items will be shorter.

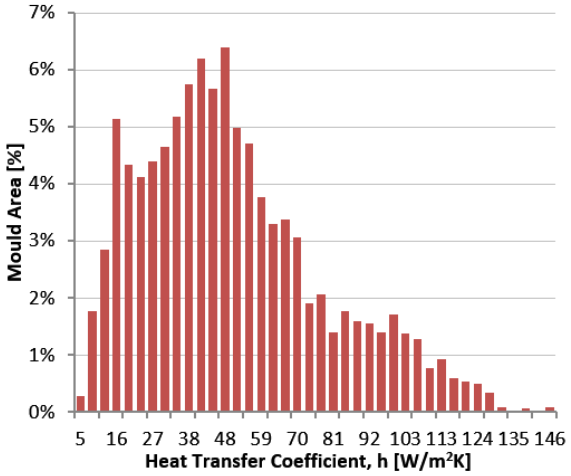

Figure 17. Histogram showing the distribution of the heat exchange coefficient on the main foundation mould surface.

IV. CONCLUSIONS

The main conclusions of this study can be summarized as below:

- Different fans type performances were assessed with the aid of CFD simulations and the TVV 4500 has been chosen due to the largest covered area with a reference level of the heat transfer coefficient around 10 W/(m^{2}K).
- Optimal fan layouts for the moulds of three typical components of wind turbines were proposed, in particular the hub will require 3 fans, the main foundation 6 fans and the main bearing house 2 fans.
- Areas which are particularly difficult to dry have been reduced to less than 2% of the mould surface and evidenced for moisture measurements during production process.
- Qualitative validation of the CFD model used was performed by comparison with infrared camera measurements for the hub mould and a satisfactory agreement was found.

V. ACKNOWLEDGEMENTS

This work was financed by Global Castings A/S, the Danish Agency for Science, Technology and Innovation (DASTI) and the Technical University of Denmark (DTU).

References

[1] U.C. Nwaogu, N.S. Tiedje, Using sol-gel component as additive to foundry coatings to improve casting quality, *Journal of Cast Metals Research*, 2012, 176-187.

[2] J. Mohammed, J. May, A. Alavi, Application of Computer Aided Design (CAD) In Knowledge Based Engineering, *Proceedings of The 2008 IAJC-IJME International Conference*, ISBN 978-1-60643-379-9.

[3] A. Patel, G. Patel, Operational Augmentation of Forced Circulation Type Solar Dryer System Using CFD Analysis, *Int. Journal of Engineering Research and Applications*, ISSN : 2248-9622, Vol. 4, Issue 4(Version 1), April 2014, pp.265-268.

[4] N. Schutze, Control Limits for the Drying of Water Based, Coatings, *Foseco Foundry Practice*, Issue 255, June 2011.

[5] G.L. Di Muoio, N.S. Tiedje, B. B. Johansen, Critical Control Variables For The Coating Process Of Furan Bonded Sand With Water Based Foundry Coatings, *71st World Foundry Congress*, Bilbao, Spain.

[6] G.L. Di Muoio, N.S. Tiedje, *Evaporation Rates of Water Based Foundry Coatings on Furan Bonded Sands*, International Foundry Research, 2015.

[7] R.H. Perry, D.W. Green, *Perry's Chemical Engineers' Handbook (7th Edition)*, McGraw-Hill, 2008. Table 1-12 (page 1-20).

[8] G.L. Di Muoio, N. S. Tiedje, B. B. Johansen, Measurement of Moisture in Foundry Coatings using Resistance Based Measuring Devices, *19th International Drying Symposium (IDS 2014)*, Lyon, France, August 24-27, 2014.

[9]. G.N. Abramovich, G.N., The Theory of Turbulent Jets, *The MIT Press*, 2003.

[10] Yunus A. Cengel, Afshin J. Ghajar, Heat and Mass Transfer, 2010.

Supplement IX

When dry is dry?
Process design rules, simulations and industrial cases on the drying of water based foundry coatings

Giovanni Luca **Di Muoio**, Global Castings A/S, Copenhagen, Denmark, gidmu@globalcastings.com
Niels Skat **Tiedje,** Technical University of Denmark, Copenhagen, Denmark

Abstract
Drying of foundry coatings is a relatively new process in the foundry industry that has come into use with the introduction of water as a solvent for mould coatings. In this paper we present an overview of the results of several tests and simulations carried out recently at Global Castings A/S and at the Technical University of Denmark on the drying of water based foundry coatings. In particular, we focus on the critical parameters and properties to be controlled in order to achieve a stable drying process. We propose for each of these parameters simple methods for testing both at laboratory and production scale so that material characterization and model validation can be carried out also for materials different from the ones considered in this study. Finally, we present the application of a simple calculation method and more advanced simulation tools, on real industrial cases. These tools have been developed in order to simulate the drying process and reduce design time and cost of expensive drying equipment.

Keywords:
Drying process, water based foundry coating, experimental validation, design procedure, simulation

Introduction

Drying of foundry coatings is a relatively new process in the foundry industry that followed the introduction of water as a solvent. Alcohol based coatings are dried by burning, a fast but unsafe process due to the high flames generated (Figure 1). Additionally alcohol fumes and combustion gases are released in production environment posing health and safety risks for the operators. Water was introduced as a solvent to eliminate such risks, but in order to avoid moisture related defects in the castings ([1-3]) a drying step for the coated moulds is needed (Figure 2). The duration of the drying process (drying time) and the final amount of residual moisture needs to be predicted and controlled so that process capacity and quality can be maintained.
In this paper, we focus on the critical process parameters and properties to be controlled in order to achieve a stable drying process (Figure 3). The term stability means that we are able to predict the final moisture level and the drying time (the time needed to reach the specified moisture level) of a mould and keep this within a narrow range.

Figure 1. Drying by burning of core coated with alcohol based foundry coating.

In particular, we propose for each of these parameters a simple method for testing and measuring them so that material characterization

and model validation can be carried out also for materials different from the ones considered in this study. Simple calculation method and more advanced simulation tools have been developed in order to simulate the drying process and reduce design time and cost of expensive drying equipment.
Results of tests and simulations carried out recently at Global Castings A/S and at the Technical University of Denmark are used to show the application of new methods on real industrial cases.

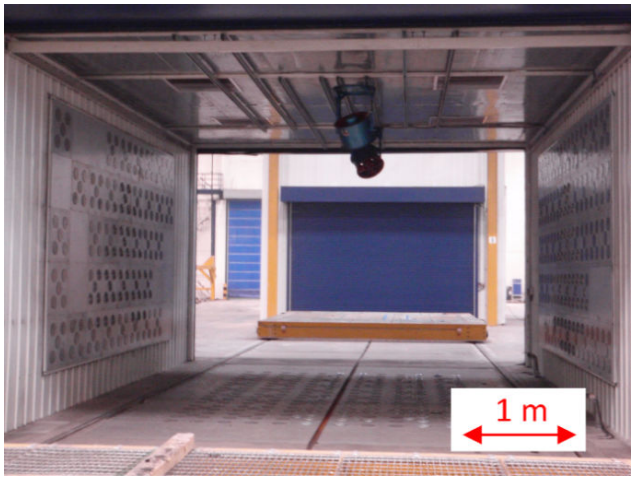

Figure 2. Example of drying cabinet used for the drying of water based coatings applied on sand moulds in the production of large size wind turbine components.

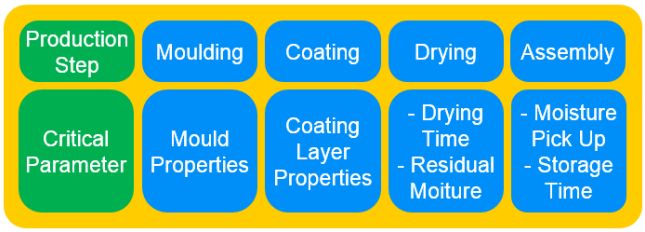

Figure 3. Overview of the critical parameters influencing the drying process for each production step.

Methods

In order to characterize and optimize the drying process our approach is to start with experiments at laboratory scale with the aim to test different properties and provide preliminary tools of assessment with low cost and risk. Hand calculations are then performed to support the initial choice of process parameter levels. Advanced CFD simulations are used when there is a need to optimize the process for a given geometry or when direct solution of equations is not possible in a simple way.
Finally, full scale tests are used for final verification and adjustments.
In the next section we describe in more detail the methods used to optimize the different process variables. The first parameters considered are the coating properties and layer thickness since they determine the amount of water to be dried and therefore the energy needed for the drying process. Next are the sorption curves of the coating and mould material that are needed in order to understand the achievable levels of moisture for given drying conditions. Then evaporation rates are used to predict coating drying times for different air drying conditions. Finally, moisture diffusion coefficients are used to estimate moisture pick up of moulds after drying and reduce gas defects risks.

Coating Layer Control

The first step towards achieving a stable coating layer is done by controlling the coating properties. In particular coating viscosity can be directly correlated with density however results can be compared only if the test method is the same. In Figure 4 we see how viscosity can vary with density and test speed for water based coatings. In real production it important to use equipment of adequate resolution and accuracy for measurement and control of coating density and viscosity [4].
The next step to coating layer control is to achieve stable mould properties and coating process parameters such as sand compaction, dipping time and coating direction with respect to gravity [4]. As shown in Figure 5 we can see that, based on different process parameter levels, it is possible to vary amount of water in the coating layer from 0.5 kg/m^2 to more than 3.0 kg/m^2 [4] for a given coating type.

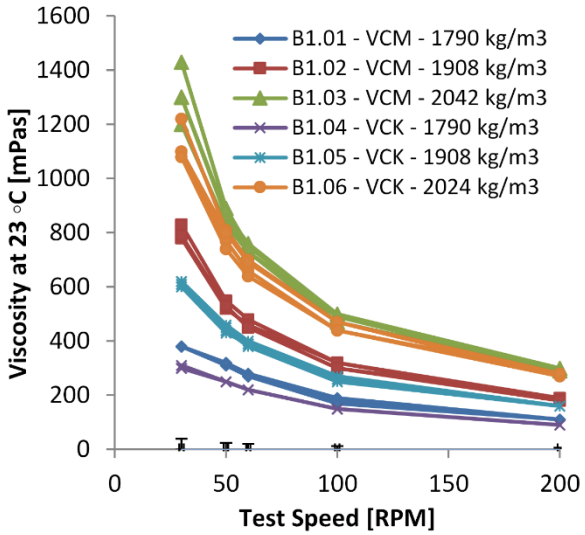

Figure 4. Viscosity measurements carried on two different batches of coating with three different densities. Viscosity can be directly correlated with density however results can be compared only if the test speed is the same [4].

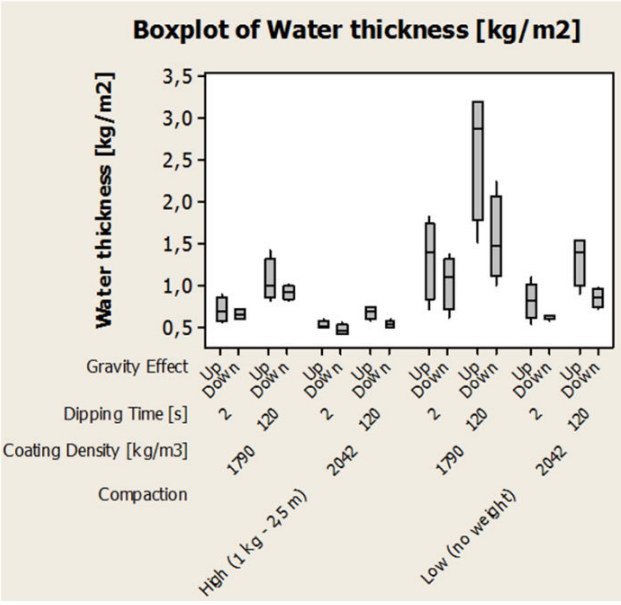

Figure 5. Water thickness deposited on furan sand samples using different levels of sand compaction, coating density, dipping time and gravity. The amount of water can vary from 0.5 kg/m² to more than 3.0 kg/m² [4].

Figure 6 shows measurements of coating penetration that can be carried out on production moulds. These measurements can be directly correlated to the amount of water in the coating layer (Figure 7). The correlation is independent from coating process variables such as compaction, density, dipping time and gravity and can be obtained for different kind of coating and sand recipes with quick laboratory tests as shown in [5].

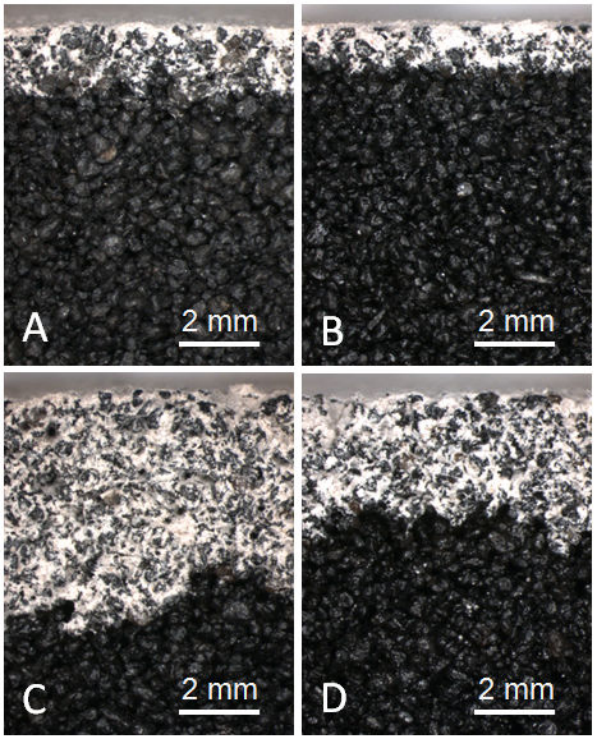

Figure 6. Coating penetration achieved with different levels of sand compaction, coating density, dipping time and gravity effect [4].

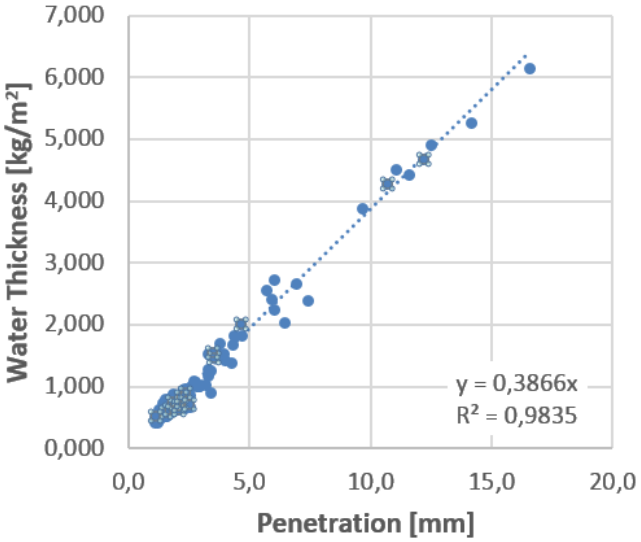

Figure 7. Coating penetration can be directly correlated to water thickness [5]. This allows to predict of coating layer water amount in large moulds.

Drying Time Control

In order avoid bottlenecks in production it is important to make sure that drying time of the moulds is equal or shorter than the needed production cycle time.

Manual Calculation Method

For constant drying air conditions the estimation of drying time can be carried out with the following manual calculation procedure:

1) Determine average evaporation rate from design map (Figure 8). Design maps display the relation between air properties, coating thickness and type (Eq.1) and can be determined experimentally as shown in [6]:

$$ER_{avg} = ER_{avg}(T_{air}, RH_{air}, V_{air}, CT_{H2O,init}, X_{final}) \quad \text{Eq.1}$$

2) Calculate estimated drying time by dividing the initial amount of water in the coating layer by the evaporation rate, as show in Eq.2:

$$t_{dry} = \frac{CT_{H2O,init}}{ER_{avg}} \quad \text{Eq.2}$$

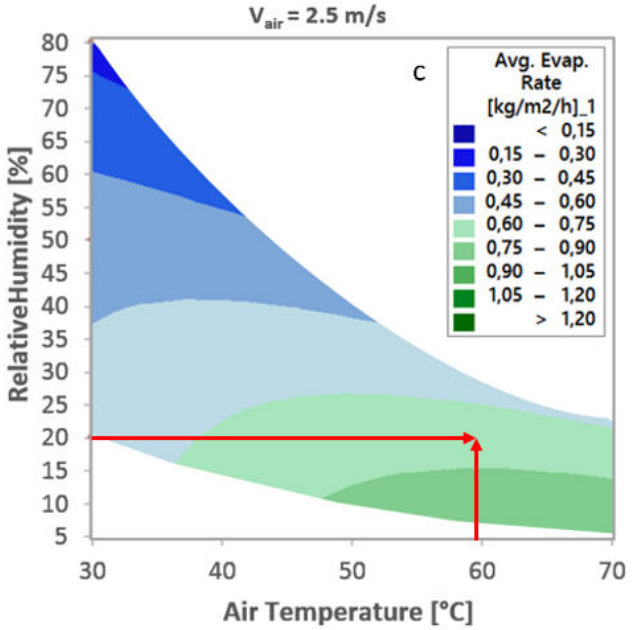

Figure 8. Average evaporation rates design maps for air speeds of 2.5 m/s, initial water thickness of < 1 kg/m2 and final moisture of < 1 % [6].

The estimated drying time can then be compared with production requirement and changes to the drying air condition or coating process can be made if needed.

Numerical Calculation Method

If there is a need to simulate varying conditions of drying air like changes in temperature, relative humidity or air speed it is possible to follow a numerical approach. In the numerical approach the properties are assumed constant only for a small amount of time Δt compared to total the length of the drying process. In this case the solution is carried out as follows:

1) Determine maximum evaporation rate from experimental equations in the form of Eq.3. Maximum evaporation rates are only a function of air properties and can be determined experimentally as shown in [6]:

$$ER_{max} = ER_{max}(T_{air}, RH_{air}, V_{air}) \quad \text{Eq. 3}$$

2) Use the ratio between current coating moisture level and initial moisture (for the first time step the ratio is 1) and the initial water thickness to obtain the correction factor from Eq.4 or Figure 9:

$$CF \quad = CF \quad (CT_{H2O,init}, X_{current}) \quad \text{Eq. 4}$$

3) Calculate current evaporation rate is as:

$$ER_{current} = ER_{max}\, CF \quad \text{Eq. 5}$$

4) Calculate water evaporated (Eq.6) and new moisture level at the next time step.

$$\Delta_{H2O} = ER_{current}\Delta t \quad \text{Eq.6}$$

5) Update drying air properties and start a new iteration from step 1.

The calculation is stopped when the calculated residual moisture is less than 1%.

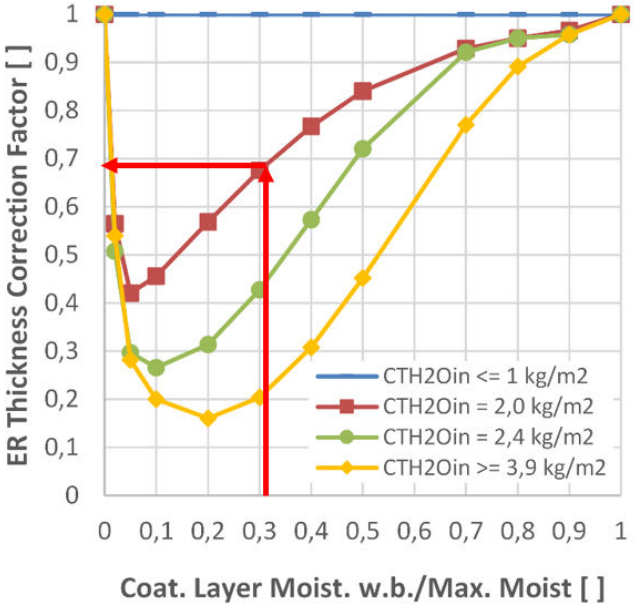

Figure 9. Correction factor for evaporation rate calculation based on initial coating water thickness and current moisture in the coating layer.

Measurement Method

In order to carry out measurements of drying time different tools have been found to be of practical use in the foundry. Moisture measurements can be carried out with portable electronic tools once the correlation between moisture in the considered coating and electrical resistance is known (Figure 10). Drying time can then be defined as the time at which a desired moisture level is reached. The accuracy of this measurements is heavily dependent on the tool used and calibration as shown in [7].

Another way to assess drying time by infrared thermography. In this case cold spots can be identified on large moulds and then moisture measurements can be carried out in the locations that have the lowest temperature and therefore will be the last to dry (Figure 11).

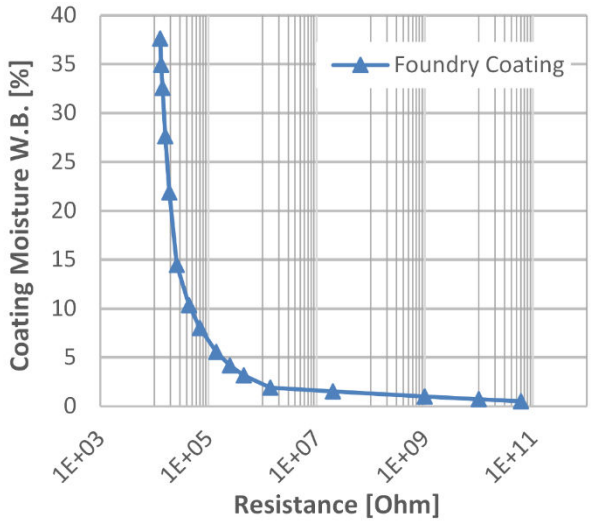

Figure 10. Example of correlation between resistance and moisture content in water based foundry coating. The knowledge of this correlation allows to improve the accuracy of resistance based measurement devices [7].

Figure 11. Thermography of a mould coated with water based coating. Cold spots can be identified as the last to dry and final moisture measurement performed.

Residual Moisture

After moulds are dried, typically in a cabinet with low relative humidity and high temperature, they are brought back to environment conditions typically with lower temperature and higher relative humidity. This will cause the moulds to pick up moisture from the surrounding air.

In order to estimate the amount of water that a mould can adsorb sorption curves can be used (Figure 12). These curves are obtained with a methodology called automatic sorption analysis as described in [8] and represent the equilibrium moisture level of different furan sands in air with a relative humidity varying from 5 to 95 %.

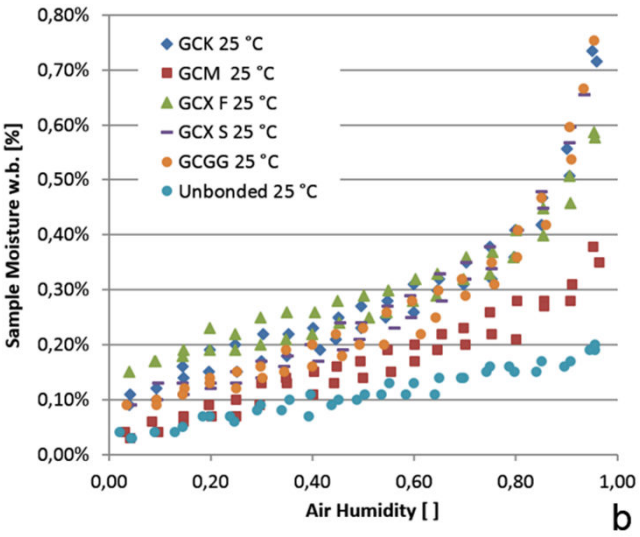

Figure 12. Sorption curves of different furan sands. Moisture levels can vary significantly both with binder brand and air relative humidity [8].

The adsorbed mass of water M_t at the time t, for a core of flat shape and thickness L, can be calculated with equation 8 where M_i is the initial mass of the core and X_e is the equilibrium moisture from the sorption curve (Figure n). The ratio between M_t/M_e is calculated from equations 6 and 7 obtained from approximate solutions of the diffusion equation [9]. The diffusion coefficient D can be determined by laboratory tests as described in [9].

$$M_t = M_e \frac{M_t}{M_e} = M_i X_e \frac{M_t}{M_e} \quad \text{Eq.8}$$

$$\frac{M_t}{M_e} = \frac{4}{L}\sqrt{\frac{Dt}{\pi}} \quad \text{for} \quad \frac{M_t}{M_e} < 0.5 \quad \text{Eq.6}$$

$$\frac{M_t}{M_e} = 1 - \frac{8}{\pi^2}\exp\left(-\frac{\pi^2 D}{L^2}t\right) \quad \text{for} \quad \frac{M_t}{M_e} > 0.5 \quad \text{Eq.7}$$

Figure 13 shows how the diffusion coefficient varies as a function of air relative humidity for different furan sand types at 25 °C. These coefficients can be used to perform moisture pick up calculation in 3D simulation software and thus make it possible to predict moisture distribution in complex shapes and varying environment conditions.

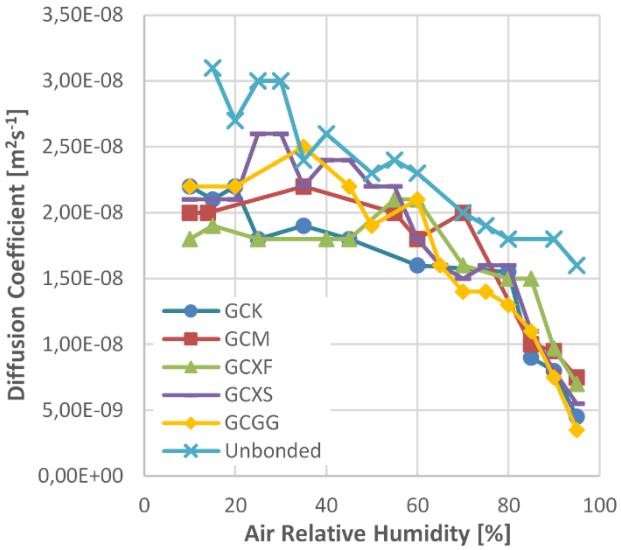

Figure 13. Diffusion coefficients for different brands of furan sands as a function of air relative humidity at 25 °C [9].

Table 1 provides an overview of the different parameters, how they can be characterized trough laboratory tests, measured in production, and what design rules and simulation tools can be used.

Results

In this section we present results from tests where the methods described have been applied to improve process stability.

Coating Layer Control

Figure 14 shows the water thickness on samples coated with tight controlled coating conditions, in

Table 1. Test methodology and design rules overview for properties affecting the drying of foundry moulds.

Properties	Lab. Tests	Production Measurements	Design Rules	Prediction Method	Ref.
Coating Properties	Rotational viscometer	In line sensors and real time control of density/viscosity	Tight control of coating density within specified range	Correlation between coating and viscosity at desired temperature	[4]
Coating Layer Properties	- Weight measurement - Penetration measurement	- Penetration measurement	Control dry and water thickness within specified range	Correlation between coating penetration and thickness	[4] [5]
Equilibrium Moisture Properties	Adsorption/Desorption tests	- Moisture sensor	Keep moisture below a critical level	- Hand calculation - 3D simulation	[8]
Diffusion Coefficients	Adsorption/desorption tests	- Moisture sensor	Reduce moisture pick up after Drying	- Hand calculation - 3D simulation	[9]
Drying Time	Evaporation rates tests	- Surface temperature - Surface moisture	Drying time and residual moisture below specified limit	Hand calculation 3D simulation	[6] [10]

particular we used good sand compaction, 1908 kg/m^2 coating density, 5 seconds dipping time and sample facing down while being coated to reduce the gravity effect. We can see that it is possible to achieve control of coating layer within a tight range by controlling relevant process variables.

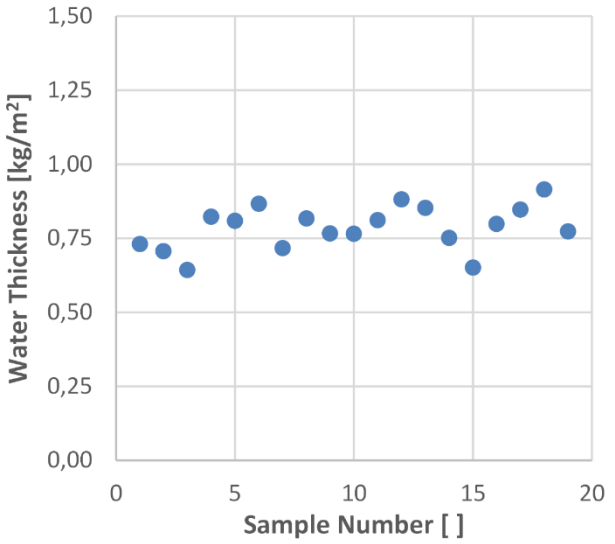

Figure 14. Water thickness on samples coated with tightly controlled coating conditions. It is possible to achieve control of coating layer by controlling relevant process variables.

Drying Time Prediction

With regard to drying time prediction Figure 15 shows how manual calculation method can be used to predict drying time of moulds drying in factory environment. Temperatures and relative humidities recorded in real production over a period of two years have been used to predict drying time of moulds drying in natural convection, low speed forced convection and high speed forced convection.

It can be seen that with natural convection drying time fluctuates from four to more than ten hours but with forced convection the drying time can be reduced to less than 6 hours.

In Figure 16 we see an application of the numerical approach to calculate the drying time of a mould dried in a drying cabinet were different return air ratios were used to save energy needed for heating the air to 65 °C. We can see that for a return air ratio of 90 % the relative humidity in the cabinet increases due to the fact that the moisture evaporated from the mould is not completely expelled. As a consequence the drying time increases form 1 hour to 1.5 hours.

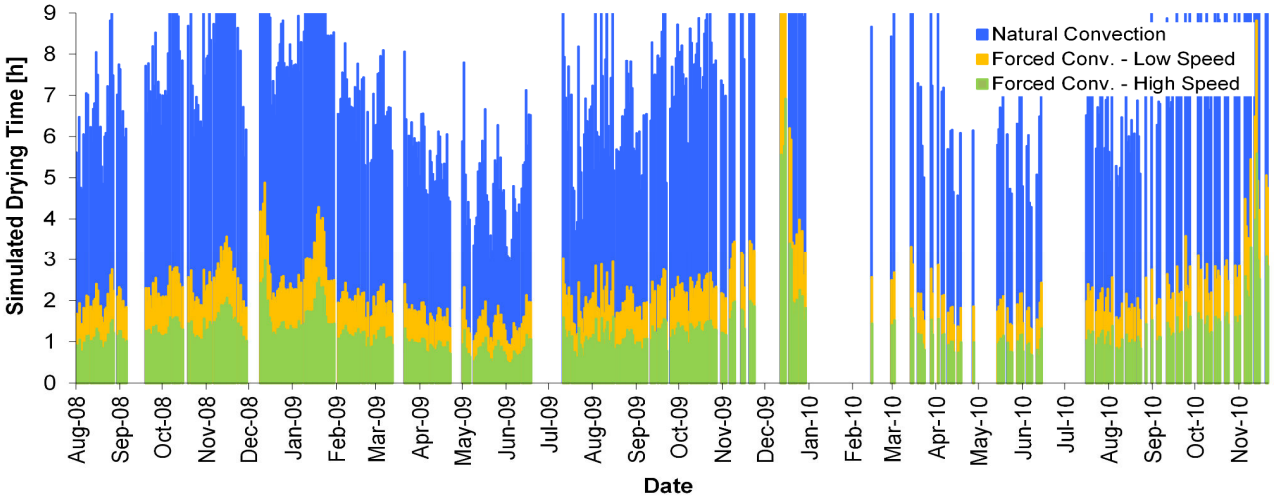

Figure 15. Drying time simulation of a mould drying at room conditions with natural convection and two different levels of forced convection. Historical temperature and relative humidity data of the specific geographic site were used.

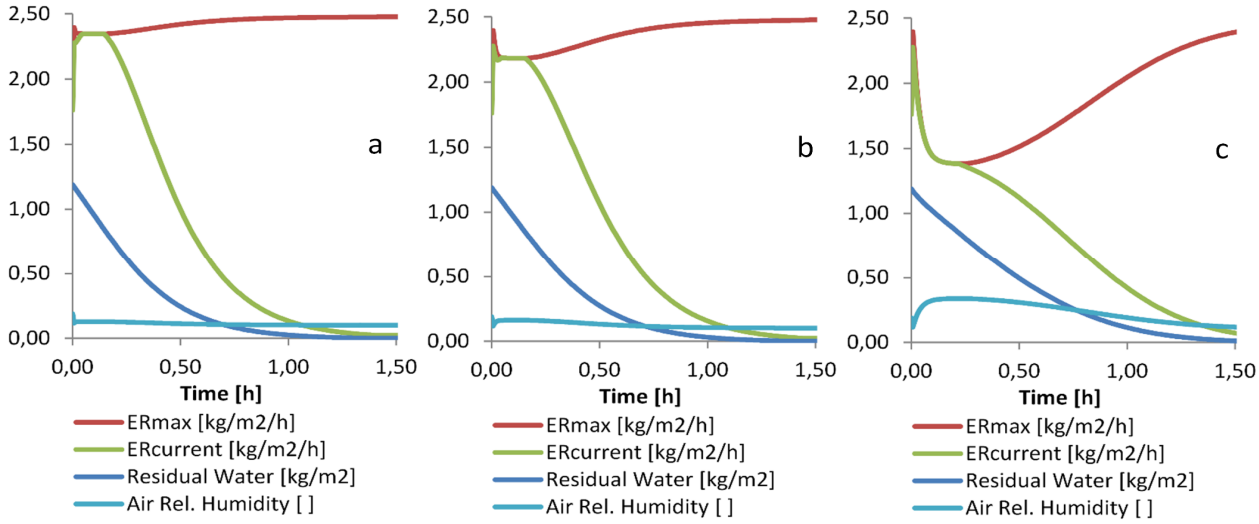

Figure 16. Simulations for drying cabinet with different return air ratios a) 10%, b) 50% and c) 90%. It can be seen how at 90% return air ratio the evaporation rate drops due to an increase in relative humidity and the drying time (residual water <0.01 kg/m^2) increases from 1 hour t 1.5 hours.

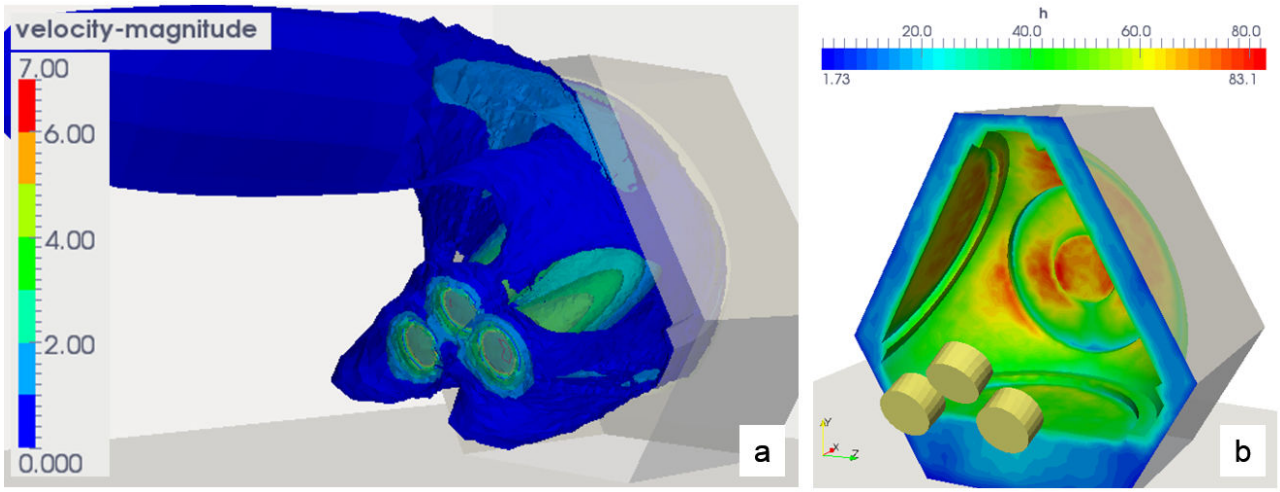

Figure 17. Velocity magnitude [m/s] iso-surfaces from 3D CFD simulation used to optimize the fan placement during the drying operation (a) and the resulting heat transfer coefficient [W/(m^{2}K)] distribution on hub mould (b).

Figures 17 a and b show the results from a computational fluid dynamic simulation where fan placement is modelled to predict the air speed distribution over the drying mould surface and calculate the heat transfer distribution [10]. The parameters in the area with lower heat transfer will then be used for process design optimization and quality control.

Residual Moisture

Figure 18 shows how resistance moisture measurements can be used assess the effect of process changes like the settings of drying cabinet. It can be see like Test 2 items have a drying time consistently shorter than test 1 items.

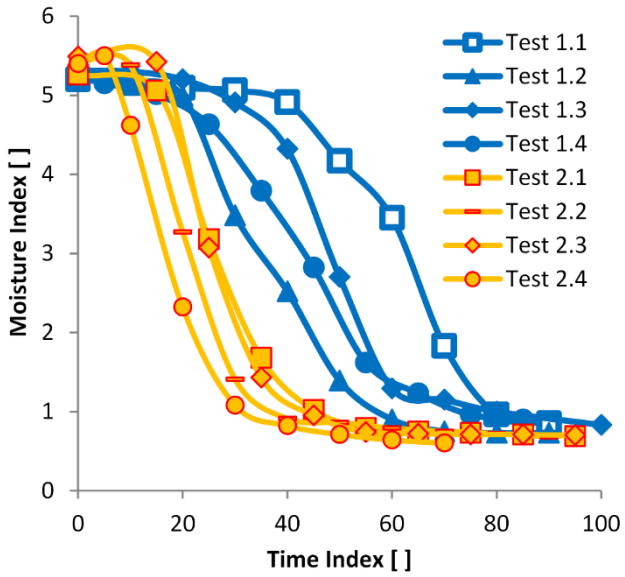

Figure 18. Moisture measurements carried out on production moulds with two different settings of drying cabinet were used. Test 2 items show a clear reduction of drying time compared to Test 1 items.

In Table 2 we see water amounts that are contained in 40 tons moulds for different binder types and relative humidity at equilibrium. It can be seen how water amount can vary from as low as 20 kg to as much as 272 kg. As consequence the risk of vapour and gas defects can be predicted.

Table 2. Water amount contained in 40 tons moulds for different binder types and relative humidity at equilibrium.

Binder Type	Air Relative Humidity [%]	Moisture [%]	Water Amount [kg] (40 tons mould)
GCK	10	0.11	44
GCK	50	0.25	100
GCK	90	0.68	272
GCM	10	0.05	20
GCM	50	0.15	60
GCM	90	0.30	120

In Figure 19 we show the effect of time and thickness on the equilibration time of furan sand cores. It can be see how a core with thickness of less 50 mm will reach equilibrium (ratio of 1) in less than 24 hours. While large core can pick up more than 30% on the equilibrated moisture values in less 3 days. This shows that it is important to minimize storage time of cores after drying in high humidity environments.

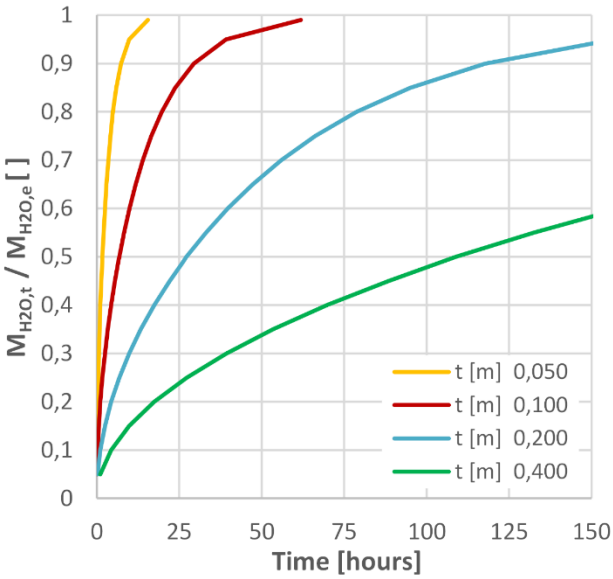

Figure 19. Effect of time and thickness on the equilibration time of furan sand cores. It can be see how core with thickness of less 50 mm will reach equilibrium in less than 24 hours.

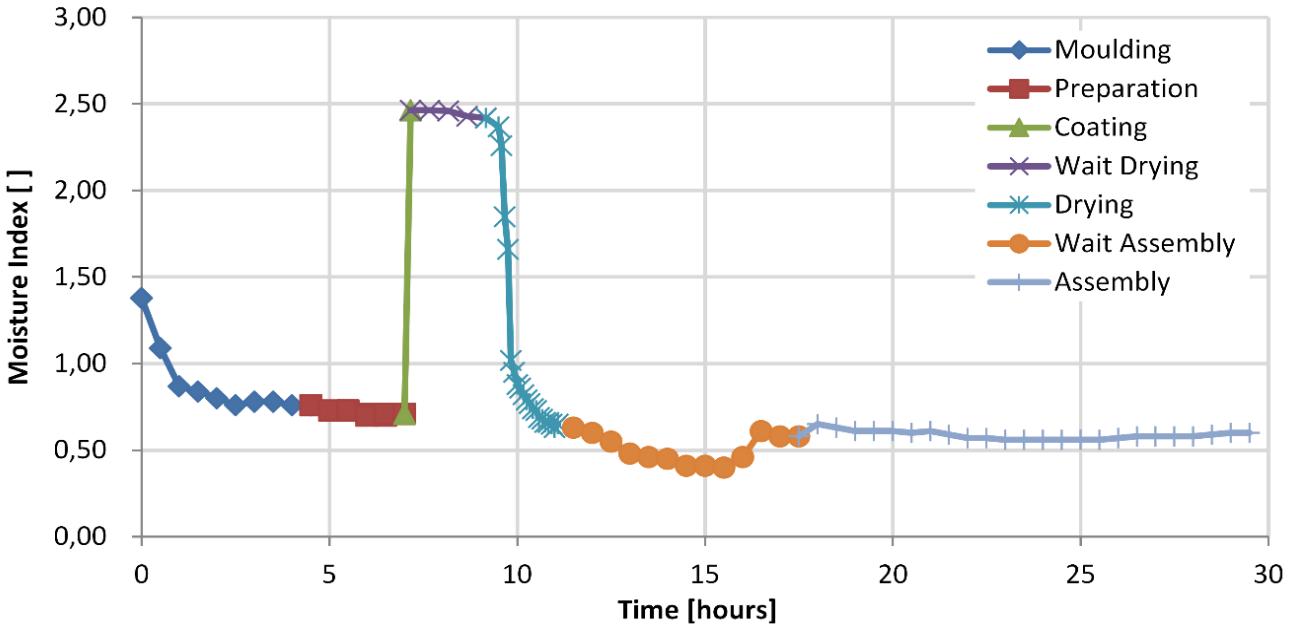

Figure 20. Example of process monitoring where moisture at the surface of the mould is measured at regular intervals in all the operations from moulding to assembly. The effect of the drying process can clearly be seen as well as the moisture pick up in during the waiting time before assembly.

Finally we show how moisture variation of the mould surface can be monitored trough the complete lifetime of the mould (Figure 20). The effect of the drying process as well as the moisture pick up during the waiting time before assembly can clearly be seen.

Conclusions

We ca summarize the results of this work in the as below:

- A set of test methods and tools for characterization and measurement of coating and moulding material properties to be used in foundry industry both at laboratory and production level has been described
- Calculation methods and simulation possibilities for moulding, coating and drying processes has been developed
- Application to real industrial cases has been shown for both measurement and simulation methods
- Possibility to significantly reduce risk of moisture related defects, cost and design time of drying operations by the use of this tool has been shown

References

[1] J. Campbell, R.A. Harding: 'Solidification Defects in Castings', Lecture 3207, The University of Birmingham, 4-8, 1994.

[2] L. Elmquist: 'Defect formation in cast iron', Presentation, School of Engineering, Jonkoping University, Sweden, 2012.

[3] B. Sarum. Ductile and Compacted Graphite Iron Casting Skin -Evaluation, Effect on Fatigue Strength and Elimination, B. Ohio State University, Ph.D Dissertation, 2013, Page 103-106.

[4] G.L. Di Muoio, N. Skat Tiedje, B. Budolph Johansen. Critical control variables for the coating of furan bonded sand with water based foundry coating. World foundry congress, 19-21 May 2014. Bilbao, Spain.

[5] G.L. Di Muoio, N.S. Tiedje, Achieving Control of Coating Process in your Foundry, Archives of Foundry Engineering, 2014.

[6] G.L. Di Muoio, N.S. Tiedje, Evaporation Rates of Water Based Foundry Coatings on Furan Bonded Sands, International Foundry Research, June 2015.

[7] G.L. Di Muoio, N. Skat Tiedje, B. Budolph Johansen, Measurement of Moisture in

Foundry Coatings Using Resistance Based Measuring Devices, 19th International Drying Symposium (IDS 2014) Lyon, France, August 24-27, 2014.

[8] G.L. Di Muoio, N. Skat Tiedje, B. Budolph Johansen, Automatic vapour sorption analysis as new methodology for assessing moisture content of water based foundry coating and furan sands, 10th International Symposium on the Science and Processing of Cast Iron, SPCI10, Argentina, Mar de Plata, Nov 2014.

[9] G.L. Di Muoio, N. Skat Tiedje, Moisture Diffusion Coefficients Determination of Furan Bonded Sands and Water Based Foundry Coatings, International Journal of Cast Metal Research, 2015 (in review).

[10] Giovanni Luca di Muoio, Alessandro Della Rocca, Niels Skat Tiedje, CFD Study for the Drying Foundry Moulds used in the Production of Wind Turbine Components, International Journal of Engineering Research and Applications, 2015.

Supplement X

An innovative integrated CAE approach for the design and optimization of foundry moulding boxes

G.L. Di Muoio[1], G. Bertuzzi, J. O. Frandsen

Casting Technology, Global Castings A/S, Diplomvej 373N, Kgs. Lyngby, 2800, Denmark

[1] E-mail: gidmu@globalcastings.com

Keywords: Process Optimization, Process Simulation, Moulding Box Design, Computer Aided Engineering, Product Development

Abstract

Moulding boxes are a critical tool in production of large cast items because they are involved in and affect most of the production steps in a foundry. Optimization of moulding boxes design allows to harvest significant savings in terms of sand consumption and possibly increase capacity by simplifying handling and shortening production times.

Optimization of such a design is not a trivial task. This is due to the many interactions with other production tools and to the need to check compliancy with the different requirements and constraints coming from each production step.

In this paper, a novel approach to the design of moulding boxes is presented with the objective to simplify the design workflow and optimization process of customized moulding boxes with the aid of CAE tools. Additionally, tools such as values stream mapping and interface diagrams are introduced to improve the management of the design process and optimize the usage of CAE tools.

Results shows that significant savings can be harvested, but that optimization generates an increase in complexity of the moulding boxes that can only be handled thanks to the newly introduced design approach where CAE tools are smartly used and integrated in design workflow.

Introduction

Moulding boxes represent a critical tool in the casting process because they are involved in and affect all the production steps: moulding, handling and turning, assembly, pouring and shake out. However, in traditional jobbing foundries moulding boxes are used in standard shapes and dimensions mainly to provide mechanical support for the sand mould and not much attention is paid to their design or optimization. The use of standard dimensions is due to the high product mix that generates the need to be able to produce different parts in the same moulding box.

On the other hand, the continuous pressure on the foundries for costs reduction makes necessary a new approach to the process design where tools and costs are minimized maintaining or improving the degree of quality of the casted items. This new approach matches mainly the requests of foundries producing large sized castings (5 to 30 tons) and that typically handle few items in medium and large series with stringent requirements in terms of dimensional tolerances and mechanical properties. The use of standard moulding

boxes for large size items leads to a high usage of sand which increases the price of the parts and puts strain on the sand transportation systems, limiting the production capacity of the factory. Finally, the casting of large cast iron sections in thick sand moulds generates long cooling times which increases the number of moulding boxes needed and the shop floor space usage in the foundry further limiting production capacity and increasing the production cost.

An optimized design of the moulding boxes can allow significant reduction of weight and price of the tools, a lower amount of sand used in the production process (Figure 1), easier handling, shorter production times and, if properly designed, final casted parts with improved quality. However, optimizing the design of such a production tool is not an easy task. This is due to the many interactions with other production tools and equipment and to the different conditions to which the box is subjected in the different production steps (mechanical, thermal, chemical, etc...).

In this paper, a novel approach to the design of moulding boxes is presented with the objective to simplify the workflow of the design and optimization process of customized moulding boxes with the aid of CAE (Computer Aided Engineering) tools. The moulding box is seen as new product to be developed and the design process is based on the analysis of the interfaces and interactions between the moulding box and other tools, of a set of requirements coming from the different production steps and of a set of economic constraints.

CAE tools are needed in order to shorten the design time and lower final cost of the moulding box, therefore maximizing the revenues (Figure 2) [1,2]. The geometries of the moulding boxes are developed from concept to detailed design using 3D CAD software. Failure modes are checked by the use of preliminary, self-developed hand calculations and finally with commercial Finite Elements software both for the moulding boxes and the casted parts.

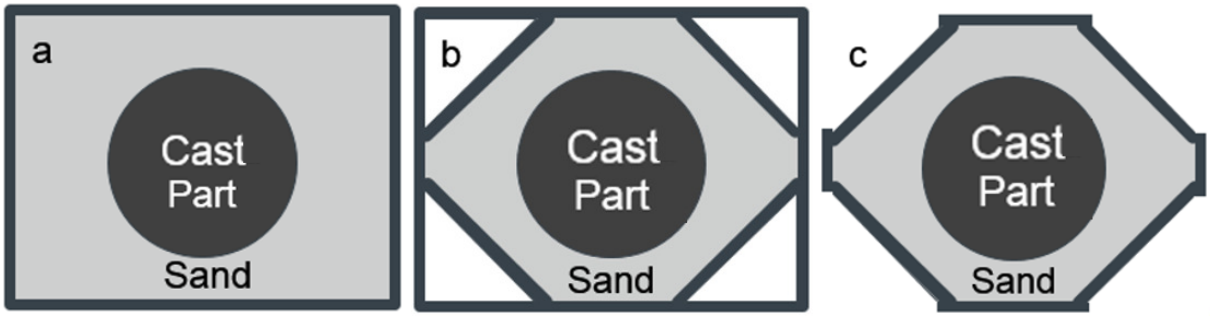

Figure 1. Sand saving concepts: a) standard moulding box, b) standard box with sand savings c) optimized moulding box.

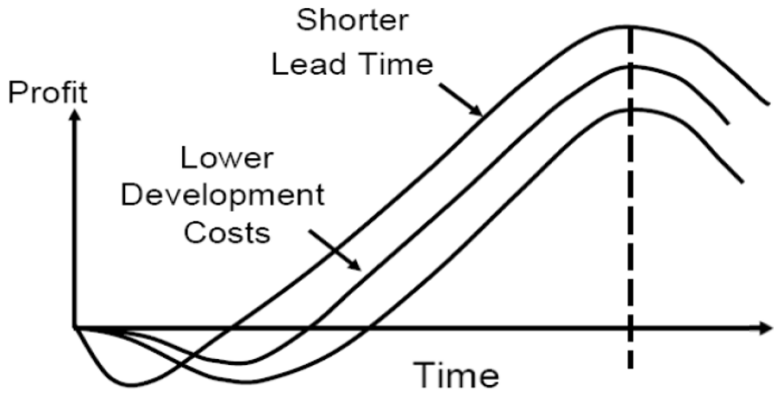

Figure 2. Effects of CAE tools on product lifecycle [1,2].

The innovative approach is used to re-design and existing moulding box and the results are then compared with a classic design. Results confirm that significant savings can be harvested by using this procedure both in investment costs and variable costs. On the other hand, the use of CAE tools on an advanced level is necessary in order to handle the increased complexity and the many design constrains.

Methods

Traditional Design Methodology

In traditional design methodology tools are developed in a sequential way as it can be seen in Figure 3.

The main drawbacks of this process are:

- Each step is handled independently with no overall view, it is therefore difficult to reach an overall optimized design
- Designers responsible for a step do not normally communicate with designers of other steps (especially if steps are not adjacent) since the process does not require this
- It is very inefficient from a time optimization point of view because the process is sequential, and one step is started only when the previous is completed
- Problems arising in one step are 'taken as they come' and designers try fix them within they knowledge areas and without challenging constraints, this results typically in delays and cost increases
- Initial steps decisions heavily hinder innovation in subsequent steps, since it is extremely difficult and expensive to make changes to an already frozen design step

From a CAE usage point of view. We note that CAE is typically used only in some steps and in a sequential way and therefore not exploiting the full potential offered. For example, PLM system is not used to design and maintain 3D documentation of production tools. 2D drawings are preferred mean of exchange between steps this slows down significantly simulation capabilities where good quality 3D geometries are instead needed.

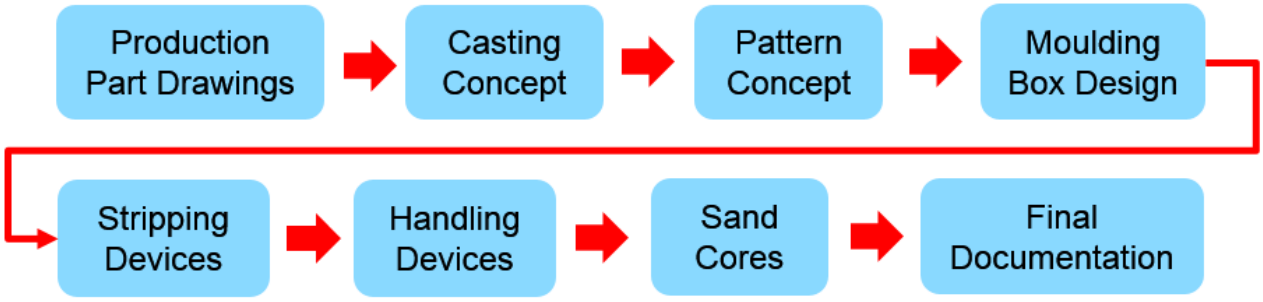

Figure 3. Traditional design methodology.

New Design Methodology

Based on methodology typically used for development of new products [3] a new desing process is introduced.

The newly introduced desing process (Figure 4) starts by defining a clear set of requirements coming from the customer. Then, two main iterative desing loops are used to initially define the design concept and then to finalized the detailed design.

The first loop is iterated until all the stakeholders approve the desing concept and no more changes are needed to the the concept. The second loop is iterated until test and 0 series are completed succesfully.

Whitin the detailed desing phase one more iteration loop is present (Figure 5). In this loop, the necessary calculations and simulations are performed and the design is optimized until all the constraints coming from the customer requirements are satisfied.

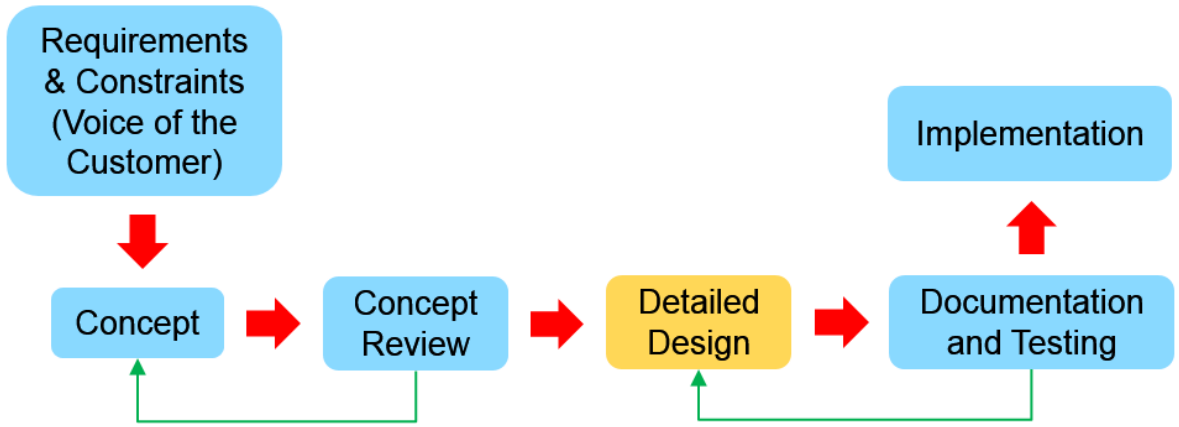

Figure 4. Overall view of new design process.

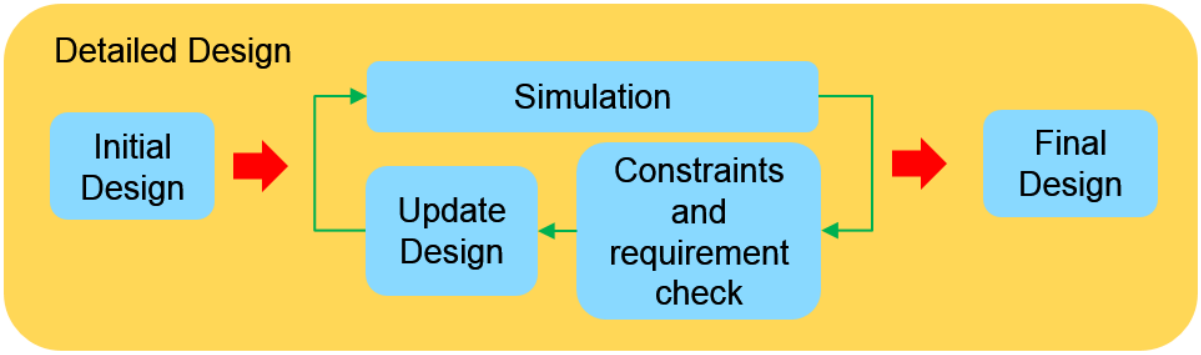

Figure 5. Schematics of detailed design phase of the new design process.

Value Stream Mapping

In order to define a clear and as complete as possible set of requirements, a value stream mapping of the process is carried out and for each operation the tool interfaces and requirements are listed (Figure 6).

It is important to point out that process mapping shall be carried out a team effort involving both design, production and management team [4]. This allows not only to reduce the risk of missing critical interfaces or requirements but also create a common shared understanding of the tool requirements for the different stakeholders [5].

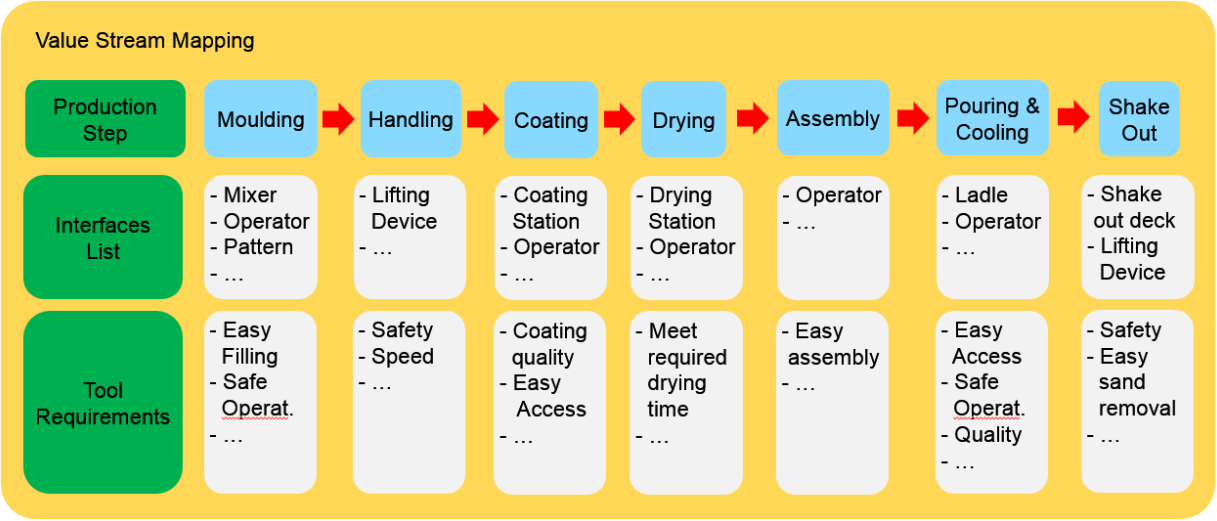

Figure 6. Requirements and interfaces identification trough value stream mapping.

Interface Diagram

Tools are grouped in systems, where a system represents a units that bears a specific function. For example the moulding system groups all the tools needed to manufacture a complete mould.

Interfaces between tools are then identified, classified and graphically visualized (Figure 7).

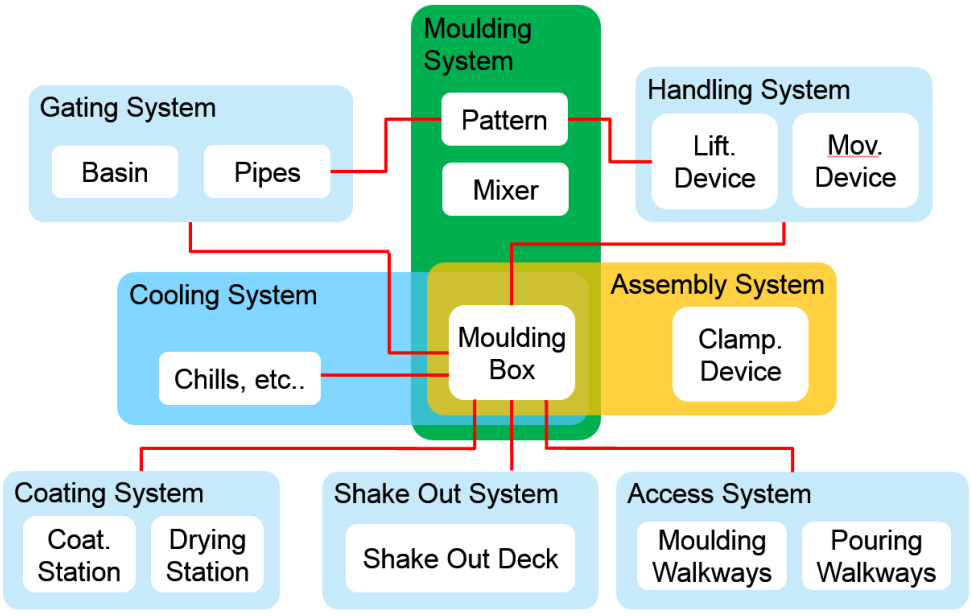

Figure 7. Interface diagram for a moulding box. This diagram helps to visualize all the interactions between the moulding box and the other production tools.

Design work is then started on each of the tools as soon as interfaces are agreed upon and resources are available (Figure 8). Design teams will keep interfaces unchanged unless there is a problem to meet a specified requirement or goal. If an interface requires modification, the involved design responsibles and affected stakeholders will review and eventually approve the change if feasible.

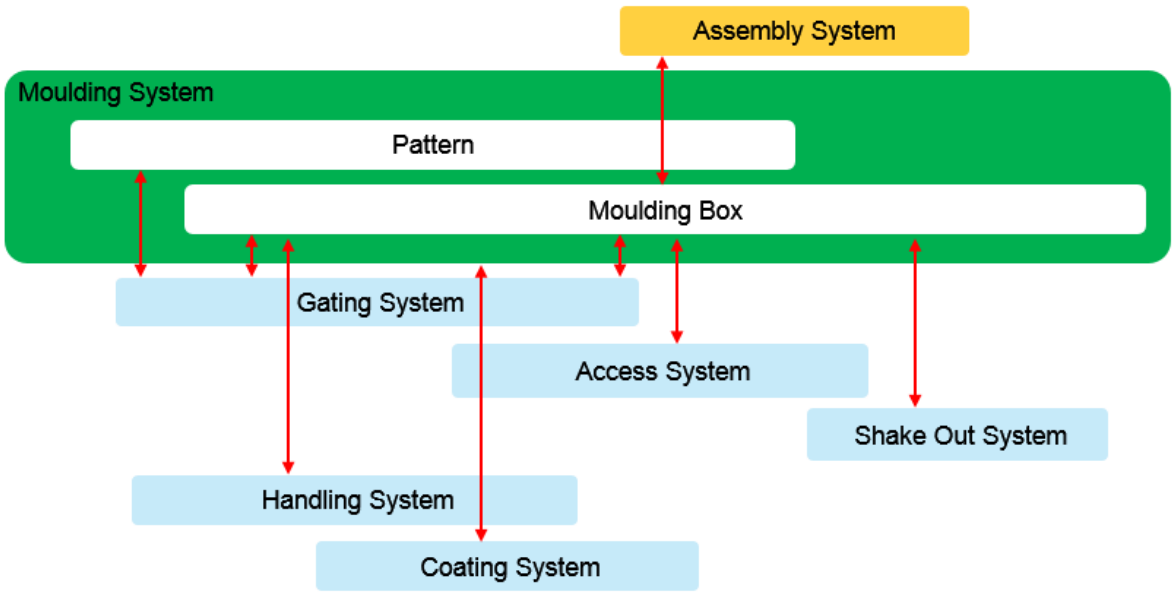

Figure 8. Planning overview of different systems designs.

Table 1 shows how CAE tools are used in the different design phases and integrated in the design workflow. It can be seen, for example, how 3D modelling is critical to all phases, from concept design (to visually evaluate the solution and speed up the review process), to detail design (where 3D models are used for simulations) and in documentation and testing (where 2D are generated from 3D). Finally PDM systems are used to maintain and track changes to the tools over their lifecycle.

Table 1. The role of CAE tools in the different phases of the new design process

Design Phase	CAE Tools Used	Role of CAE Tools
01 - Concept	3D modelling	- Quick modelling - Ideas check
02 - Review	3D modelling	- Quick visualization to reviewers - Simplify and speed up review
03 - Detailed Design	3D modelling, Structural FEA Analysis Process Simulation	- Check compliance with constraints - Optimize design - Optimize production process
04 - Documentation & Testing	2D drawing	- Manufacturing drawings - Automated BOM
05 - Implementation	PDM	- Engineering Change Management

Results

Design Process Comparison

Table 2 shows how critical aspects of the design process differ in the two proposed methods. For example, we can notice that 3D design competence, previously outsourced, is now handled in house to allow for better integration and communication [6]. Additionally, overall competences of the staff were increased to be able to be able to use CAE tools in an advanced manner.

The level of innovation achieved is much higher since now the work on different tools is carried out in parallel and decision on design or interface changes are done based on a total cost evaluation, not just in respect to one production step.

Documentation process followed naturally and was speeded up by the in house availability of 3D models.

Finally, the process helped to foster innovation by having a quantitative assessment of the ideas (based on calculation, simulation or tests) as compared to a qualitative assessment criteria that was often used previously.

Table 2. Comparison between the caracteristics of a classic sequential design process and the new CAE integrated design process.

		Classic Sequential Design Process	New Integrated CAE Design Process
Design Process Characteristic	3D Design competence	Outsourced	In house
	Staff overall competences	Low-Medium	Medium-High
	Possibility of innovation	Low (design dependent on decisions made at previous steps)	High (design teams work in parallel and independently, but communicating often about interfaces changes)
	Interface design	Locked in initial stages	Locked when optimal solution reached
	Perceived need for communication between designers	Low	High
	Documentation system	Different and difficult to access	Standardized
	Idea selection criteria	Qualitative	Quantitative

Mouldbox Comparison

The design that resulted from the application of this process to a standard tool like the mouldbox show a general increase in complexity. In Figure 9 we can see general level of complexity of a mould box and how it increases when from a standard design we go towards optimized design. Such complexity could not have

been handled optimally only with the use of old simple 2D drawing softwares and without a management process that focused on clear requirements and interfaces defintion.

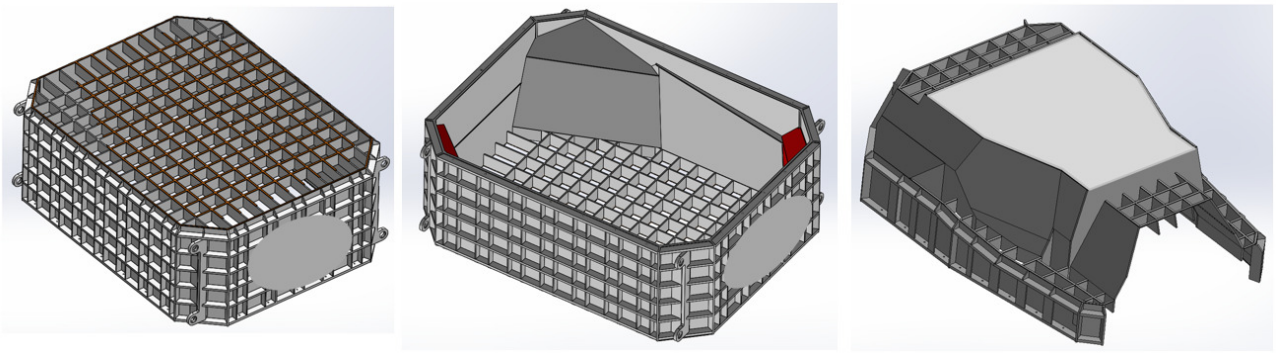

Figure 9. Example of standard moulding box (on the left), sand saving moulding box (at the centre) and optimized moulding box (on the right). 3D cad models are build and used as starting point for advanced software simulations. (Some parts have been hidden for commercial reasons)

Table 3 summarizes the main key performance indicators for a tool like a moulding box. It can be see how the steel amount used can be reduced in an optimized moulding box, but the percentage of custom plates increases drastically as well as the number of different BOM item. This results in a higher cost per kg of steel (due to increased amount of welds and custom plates) in the optimized moulding box but in a lower final total cost due to the material savings achieved.

Also we can see how sand usage quantity was drastically reduced, as well as the effect on the cost of the produced item.

Table 3. Overview of key performance indicators for the three different moulding boxes designs (values relative to standard moulding box).

		Standard Moulding Box	Moulding Box With Sand Saving	Optimized Moulding Box
Moulding Box Design KPI	Steel Amount [%]	100	120	70
	Welds Amount [%]	100	110	70
	# Custom plates # Square shape Plates [%]	5	15	75
	# of Different Items in BOM	25	40	80
	Sand Amount	100	80	55
	Moulding Box Cost	100	120	70
	Direct Savings on Casted Item [%]	0	2%	5%

Conclusions

A new design methodology that heavily relies on CAE tools as well as on an improved management of the different systems and their interaction was implemented. The results was an increased capability to handle complex design in an easy way and a significant savings achieved both in investment and variable costs.

Acknowledgments

We wish to thank the management team of Global Casting A/S, for supporting such an innovative initiative, as well as all the people involved in the project from the design team, to project management office and factory floor for the hard work that made this a successful implementation.

Literature

[1] J. Mohammed, J. May, A. Alavi, *Application of Computer Aided Design (CAD) In Knowledge Based Engineering*, Proceedings of The 2008 IAJC-IJME International Conference, ISBN 978-1-60643-379-9.

[2] Giesecke, F., Mitchell, A., Spencer, H., & Hill, I. (2003). *Technical drawing*. Upper Saddle River, NJ: Prentice Hall.

[3] Karl T. Ulrich and Steven D. Eppinger, *Product Design and Development*, 2nd Edition, Irwin McGraw-Hill, 2000.

[4] P.G. Smith, *Cross-Functional Design Teams*, ASM Handbook, Volume 20, Materials Selection and Design, 1997, pp 49-53.

[5] Manuel E. Sosa, Steven D. Eppinger, Craig M. Rowles, *Are Your Engineers Talking to One Another When They Should?,* November 2007, Harvard Business Review, Page 133, hbr.org.

[6] D.I. Cleland, *Field Guide to Project Management, Concurrent Engineering (Chapter 32),* John Wiley & Sons, 1998.

Appendix B

Test Equipment Specifications

Coating Properties Tests

MLC608I

Rated load: 20,30,50,100,200G; Precision: C3
Safe overload:150% Ultimate overload: 200%
Material: Alloy aluninum
Apply to: handle scale,kitchen scale,fish scale,body scale,baby scale,post scale,microfore test equipment

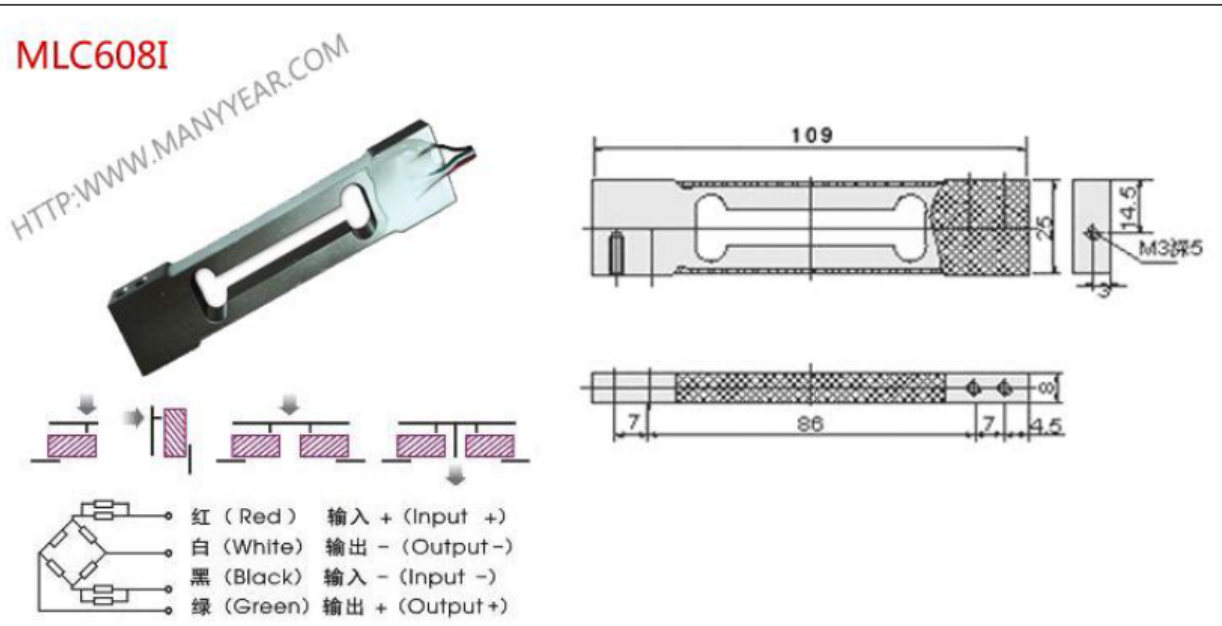

Specification			
comprehensive error:	0.05FS	output resistance:	1000±10Ω
Rated output:	0.5±0.1mv/v(1kg); 2mv/v(3kg)	Insulation resistance:	≥2000 MΩ/50V
Non-linearity:	±0.05%F.S.	Excitation voltage:	5~10VDC
Hysteresis:	±0.05%F.S.	compensated temp:	-10~+40ºC
Repeatability:	±0.05%F.S.	use temperature:	-20~+55ºC
Creep:	±0.05%F.S.5min	temp effect on zero:	±2.0%F.S./10ºC
Zero balance:	±0.1%FS	Temp effect on span:	±0.05%F.S./10ºC
Input resistance:	1055±10Ω	defend grade:	IP66

Figure B.1 Load cell specifications for self-developed cut time measurement.

Main characteristic AD MODULE	
1. Digital filter;	
2. digital demarcate:	
3. characteristic parameter store;	
4. sample rate option;	
5. set all item by series port;	
6. zero track range; ±2%	
7. zero adjust range when power on; ±2%~±20%	
8. linearity correct point option(4~8);	
9. temperature correct, adjust time can be option ;	
10. short response time of measure;	
11. Prevent versatility Intension option ;	
technology parameter	
1. Max signal range:	±10mV~±5V;
2. A/D resolution :	2000k/mV(12.5Hz);
3. A/D sampling speed:	6.25Hz，25Hz、50Hz、100Hz、200Hz、(option);
4. Filter mode:	standard low-filter and FIR filter;
5. Nor-linearity:	±0.001%F·S
6. Temperature characteristic:	<±1ppm/°C
7. Communication mode:	RS232/RS485/MODBUS/WIRELESS
8. baudrate:	1200,2400,4800,9600,19200 ,38400 bps (option);
9. Power supply:	16V~24V DC;
10. Current:	< 30 mA < 35mA (MAX);
11. Work temperature range:	,-20°C~+60°C;
12. Stock temperature range:	,-40°C~+80°C;
13. Indicator	6 bits LED
14. Keyboard	5 keys
15. output voltage (for load cell)	5vdc
16. analog signal output	4-20MA, 0-5vdc, 0-10vdc (option)
17 install mode	35mm standard guid rail
18. Prevent Thunder Strike dimension(mm):	100*75*25(L×W×H);
16. Weight	47g

Figure B.2 A/D converter specifications.

		Elcometer 2300 RV1-L
Low to medium viscosity		•
Medium to high viscosity		
Backlit LCD		•
Readings (cP & mPa)		•
Sample temperature measurement		•
Measuring range		3 – 2,000,000mPa
Accuracy of full scale		±1%
Max. altitude above sea level		2000m
Surge Class II		•
Contamination level 2		•
Operating voltage	UK 240VAC 50Hz	•
	EUR 220VAC 50Hz	•
	US 110VAC 60Hz	•

Speeds		0.3, 0.5, 0.6, 1, 1.5, 2, 2.5, 3, 4, 5, 6, 10, 12, 20, 30, 50, 60, 100, 200
Speed accuracy		< 0.5 of the absolute value
Thermometer	Range	-15°C to +180°C / 5°F to 356°F
	Resolution	0.1°C / 0.1722°F
	Accuracy	± 0.1°C / 0.1722°F
Power consumption		23W
Dimensions (of carry case)		495 x 420 x 200mm / 19.5 x 16.5 x 8"
Weight (including carry case)		9kg / 20lb

Figure B.3 Rotational viscometer specifications.

Infrared heating with metal heating elements
The robust heating elements deliver reliable results.

Routine operation without touching a button
The MJ33 guides the operator step by step through the analysis for simple, reliable routine inspection.

Compact display for ease-of-use
The compact display shows the key information. Icons guide the user.

Good access, easy to clean
The wide opening provides good access to the sample chamber. For easy operation and fast cleaning.

Optional printer for full documentation
The MJ33 features time and date for GMP/GLP compliant documentation.

Specifications MJ33

Part No. MJ33 **11121810**

Measurement values	**Moisture Content**
Readability	0.01%
Repeatability (sd) with 2 g sample	0.15%
Repeatability (sd) with 10 g sample	0.05%
Evaluation	
Moisture and dry content in %	✓
Weight in g	✓
ATRO moisture	✓
Balance	
Max. sample weight	35 g
Readability	1 mg
Drying unit	
Technology	Infrared; metal heating elements
Temperature range	50–160 °C
Adjustment increments	1 °C
Temperature programs	Standard
Switch-off	
Fully automatic, fixed	✓
Time controlled (minutes) & manual	1–99 min.

Figure B.4 Moisture analyser specifications.

Evaporation Rates Tests

Parameter	Conditions	Specification
A/D converter type		ADS1256, 24-bit Sigma Delta
A/D data rates		3750 samples per second (S/s), 2000 S/s, 1000 S/s, 500 S/s, 100 S/s, 60 S/s, 50 S/s, 25 S/s, 10 S/s, 5 S/s, 2.5 S/s
Throughput		▪ Single channel: 2.5 Hz to 1102.94 Hz, software selectable ▪ Multiple channels: 0.16 Hz to 1102.94 Hz, software selectable See Table 18 and Table 19 for details.
Number of channels		Up to 32 channels individually software-configurable as single-ended or differential Thermocouples require differential mode. For each channel configured as differential, you essentially lose one single-ended channel. You can add channels by connecting to an AI-EXP32.
Input isolation		*500 VDC minimum between field wiring and USB interface*
Channel configurations		Temperature sensor input, software programmable to match sensor type
		Voltage input
Input voltage range	Thermocouple mode	±0.078125 V
	Voltage mode (Note 1)	±20 V, ±10 V, ±5 V, ±2.5 V, ±1.25 V, ±0.625 V, ±0.3125 V, ±0.15625 V, ±0.078125 V, software-configurable
Absolute maximum input voltage	*CxH-CxL relative to GND*	▪ *±30 V maximum (power on)* ▪ *±10 V maximum (power off)*
Input impedance		▪ *2 GΩ (power on)* ▪ *390Ω (power off)*
Input leakage current		*±10.6 nA*
	▪ *Input voltage >±30 V (power on/off)*	*±1 µA maximum*
Input capacitance		590 pf
Maximum working voltage (signal + common mode)	Voltage mode: ±20 V range	±20.01 V maximum
	Voltage mode: all other voltage input ranges	±10.25 V maximum
Common mode rejection ratio (Note 1)	*Thermocouple mode, (f_{IN} = 60 Hz)*	*110 dB*
	Voltage mode, (f_{IN} = 60 Hz, all input ranges)	*90 dB*
ADC resolution		24 bits
Crosstalk	Adjacent channels	100 dB

Figure B.5 Voltage acquisition card USB-24-16-4AO specifications.

Parameter	Conditions	Specification
A/D converters		Four dual 24-bit, Sigma-Delta type
Number of channels		8 differential
Input isolation		*500 VDC minimum between field wiring and USB interface*
Channel configuration		*Software programmable to match sensor type*
Differential input voltage range for the various sensor categories	*Thermocouple*	*±0.080 V*
	RTD	*0 to 0.5 V*
	Thermistor	*0 to 2 V*
	Semiconductor sensor	*0 to 2.5 V*
Absolute maximum input voltage	*±C0x through ±C7x relative to GND (pins 9, 19, 28, 38)*	±25 V power on, ±40 V power off
Input impedance		5 GΩ, min
Input leakage current	Open thermocouple detect disabled	30 nA max
	Open thermocouple detect enabled	105 nA max
Normal mode rejection ratio	*f_{IN} = 60 Hz*	*90 dB min*
Common mode rejection ratio	*f_{IN} = 50 Hz/60 Hz*	*100 dB min*
Resolution		24 bits
No missing codes		*24 bits*
Input coupling		DC
Warm-up time		30 minutes min
Open thermocouple detect		Automatically enabled when the channel pair is configured for thermocouple sensor. The maximum open detection time is 3 seconds.
CJC sensor accuracy	*15 °C to 35 °C*	*±0.25 °C typ,±0.5 °C max*
	0 °C to 70 °C	*–1.0 °C to +0.5 °C max*

Figure B.6 Temperature acquisition card USB-Temp specifications.

Output specification

Number	8
Contact configuration	8 FORM C (SPDT) NO, NC and Common available at connector
Contact rating	*6 amperes (A) @ 120 volts AC (VAC) or 28 volts DC (VDC) resistive*
Contact resistance	100 milliohms (mΩ) max
Operate time	*10 milliseconds(ms) max*
Release time	*5 ms max*
Vibration	*10 to 55 hertz (Hz) (Dual amplitude 1.5 millimeters (mm))*
Shock	*10 G (11 ms)*
Dielectric isolation	*500 V (1 minute)*
Life expectancy	*10 million mechanical operations, min*
Power on RESET state	Not energized. NC in contact to Common.

Figure B.7 Digital output card Switch & Sense 8/8 specifications.

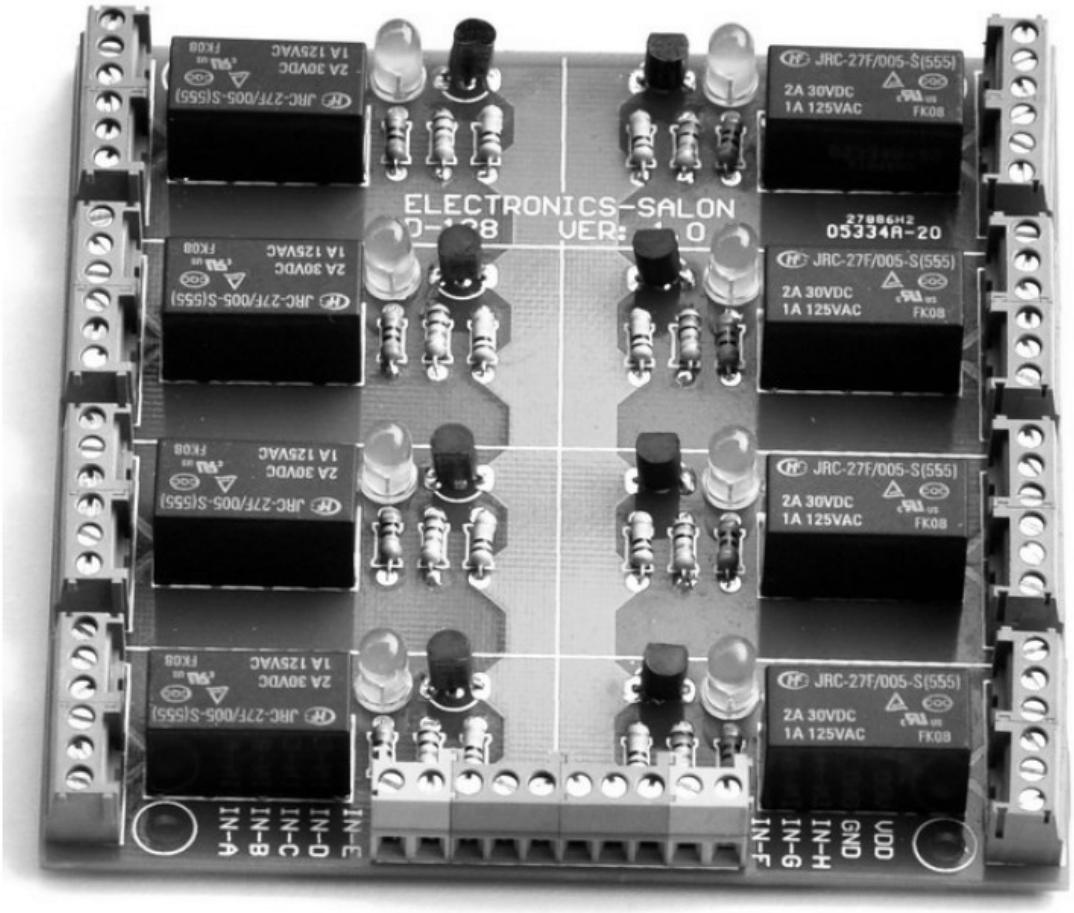

Led indicator for each relay.
BC517 Darlington transistor driving relay, Improve the reliability of action.
FR-4 Fiber glass PCB (Double Layer).
PCB thickness: 1.6mm.
Size: 100 x 100 x 16 mm (approximately 4 x 4 x 0.64 inch).

Power Supply:
24V version: 24VDC / 150mA (relay all ON).
Input control signal voltage:
0V - 0.5V Low stage (relay is OFF)
0.5V – 2.5V (unknown state).
2.5V - 20V High state (relay is ON)

Contact Rating:
5V and 12V version:
Contact Resistance: <0.05 ohm.
Contact Capacity: 125V AC 1 Amp, 30V DC 2 Amp.

Figure B.8 Double pole double throw (DPDT) relay card for power and signal switching.

■ FEATURES

- Ultra high sensitivity
- UL, CSA recognized
- Conforms to FCC rules and regulations Part 68
  —Surge strength 1,500 V
- High dielectric strength type available (RY-WF type)
- Contact arrangement MBB type available (RY-D type)
- High reliability-bifurcated contacts
- Wide operating range
- DIL pitch terminals
- Plastic sealed type
- RoHS compliant since date code: 0438B9
  Please see page 8 for more information

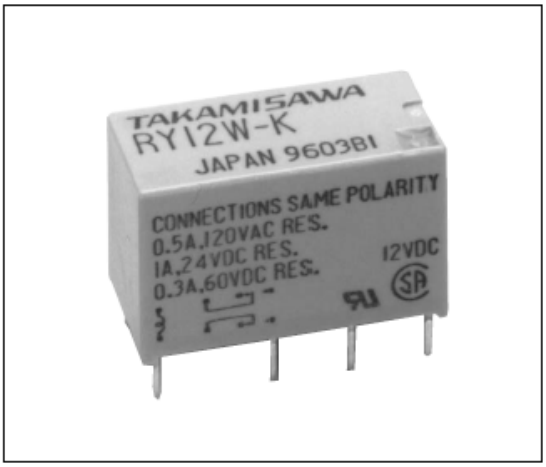

Item			High Sensitive Type	500 mW Type	High Dielectric Strength	2 A Type	Continuous (MBB) Type
			RY-( ) W-K	RY-( ) WZ-K	RY-( ) WF-K	RY-( ) WFZ-K	RY-( ) D-K
Contact	Arrangement		2 form C (DPDT)				2 Form D (2 MBB)
	Material		Gold overlay silver-palladium			Gold overlay silver-nickel	Gold overlay silver-palladium
	Style		Bifurcated (cross bar)				Single
	Resistance (initial)		Maximum 100 mΩ (at 1 A 6 VDC)				
	Maximum Carrying Current		1.25 A			2 A	0.6 A
	Rating (resistive)		1 A 24 VD 0.5 A 120 VAC		1 A 24 VDC 0.25 A 120 VAC	2 A 30 VDC 0.5 A 125 VAC	0.15 A 48 VDC 0.3 A 120 VAC
	Maximum Switching Power		60 VA/24 W		30 VA/24 W	62.5 VA/60 W	36 VA/7.2 W
	Maximum Switching Voltage		120 VAC, 60 VDC			125 VAC, 150 VDC	120 VAC, 60 VDC
	Maximum Switching Current		1 A			2 A	0.6 A
	Minimum Switching Load*1		0.01 mA 10 mVDC				0.1 mA 10 mVDC
	Capacitance (at 10MHz)		Approx. 0.9 pF (between open contacts) 1.4 pF (adjacent contacts) Approx. 1.9 pF (between coil and contacts)				
Coil	Nominal Power (at 20°C)		150 to 300 mW	500 to 580 mW	450 to 460 mW	500 to 580 mW	450 to 480 mW
	Operate Power (at 20°C)		75 to 140 mW	125 to 145 mW	200 to 210 mW	200 to 324 mW	200 to 210 mW
	Operating Temperature (No frost)		–30°C to +90°C (*+80°C)	–30°C to +60°C (refer to the CHARACTERISTIC DATA)			–30°C to +70°C (*2 +65°C)
Time Value	Operate (at nominal voltage)		Maximum 6 ms				
	Release (at nominal voltage)		Maximum 3 ms				
Life	Mechanical		2×10^7 ops. min.	1×10^7 operations minimum			1×10^6 ops. min.
	Electrical (at contact rating)		2×10^5 ops. min. (0.5 A 120 VAC) 5×10^5 ops. min. (1A 24 VD C)		5×10^5 ops. min. (0.25 A 120 VAC 1 A 24 VDC	1×10^5 ops. min. (2 A 30 VDC)	2×10^5 opsmin. (0.3 A 120 VAC) 5×10^5 ops. min. (0.15 A 48 VDC)
Other	Vibration	Misoperation	10 to 55 Hz (double amplitude of 1.5 mm)				
	Resistance	Endurance	10 to 55 Hz (double amplitude of 4.5 mm)				
	Shock	Misoperation	100 m/s² (11±1 ms)				
	Resistance	Endurance	1,000 m/s² (6±1 ms)				
	Weight		Approximately 5 g				

Figure B.9 Signal switching relay general specifications.

Orion Series Specifications

Capacity / Resolution		HR-60	HR-120	HR-200
Gram	(g)	60x0.0001	120x0.0001	210x0.0001
	(mg)	60,000x0.1	120,000x0.1	210,000x0.1
Decimal Ounce	(oz)	2.1x0.000005	4.2x0.000005	7.4x0.000005
Troy Ounce	(ozt)	1.9x0.000005	3.8x0.000005	6.7x0.000005
Pennyweight	(dwt)	38x0.0001	77x0.0001	135x0.0001
Carat	(ct)	300x0.001	600x0.001	1050x0.001
Momme	(mom)	16x0.00005	32x0.00005	56x0.00005
Grain Unit	(GN)	925x0.002	1851x0.002	3240x0.002
Tola	(t)	5x0.00001	10x0.00001	18x0.00001
Tael	(TL)	1.5x0.000005	3.1x0.000005	5.5x0.000005
Percentage Min Div		0.01%, 0.1% or 1		
Counting Min Weight		0.1		
Linearity		±0.0002 g		
Repeatability / Std Dev		0.0001 g		
Stabilization Time		3 seconds (typically)		
Sensitivity Drift		±2ppm / °C (when automatic		
Display Refresh		5 times per second /		
Pan Size		Ø 85 mm / 3.3 inches		
Physical Dimensions	(mm)	213(W) x 319(D) x 301(H)		
	(in)	8.4(W) x 12.6(D) x 11.9(H)		
Breeze Break Dimensions	(mm)	180(W) x 192(D) x 200 (H)		
	(in)	7.1(W) x 7.5(D) x 7.9(H)		
Operating Temperature		5°C to 40°C (41 °F to 104 °F), 85		
Weight		Approximately 5.7 kg / 12.5 lb		
Power		100, 120, 220, 240 VAC (AC Adaptor) 50 Hz / 60 Hz 10 hours continuous operation with rechargeable battery pack		
Standard Accessories		Manual, AC Adaptor, Protective Cover		
Ext. Cal. Mass (optional)		50 g	100 g	200 g

Figure B.10 Scale for gravimetric moisture measurement.

Power : 24(W)
Working Voltage: 24(V)DC
Working frequency: 1700±50(KHZ)
Transduction Slice Diameter : Φ20mm
Automization Volume :>300ml/h
Effective water level:15mm~35mm
Working Temperatture :5~45°C
coloured lantern:Circle 12 LED light
Water Level Inductive switch:Gate Shape Hight 20mm
Automization Head Diameter:Φ45mm H27mm
Wire rod specification:Black 3.8mmPVC wire,Long 1400±20mm
Plug Type :Φ 5.5×2.1mm Mother Plug
Rubber stuff :Φ 12mm
Back astern frame Hight105MM)

Figure B.11 Moist air generator (piezoelectric water atomizer) general specifications.

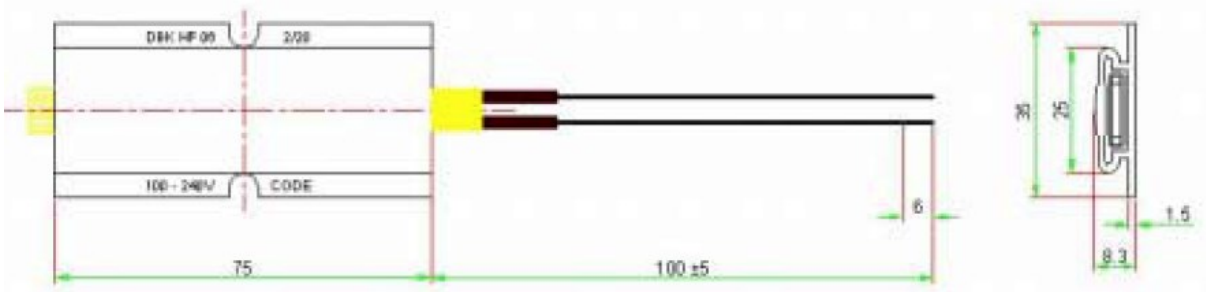

Product Type: **HP06 2/20 100-240V**
DBK Part Numbers: **FG800006**

Silicone Insulated Wire, 20awg, 300V

Description
A PTC surface and natural convection heater that will provide enough power to heat its surface to 200°C. In certain circumstances where heat loss is minimal, a surface temperature of 240°C is possible. The maximum power that the heater can supply when attached to a large heatsink is 180W at a lower surface temperature.

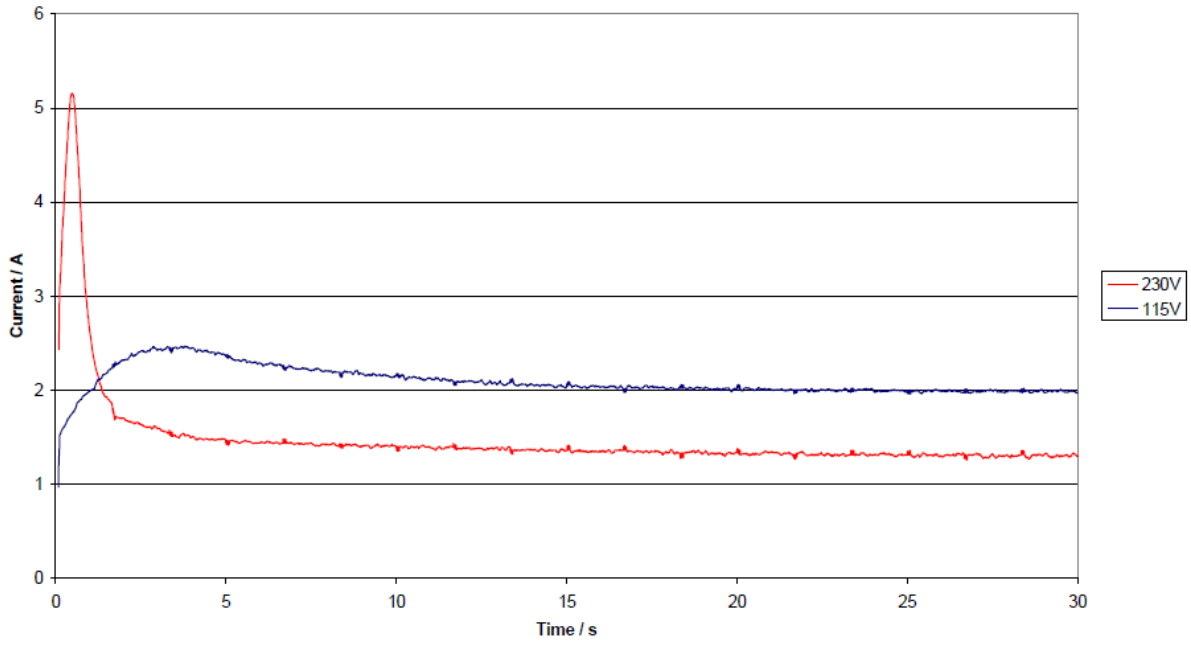

Thermal Performance – In free air

Ambient Temperature (degrees C)	Power Output (W)	Supply Voltage	Surface Temp (degrees C)
-20	25	230Vac	200
25	20	230Vac	210

Absolute maximum power available with natural convection and a large thermal mass at -20C is 180W.

Figure B.12 Electric PTC heater general specifications.

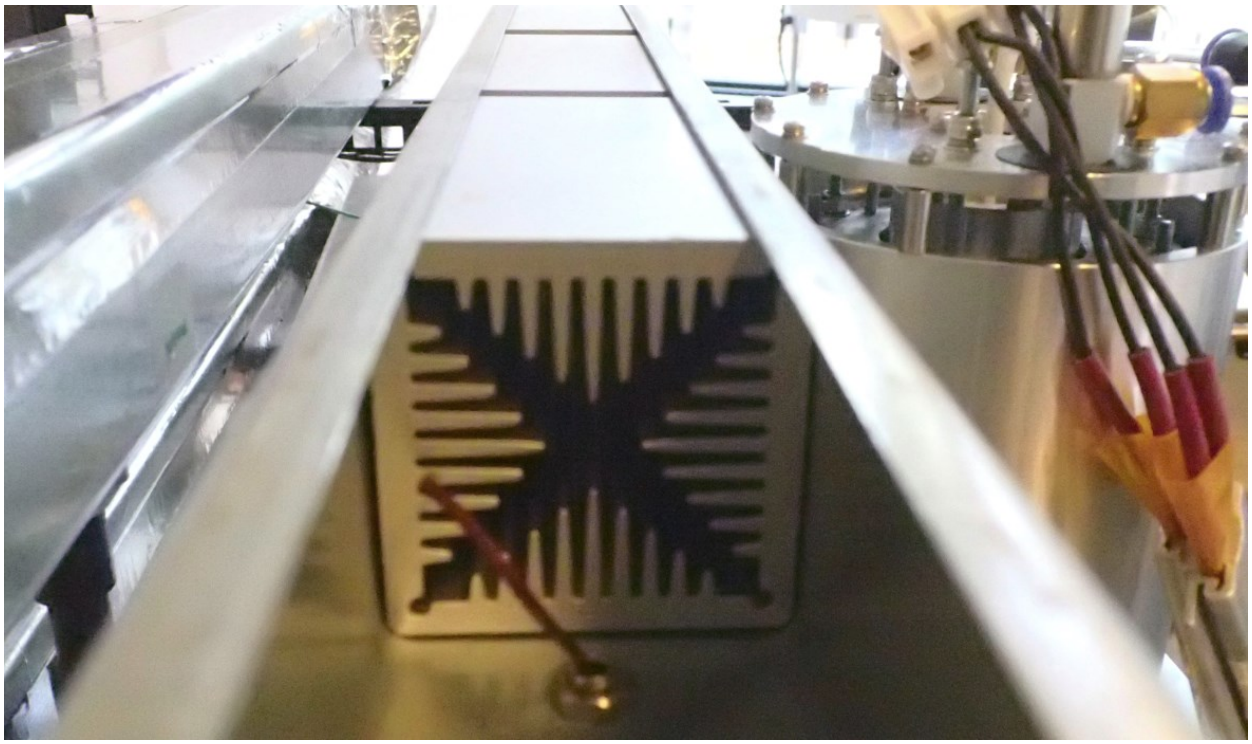

Figure B.13 Heat exchanger for electric heater.

SUNON 153~190 CFM 120x120x38 mm

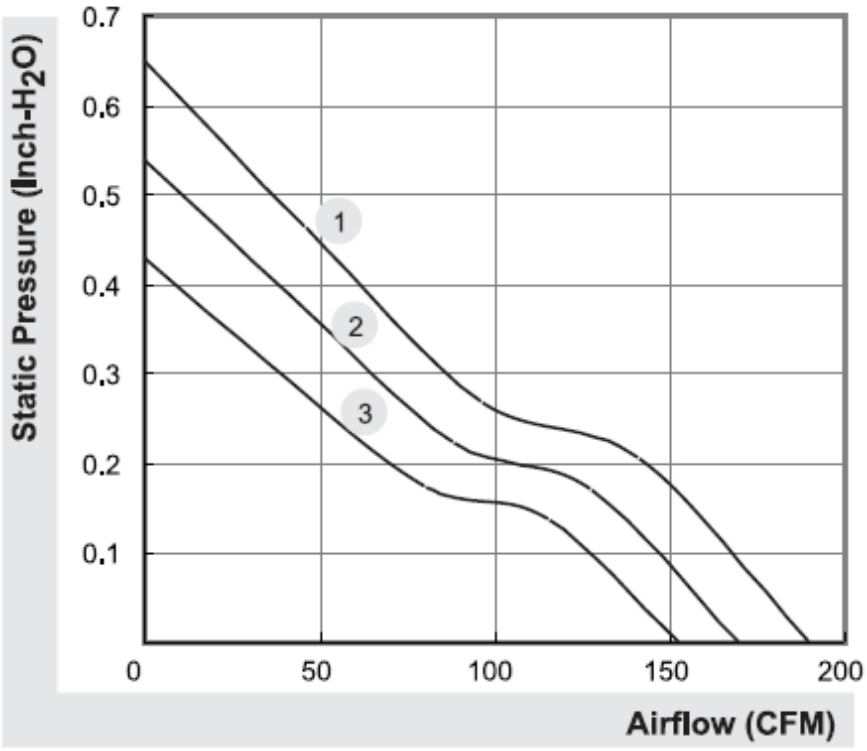

Model	P/N	Bearing ● 2BALL ○ Sleeve	Rating Voltage (VDC)	Power Current (AMP)	Power Consumption (WATTS)	Speed (RPM)	Air Flow (CFM)	Static Pressure (Inch-H2O)	Noise (dBA)	Weight (g)	Curve
PMD1212PMB1-A	(2).GN	●	12	1.6	19.2	4200	190	0.65	54	330	1
PMD1212PMB2-A	(2).GN	●	12	1.2	14.4	3800	170	0.54	51	330	2
PMD1212PMB3-A	(2).GN	●	12	0.83	10.0	3400	153	0.43	48	330	3

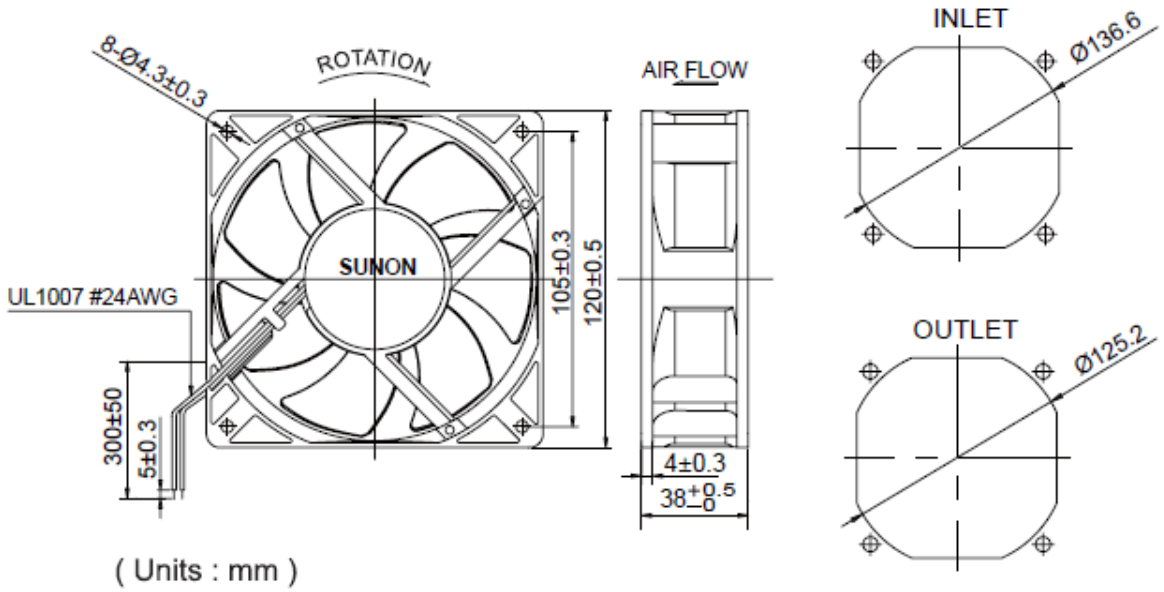

Figure B.14 Fan specifications (4 fans in series).

Thermocouple wire Type T is usable from 0 to 350 c or 32 to 660 f and very stable in cryogenic and low temperature applications.

T	Copper (+) Constantan (-)	Pure Copper 45% Nickel - 55% Copper

When protected or isolated with ceramic beads or insulation material.
Type T can be used in either oxidizing or reducing atmospheres, though for longer life, a protecting tube is recommended. Because of its stability at lower temperatures, this is a superior thermocouple for a wide variety of applications in low and cryogenic temperatures. It's recommended operating range is -200° to 350°C (-330° to 660°F), but it can be used to -269°C (-452°F) (boiling helium).

When protected by compacted mineral insulation and outer metal sheath (MGO).
Type T is usable from 0 to 350°C (32 to 660°F) and very stable in cryogenic and low temperature applications. For applications below 0°C (32°F) special alloy selections may be required.

Figure B.15 Thermocouple wire type T specifications.

16bar PVC-U pipe(x9),25mm ODx2m L

High quality PVC-U fittings, valves, pipework and accessories for a wide range of exterior and interior applications
PVC has excellent chemical resistance which combined with smoothness of bore eliminates build up of scale and gives good flow characteristics
Being odourless and tasteless it is suitable for conveying drinking water and many food products
Jointing is by solvent weld cement
The chemical resistance properties of PVC-U are excellent; it is resistant to most solutions of acids, alkalis and salts and to solvents that can be mixed with water. PVC-U is not resistant to aromatic and chlorinated hydrocarbons.
Tin stabilised compound conforming to the EEC safety levels for vinyl chloride monomer (VCM) and the WRAS requirements for use with potable water
Water Regulations Advisory Scheme, approved product for potable water
Permissible working temperature range for PVC-U systems is 0°C to 60°C
PVC-U fittings in imperial sizes for solvent cement jointing are manufactured in accordance with BS4346: Part 1, and are suitable for jointing PVC-U pipe to BS3505 & BS3506
All PVC-U metric pipe and fittings are manufactured in accordance with ISO/EN 15493

Bulk density	1.38g / cm^3
Tensile strength	55 N / mm^2
Elongation at break	>30%
Impact strength	No failure KJ / m^2 (23°)
Module of elasticity	3000 N / mm^2
Thermal expansion coefficient	0.08 mm / m°C
max. Operating temperature	60 °C
Vicat softening temperature	>76 °C (VST/B 50)
Moisture absorption	<4 mg / cm^3
Surface resistance	approx. 10^{13} Ω

Figure B.16 Low moisture, corrosion resistant plastic for sample holder specification.

Figure B.17 Drying sample placement in evaporation rates test setup.

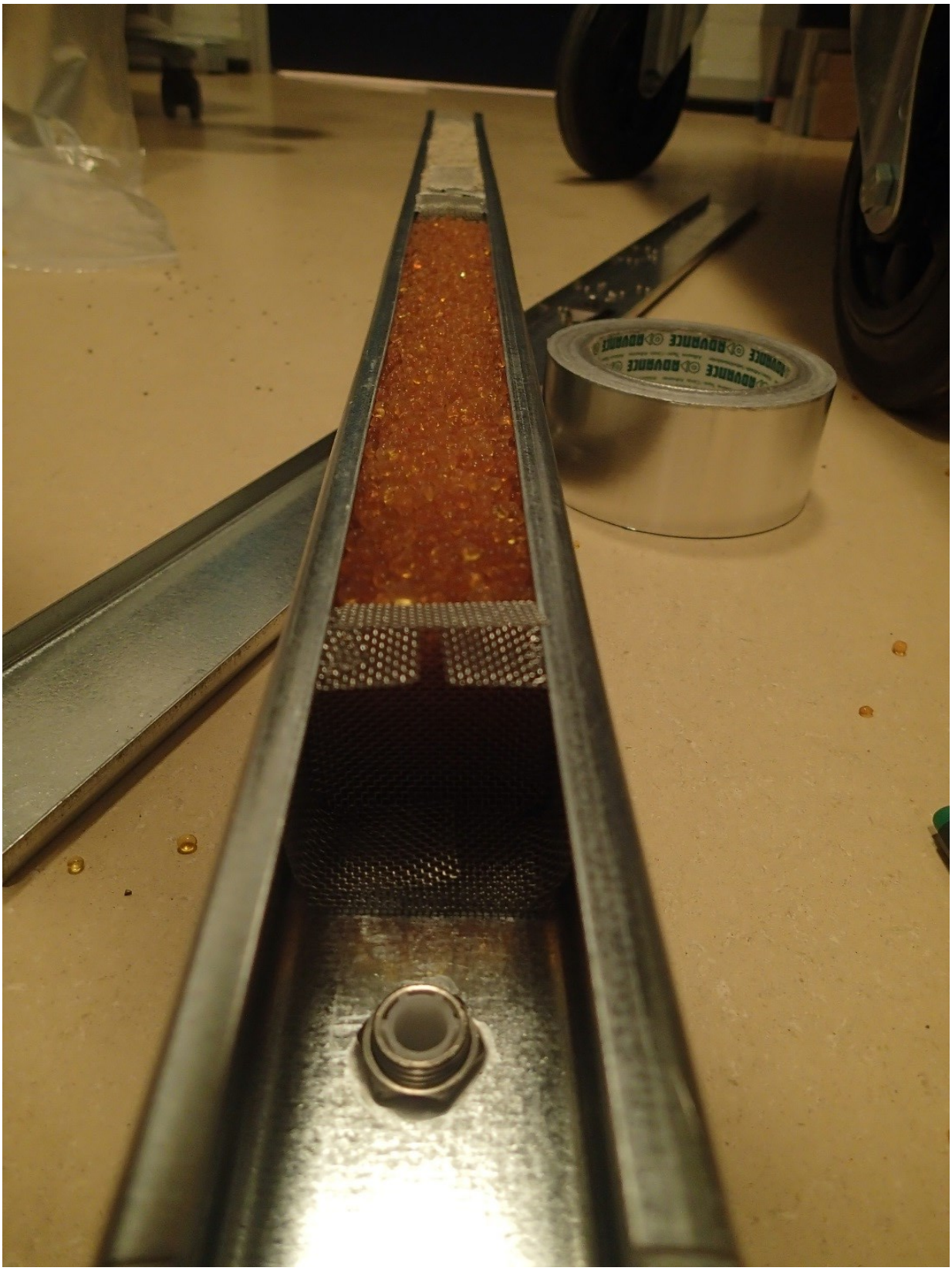

Figure B.18 Silica gel and molecular sieve used to obtain dry air for injection in the evaporation rates test setup.

	MiniAir64 Micro
Measuring range	0.5 - 20 m/s
or	0.7 - 40 m/s
Accuracy +/-	1.0% fs, 3.0% rdg
Operating temp.	-10 to +80°C
Power req. (external)	9 - 24 V DC (depending on the used resistance)
Output signal, 2-wire	**4 - 20 mA**
Head dim.	∅ 11 x 15 mm
Access opening	16 mm
Probe length	165 mm
Cable	5 m
Storage temp.	-65 to +150°C

Figure B.19 Air velocity sensor

XB Humidity Temperature Transmitter

Rotronic AG
Bassersdorf, Switzerland

Humidity measurement	XB2	XB3
Sensor	ROTRONIC Hygromer ® IN1	
Measuring range	0…100 %RH	
Measurement accuracy at 23 °C	±1.0 %RH	
Repeatability	0.3 %RH	
Long term stability	< 1 %RH / year	
Sensor time constant	Typical 10 sec, 63% of a 35 to 80 %RH step change (1m/sec air flow at sensor)	

The XB transmitter can be configured to calculate either the dew point or frost point based on the measurement of relative humidity and temperature. The accuracy of this conversion varies, depending on the humidity and temperature conditions as shown in the graph below:

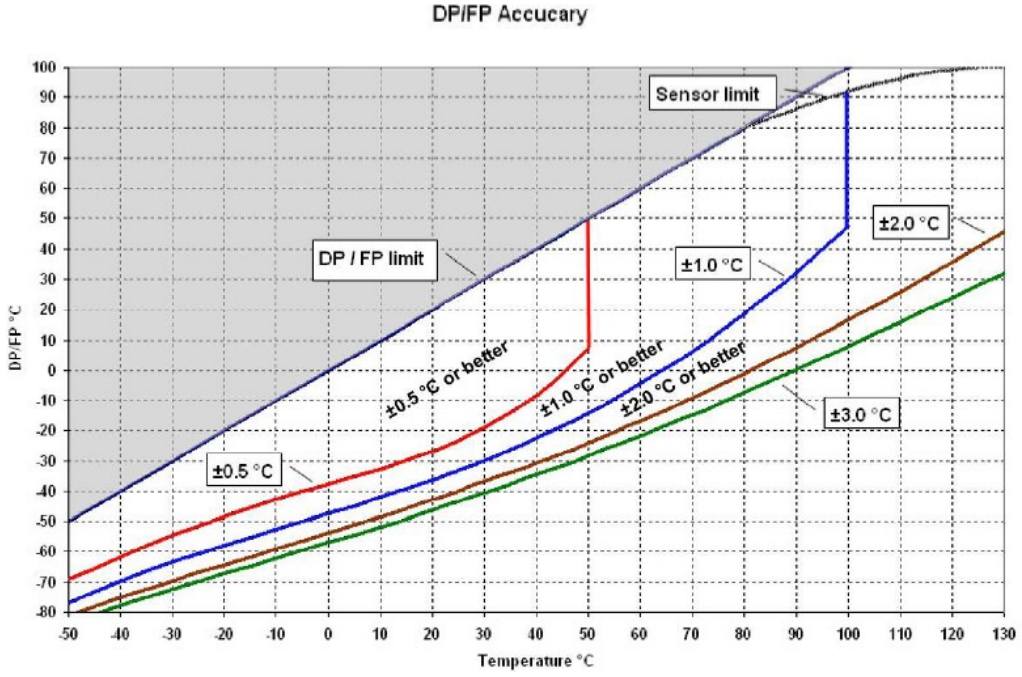

Figure B.20 Dew point and relative humidity sensor.

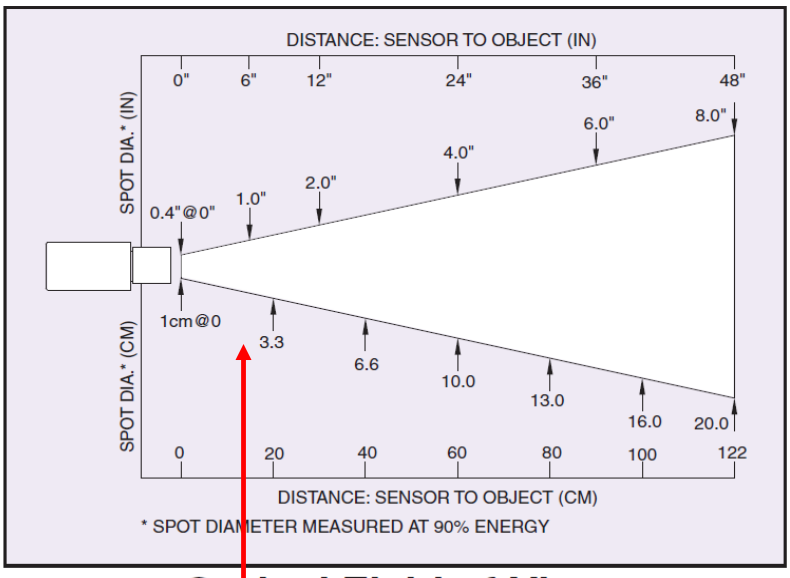

Optical Field of View

Temperature Range	-18 to 538°C (0 to 1000°F)
Accuracy @ 22°C (72°F) ambient temperature & emissivity of 0.95 or greater	± 2% of Rdg. or 2.2°C (4°F) whichever is greater
Optical Field of View	6:1 (Distance/Spot Size)
Repeatability	± 1% of Rdg.
Spectral Response	5 to 14 microns
Response Time	100 msec (0 to 63% of final value)
Emissivity Range	0.1 to 1.00, adjustable
Operating Ambient Temperature	
Main Transmitter	0 to 50°C (32 to 122°F)
Sensor Head	0 to 70°C (32 to 158°F)
Sensor Head (-HT Model)	0 to 85°C (32 to 185°F)
Sensor Head with OS100-WC (Water Cooling Jacket)	0 to 200°C (32 to 392°F)
Operating Relative Humidity	Less than 95% RH, non-condensing

Figure B.21 Non-contact infrared surface temperature transmitter specifications

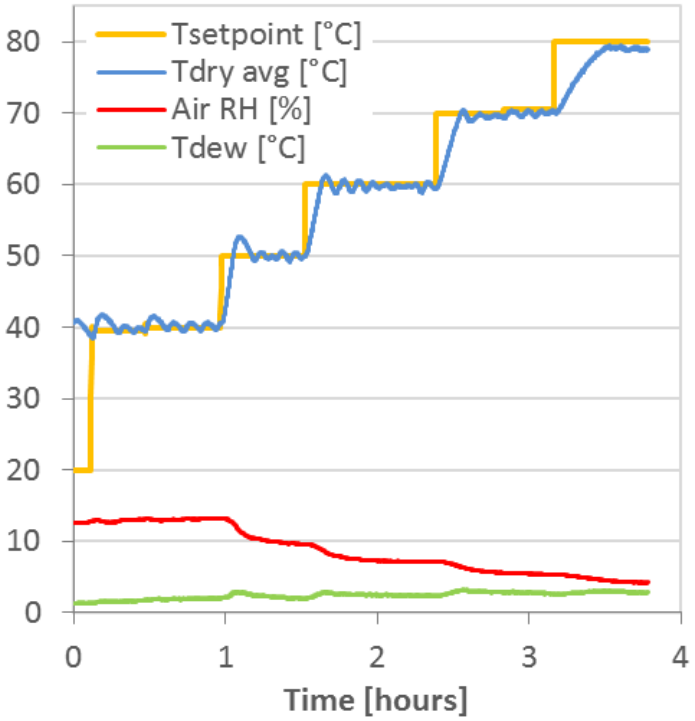

Figure B.22 **Precision of PID temperature control in evaporation rates test setup shown at different test temperatures.**

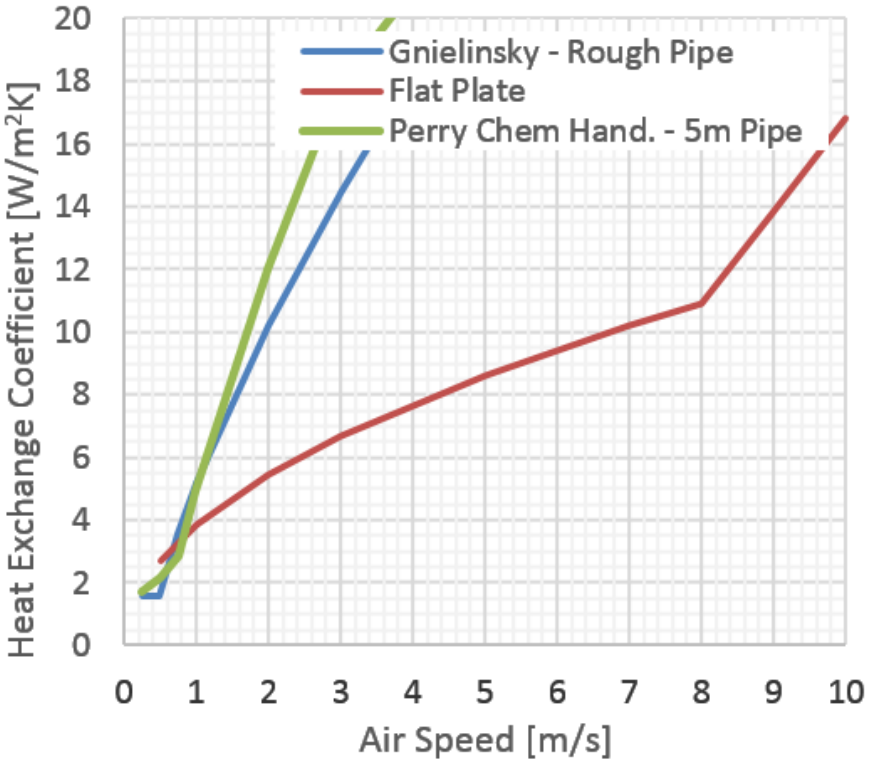

Figure B.23 **Heat exchange coefficient for a flat plate and for a 50 mm diameter test duct as a function of air speed**

Residual Moisture and Moisture Diffusion Tests

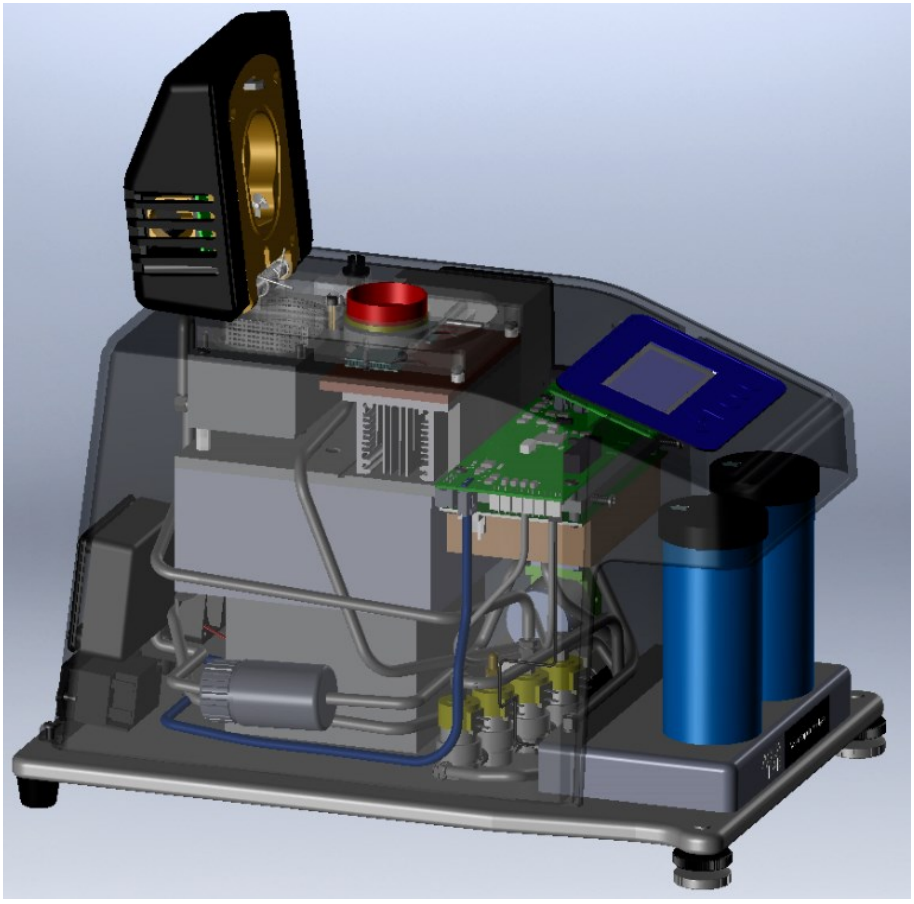

Accuracy : ±0.005aw

Repeatability : ±0.003 aw

Range: 0.030 to 0.950 aw

Isotherm Methods: Dynamic Dewpoint Isotherm (DDI) & Static (DVS)

External Gas: Not needed. If external gas, no more than 7PSI.

Computer Interface: USB

Mass Resolution: ±0.1 mg

Water Reservoir: 20ml

Sample Cup Volume: 10cc

Sample Weight: 500 to 5,000mg

Power : 110 V to 220 V AC, 50/60 Hz

Weight: 28 lbs

Temperature: 15 to 60 °C (sample chamber temperature; sample temperature is measured separately, and may vary)

Temp Stability: ±0.1 °C

Dimensions: W 10" x L 15" x H 12" , 25.4cm x 38.1cm x 30.5cm

Figure B.24 Automatic vapour sorption analyser specifications.

Kestrel® 4300 CONSTRUCTION WEATHER TRACKER

www.r-p-r.co.uk

FUNCTIONS

- Wind Speed
- Temperature
- Wind Chill
- Relative humidity
- Heat index
- Dew point
- Wet bulb temperature
- Evaporation rate
- Barometric pressure
- Altitude
- Density altitude
- Time & Date

Bluetooth® model available

Ideal for streaming real-time data to laptop or PDA

actual size (A4 page)

FEATURES

- High accuracy
- Wide operating range
- Compact, rugged design
- User-replaceable, precision Zytel®-mounted impeller
- Fast response temperature sensor

- Easy to read back-lit display
- Min/max/average values or graphical data
- User selectable units and language
- User customisable screens

- Data logging - up to 3200 readings
- Data upload (with optional PC interface or integrated *Bluetooth*® wireless technology)
- Runs from 2 AAA batteries
- Available in lime green

Speed (1 sec response)	Operational range	0.6m/s to 60m/s (1.3 to 135.0mph)
	Specification range	0.6m/s to 40m/s (1.3 to 89.0mph) Start-up speed stated as lower limit, readings may be taken down to 0.4 m/s | 79 ft/min | 1.5 km/h | .9 mph | .8 kt after impeller start-up.
	On axis accuracy	± 3% of reading or ± 0.1 m/s. (Some loss of accuracy from bearing wear may occur with sustained operation at or near maximum speed)
	Off -axis response	-1% @ 5°, -2% @ 10°, -3% at 15°
	Calibration drift	<1% after 100hrs operation at 7m/s
	Resolution	0.1 kt, m/s, km/h, mph. 1 FPM below 1999 FPM, 10 FPM above 2000 FPM. 1 Beaufort (0 to 12)
Temperature (1 sec response)	Operational range	-45.0°C to +125.0°C
	Specification range	-29.0°C to +70.0°C
	Accuracy	±1°C
	Resolution	0.1°
Wind chill accuracy		±1.0°C (from wind speed and temperature)
Relative Humidity (1 min response)	Operational range	0% to 100%
	Specification range	5% to 95% non-condensing
	Resolution	0.1%
	Accuracy	±3% (when unit allowed to equilibrate to external temperature)
	Calibration drift	±2% over 24 months (correctable)
Dew point accuracy		±2°C (above 20% relative humidity)

Figure B.25 Air temperature, speed and relative humidity logger.

Moisture Measurement

BM20 moisture indicator with pins

Moisture indicator needle for measuring moisture in wood, building materials.

- Moisture in wood in the range 1 - 45%
- Measurement of building materials in the range 0.2 -2.4%
- Max depth of 8 mm
- Environmental conditions
  - 0-40 ° C
  - 0-85% rh
- Digital display
- Automatic shutoff
- Alarm function
- Hand Model
- Weight 100 gr.

Figure B.26 Trotec concrete and wood moisture meter.

MODELS MTC-60 AND MTV-60 FOR WOOD

The Delmhorst moisture transmitters measure moisture in wood or other hygroscopic materials (in conjunction with any Delmhorst electrode) and generate either a current (MTC-60) or voltage output (MTV-60). The transmitters do not have a display. They use a 4-wire transmission method (i.e., DC voltage is brought in to power the unit by a separate wire from the wire used to carry the voltage or current output.)

The transmitters are ideally suited for applications requiring continuous monitoring of moisture in hygroscopic materials and interfacing the sensor to a data logger. The transmitters are housed in an ABS wall-mounted case for easy mounting near the sensor or in a control room.

SPECIFICATIONS: MTC-60

MOISTURE RANGE:	6% - 60% Wood (DOUGLAS FIR @ 70ºF)
NO. OF INPUTS:	ONE
OUTPUTS:	D.C. CURRENT 4 to 20 mA (Non-linear, inversely proportional) or, VOLTAGE 1-5 VDC, or 0-2 VDC
POWER REQUIREMENT:	D.C. VOLTAGE between 15 to 30 volts
SUPPLY CURRENT:	Minimum 50 mA
CASE SIZE:	3.5" x 1.75" x 2.5"; mounting base 3.53" x 2.28"
TERMINALS:	A 2.5 mm (Center Positive) POWER JACK for POWER INPUT, TERMINAL STRIP and UHF connector for MOISTURE INPUT

INCLUDES: MTC-60 or MTV-60, 15V POWER ADAPTER NO.219ADA-0011, OUTPUT PLUG NO. 216CAB-0023

Figure B.27 Delmhorst wood moisture meter.

Ultra-High Value Precision Resistors

TT electronics

3810 Series

- **Resistance range up to 100 T ohms (10^{14} ohms)**
- **Designed for low current (picoampere level) measurements**
- **Low voltage coefficient**
- **Hermetically sealed**
- **Leakage current minimised by hermetic sealing and guard ring**

		3810	3811	3812
Resistance range	ohms	100M to 1T	100M to 1T	1T to 100T
Limiting element voltage	volts	500	1000	1000
TCR (20°C to 70°C)	ppm/°C	-500 to -3500		
Resistance tolerance	%	10, 20	1, 2, 5, 10	1T to 10T; 2, 5, 10 >10T; 5, 10
Values		E24 preferred		
Ambient temperature range	°C	-40 to 100		

			Maximum	Typical
Load at rated voltage: 1000 hours at 20°C		ΔR%	2	1
Shelf life: 12 months at room temperature		ΔR%	1	0.5
Resistance to solder heat		ΔR%	0.2	<0.1
Capacitance	3810	pF	0.4	
	3811	pF	0.2	

Figure B.28 GOhm range resistors used for reference.

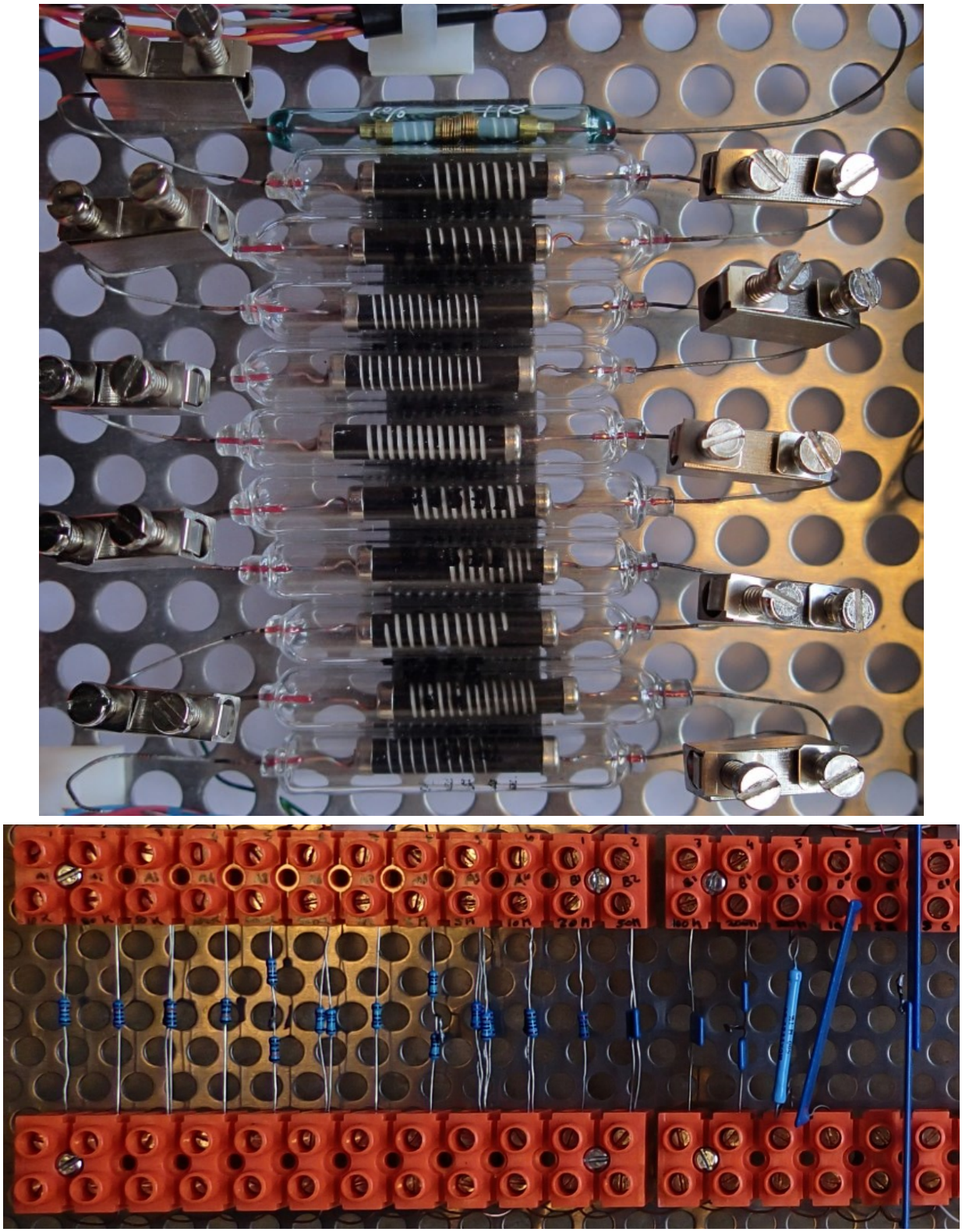

Figure B.29 Assembled reference resistor banks.

Properties	Unit	Test method DIN ASTM	
Thermal			
Max. service temperature short term long term	°C °C		260 260
Coefficient of thermal conductivity	W/(m · K)		0.25
Specific heat	J/(g · K)		1
Coefficient of thermal expansion	10^{-5}/K		12
Electrical			
Dielectric constant at 10^5 Hz		53 483	2.1
Dielectric loss factor at 10^5 Hz		53 483	0.0002
Specific volume resistance	Ω · cm	53 482	10^{18}
Surface resistance	Ω	53 482	
Dielectric strength 1 mm	kV/mm	53 481	48
Tracking resistance		53 480	KA 3c/KB > 600
Miscellaneous			
Moisture absorption: Equilibrium in standard atmosphere (23 °C / 50 % relative humidity)	%	53 714	0
Water absorption at saturation at 23 °C	%	53 495	
Resistance to hot water, washing soda			resistant
Flammability		UL 94	V0
Resistance to weathering			resistant

Figure B.30 Teflon material specifications. Used for resistance based moisture measurement device calibration.

Technical data		V Series	LV Series
Article no.		IC 080 V: 3.110.003.011 IC 0120 V: 3.110.003.019	
Measuring	Temperature range	-20 °C to +600 °C -20 °C to +1.500 °C	-20 °C to +600 °C -20 °C to +1.500 °C
	Accuracy	±2 °C, ±2% of the measured value	
	Detector type	Focal Plane Array (FPA), uncooled microbolometer	
	Detector resolution	160 x 120 pixels	384 x 288 pixels
	Spectral range	8 to 14 µm	7,5 to 14 µm
	Field of Vision (FOV)	20 °C x 15 °C	24 °C x 21 °C
Image output radiometric	Geometric resolution	2.2 mrad	1.1 mrad
	Thermal sensitivity	0.08 °C to 30 °C	0.05 °C to 30 °C
	Image refresh rate	50/60 Hz	
	Focus	manual	
	Min. focusing distance	0,10 m	

Figure B.31 Infrared camera for thermo-imaging.

DTU Mechanical Engineering
Section of Manufacturing Engineering
Technical University of Denmark

Produktionstorvet, Bld. 427A
DK- 2800 Kgs. Lyngby
Denmark
Phone (+45) 4525 4763
Fax (+45) 4593 0190
www.mek.dtu.dk
ISBN: 978-87-7475-412-1